

I. Ground and Excited State Studies of
Persistent 1,1-Diazenes
and
II. Design of Sequence Specific DNA Cleaving Molecules

Thesis by
Peter G. Schultz

In Partial Fulfillment of the Requirements
for the Degree of
Doctor of Philosophy

California Institute of Technology
Pasadena, California

1984

(submitted September 19, 1983)

To Mom and Dad

ACKNOWLEDGMENTS

Many thanks to a terrific advisor, Peter Dervan, for providing the research opportunities which made this thesis possible. His insight, enthusiasm, and friendship will always be appreciated.

I would also like to thank all those people who have contributed to the great times during my stay at Caltech. I would especially like to thank John Taylor and Bill Hinsberg for their valuable scientific contributions. Debbie Chester cheerfully and expertly typed this thesis. NSF and IBM provided financial support.

Finally, thanks to Jocelyn for her love and companionship.

Abstract

CHAPTER I

Direct studies of the ground and excited state properties of kinetically persistent 1,1-dialkyldiazenes are reported. The electronic absorption spectrum of N-(2,2,5,5-tetramethylpyrrolidyl)nitrene **3** reveals a structured absorption band for the n, π^* transition: $\lambda_{\max} = 497$ nm, $\lambda_{0,0} = 572$ nm ($\lambda_{\max} = 20 \pm 3$) in CH_2Cl_2 ; $\lambda_{0,0} = 552$ nm in *i*-PrOH. The infrared spectrum shows a strong absorption at 1638 cm^{-1} , providing evidence that the 1,1-diazene N-N stretch has considerable double bond character. The major products resulting from pyrolysis of **3** at 0°C are isobutylene **21**, tetramethylcyclobutane **20**, and tetrazene **24**, consistent with unimolecular and bimolecular decomposition pathways. The activation parameters for unimolecular fragmentation are: $\log A = 12.4 \pm 0.4$, $E_a = 19.0 \pm 0.6 \text{ kcal mole}^{-1}$ in Et_2O ; $\log A = 12.1 \pm 0.3$; $E_a = 19.1 \pm 0.4 \text{ kcal mole}^{-1}$ in THF; $\log A = 10.9 \pm 0.3$, $E_a = 16.8 \pm 0.5 \text{ kcal mole}^{-1}$ in hexane. The activation parameters for the bimolecular dimerization of **3** could not be measured, however $\log A = 3.8 \pm 0.7$ and $E_a = 6.4 \pm 0.9 \text{ kcal mole}^{-1}$ for the dimerization of N-(2,2,6,6-tetramethylpiperidyl)nitrene **2** in CDCl_3 .

The fluorescence spectrum of **3** has a 0-0 band at 607 nm which is the maximum. The spacing between the peaks at 607 and 672 nm is consistent with the N=N stretch of S_0 obtained from the infrared spectrum. The fluorescent quantum yields are $\phi_F = 2 \times 10^{-3}$ (MIHF, -78°C), 7×10^{-8} (CFCl_3 , -196°C) and 1×10^{-3} (EPA, -196°C). The fluorescent lifetime of **3**, τ_F is 5×10^{-9} sec (CFCl_3 , -78°C) and 2.3×10^{-8} sec (CFCl_3 ,

-196°C). Direct irradiation of **3** in the visible (-78°C) affords 54% **21**, 44% **20**, and tetrazene **24**, again consistent with unimolecular and bimolecular decomposition pathways. Triplet sensitized photolysis affords a high cleavage/closure ratio: 74% **21** and 24% **20**. An approximate quantum yield for decomposition of **3** on direct irradiation (-78°C) is $\phi_D = 1.1 \times 10^{-2}$.

D,L-N(2,5-diethyl-2,5-dimethylpyrrolidyl)nitrene **26** has a structured visible absorption with λ_{\max} at 507 nm. The maximum of the fluorescence spectrum is 620 nm, $\phi_F = 9 \times 10^{-3}$ (MTHF, -196°C). Direct and sensitized irradiation of **26** in the visible (-78°C) affords closure, cleavage, and disproportionation products as well as tetrazene. The retention of configuration in the cyclobutane products was 98% and 68% for direct and sensitized decompositions, respectively. This spin correlation effect indicates that $k_{ISC} \ll k_{N_2}(S_1)$, consistent with the large calculated S_1-T_1 gap in 1,1-diazene. Comparison of these results with those in the literature for the isomeric 1,2-diazene provides information on the nature of intersystem crossing in nonconjugated diradicals. The deactivation rates for S_1 of 1,1-diazene **3** have been determined: $k_{IC} = 2 \times 10^8 \text{ sec}^{-1} (-78^\circ\text{C})$; $k_F = 3 \times 10^5 \text{ sec}^{-1}$; $k_{DIM} \sim 8 \times 10^7 \text{ M}^{-1} \text{ s}^{-1} (-78^\circ\text{C})$; $k_{N_2} \sim 3 \times 10^5 \text{ sec}^{-1} (-78^\circ\text{C})$; $E_T \leq 31 \text{ kcal mole}^{-1}$.

The photochemistry of the six-membered ring cyclic 1,1-diazene **2** was also examined.

CHAPTER II

The ability of restriction endonucleases to cleave double helical DNA on opposite strands at or near 4-6 base pair recognition sequences makes possible DNA sequencing, gene isolation and recombinant DNA technology. Studies aimed at defining those elements necessary for the design of synthetic double strand DNA cleaving molecules with defined target sequences and binding site sizes are described.

The covalent modification of sequence specific DNA binding molecules with a chelated metal capable of redox chemistry generates bifunctional DNA cleaving molecules. Attachment of EDTA to the amino or carboxy terminus of the N-methylpyrrole oligopeptide distamycin A affords distamycin-EDTA (**DE**) and EDTA-distamycin (**ED**), respectively. **DE**·Fe(II) and **ED**·Fe(II) (10^{-6} M) sequence specifically single strand cleave pBR-322 plasmid DNA (10^{-5} M bp) in the presence of O_2 and dithiothreitol (DTT). Cleavage occurs over three to five base pairs adjacent to a five base pair 5'-XXTTT-3' (X = A or T) binding site and is consistent with oxidative degradation of the deoxyribose. Analysis of the DNA cleavage patterns generated by **DE**·Fe(II) and **ED**·Fe(II) (high resolution denaturing gel electrophoresis) provides information on the location, size, and orientations of distamycin binding sites on DNA. This direct method for defining small molecule binding sites on DNA, "DNA affinity cleaving", is compared to methidiumpropyl-EDTA·Fe(II) (**MPE**·Fe(II)) footprinting. A model for distamycin binding is proposed.

Attachment of EDTA to the amino terminus of a penta-N-

methylypyrrole peptide yields **P5E**. In the presence of O_2 and DTT, **P5E**·Fe(II) ($10^{-8}M$ bp) converts supercoiled pBR-322 DNA ($10^{-3}M$) to 40% open circular DNA, indicating that cleavage is catalytic, with a minimum of nine turnovers. **P5E**·Fe(II) sequence specifically double strand cleaves linear pBR-322 DNA (4362 base pairs) into discrete fragments. The cleavage sites are located at 4.3, 4.2, 3.3, 3.2 kb (major) and 2.6, 2.4, 2.0, 1.8 kb (minor). **P5E**·Fe(II) binds preferentially to 6-7 base pair poly(dA)·poly(dT) sites.

EBD and **BED** consist of two N-methylpyrrole tripeptide units coupled at the amino termini via a flexible linker with EDTA tethered to one or both carboxy termini, respectively. **BED**·2Fe(II) and **EBD**·Fe(II) cleave pBR-322 ($10^{-5}M$ bp) DNA at nanomolar concentrations. These reagents cleave linear pBR-322 plasmid DNA at 4.3 and 3.3 kb to afford discrete fragments. **BED**·Fe(II) and **EBD**·Fe(II) bind as dimers to 8-9 base pair A+T sites and monomers to 5-6 base pair A+T sites.

TABLE OF CONTENTS

CHAPTER I

PAGE

INTRODUCTION.....	2
Theoretical Studies.....	3
Generation and Chemistry of 1,1-Diazenes.....	7
Nomenclature.....	14
Experimental Strategy.....	14
RESULTS AND DISCUSSION.....	17
Synthesis and Characterization of N-(2,2,5,5-Tetramethyl- pyrrolidyl)nitrene.....	17
Synthesis of N-(2,2,5,5-tetramethylpyrrolidyl)nitrene.....	17
Electronic Absorption Spectrum of N-(2,2,5,5- Tetramethylpyrrolidyl)nitrene	19
Infrared Spectrum of N-(2,2,5,5-Tetramethyl- pyrrolidyl)nitrene.....	22
Nuclear Magnetic Resonance Spectra of N- (2,2,5,5-Tetramethylpyrrolidyl)nitrene.....	26
Thermolysis of N-(2,2,5,5-Tetramethyl- pyrrolidyl)nitrene	29
Unimolecular Decomposition Kinetics of N-(2,2,5,5- Tetramethylpyrrolidyl)nitrene and Bimolecular Decomposition Kinetics of N-(2,2,5,5-Tetramethyl- pyrrolidyl)nitrene and N-(2,2,6,6-Tetra- methylpiperidyl)nitrene ..	32
Photochemistry of 1,1-Diazenes. Photochemical Studies of N-(2,2,5,5-Tetramethylpyrrolidyl)nitrene, dl,-N(2,5-Diethyl-2,5-Dimethylpyrrolidyl)nitrene and N-(2,2,6,6-Tetramethylpiperidyl)nitrene.....	44
Photophysical Properties of N-(2,2,5,5-Tetramethyl- pyrrolidyl)nitrene and N-(2,2,6,6-Tetramethyl- piperidyl)nitrene.....	46
Direct and Sensitized Photolyses of N-(2,2,5,5- Tetramethylpyrrolidyl)nitrene and N-(2,2,6,6- Tetramethylpiperidyl)nitrene	54
Spin Correlation Effects in the Photodecomposition of dl,-N(2,5-Diethyl-2,5-Dimethylpyrrolidyl)nitrene and the Behavior of the Incipient Biradical.....	66
Summary.....	79
EXPERIMENTAL.....	82
REFERENCES.....	118

CHAPTER II

INTRODUCTION.....	128
Restriction Endonucleases.....	128
Experimental Strategy.....	133
RESULTS AND DISCUSSION.....	143
Distamycin-EDTA (DE).....	143
Synthesis.....	143
Cleavage Efficiency.....	145
Double Strand Cleavage.....	150
Cleavage Specificity.....	154
EDTA-Distamycin (ED).....	175
Synthesis.....	175
Cleavage Efficiency.....	176
Double Strand Cleavage.....	178
Cleavage Specificity.....	182
Affinity Cleaving with ED ·Fe(II) and DE ·Fe(II).....	182
Comparison of Affinity Cleaving with MPE ·Fe(II)	
Footprinting.....	195
Penta-N-Methylpyrrolecarboxamide-EDTA (PSE).....	204
Synthesis.....	204
Cleavage Efficiency.....	205
Double Strand Cleavage.....	209
Cleavage Specificity.....	214
Bis(distamycin-EDTA) (BED) and EDTA-bisdistamycin (EBD)	227
Synthesis.....	228
Cleavage Efficiency.....	231
Double Strand Cleavage.....	233
Cleavage Specificity.....	237
Conclusion.....	246
EXPERIMENTAL.....	247
REFERENCES.....	275
PROPOSITIONS.....	286

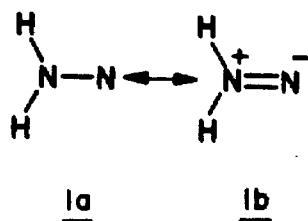
CHAPTER I

Ground and Excited State Studies of

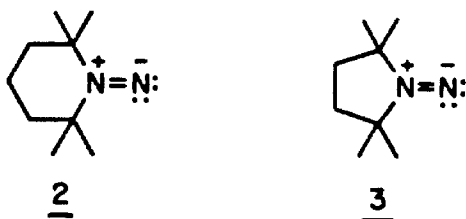
Persistent 1,1-Diazenes

INTRODUCTION

1,1-Diazenes, nitrenes in which (formally) monovalent nitrogen is substituted with an amino group, are isoelectronic to carbonyls and isomeric to 1,2-diazenes (azo compounds). Although the intermediacy of 1,1-diazenes has been postulated in a substantial number of chemical



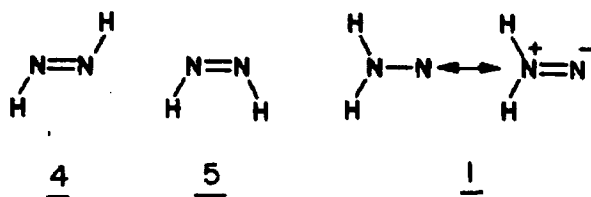
reactions,¹ only recently has this elusive species been directly observed. In 1978, Hinsberg and Dervan reported the synthesis and characterization of the kinetically persistent 1,1-dialkyldiazene N-(2,2,6,6-tetramethylpiperidyl)nitrene² **2**. Shortly thereafter, Schultz and Dervan reported the isolation of a second 1,1-diazene, N-(2,2,5,5-tetramethylpyrrolidyl)nitrene³ **3**. The synthesis and isolation of these kinetically persistent 1,1-diazenes have made possible the first direct



studies of both the ground and excited state properties of this functional group.

Theoretical Studies

Theorists have devoted considerable effort to the N_2H_2 surface with regard to the nature of bonding, state energetics, the mechanism of



isomer interconversion and the N-H bond energies.⁴⁻³⁰ The most important question concerning the electronic structure of H_2N-N is the nature of the ground state. Unlike other nitrenes, the chemical behavior of 1,1-diazenes suggests that the singlet is the ground state.¹ Early *ab initio* studies of H_2N-N resulted in a triplet ground state, but more recent calculations employing larger basis sets and configuration interaction find that the singlet is the ground state (Table I).

Table I - Singlet-Triplet Energy Gap in H_2N-N

Calculational Method	Ground State	S-T Gap ^a	Reference
STO-3G	Triplet	26.3	Baird, 1973 (12)
4-31G	Triplet	11.7	Pople, 1978 (25)
HF	Triplet	5.2	Ahlrichs, 1976 (17)
SCF	Triplet	2.1	Wagniere, 1973 (13)
4-31G-Cl	Singlet	1.6	Baird, 1977 (23)
GVB-Cl	Singlet	13.8	Goddard, 1977 (24)

a) kcal/mol⁻¹, both states at equilibrium geometries.

From recent calculations of Davis and Goddard (GVB-CI)²⁴ the following theoretical picture of the parent 1,1-diazene emerges. The ground state is a singlet (1A_1) with the triplet (3A_2) lying 0.6 eV (13.8 kcal) higher in energy. Stabilization of the singlet state is due to the large amount of double bond character in the NN bond ($H_2\ddot{N}=\ddot{N}:$) as reflected in the short bond length ($R_e = 1.25 \text{ \AA}$, $R_e = 1.25 \text{ \AA}$ for $t\text{-HN=NH}^{30}$) and the large dipole moment ($\mu = 4.036 \text{ D}$). Due to strong bonding interaction S_0 is planar. The calculations suggest that electron withdrawing substituents should destabilize the S_0 state relative to T_1 , thereby compressing the S_1 - T_1 gap. The first excited singlet, S_1 , corresponds to an n,π^* state and lies 2.2 eV (50.7 kcal/mole) above the ground state. Important to the experimentalist, the calculations predict that the 1,1-diazene should absorb light in the visible region.

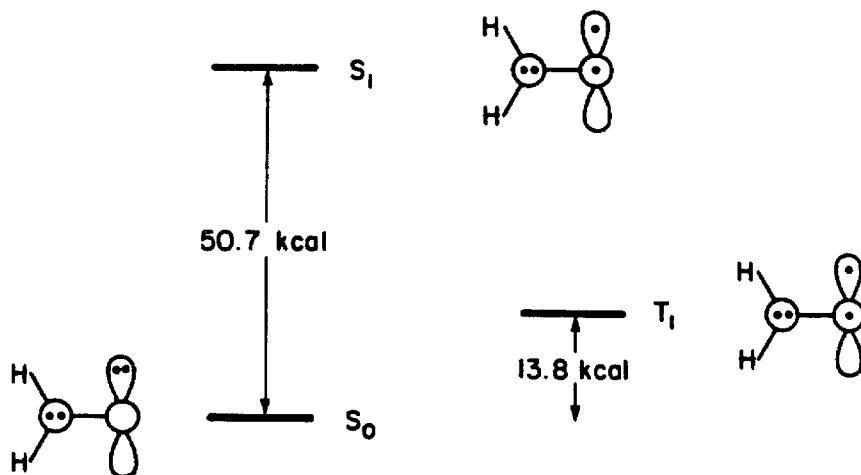


Figure 1. GVB-CI Calculations for H_2N-N

In the S_1 and T_1 states there are two opposing forces: pyramidalization which reduces antibonding interactions, and planariti-

zation which leads to a favorable 3 electron, 2 center bond. These effects are actually comparable and lead to an optimum pyramidal geometry (21° angle between the H_2N plane and N-N axis) with an inversion barrier of <1 kcal/mole (the inversion barrier of NH_3 is 6 kcal/mole).³¹ Delocalization of the internal nitrogen lone pair is reflected in an optimum bond length of 1.37 Å (hydrazine is 1.45 Å)³² and dipole moment of 2.35 D. The $\text{S}_1\text{-T}_1$ gap in 1,1-diazenes (36 kcal) is the same as that in $\text{H-N}\cdot$; the amino substituent effecting S_1 and T_1 identically.

The thermochemistry of the N_2H_2 surface has also been examined by theory.^{5,29} The *ab initio* (GVB-CI) calculations of Casewit and Goddard⁵ are summarized in Figure 2.

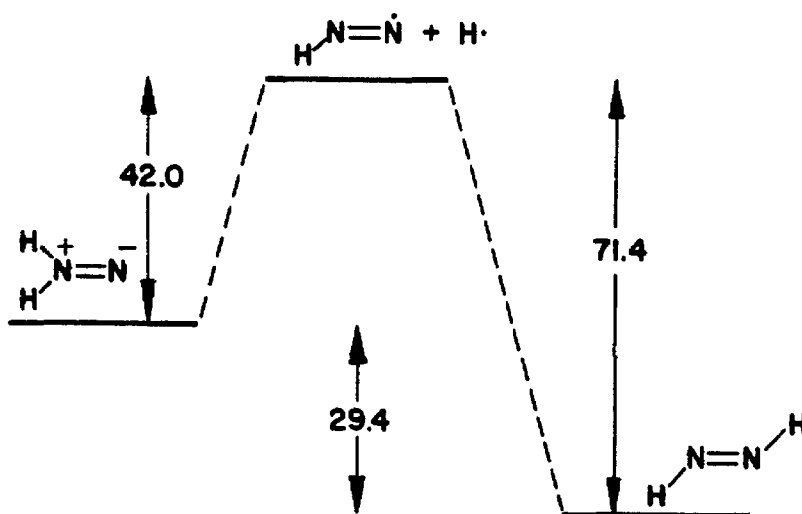
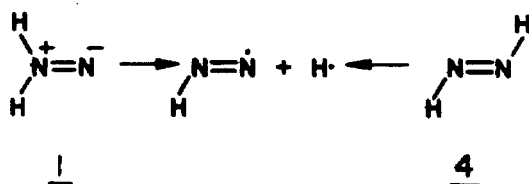


Figure 2. GVB-CI calculations for the N_2H_2 energy surface and the diazenyl radical $\text{H-N=N}\cdot$.

Their calculations afford an N-H bond energy in 1,1 diazene **1** of 42



kcal/mole and an N-H bond energy in 1,2-diazene **4** of 71.5 kcal/mole.

Correcting for the difference between a N-CH₃ and N-H bond (D(HMeN-H) - D(HMeN-Me) = 18.5 kcal/mole)³³ gives an estimate of the bond energy in 1,1-dimethyl diazene of 23.5 kcal/mole. Application of this correction to the N-H bond energy of **4** leads to a value of 52.9 kcal/mole for the C-N bond energy in trans-1,2-dimethyldiazene (azomethane). This value is in excellent agreement with the experimental value of 52.5

kcal/mole³⁴ for the thermal decomposition of azomethane. However the 18.5 kcal/mole correction factor may not be valid for the 1,1-diazene.

One must therefore be cautious in applying the GVB-CI results to

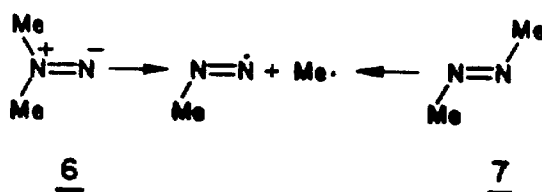
1,1-dialkyldiazene thermochemistry. Qualitatively, the N-H bond energy in 1,1-diazenes is lower than in 1,2-diazenes because α cleavage in

$\text{H}_2\text{N}^+\text{N}^-$ results in formation of a full π bond, i.e., $\text{HN}=\text{N}\cdot$ (without the need for charge separation as in $\text{H}_2\text{N}^+\text{N}^-$). Although an N-H bond is

broken, substantial π bonding is gained and $D_e(\text{N-H})$ is 26 kcal/mole. On the other hand, there is a full π bond in the ground state of

1,2-diazenes so only three electron two center bonding is gained in

$\text{HN}=\text{N}\cdot$, resulting in $D_e(\text{N-H}) = 56 \text{ kcal/mole}$.



HF calculations of Pasto and Chipman²⁹ result in a 40 kcal/mole N-H bond energy for **1** (26 kcal/mole for the C-N bond of 1,1-dimethyl diazene **6**), in good agreement with Casewit and Goddard.

Casewit and Goddard⁵ also find the following heats of formation: $\Delta H_f(298) (\textbf{4}) = 56.9 \text{ kcal/mole}$; $\Delta H_f(298) (\textbf{1}) = 86.3 \text{ kcal/mole}$. For comparison, the latest experimental value for the heat of formation of **4** is $50.7 \pm 2 \text{ kcal/mole}$.³⁵

Generation and Chemistry of 1,1-Diazenes

In the last three decades the chemistry of 1,1-diazenes has been investigated extensively.¹ There are a variety of methods reported for generating the presumed diazene intermediate. The most versatile of these is the oxidation of 1,1-disubstituted hydrazines **8** by such oxidants as t-butyl hypochlorite,³⁶ manganese oxide,³⁷ lead tetraacetate,³⁸ bromine,³⁹ mercuric oxide⁴⁰ and nickel peroxide.⁵⁸ Base induced or thermal decomposition of 1,1-disubstituted-2-sulfonyl hydrazines **9**⁴¹ and the thermal or photochemical cleavage of N-amino-sulfoximes **10**⁴² are also attractive routes to 1,1-diazenes.

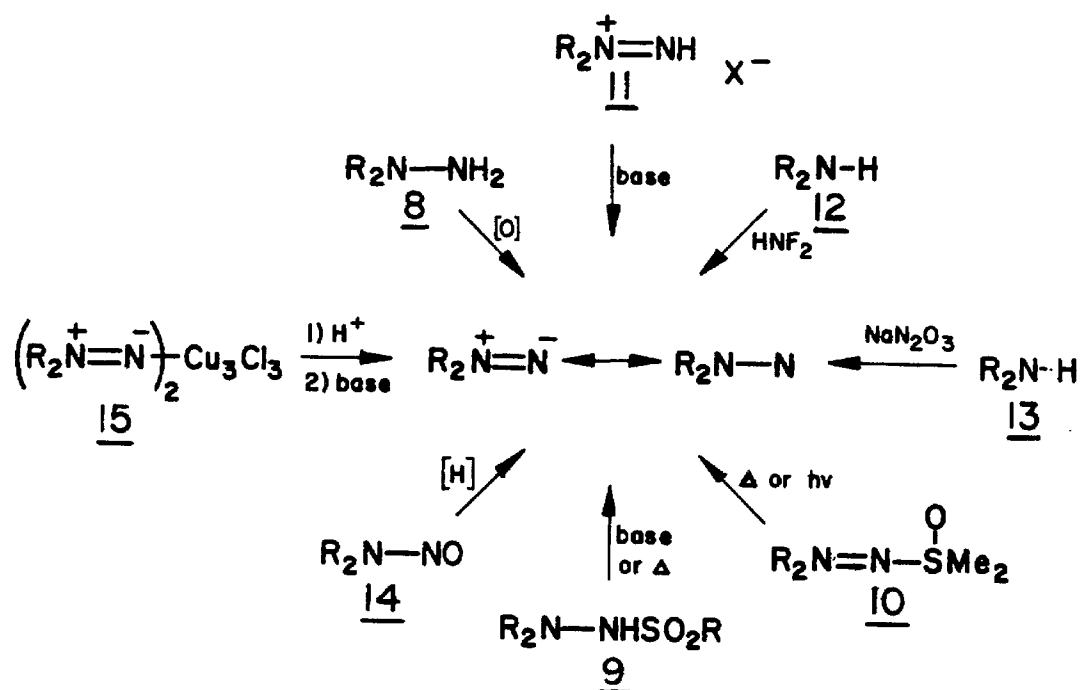


Figure 3. Methods for generation of 1,1-diazenes

The reactions of 1,1-diazenes¹ can be divided into three general classes (Figure 4): (a) fragmentations, (b) isomerizations, and (c) bimolecular reactions. The actual reaction pathway depends on structure, substitution, reaction conditions, and mode of generation.

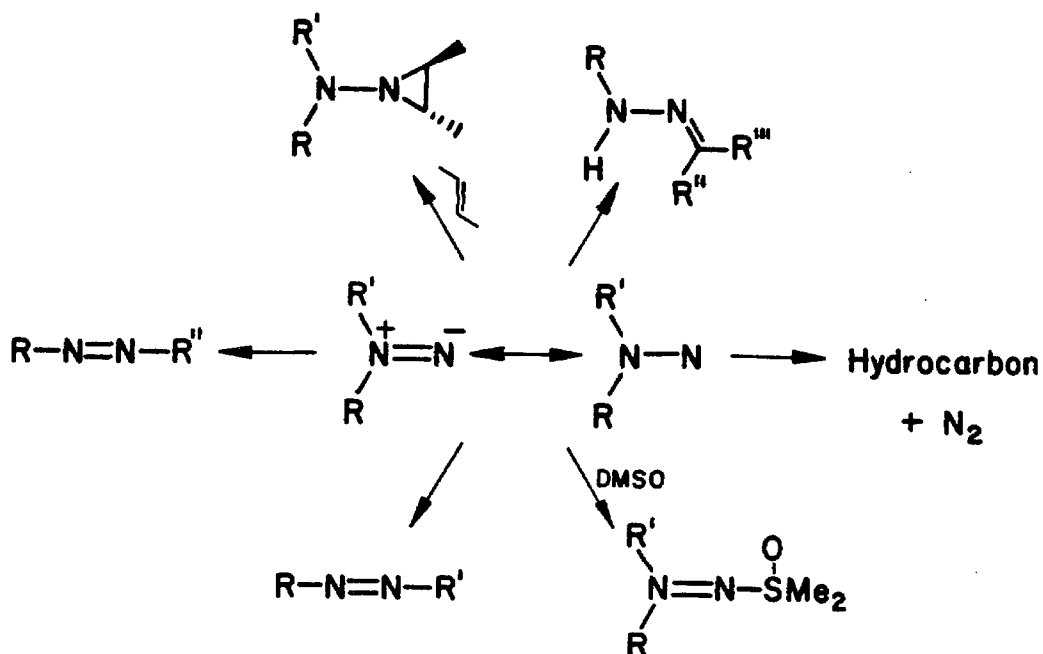
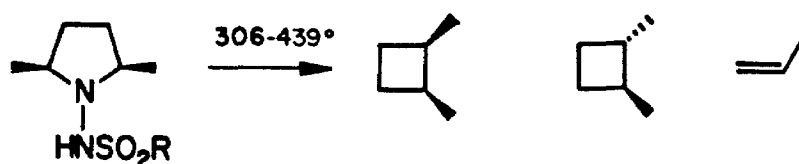


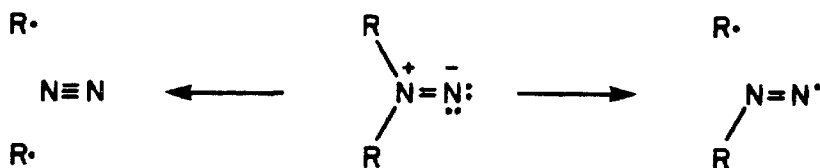
Figure 4. Characteristic reactions of 1,1-diazenes

Fragmentation reactions of 1,1-diazenes generally occur when the carbons α to the diazene function have radical stabilizing substituents, the diazene has a small ring structure, or there exists a concerted pathway to fragmentation. Dibenzyl hydrazine yields dibenzyl and nitrogen upon oxidation at 250°C with mercuric oxide.⁴³ Pyrolysis of

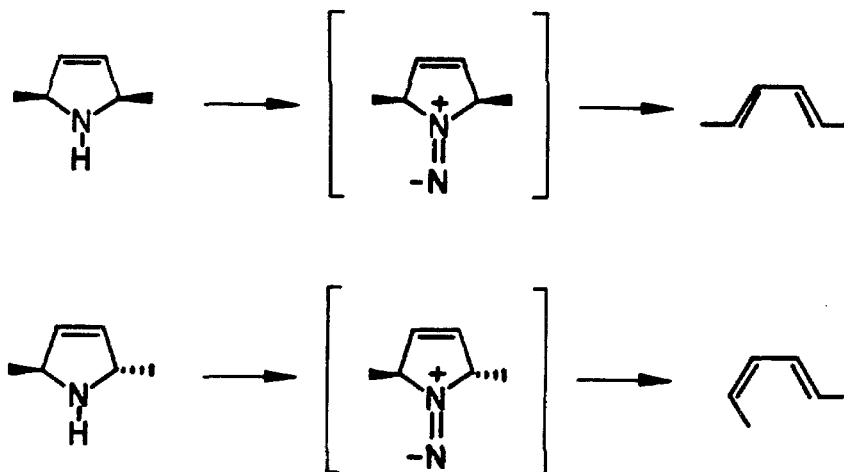
2-sulfonyl-2,5-dimethylpyrrolidylhydrazine^{41c} at 400°C yields 1,2-dimethylcyclobutane, 2-methylpropene and nitrogen. This reaction occurs



62% by nitrogen extrusion to the tetramethylene biradical, followed by cleavage and closure, and 38% by direct cleavage to alkenes and nitrogen. In general, 1,1-diazene decompositions are in accord with a mechanism involving radical or biradical intermediates, analogous to their 1,2-diazene isomers. The question of whether 1,1-diazenes decompose by sequential one bond or simultaneous two bond cleavage of the C-N bonds remains unanswered.⁴⁴

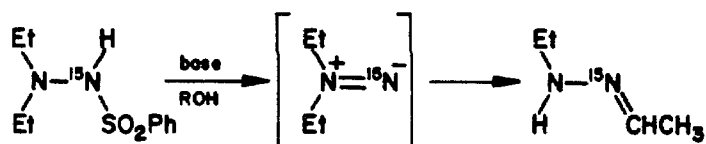


Concerted fragmentation of 1,1-diazenes may occur in a number of cases. For example, it was found that cis and trans-2,5-dimethyl-3-pyrroline, when treated with sodium nitrohydroxamate, yielded only the trans-trans and the cis,trans-hexadienes.⁴⁵



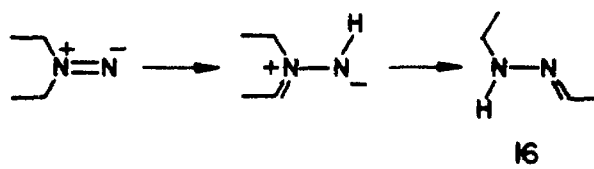
These results are consistent with the orbitally allowed disrotatory opening of the intermediate 1,1-diazene.

Isomerizations of 1,1-diazenes generally take one of two forms: (a) rearrangement of the 1,1-diazene to an isomeric hydrazone or (b) rearrangement to a 1,2-diazene. The formation of hydrazones is a general reaction for 1,1-dialkyldiazenes possessing a C-H bond α to the diazene function,¹ but only when the diazene is generated in a protic medium. Labeling studies⁴⁶ have demonstrated that the nitrene

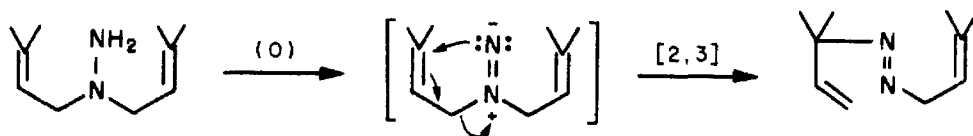


nitrogen ends up as the doubly bonded nitrogen in the product. Although this rearrangement has been the subject of extensive research, the

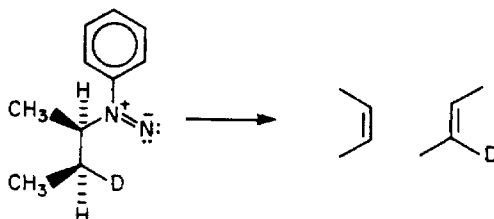
mechanism remains unknown. Diaziridines and 1,2-diazenes have been ruled out as possible intermediates,⁴⁷ since both, when independently generated, are stable to the reaction conditions. At present the reaction is regarded as proceeding through an azomethinimine¹⁶ (analogous to the enol form of a ketone.) The function of the protic solvent may be to facilitate tautomerization of the 1,1-diazenes.



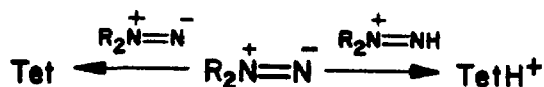
Rearrangement of 1,1-diazenes to 1,2-diazenes can occur in cases where the resulting azo linkage is incorporated into an aromatic system.⁴⁸ 1,2-Diazenes have also been shown to occur from 2,3-sigmatropic rearrangements of alkyl substituted 1,1-diazenes.⁴⁹



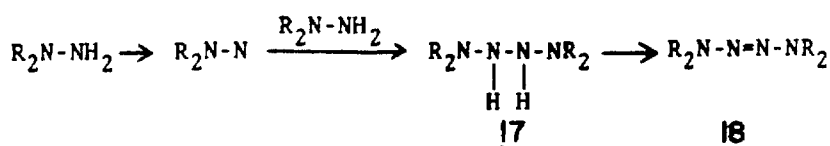
Finally, Duan and Dervan have recently demonstrated the existence of a concerted 2,3-elimination pathway for 1,1-diazenes.⁵⁰



1,1-Diazenes react bimolecularly to form tetrazenes, add to π bonds, and are trapped by sulfoxides.¹ The formation of tetrazenes is a general reaction for 1,1-diazenes. However, the mechanism of tetrazene formation may vary depending upon the method of diazene generation and only in a few cases is the mechanism known. Neutralization of solutions of 1,1-dialkyldiazenium ions leads to the formation of tetrazenes,⁵¹ probably by the reaction of the diazenium ion with diazene.



Rees and coworkers⁵² isolated a tetrazane 17 from the lead tetraacetate oxidation of N-aminophthalimide, which upon further oxidation yielded the corresponding tetrazene 18.



Simple bimolecular dimerization has also been shown to occur (see page 40).

1,1-Diazenes substituted with acyl groups and 1,1-diazenes in which the lone pair on the trivalent nitrogen is part of an aromatic system add to π bonds and sulfoxides, suggesting that these additions are electrophilic in nature.¹ Addition to olefins is greater than 95% stereospecific even at low alkene concentrations.⁵³ By analogy to carbene chemistry this is taken as evidence for a singlet ground state. Dialkyldiazenes have yet to be trapped by alkenes or sulfoxides.

Nomenclature

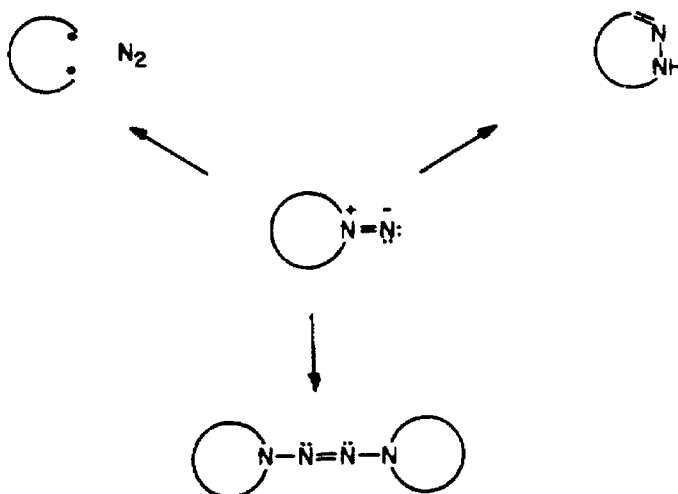
There exists no IUPAC nomenclature for the $R_2N^+=N^-$ functional group. Because the name aminonitrene is misleading with regard to structure and function, I have used here the name 1,1-diazene, introduced by McBride^{51b}. This nomenclature has been used in all key reviews of 1,1-diazene chemistry.^{1,44}

Experimental Strategy

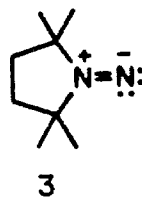
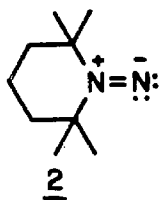
A number of elegant methods have been applied to the study of reactive intermediates in recent years including matrix isolation techniques, flash spectroscopy, and reactant design such that subsequent reactions⁵⁷ of a reactive intermediate are slowed. We have used this last approach in generating kinetically persistent 1,1-diazenes for direct studies.

Recall that once generated 1,1-diazenes undergo three general

reactions. In order to slow the 1,1-diazeno to tetrazene dimerization reaction, the diazene has been substituted with methyl groups at the position. These substituents provide steric interactions in the transition state unfavorable to dimerization. Substitution also eliminates the possibility of



the 1,1-diazeno to hydrazone rearrangement. In order to slow the rate of unimolecular nitrogen extrusion we have made the 1,1-diazeno cyclic, i.e., bonded α, α' methyl groups. The synthetic targets chosen were N-(2,2,6,6-tetramethylpiperidyl)nitrene 2 and N-(2,2,5,5-tetramethylpyrrolidyl)nitrene 3.



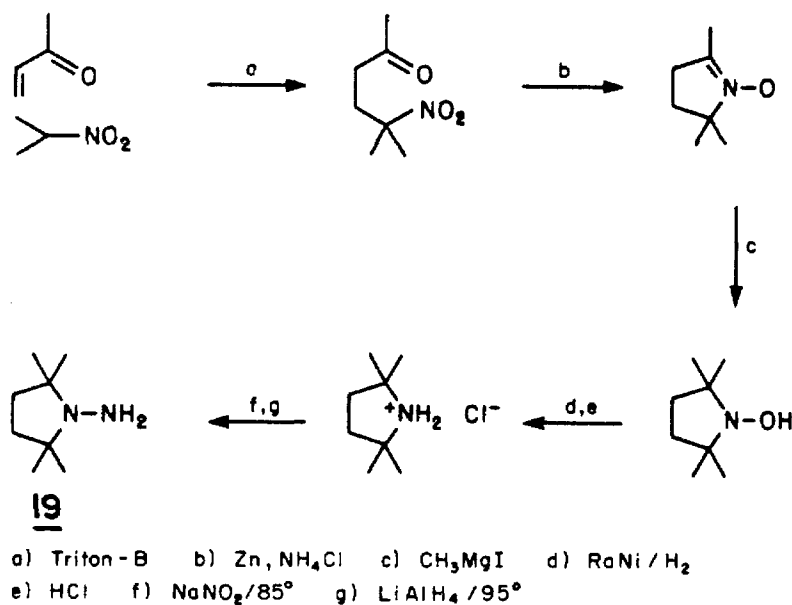
An investigation of the ground and excited state properties of N-(2,2,5,5-tetramethylpyrrolidyl)nitrene 3 is presented below.

RESULTS AND DISCUSSION

Synthesis and Characterization of N-(2,2,5,5-Tetramethylpyrrolidyl)nitrene

Synthesis of N-(2,2,5,5-tetramethylpyrrolidyl)nitrene

The precursor to the five membered ring 1,1-diazene 3, 1-amino-2,2,5,5-tetramethylpyrrolidine **19**, was synthesized in six steps from methyl vinyl ketone and 2-nitropropane.⁵⁴⁻⁵⁷ The overall yield of nitrosamine is 30%. Reduction to hydrazine **19** requires vigorous conditions and is accomplished in 35% yield.



Addition of tert-butyl hypochlorite⁴⁹ to a stirred solution of hydrazine **19** and triethylamine (Et_3N) in anhydrous dimethyl ether affords, in addition to an insoluble white precipitate ($\text{Et}_3\text{N}\cdot\text{HCl}$), a red

solution which is stable for days at -78°C , but decolorizes rapidly upon warming to 0°C . 1,1-Diazene 3 can also be generated by nickel peroxide⁵⁸ oxidation (10 fold excess oxidant, -78°C) in the presence of triethylamine, and by photolysis (-78°C , pyrex filter) in the presence of di-*t*-butylperoxide. Oxidations with *t*-butyl hypochlorite and nickel peroxide typically yield 30% and 90%, respectively, of 1,1-diazene 3, with the major remaining component being unreacted hydrazine.

Generation of the colored 1,1-diazene solution at -78°C (*t*-butyl hypochlorite), followed by filtration at -78°C , affords a clear red solution. This solution can be concentrated and further purified by low temperature chromatography (-88°C) on deactivated alumina (using dimethyl ether/propane mixtures as the eluting solvent) to yield a solution >95% 3 and <5% tetrazene 24 (low temperature ^1H NMR). Addition of triethylamine after chromatography is necessary to prevent decomposition because 1,1-diazene is sensitive to trace acid. A variety of solvents can then be added to the purified solution of 3 at -78°C and the chromatography solvents, propane and dimethyl ether, can be removed at reduced pressure.

Significantly, oxidation of cis or trans-1-amino-2,5-dimethylpyrrolidine with either *t*-butyl hypochlorite or nickel peroxide (-78°C) leads to colorless solutions. After warming the corresponding tetrazenes were detected as the major reaction products. Photolysis of diisopropyl hydrazine in the presence of di-*t*-butyl peroxide (-78°C) affords a purple solution which has $\tau_{1/2} = 300$ sec at -78°C . Tetrazene is the major reaction product. These observations support the notion that the kinetic persistence of 3 results from steric hindrance to

dimerization.

**Electronic Absorption Spectrum of N-(2,2,5,5-tetramethylpyrrolidyl)-
nitrene 3**

The visible absorption spectrum of chromatographed 1,1-diazene 3 was obtained at -78°C using a low temperature spectroscopic cell.⁶¹

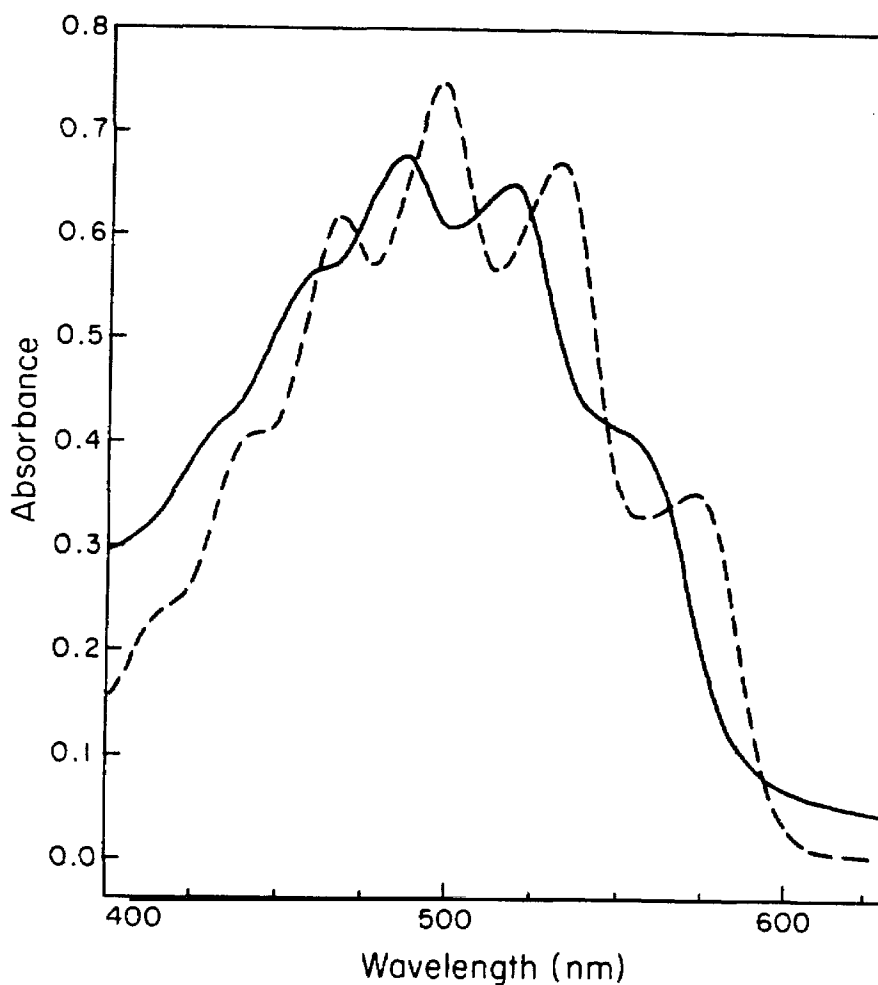


Figure 5. Absorption spectrum of 3 at -78°C in CH_2Cl_2 (—) and $i\text{-PrOH}$ (---).

The spectrum of 3 in CH_2Cl_2 consists of a structured absorption band with a λ_{max} of 497 nm and $\lambda_{0,0}$ of 572 nm (50 kcal). This absorption is close to the n, π^* electronic transition calculated by Davis and Goddard for the parent 1,1-diazene $\text{H}_2\text{N}=\text{N}$. The spacing between the maxima is 1238 cm^{-1} , corresponding to the vibrational level spacing of the N-N stretch in S_1 . The prominence of the N=N stretching mode is indicative of a substantial change in $R_e(\text{N}=\text{N})$ on excitation from S_0 to S_1 . Using the ratio of force constants predicted by Goddard and Davis²⁴ for the N-N stretch of S_0 and S_1 of $\text{N}=\text{NH}_2$, $\nu(\text{N}=\text{N})$ in S_1 of 3 should be 1409 cm^{-1} . The experimental value of 1238 cm^{-1} is substantially lower, suggesting that pyramidalization may be more important than electron delocalization in stabilizing S_1 of 3. In fact 3 is probably prevented from achieving maximum pyramidalization due to steric interactions between the bulky methyl groups.

The position of an n, π^* absorption involving nonbonding electrons is sensitive to solvent polarity and hydrogen bonding effects.⁵⁹ Replacement of CH_2Cl_2 with isopropyl alcohol affords $\lambda_{\text{max}}(\text{i-PrOH}) = 487 \text{ nm}$ and $\lambda_{0,0} = 552 \text{ nm}$, a blue shift of 20 nm to shorter wavelength (0,0 transition) (Figure 5). The shift in 0,0 bands suggests that the thermally equilibrated ground and excited states must be differentially solvated, consistent with the differing degrees of electron delocalization in S_0 and S_1 . For comparison, the n, π^* transition of acetone shifts from 277 nm in CHCl_3 to 272 nm in ethanol.⁶⁰

Because n, π^* transitions are symmetry forbidden, one would expect 3 to have a low extinction coefficient.⁶¹ In diethyl ether ϵ_{\max} is 20 ± 3 for 1,1-diazene 3 as measured by a combination of low temperature proton NMR and electronic absorption spectroscopy. In addition it has been determined that any absorption of 1,1-diazene 3 greater than 220 nm has $\epsilon_{\max} \leq 50 \pm 10$. It is therefore likely that the S_2 state is higher in energy than 130 kcal.

A comparison of the visible absorption spectra of the five (3) and six-membered ring (2)² 1,1-diazenes is instructive (Table II). The S_1 - S_0 energy separation is lower for the six-membered ring

Table II - Electronic Absorption Spectra of 1,1-Diazenes 3 and 2

1,1-Diazene	Solvent	$\lambda_{\max},$ nm	$\lambda_{0,0},$ nm	$E_{0,0}$ kcal	$\nu(N-N)$ of S_1 cm^{-1}
3	$CFCl_3$	497	565	50.6	1238
3	iPrOH	487	552	51.8	1230
2	$CFCl_3$	543	620	46.1	1113
2	iPrOH	526	592	48.5	—

1,1-diazene 2 than for the five membered ring 1,1-diazene 3. One explanation is that S_1 of 2 has less steric hindrance to pyramidalization than S_1 of 3. Pyramidalization should stabilize 1,1-dialkyldiazene S_1 states by relieving nitrogen lone pair-alkyl interactions. The lower N-N stretching frequency of S_1 for 2 versus 3 is consistent with this explanation. The analogous cyclic alkanones behave much the same way. In Et_2O , tetramethylcyclopentanone has a λ_{\max} of 296 nm while tetramethylcyclohexanone has a λ_{\max} of 305 nm.⁶¹ However the λ_{\max} of cyclopentanone (299 nm) is lower in energy than λ_{\max} of cyclohexanone (285 nm).⁶² In the absence of α substitution, S_1 of

cyclopentanone can pyramidalize more than S_1 of cyclohexanone due to differences in $C(=O)C$ bond angles. Ground state effects should be the same in all the systems considered.

The nitrogen lone pair interactions in S_1 of H_2N-N should be less severe than in 1,1-dialkyldiazenes. In S_0 , however, there should be little difference between H_2N-N and R_2N-N since the nitrogen lone pair is largely delocalized ($\langle HNH \text{ angle} \approx \langle RNR(2) \rangle$). We would then predict H_2N-N to have $\lambda_{\max} > 540 \text{ nm}$.

Infrared Spectrum of N-(2,2,5,5-Tetramethylpyrrolidyl)nitrene

When chromatographed 1,1-diazene 3 (-78°C , CH_2Cl_2) is introduced into a copper jacketed low temperature infrared cell, the infrared spectrum shows a strong absorption at 1638 cm^{-1} that disappears when the solution is warmed to 25°C and subsequently recooled to -78°C . This absorption is assigned to the $N=N$ double bond stretching frequency. In order to test this assignment, application of Hooke's law⁶² allows an approximation of the stretching frequency change for the appropriate $^{14}\text{N}=^{15}\text{N}$ isotopically labeled isomer. The calculated $\nu(^{14}\text{N}=^{14}\text{N})/\nu(^{14}\text{N}=^{15}\text{N})$ ratio is 1.0171 or a predicted shift for the $^{14}\text{N}=^{15}\text{N}$ species to 1611 cm^{-1} . Successive treatment of 2,2,5,5-tetramethylpyrrolidine with sodium nitrite- ^{15}N , lithium aluminum

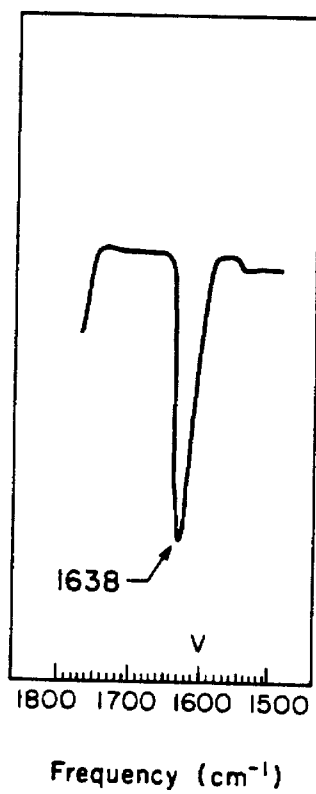


Figure 6. Infrared spectrum of chromatographed 3 in CH_2Cl_2 (-78°C).

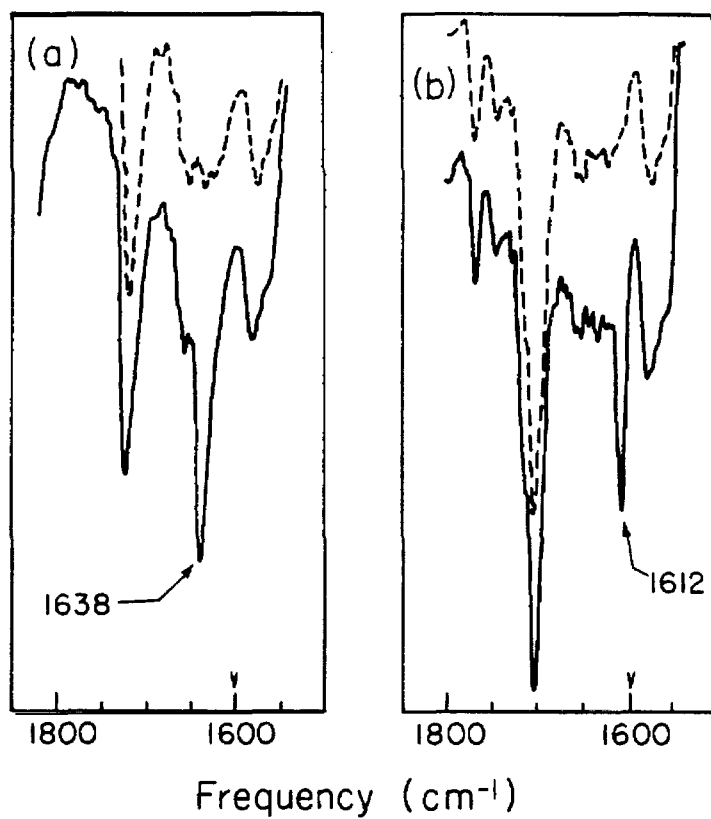


Figure 7. Infrared spectra of 3 (a) R₂ ¹⁴N=¹⁴N and (b) R₂ ¹⁴N=¹⁵N at -78°C (—) and at -78°C after warming to 25°C (---).

hydride and *t*-butyl hypochlorite/triethylamine afforded the ^{15}N -labeled 1,1-diazene. The infrared spectrum showed no absorption at 1638 but rather a new absorption at 1612 cm^{-1} , a shift of 26 cm^{-1} , consistent with the $\text{N}=\text{N}$ stretch assignment for the 1,1-diazene **3** (see Figure 7). These results suggest that there is considerable double-bond character in the 1,1-dialkyldiazene $\text{N}=\text{N}$ bond, in accord with the calculations of Davis and Goddard. For comparison, the 1,2-diazene isomer 3,3,6,6-tetramethyltetrahydropyridazine **25** has an absorption at 1565 cm^{-1} ($\text{N}=\text{N}$ stretch).⁶³

The change from a five-membered to six-membered ring 1,1-diazene causes a shift to higher energy for the ground state $\text{N}=\text{N}$ stretching frequency (Table III).

Table III - Infrared Spectra of 1,1-Diazenes **3** and **2a**

1,1-Diazene	$(\text{R}_2^{14}\text{N}=\text{N}^{14}\text{N})$, cm^{-1}	$(\text{R}_2^{14}\text{N}=\text{N}^{15}\text{N})$, cm^{-1}
2	1595	1569
3	1638	1612

a) In CH_2Cl_2 .

This is likely the result of increasing p-orbital character in the ring orbitals with increasing CNC bond angle. Consequently the s-orbital character in the $\text{N}-\text{N}$ σ bond increases, with a concomitant increase in the $\text{N}-\text{N}$ stretching vibration. For comparison the $\text{C}=\text{O}$ stretching frequency of tetramethylcyclopentanone is 1730 cm^{-1} and $\nu(\text{C}=\text{O}) = 1690\text{ cm}^{-1}$ for tetramethylcyclohexanone.⁶¹ $\text{H}_2\text{N}-\text{N}$ and **2** should have similar bond angles and therefore we might expect similar stretching frequencies.

Nuclear Magnetic Resonance Spectra of N-(2,2,5,5-Tetramethyl-pyrrolidyl)nitrene 3

The proton and carbon-13 NMR spectra of chromatographed 1,1-diazene 3 ($2 \times 10^{-2}M$) were recorded in $CDCl_3$ at $-65^\circ C$. The 1H NMR spectrum revealed absorptions at 1.04 and 2.32 ppm in a 3:1 ratio. These are assigned to the methyl protons and ring protons, respectively (Figure 8). Warming the sample results in the disappearance of the 1.04 and 2.32 ppm signals while tetrazene signals and signals due to the hydrocarbon products appear. ^{13}C spectra recorded under the same conditions ($2 \times 10^{-2}M$, $-65^\circ C$) showed three absorptions which disappeared on warming to $25^\circ C$. Again tetrazene and hydrocarbon absorptions grew in on warming. Assignment of the ^{13}C shifts are based on ^{13}C shifts in tetraalkylammonium salts.

The ^{13}C resonances are consistent with delocalization of the internal amino lone pair onto the external nitrene nitrogen. An ^{15}N NMR spectrum of the six membered ring 1,1-diazene 2 has been reported.⁷⁰ The nitrene and amino nitrogens have resonances in dimethyl ether at 917.0 and 321.4 ppm, respectively (downfield from anhydrous $^{15}NH_3$). The chemical shift of the ring nitrogen is consistent with a delocalized amino lone pair. The large downfield shift of the nitrene nitrogen is consistent with a large paramagnetic term due to a low lying n, π^* transition.

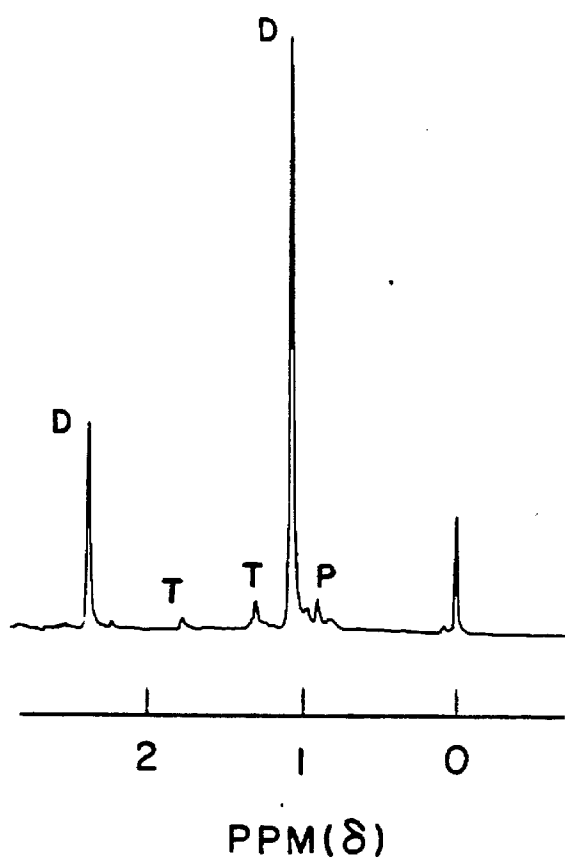


Figure 8. Proton NMR spectrum of 3 at -65°C in the region 0 to 3 ppm. D = 1,1,-diazene; T = tetrazene; P = propane.

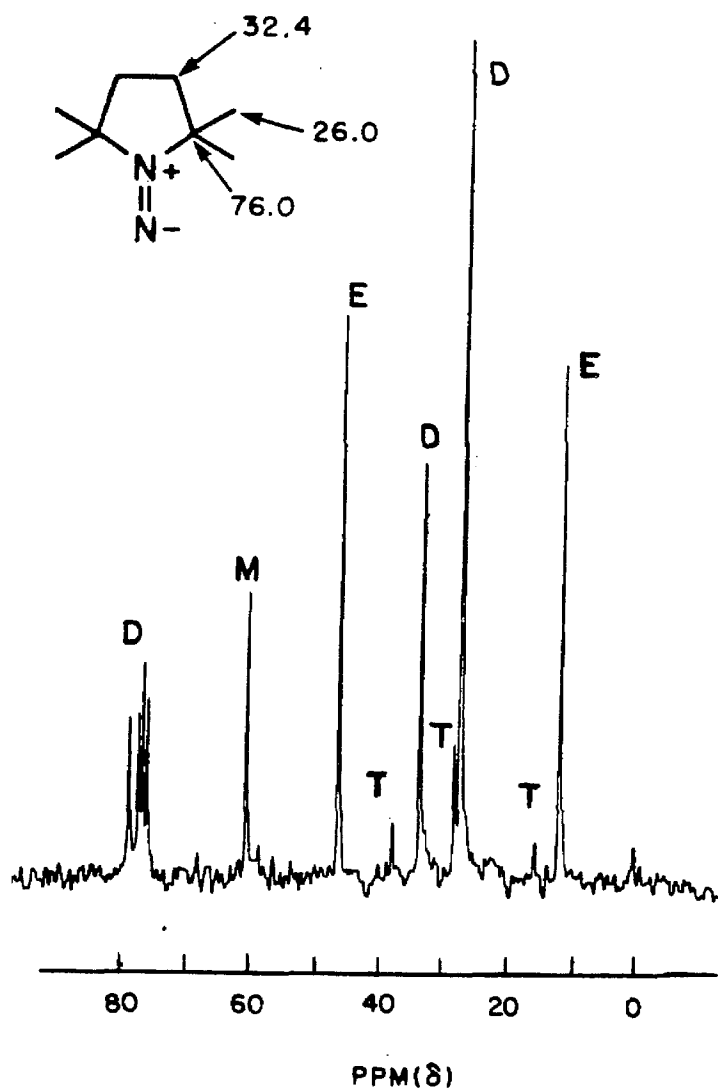
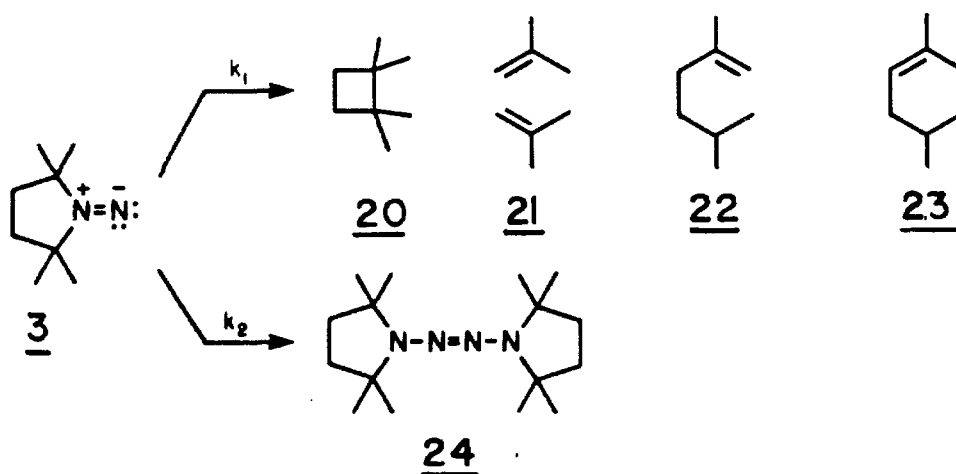


Figure 9. Carbon-13 NMR spectrum of 3 at -65°C in CDCl₃. D = 1,1-diazene; T = tetrazene, E = triethylamine, M = methyl ether.

Thermolysis of N-(2,2,5,5-Tetramethylpyrrolidyl)nitrene 3

Pyrolysis of chromatographed 1,1-diazene 3 at 0°C in diethyl ether yielded hydrocarbon products **20-23** and tetrazene **24**.



Products were analyzed by ^1H NMR and vapor phase chromatography.

Tetrazene **24** was synthesized independently by O_2 oxidation (25°C) of hydrazine **19**. 1,1,2,2-Tetramethylcyclobutane was synthesized independently by pyrolysis of 3,3,6,6-tetramethyltetrahydropyridazine **25**.⁶³ The remaining hydrocarbons are commercially available. For comparison, the isomeric azo compound **25** was also pyrolyzed and the hydrocarbon product ratios determined. The product ratios from 1,1-diazene **3** and the isomeric 1,2-diazene **25** are listed in Table IV.

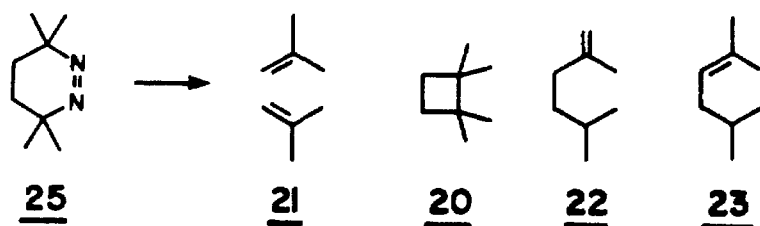


Table IV. Product Ratios from 1,1-Diazene **3** and 1,2-Diazene **25**

Compound	Conditions	20	21	22	23	24
3	0°C (Et ₂ O)	49	47	2.0	1	320
25	140°C (benzene)	46	52	1.5	0.5	—

The pyrolysis products of **3** and **25** are consistent with the intermediacy of a tetramethylene diradical which can cleave, close, or disproportionate. A direct pathway to isobutylene may also be involved.⁶⁴ Interestingly, although the 1,1- and 1,2-diazene isomers were pyrolyzed at very different temperatures the product ratios are similar. Pyrolysis temperature has a substantial effect on the product ratios of 1,1-diazene **3** (Table V).

Table V. Temperature Effect on Product Ratios of 1,1-Diazene **3**

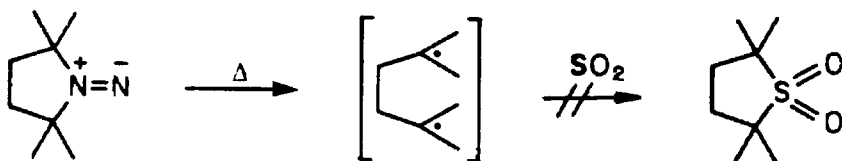
Diazene	Conditions	20	21	22 + 23
3	0°C, CFC1 ₃	49	47	4.0
3	-10°C, CFC1 ₃	44	53	3.5
3	-20°C, CFC1 ₃	39	59	2.0

These data suggests (ignoring solvent effects which should be minor) that either a) diazenes **3** and **25** are producing substituted tetramethylenes in different conformations which cleave, close and

disproportionate in differing ratios before equilibrating, b) differing degrees of a direct pathway to isobutylene and N_2 are involved in 3 and 25, or c) differing degrees of a diazenyl pathway are involved in the decomposition of 3 and 25. It was shown that 1,2-diazene 25, which could arise by recombination of an intermediate diazenyl radical, was not present in the pyrolysis products of 3.



An attempt was made to chemically trap the hypothetical tetramethylene intermediate in the thermal decomposition of 1,1-diazene 3. Sulfur dioxide is known to trap methyl radicals with a log A of 10.82 and E_a of 1.5 kcal/mole. Pyrolysis of chromatographed 1,1-diazene 3 in neat 15M SO_2 (bp $-15^\circ C$) yielded no tetramethyl sulfolane, although tetramethylcyclobutane was found in the reaction mixture. Authentic tetramethylsulfolane was prepared by a Diels Alder reaction of SO_2 and 2,5-dimethyl-2,4-hexadiene (sealed tube, $140^\circ C$) followed by catalytic hydrogenation over platinum.



Unimolecular Decomposition Kinetics of N-(2,2,5,5-Tetramethylpyrrolidyl)nitrene 3 and Bimolecular Decomposition Kinetics of N-(2,2,5,5-Tetramethylpyrrolidyl)nitrene 3 and N-(2,2,6,6-Tetramethylpiperidyl)nitrene 2.

The unimolecular decay of 3 was studied in dilute solutions ($\leq 3 \times 10^{-3} \text{M}$) in order to slow the competitive higher order decay. Decomposition kinetics of chromatographed 3 were examined in three different solvents (tetrahydrofuran, ethyl ether, and n-hexane) typically in the range of $+4^\circ$ to -21.6°C by monitoring the optical density of the red solution at 497 nm as a function of time. In dilute solutions ($\leq 3 \times 10^{-3} \text{M}$) the disappearance of 3 was strictly first order in THF and Et₂O. In n-hexane, the disappearance of 3 was first order at higher temperatures (-4.8 to $+9.0^\circ \text{C}$). However plots of \ln absorbance versus time at lower temperatures afforded a curved segment at short times, followed by a linear segment at longer times. First order rate constants were taken to be the slopes of the linear portions of these plots. The activation parameters for the unimolecular decomposition of 3 are given in Table VI.

Table VI - Unimolecular Arrhenius Parameters of 3 in Different Solvents

Solvent	Ea ^a	Log A	ΔH^\ddagger ^a	ΔS^\ddagger ^b
n-Hexane	16.8 \pm 0.5	10.9 \pm 0.3	16.2 \pm 0.5	-10.7 \pm 1.4
Et ₂ O	19.2 \pm 0.6	12.4 \pm 0.4	18.5 \pm 0.4	- 5.2 \pm 1.4
THF	19.1 \pm 0.4	12.1 \pm 0.3	18.4 \pm 0.6	- 3.8 \pm 1.8

a) kcal/mole; b) e.u.

FIRST ORDER RATE CONSTANTS IN THF

Temperature(°C)	$k_1(\text{sec}^{-1})$
+6.8	1.55×10^{-3}
+3.5	1.07×10^{-3}
+1.2	7.62×10^{-4}
-1.3	5.59×10^{-4}
-3.5	4.26×10^{-4}
-6.0	2.89×10^{-4}
-8.8	2.10×10^{-4}

FIRST ORDER RATE CONSTANTS IN Et₂O

+5.1	2.77×10^{-3}
+3.0	2.07×10^{-3}
-0.6	1.32×10^{-3}
-3.8	8.50×10^{-4}
-6.8	5.59×10^{-4}
-9.8	3.74×10^{-4}
-11.8	3.10×10^{-4}

FIRST ORDER RATE CONSTANTS IN n-HEXANE

-4.8	2.29×10^{-3}
-6.3	1.97×10^{-3}
-9.0	1.42×10^{-3}
-12.8	8.42×10^{-4}
-17.2	5.26×10^{-4}
-21.4	2.98×10^{-4}

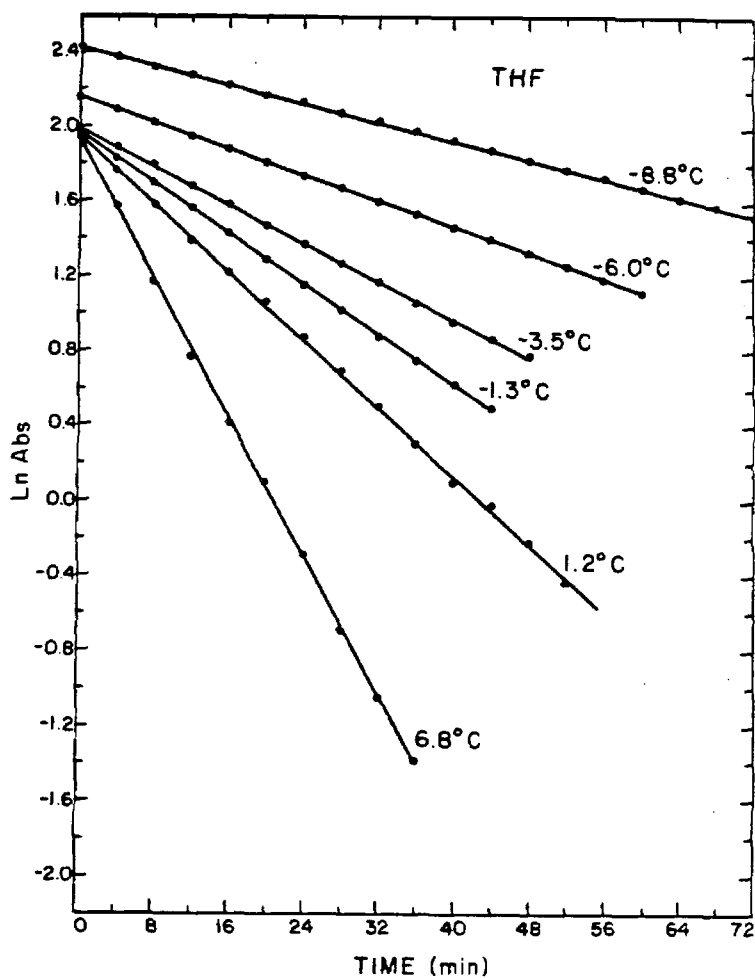


Figure 10. Ln Abs versus time plots for unimolecular decomposition of 3 in tetrahydrofuran

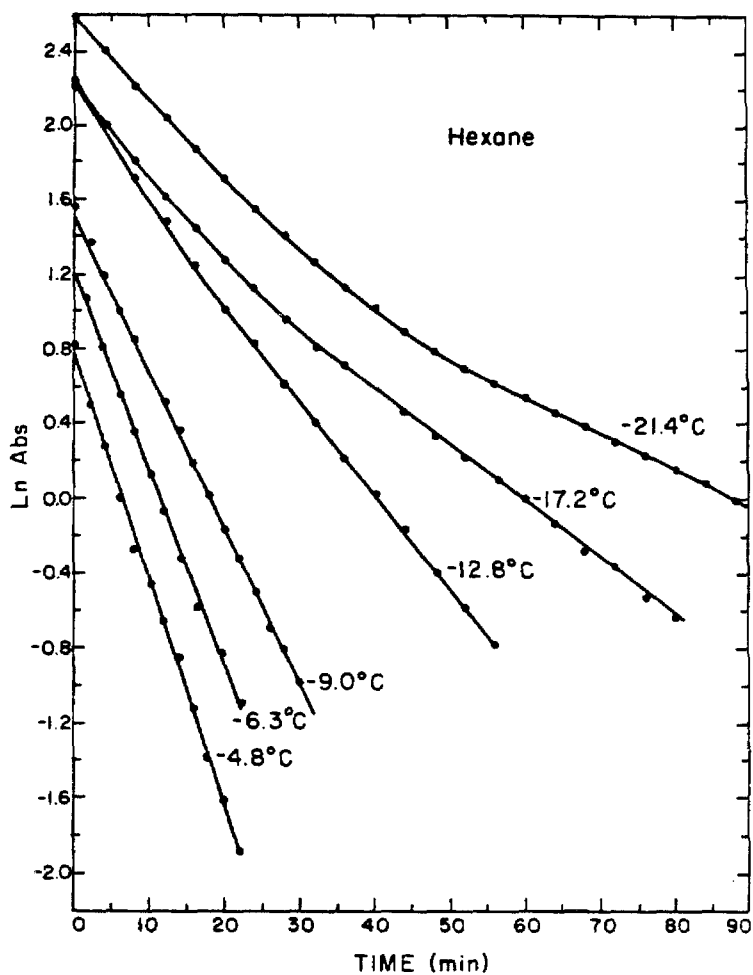


Figure 11. $\ln \text{Abs}$ versus time plots for unimolecular decomposition of 3 in *n*-hexane

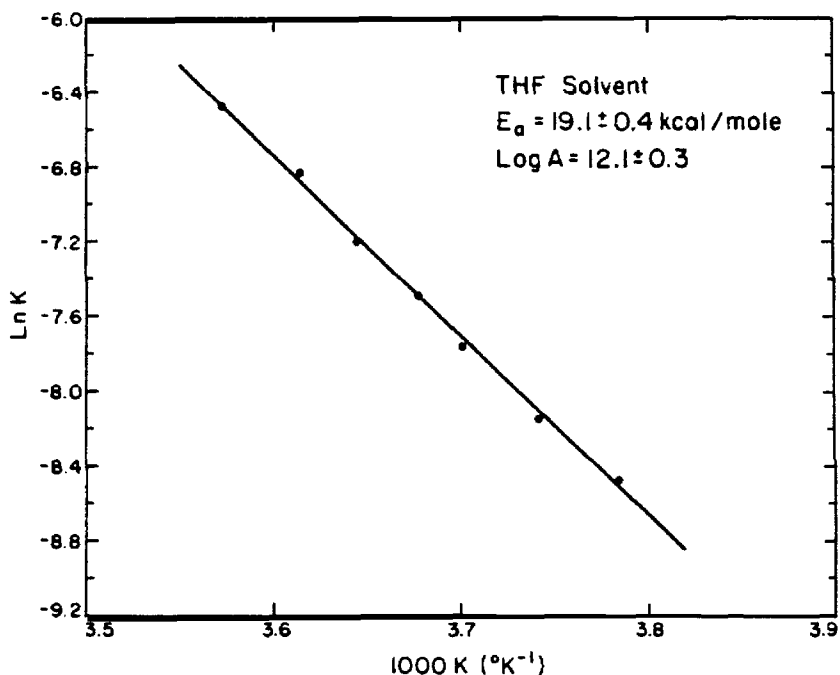


Figure 12. Arrhenius plot of diazene first order decomposition kinetics in THF.

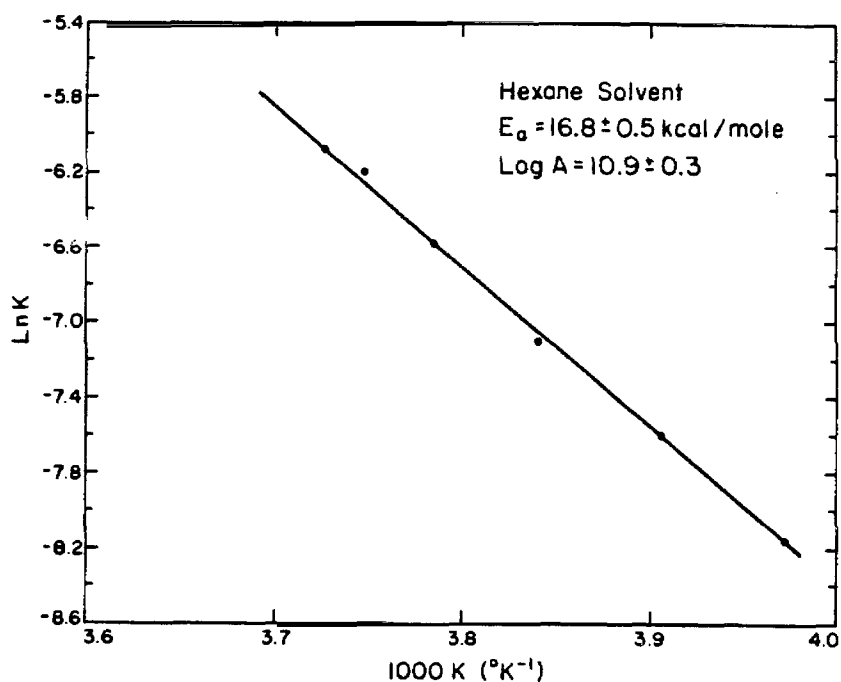


Figure 13. Arrhenius plot of diazene first order decomposition kinetics in hexane.

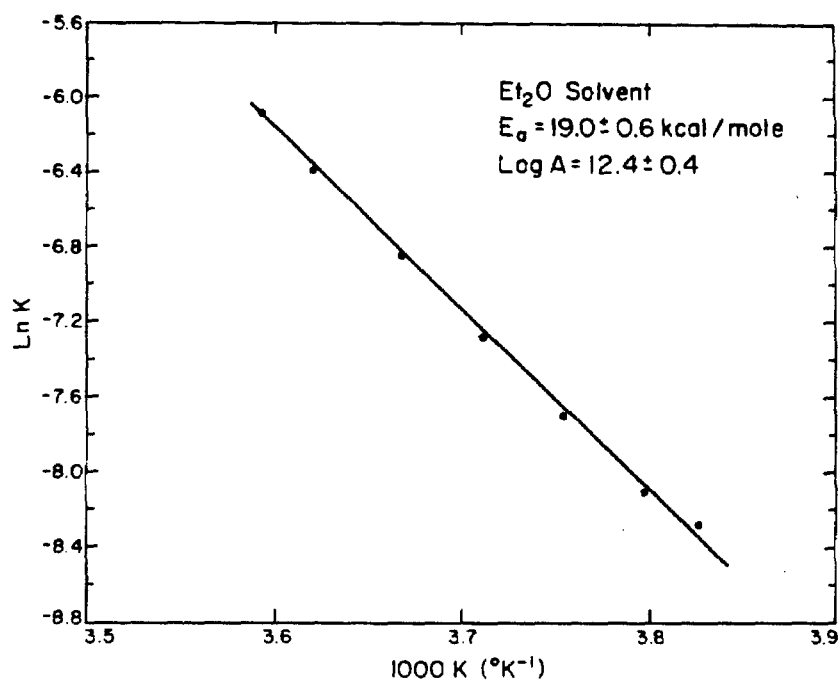


Figure 14. Arrhenius plot of diazene first order decomposition kinetics in diethyl ether.

The rate of decomposition of 3 is sensitive to solvent, the rate increasing with decreasing solvent polarity. This is consistent with a polar ground state decomposing by a less polar transition state.

Table VII - Solvent Effects on the Decomposition of 3

Solvent	E_T^{65}	k_{rel}	G^\ddagger (kcal/mole)
n-hexane	30.9	5.1	19.0
Et ₂ O	34.6	2.4	19.9
THF	37.4	1.0	19.4

The activation energy for unimolecular extrusion of nitrogen from 1,1-diazene 3 ($E_a = 16.8 \pm 0.5$ kcal/mole in n-hexane) is substantially lower than that of the corresponding 1,2-diazene 25 ($E_a = 36.7 \pm 0.5$ kcal/mole in hexane).⁶⁶ These results are in accord with the theoretical results of Casewit and Goddard⁵ and Pasto and Chipman.²⁹ If the strain energy of 3 is estimated to be 9 kcal/mole (based on strain energy of 25)⁶⁶ and the methyl stabilization of 3 is assumed to be the same as in diisopropyldiazene, the predicted ΔH^\ddagger for dimethyl-1,1-diazene decomposition is 31 kcal/mole (based on the difference in N-R bond strengths of azo alkanes⁶⁶). This is not too different from the theoretical value of 26 kcal/mole.⁵

The relatively low A factors for the thermal decomposition of 1,1-diazene 3 suggest the possibility of a concerted elimination pathway as has been postulated for pyrazolines.⁶⁸ However, Uyehara and Dervan⁶⁷ have presented evidence favoring a biradical pathway in the decomposition of cyclic 5 membered ring 1,1-diazenes. Tetramethyl

substitution would be expected to stabilize the diradical pathway further. In any case, the transition state must have severe geometric constraints.

A comparison of the unimolecular decomposition rates of the five- and six-membered ring cyclic 1,1-diazenes is shown in Table VIII.

Table VIII - Relative Rates of Unimolecular Decomposition of 1,1-Diazenes 3 and 2 at -10.0°C

1,1-diazene	solvent	E _T	k, s ⁻¹	k _{rel}	ΔG [‡] , kcal mol ⁻¹
3	hexane	30.9	1.1 x 10 ⁻³	5.1	19.0 ± 0.9
3	Et ₂ O	34.6	5.2 x 10 ⁻⁴	2.4	19.9 ± 1.0
3	THF	37.4	2.2 x 10 ⁻⁴	1.0	19.4 ± 0.9
2	hexane	30.9	3.49 x 10 ⁻³	4.8	18.3 ± 1.3
2	Et ₂ O	34.6	1.23 x 10 ⁻³	1.7	18.9 ± 0.8
2	THF	37.4	0.73 x 10 ⁻³	1.0	19.1 ± 0.8

1,1-Diazenes 3 and 2 have similar E_a values for unimolecular decomposition. If similar mechanisms are operating in the unimolecular decomposition of 3 and 2, the data suggest that the difference in strain energies of these cyclic diazenes is small. For comparison ΔE_{strain} = 5.5 kcal/mole in the isomeric five- and six-membered cyclic 1,2-diazenes.⁶⁶

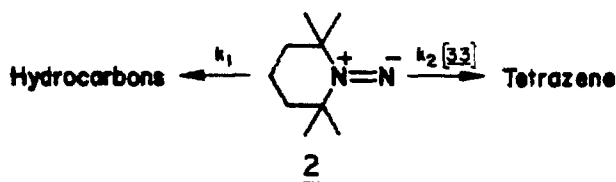
Our qualitative observations on the dimerization of 1,1-diazenes 2 and 3 indicated that the five-membered species was significantly more persistent than its six-membered counterpart. By studying 1,1-diazene decomposition at temperatures (-30°C to -90°C) where unimolecular decomposition is slow and at high concentrations (0.1M), one can examine the kinetics of the dimerization reaction. The disappearance of chromatographed 1,1-diazene (CDCl₃, 0.1M) and formation of tetrazene

were followed by low temperature proton NMR. In the temperature range -30°C to -90°C we were unable to obtain accurate Arrhenius parameters for 3 due to the exceedingly small bimolecular rate constant for dimerization. A rate constant of 2.83×10^{-4} liter/mole-sec was measured at -41.1°C. For 1,1-diazene 2, Arrhenius parameters could be obtained.

Table IX - Bimolecular Decomposition of 1,1-Diazene 2

Temperature °C	k_2 (l/mole-sec)
-30.6	1.53×10^{-2}
-41.1	7.36×10^{-3}
-50.4	3.91×10^{-3}
-60.5	2.23×10^{-3}
-70.2	1.17×10^{-3}

Plotting $\ln k$ as a function of $1/T$ affords a straight line from which the Arrhenius parameters were determined, $E_a = 6.4 \pm 0.9$ kcal/mole, $\log A = 3.8 \pm 0.7$ ($\Delta H^\ddagger = 5.8$ kcal/mole, $\Delta S^\ddagger = -43.2$ e.u.). Hinsberg and Dervan have modeled curved $\ln A$ versus time plots for decomposition of 2 (-13°C to -22°C) in diethyl ether as competitive



unimolecular and bimolecular reactions ($k_{obs} = k_{uni} + k_{bim}[2]$). The fit between experimental and calculated data was excellent yielding $\log k_1 = 11.4 - 17.4/\theta$ and $\log k_2 = 4.5 - 6.8/\theta$. These results are in close agreement with the Arrhenius parameters determined directly by NMR. This is the first kinetic evidence for a direct bimolecular pathway for the formation of tetrazenes from 1,1-diazenes, as opposed to the

alternative indirect pathways discussed earlier (see Introduction). The results indicate that the temperature dependence of the dimerization rate is small, and that there are severe stereochemical constraints for dimerization. For comparison, the A factor for dimerization of tri-*t*-butylcycloheptatrienyl radical is $10^{6.69}$

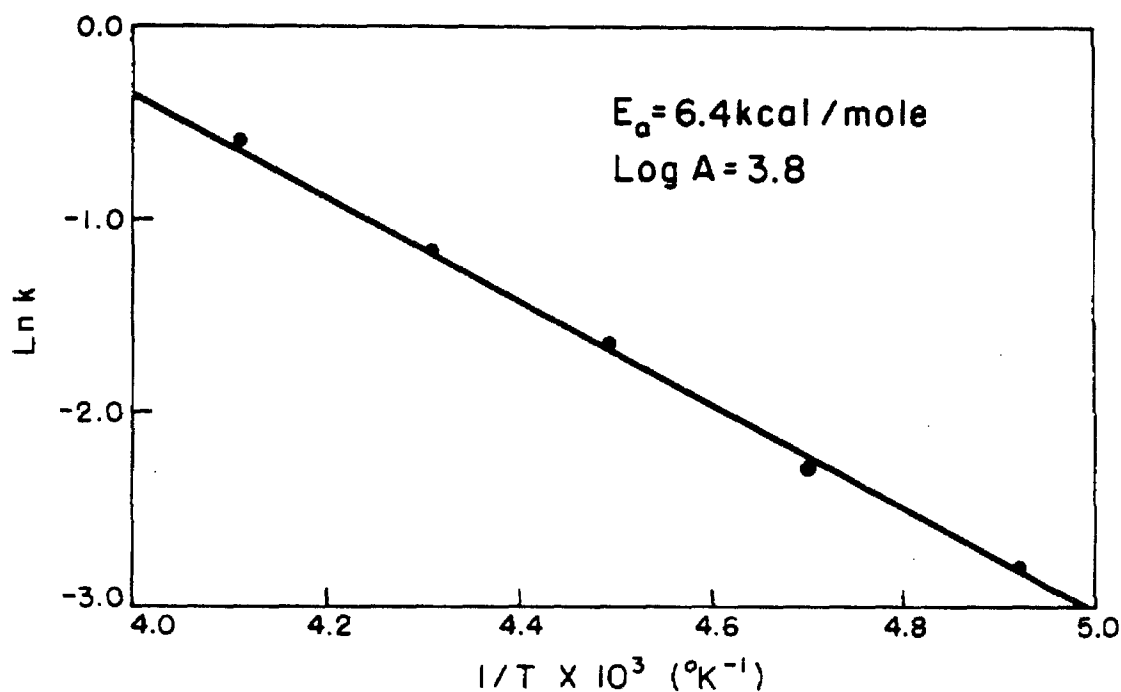


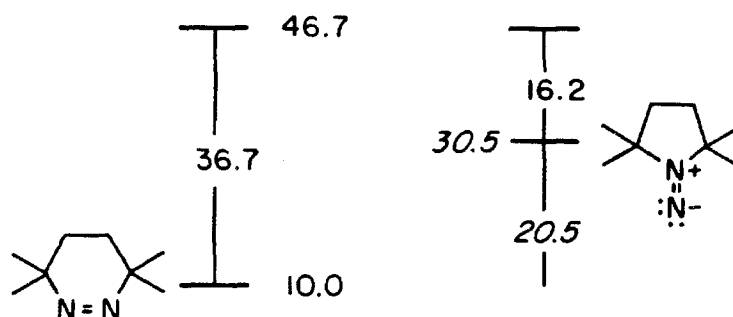
Figure 15. Arrhenius plot of bimolecular decomposition kinetics of 2 in CFCl_3

The bimolecular dimerization rate of diazene 2 at -41.1°C is 2.8×10^{-4} liter/mole-sec. At this temperature the dimerization of 1,1-diazene 3 is two orders of magnitude slower than the dimerization of 2. This result is surprising in light of the structural similarity of 2 and 3.

Table X - Relative Rates of Dimerization of 1,1-Diazenes 2 and 3

1,1-Diazene	Temperature	k_2 liter/mole-sec	k_{rel}
2	-41.1°C	7.4×10^{-3}	90
3	-41.1°C	8.6×10^{-5}	1

The heat of formation of a 1,1-diazene has never been determined and may be a difficult value to obtain due to the lability of 1,1-diazenes. The heat of formation ($\Delta H_f = 10.0 \pm 0.6$ kcal/mol) and the enthalpy of activation ($\Delta H^\ddagger = 36.7 \pm 0.5$ kcal/mol) for decomposition of 3,3,6,6-tetramethyltetrahydropyridazine (25) are known.⁶⁶ The sum of these two values affords a value for the heat of formation of the corresponding transition state, $\Delta H_f^\ddagger = 46.7$ kcal/mol. If similar intermediates of similar energy intervene in the decomposition of 3 and 25, subtraction of the enthalpy of activation for the decomposition of 3 ($\Delta H^\ddagger = 16.2$ kcal/mole in hexane) affords an approximate value for the heat of formation of 1,1-diazene (3) i.e., $\Delta H_f(3) = 30.5$ kcal/mol. This value would indicate that 1,1-diazene 3 has a higher heat of formation than the cis-1,2 isomer 25 by 20 kcal/mol.

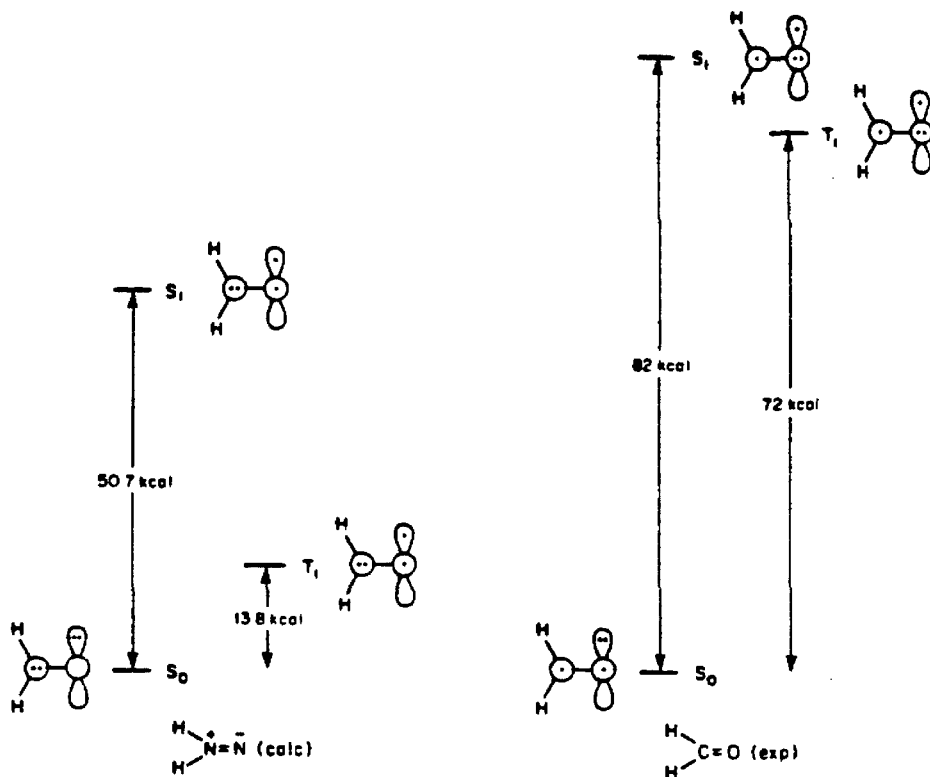


Using standard thermochemical group values³³ and the theoretical heat of formation of 86.3 kcal/mol for $\text{H}_2\text{N}-\text{N}$ (Casewit & Goddard)⁵ yields a calculated ΔH_f for 1,1-diazene 3 of 44 kcal/mol plus 10 kcal/mol (strain energy) = 54 kcal/mol (from $\Delta H_f(\text{Me}_2\text{N}-\text{N}) = \Delta H_f(\text{H}_2\text{N}-\text{N}) + 2[\Delta H_f(\text{Me}\cdot) - \Delta H_f(\text{H}\cdot)] + 2[\text{De}(\text{HMeN}-\text{Me}) - \text{De}(\text{HMeN}-\text{H})] = 86.3 + 2(18) + 2(-18.5) = 85.3$). The large discrepancy, 24 kcal/mol, between the "experimental ΔH_f " and the theoretical ΔH_f can be accounted for by either very different transition state energies for decomposition of 3 and 25 or by the use of dimethylamine to model the differences in the 1,1-diazene N-H/N-R bond strengths.

Photochemistry of 1,1-Diazenes. Photochemical Studies of N-(2,2,5,5-Tetramethylpyrrolidyl)nitrene, dl-N-(2,5-Diethyl-2,5-Dimethylpyrrolidyl)nitrene, and N-(2,2,6,6-Tetramethylpiperidyl)nitrene

The synthesis of kinetically persistent 1,1-diazenes makes possible direct studies of this reactive chromophore's photochemistry. One might expect the excited state properties of the 1,1-diazene to resemble those of the isoelectronic carbonyl.⁷¹ However, 1,1-diazenes differ from carbonyls in several key aspects. The ground state N-R bond energy in 1,1-dialkyldiazenes is substantially lower than the ground state C-R bond energy of carbonyls. Secondly, the (n, π^*) singlet state of 2 and 3 lies at 53-58 kcal (λ_{max}), whereas the lowest (n, π^*) state of the analogous ketones lies at 94-97 kcal. Goddard's GVB-CI calculations²⁴ place the $^3(n, \pi^*)$ state of $\text{H}_2\text{N}-\text{N}$ at 13.8 kcal, resulting in an S_1-T_1 gap of 37 kcal. (This value is the same as that for the triplet-singlet splitting in $\text{H}-\dot{\text{N}}$ since amino substitution effects S_1 and T_1 identically. Because the calculated energy of S_1 agrees well with experiment, the calculated value for the energy of T_1 should be reliable.) Formaldehyde has an S_1-T_1 gap of only 10 kcal.^{72,73} This difference arises out of differences in the exchange integrals of the n and π^* electrons in the diazene and carbonyl excited states. The n, π^* excited states of the 1,1-diazene are nitrene-like with the n and π^* orbitals localized on the terminal nitrogen.⁷⁴ In contrast, there is considerable delocalization of the π^* orbital onto carbon in the carbonyl S_1 and T_1 states. As a result of differences in $\Delta E_{S_1-T_1}$, 1,1-diazenes and carbonyls should have much different S_1-T_1 intersystem crossing rates^{75,76} ($k_{\text{ST}} = 5 \times 10^8 \text{ sec}^{-1}$ for acetone⁷⁷). Furthermore,

because the 1,1-diazene $^3(n, \pi^*)$ state is predicted to lie only 13.8 kcal above S_0 , the T_1 - S_0 internal conversion rate in diazenes should be considerably faster than in carbonyls ($k_{TS} = 1.8 \times 10^3 \text{ sec}^{-1}$ for acetone)⁷⁸.



For photochemical studies 1,1-diazenes 2 and 3 were carefully purified. Modifications in the chromatographic technique previously described (see experimental) afforded diazene 3 with only 2% tetrazene contamination and small amounts of dimethyl ether (1H NMR, $-65^\circ C$). Diazene 2 was more difficult to purify, a typical solution containing 70% 2, 25% 1-amino-2,2,6,6-tetramethylpiperidine and 5% tetrazene. Importantly, these solutions are stable at $-78^\circ C$ in the absence of

triethylamine, a common excited state quencher.

**Photophysical Properties of N-(2,2,5,5-Tetramethylpyrrolidyl)-
nitrene and N-(2,2,6,6-Tetramethylpiperidyl)nitrene**

Once formed, the n, π^* singlet state is, in general, deactivated by four pathways: (1) fluorescence; (2) intersystem crossing; (3) decomposition; and (4) radiationless conversion back to the ground state. If k_F , k_{ST} , k_D , and k_{IC} are the rate constants for these deactivation modes, then the measured lifetime, τ_F , of S_1 is given by $\tau_F = (k_F + k_D + k_{ST} + k_{IC})^{-1}$. The photochemical studies described below will enable us to define the rates of these processes and the various factors controlling them.

The singlet n, π^* transition in 1,1-dialkyldiazenes is symmetry forbidden. As a result only weak emission is detected on direct excitation of 3. The fluorescence spectrum of 1,1-diazene 3 in $CFCl_3$ is shown in Figure 16. The correction for instrument response is 10% in the 600-700 nm range. The absorption spectrum (λ_{max} 497 nm, 0-0 band 565 nm, $CFCl_3$) is included for comparison. The vibrational spacing of S_1 is 1230 cm^{-1} (N=N stretch) consistent with some two center, three electron bonding. The 0-0 band of the fluorescence spectrum is at 607 nm and is the maximum. The spacing between the peaks at 607 and 672 nm is consistent with the 1638 cm^{-1} N=N stretch of S_0 obtained from the infrared spectrum of 3. On warming and subsequent recooling the emission signal disappears. 0-0 Band assignments for the absorption and fluorescence spectra have been made with the assumption that these bands should not overlap.

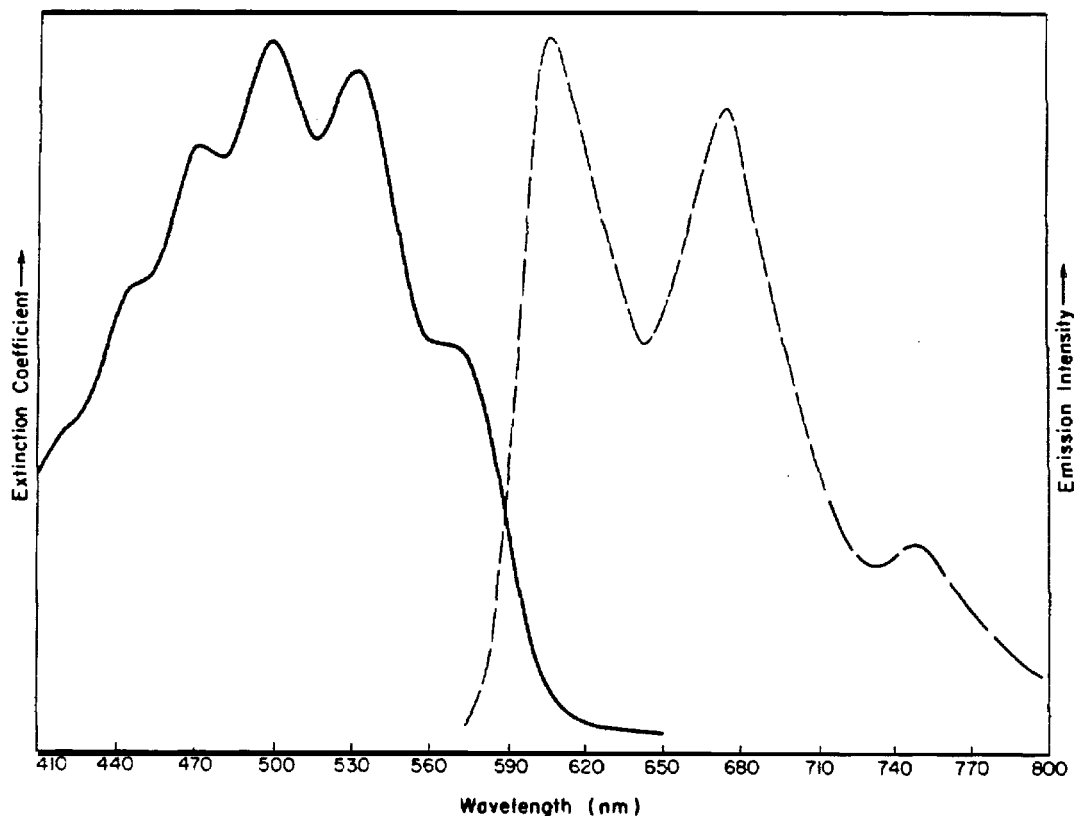


Figure 16. Absorption spectrum of 3 at -78°C (—)
Fluorescence spectrum of 3 at -196°C (---).

The absorption and fluorescence λ_{max} are separated by 100 nm, indicating that the equilibrium geometries of the S_0 and S_1 states of 1,1-diazene 3 differ substantially. This is consistent with the difference in N-N bond lengths predicted by theory, $R_e(\text{N-N}) = 1.25 \text{ \AA}$ for S_0 and $R_e(\text{N-N}) = 1.37 \text{ \AA}$ for S_1 .²⁴ The λ_{max} (0-0 band) of the fluorescence spectrum red shifts to 614 nm in the more polar solvent, isopropanol. The solvation of the excited state presumably corresponds to a high energy solvation geometry for the ground state. In both the

absorption and fluorescence spectra the 0-0 bands and λ_{max} change with solvent polarity. This shift in 0-0 bands suggests that the thermally equilibrated ground and excited states must be differentially solvated, which is consistent with the differing degrees of electron delocalization in S_0 and S_1 . Recall that the theoretical value for the dipole moment of S_0 is 4.0D and for S_1 , 2.4D.²⁴ In addition the shapes of the absorption and corrected fluorescence spectra of 3 differ substantially. The Franck-Condon factors for absorption and emission must therefore differ. The $S_1 \rightarrow S_0$ transition may be coupled to an $R_2N=N$ bending mode.

Interestingly, in diethyl ether, the absorption spectrum of 3 appears to be the superposition of two species. One may be the 1,1-diazene monomer and the second, a π stacked S_0 dimer. This effect is not observed in CH_2Cl_2 , CFCl_3 , isopropanol, or dimethyl ether.

The fluorescence rate constant, k_F , can be calculated from the integrated absorption spectra of 3, $k_F = 1.3 \times 10^5 \text{ sec}^{-1}$.⁷⁹ The fluorescence quantum yields, $\phi_F = k_F / (k_F + k_{IC} + k_{ST} + k_D)$, determined relative to rubrene ($\phi_F = 1$),⁸⁰ are 2×10^{-3} (methyltetrahydrofuran (MTHF), -78°C), 7×10^{-3} (MTHF, -196°C) and 1×10^{-3} (EPA, -196°C). The modest sensitivity of ϕ_F to hydrogen bonding effects is surprising, in light of dramatic solvent effects on the lifetimes of cyclic ketones⁷¹ and azoalkanes.⁸¹ The temperature insensitivity of ϕ_F suggests that internal conversion (k_{IC}) or intersystem crossing (k_{ST}) may be the rate

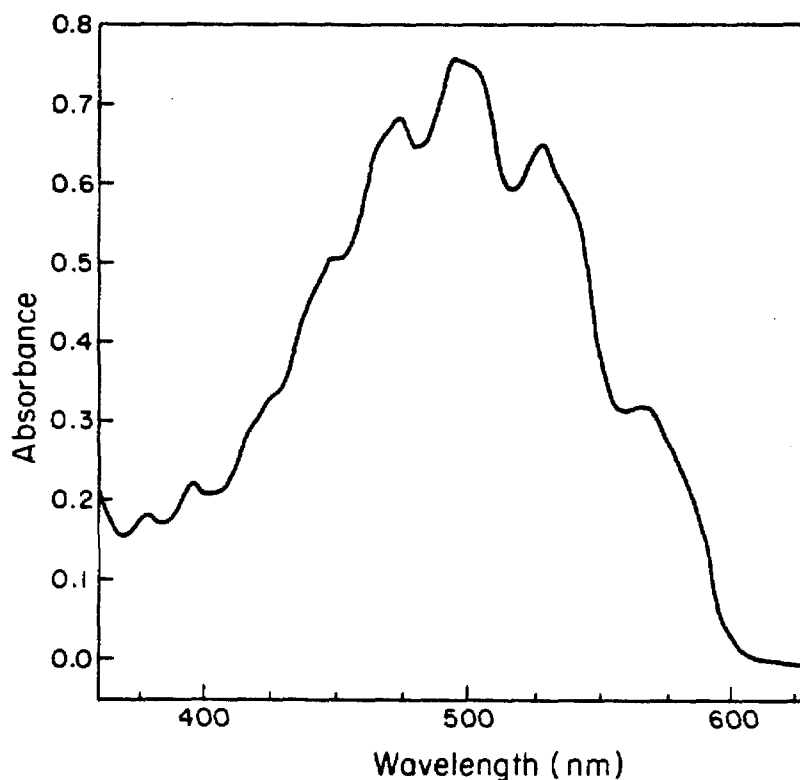


Figure 17. Absorption spectrum of 1,1-diazene 3 in diethyl ether.

determining deactivation mode for S_1 . A temperature dependent process such as α bond scission would be expected to show a more dramatic temperature effect. In the absence of vibrationally induced surface crossings and a low lying π, π^* triplet, internal conversion (k_{IC}) and intersystem crossing (k_{ST}) rates will be determined by Franck-Condon overlap and will therefore be proportional to $\Delta E_{state1, state2}$.^{75,76} Intersystem crossing in 1,1-diazenes should then be considerably slower

than in cyclic alkylketones (k_{ST} of tetramethylcyclopentanone = 10^8 sec^{-1})⁸² and the $S_1 \rightarrow S_0$ internal conversion rate, k_{IC} , should be quite fast. In azulene, for instance, $\Delta E_{S_1-S_0}$ is 42 kcal and $k_{IC} > 10^{10} \text{ sec}^{-1}$.⁸³ A rough estimate affords $k_{IC}(3) = 1 \times 10^8 \text{ sec}^{-1}$ ^{71d} (and $1 \times 10^6 \text{ sec}^{-1}$ for tetramethylcyclopentanone).

The fluorescence lifetime of 3, $\tau_F = 2.3 \times 10^{-8} \text{ sec}$ (CFCl_3), was determined at -196°C using a pulsed nitrogen dye laser. The decay rate of S_1 , $1/\tau_F$, is then $4 \times 10^7 \text{ sec}^{-1}$ (-196°C). We can now experimentally determine the fluorescence rate, $k_F = 1/\tau_F \cdot \phi_F$ (-196°C) = $3 \times 10^5 \text{ sec}^{-1}$. This value is not too different than that calculated from the integrated absorption spectrum. Unfortunately τ_F was too short to be measured at -78°C , but since k_F should be temperature insensitive, $\tau_F(-78^\circ\text{C}) = \tau_F(-196^\circ\text{C})/k_F = 2 \times 10^{-3}/3 \times 10^5 = 6.7 \times 10^{-9} \text{ sec}$. The n, π^* singlet decay rate (-78°C) is then $1.5 \times 10^8 \text{ sec}^{-1}$, not too different from the internal conversion rate of 10^8 sec^{-1} based on the S_1-S_0 energy gap. These results are consistent with k_{IC} controlling the S_1 lifetime. However we will experimentally demonstrate that k_{ST} and k_D are slower than internal conversion.

Attempts to locate T_1 of 3 have, to date, been unsuccessful. No phosphorescence signals have been detected above 1100 nm (detection limit of instrument) on direct or sensitized irradiation. Nor has an S_0-T_1 absorption been detected in the visible or near infrared using 1M solutions of 3. Assuming $\epsilon = 10^{-2}$,⁸⁴ $c = 1\text{M}$, and $\ell = 1$, $A = 0.1$ for an S_0-T_1 absorption. Direct and sensitized irradiation (see next section) of 1,1-diazene 3 (0.05M) in an ESR probe (at 78°K or 10°K , CFCl_3 or MTHF) failed to produce a triplet signal, suggesting that T_1 may be very

short lived (fast T_1-S_0 internal conversion or photochemical decomposition). The ESR spectrum of a triplet 1,1-diazene would be expected to exhibit a signal in the region of 5000-8000G for a microwave frequency of 9.234 GHz.⁸⁵ At 78°K a strong signal from a doublet state grows in at 3300G on direct photolysis (pyrex filter). The signal disappears on warming to 298°K. Irradiation of solutions of tetrazene 24 under the same conditions affords the same

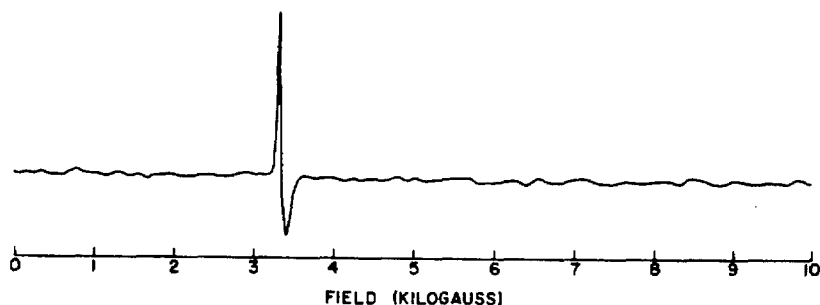


Figure 18. EPR spectrum of 0.05M solution of 3 in MTHF at 77°K (9.234 GHz) photolyzed using a pyrex filter and 200 watt mercury lamp.

doublet. The signal is most likely due to the presence of 2,2,5,5-tetrapyrrolyl amino radical. It may be possible to determine the S_1 - T_1 energy gap by electron photodetachment from the $R_2N-\bar{N}$ radical anion⁸⁶ (if this is a bound species). The radical anion might be generated from the amino isocyanate $R_2N-N=C=O$ (microwave discharge) which is produced on photolysis of $R_2N-NOON_3$.⁸⁷

The absorption and fluorescence spectra of 1,1-diazene 2 in $CFCl_3$ are shown in Figure 19. The absorption spectra has a λ_{max} at 543 nm and a 0-0 band at 620 nm. The vibrational spacing is 1113 cm^{-1} . As we noted earlier, the S_0 - S_1 gap and $S_1(N=N)$ vibrational frequencies of the six-membered cyclic 1,1-diazene 2 are lower than in the five-membered ring 1,1-diazene 3, consistent with more pyramidalization (stabilization) in S_1 of 2.

The fluorescence spectrum, corrected for instrument response to 900 nm, has only a single maximum at 684 nm which also corresponds to the 0-0 band. This band disappears on warming to 0°C and subsequent recooling to -196°C . A second maxima would appear at 767 nm ($\nu[N=N] = 1595\text{ cm}^{-1}$) and should be readily discernable. The λ_{max} of the absorption and fluorescence spectra differ by 141 nm consistent with substantially different S_0 and S_1 geometries. As was the case with diazene 3, the absorption and fluorescence spectra differ substantially in shape probably as a result of vibronic coupling in the pyramidal S_1 state of 2.

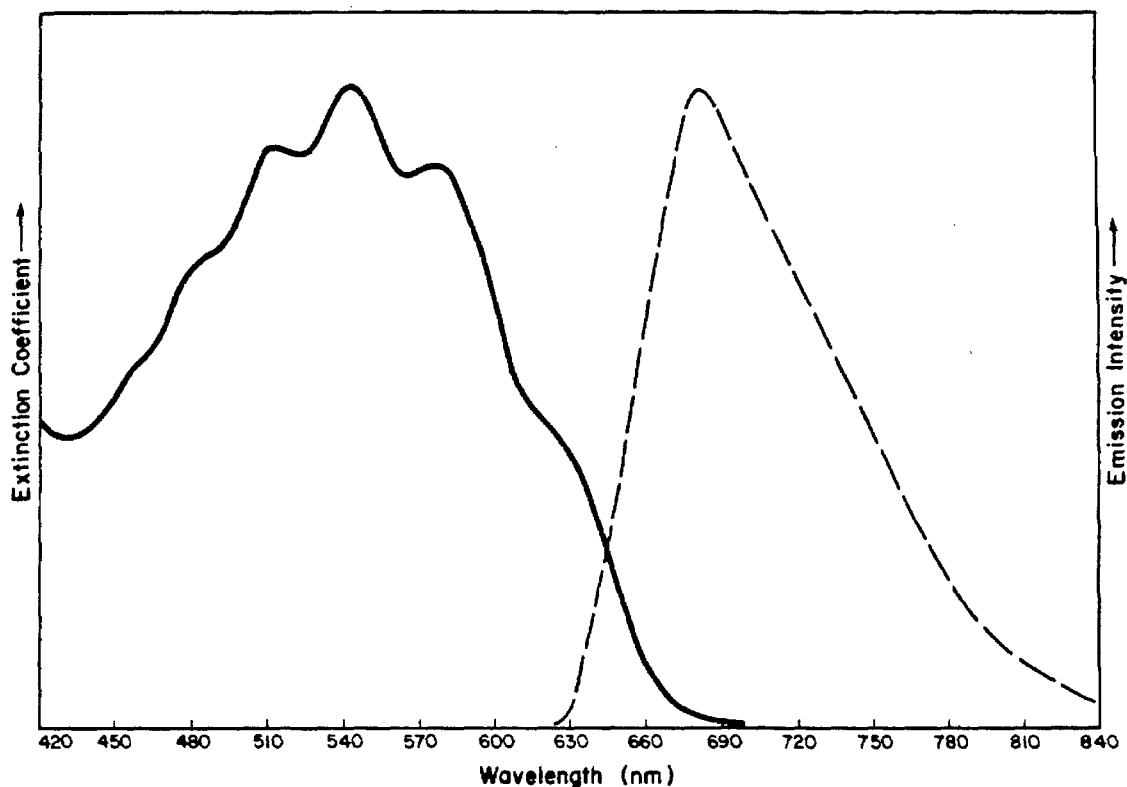


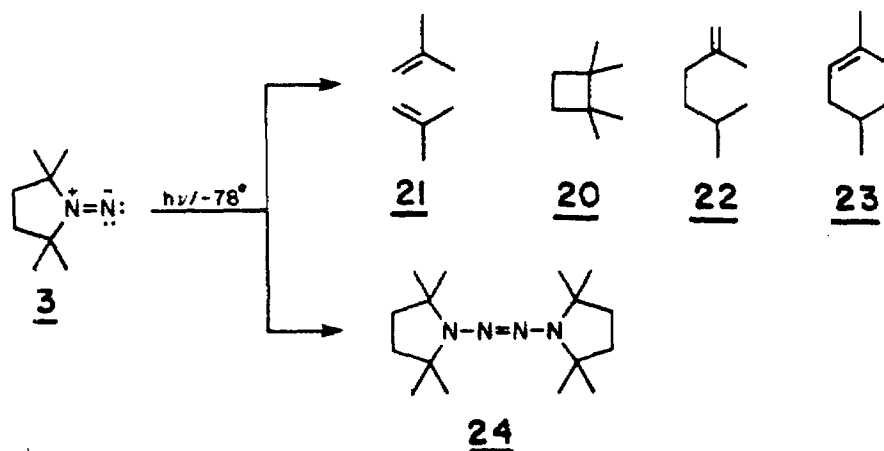
Figure 19. Absorption (—) and fluorescence (---) spectra of 2 in CFCl_3 at -78°C and -196°C , respectively.

The fluorescence rate constant, k_F , calculated from the integrated absorption spectrum, is $9.9 \times 10^4 \text{ sec}^{-1}$. The fluorescence quantum yield, ϕ_F , (-196°C (MTHF)) is 4×10^{-4} and approximately 1×10^{-4} at -78°C (MTHF). The fluorescence lifetime, τ_F , was too short to be measured ($< 10^{-8} \text{ sec}$), but from $\tau_F = \phi_F/k_F$, $\tau_F = 4 \times 10^{-9} \text{ sec}$ (-196°C)

and $\tau_F = 10^{-9}$ sec (-78°C), an order of magnitude shorter than the lifetime of the five-membered ring 1,1-diazene S_1 state. If k_{IC} is lifetime determining for S_1 , these results are consistent with $\Delta E_{S_0-S_1}(2) < E_{S_0-S_1}(3)$. In addition, internal conversion in 2 may be accelerated relative to 3 due to decreased rigidity of 1,1-diazene 2.

Direct and Sensitized Photolyses of N-(2,2,5,5-Tetramethylpyrrolidyl)nitrene 3 and N-(2,2,6,6-Tetramethylpiperidyl)nitrene 2

For photochemical studies a degassed, chromatographed solution of 3 (0.03M, CFCl_3) was irradiated at 466 to 610 nm at -78°C with a 1000 watt xenon lamp. The intensity of the lamp is linear over this range. Irradiation with the full spectrum of the lamp was avoided due to the possibility of energy transfer from tetrazene 24 to S_1 or T_1 of 3. After 12 hours of irradiation, the red color of 3 had completely disappeared. Vapor phase chromatography and ^1H NMR spectroscopy revealed the presence of four hydrocarbon products 20-23 and tetrazene 24 in a ratio of 1:4. Controls showed 3 (-78°C ; 0.03M, CFCl_3) to be stable in the dark. The hydrocarbon products 20-23 appear to result from the photochemical extrusion of nitrogen from 3. Tetrazene 24 will be shown to result from bimolecular reaction of S_1 with S_0 .



An approximate quantum yield for the decomposition of 3 on direct irradiation is $\phi_D = 1.1 \times 10^{-2}$. The decomposition rate for direct irradiation, k_D , equals ${}^3\phi_D k_{ISC} + k_{N_2} + k_{DIM}[S_0]$, where k_{N_2} is the rate for loss of N_2 from S_1 , k_{DIM} is the rate of dimerization of S_1 with S_0 , and ${}^3\phi_D(k_{ISC})$ is the rate of decomposition via the triplet. It will be shown that $k_{ISC} \ll k_{N_2} + k_{DIM}[S_0]$, so that $k_D = k_{N_2} + k_{DIM}[S_0]$. From $\phi_D = 1.1 \times 10^{-2}$ and $\tau_F = 6.7 \times 10^{-9}$ sec (-78°C), $k_D = \phi_D/\tau_F = 1.6 \times 10^6$ sec $^{-1}$. The ratio of hydrocarbon/tetrazene products (0.25) allows calculation of k_{N_2} and k_{DIM} from S_1 of 3: $k_{N_2} \sim 3 \times 10^5$ sec $^{-1}$; $k_{DIM} \sim 8 \times 10^7$ liter/mole sec. By assuming an A factor of 10^{13} , we can estimate a value for k_{N_2} at 25°C . The resulting E_a is 6.7 kcal/mole affording $k_{N_2}(25^\circ\text{C}) = 1 \times 10^8$ sec $^{-1}$.

In the isoelectronic alkanones, it is known that both α methyl substitution (radical stabilizing effect) and ring strain increase the

rate of α cleavage in the S_1 and T_1 states. If these effects are generalizable to 1,1-dialkyldiazenes, then k_{N_2} for the six-membered ring cyclic 1,1-diazene 2 will be less than k_{N_2} (3). Furthermore, 1,1-dimethyldiazene by this argument, should be stable to C-N bond scission. Values for k_α of S_1 and T_1 states of alkanones are listed in Table XI.

Table XI - Rate Constants for α -Cleavage in Carbonyls

Molecule	$k_\alpha(S_1)\text{sec}^{-1}$	$k_\alpha(T_1)\text{sec}^{-1}$
cyclohexanone ⁸⁹	$< 10^8$	2×10^7
cyclopentanone ⁸⁹	$< 10^8$	2×10^8
tetramethylcyclopentanone ⁸⁹	$< 10^8$	$> 10^{10}$

One might expect the N-R bond energies of 1,1-diazenes in the excited S_1 state to more closely parallel those of the isoelectronic carbonyls and isomeric azo compounds than in the ground state. Recall that in S_0 of R_2N-N , N-R cleavage results in formation of a normal N-N π bond, $R-N=N\cdot$ (not present in $H_2\ddot{N}=\ddot{N}$), and thereby lowers the normal $D_e(N-R)$.

Carbonyls and 1,2-diazenes already have normal π bonds so only 2 center 3 electron bonding is gained on α -cleavage, and bond energies are higher. However in the excited states of 1,1-diazenes, 1,2-diazenes, and carbonyls, the N=N bond has become a 3 electron, 2 center bond. Now, in all three cases, α cleavage has the same effect, a full π bond and a 2 center-3 electron bond are formed. This argument assumes that excited state decomposition does not occur through vibrationally excited

S_0 . For comparison, k_α 's of 1,1-diazene 3, 1,2-diazene 25 and tetramethylcyclopentanone are listed in Table XII.

Table XII - Comparison of k_α 's in 1,1-Diazene, 1,2-Diazenes and Alkanones

Molecule	$k_\alpha(S_0)^a \text{ sec}^{-1}$	$k_\alpha(S_1)^a \text{ sec}^{-1}$
3	10^{-1}	10^8
25	$10^{-11.66}$	$5 \times 10^{8.81}$
15	$10^{-45.90}$	$\leq 10^{8.89}$

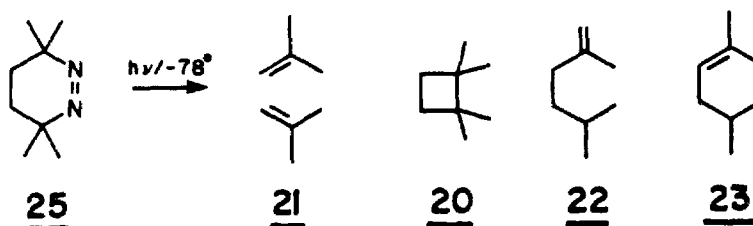
a) 25°C

The rate of dimerization of S_1 with S_0 , $^1k_{\text{DIM}} = 4 \times 10^7$ liter/mole sec is approximately 12 orders of magnitude greater than dimerization of S_0 , $^0k_{\text{DIM}} = 10^{-5}$ liter/mole sec, reflecting the nitrene like character of the terminal nitrogen in S_1 . In ground state 1,1-diazenes in which the internal nitrogen lone pair electrons are delocalized onto α substituents, again making the external nitrogen nitrene like, tetrazene is typically the only observed decomposition product.¹

Triplet sensitized photodecompositions were carried out at longer wavelengths (-78°C). Irradiation of degassed chromatographed solutions of 1,1-diazene 3 (0.03M in CFCl_3) at $> 608 \text{ nm}$ in the presence of 0.02-0.05M azulene sensitizer ($E_T = 31 \text{ kcal}$),⁹¹ affords hydrocarbons 20-23 and tetrazene 24 in a 1:9 ratio. Controls show that diazene 3 is unreactive upon direct irradiation at wavelengths $> 608 \text{ nm}$. Although k_{N_2} or k_{DIM} for the T_1 state have not been determined, one might expect $k_{\text{DIM}}(T_1 + S_0) \ll k_{\text{DIM}}(S_1 + S_0)$ (lower T_1 energy, spin restrictions).

This would imply that $k_{N_2}(T_1) \ll k_{N_2}(S_1)$, which is opposite the behavior of cyclopentanones (Table XI). The 1,2-diazene, 3,3,6,6-tetramethyl-tetrahydropyridazine **25**, was not present ($< 0.5\%$) among the direct or sensitized decomposition products. However, S_1 (3) could rearrange to a photoexcited state of **25** which subsequently reacts.

Because photolysis of the 1,1- and 1,2-diazenes isomers could produce common intermediates, the products from direct and sensitized irradiation (-78°C) of 1,2-diazene **25** were also examined. Photolysis of **25** at > 310 nm yielded



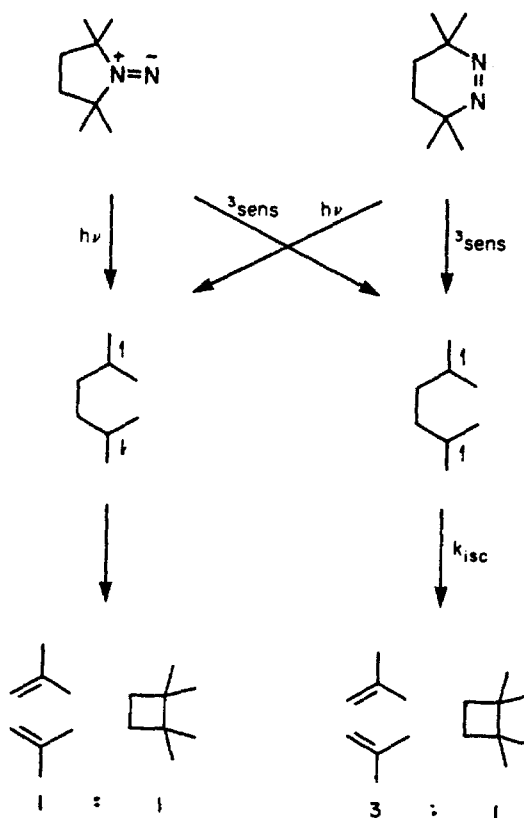
hydrocarbon products **20-23**. Sensitized photodecompositions in the presence of thioxanthanone⁹² also gave hydrocarbons **20-23**. The product compositions from the thermal, direct, and sensitized photodecompositions of 1,1-diazene **3** and the isomeric 1,2-diazene **25** are summarized in Table XIII.

Table XIII - Hydrocarbon Products from 1,1- and 1,2-Diazene 3 and 25

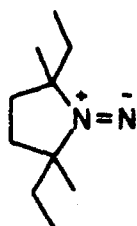
diazene	conditions	21	20	22 and 23
3	0°C, thermal ^a	47	49	4.0
3	-10°C, thermal ^a	53	44	3.0
3	-20°C, thermal ^a	59	39	2.0
3	-78°C, h ν (direct) ^a	54	44	2.0
3	-78°C, h ν (sens) ^{a,b}	74	24	2.0
25	140°C, thermal ^c	52	46	2.0
25	-78°C, h ν (direct) ^a	56	42	2.0
25	-78°C, h ν (sens) ^d	72	26	2.0

a) CFC1₃; b) Azulene; c) Benzene; d) CH₂Cl₂, thioxanthone

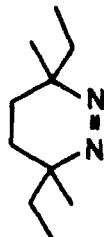
The 2-methylpropene/tetramethylcyclobutane (21/20) ratios for direct and sensitized photodecomposition of 1,1-diazene 3 are 1.14 and 3.09, respectively. Importantly, the 21/20 product ratios are similar in the 1,1- and 1,2-diazene direct and sensitized photolyses. Common singlet and triplet 1,4-biradicals⁶⁷ (formed from loss of nitrogen from S₁ and T₁, respectively) from 3 and 25 would be sufficient to explain these results. The different propene/cyclobutane ratios from direct and sensitized photodecomposition may reflect cleavage and closure from different biradical conformations which are in turn spin dependent. Such an effect, a radical pair giving different products depending upon its multiplicity, is called a spin correlation effect (SCE).⁹³ Bartlett and Porter⁹² have demonstrated such an effect on the products produced from direct and sensitized photodecomposition of the cyclic 1,2-diazene 27. The observation of an SCE demands that direct and sensitized photolyses proceed via different pathways, that is, $k_{ISC} \ll k_{N_2}$. The fact that the hydrocarbon product ratios from 3 are different in the direct and sensitized photolyses, but in agreement



with the product ratios from the 1,2-diazenes isomer **25**, is permissive evidence for a spin correlation effect in the 1,1-diazenes case. Such behavior would be consistent with the large S_1 - T_1 gap predicted for the 1,1-diazenes. To test explicitly whether $k_{\text{ISC}} \ll k_{\text{N}_2}$ in S_1 of the 1,1-diazenes, we have synthesized and studied the direct and sensitized photodecomposition of d,l-N-(2,5-diethyl-2,5-dimethylpyrrolidyl)nitrene **26**. These studies will be described in the next section. It is unlikely that interpretable data on 1,1-diazenes intersystem crossing rates can be obtained from triplet quenching studies due to the diazenes' lability and the small S_0 - T_1 gap.

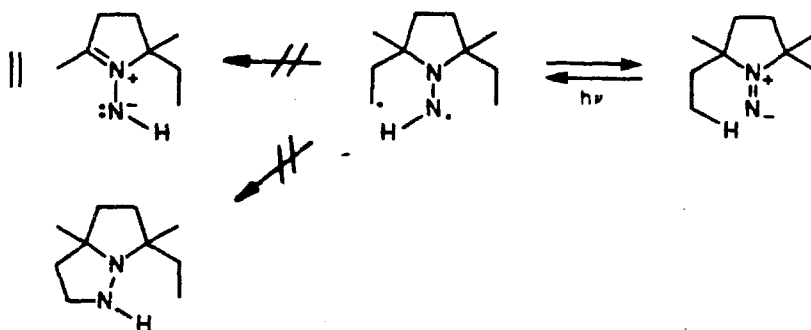


26



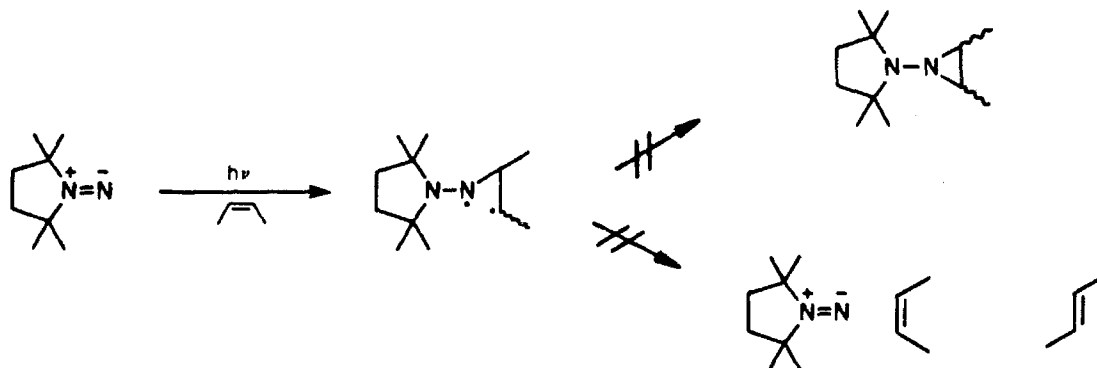
27

Unlike the case with the isoelectronic carbonyls⁹⁴, neither direct nor sensitized photolysis of 1,1-diazenes 3 in the presence of high concentrations of hydrogen donors (e.g., 4M 1,4-cyclohexadiene) yielded products resulting from hydrogen abstraction (hydrazines). A hydrazinyl radical formed by hydrogen abstraction could also lead to tetrazene formation, however the tetrazene/hydrocarbon ratio was unaffected by the presence of 1,4-cyclohexadiene. Unfortunately, thermal decomposition of 3 in the presence of thiols or tri-n-butyltin hydride prohibited photochemical experiments with these excellent hydrogen donors. Triethylamine has no effect on the photodecomposition of 3. These results suggest that diazenes with γ -hydrogens will not undergo Norrish Type II photochemistry. This in fact the case, products consistent with either β or γ hydrogen abstraction were not found in the direct or sensitized photodecompositions of N-(2,2,5,5-tetramethylpyrrolidyl)nitrene 3 or N-(2,5-diethyl-2,5-dimethyl-

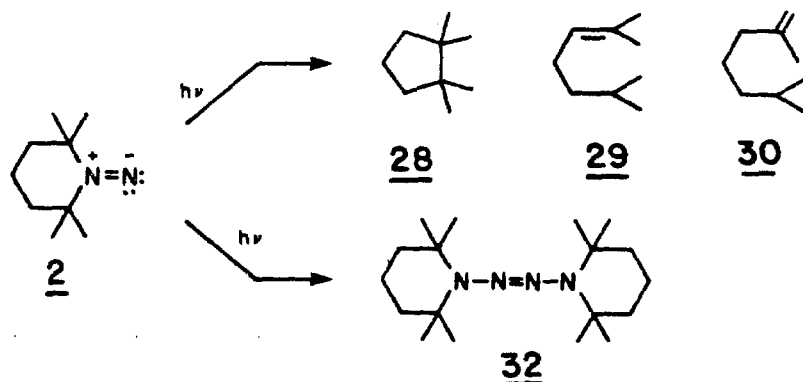


pyrrolidyl)nitrene 26 (next section). Interestingly, hydrogen abstraction or Type II reactions have not been observed in ground state reactions of 1,1-diazenes with electron withdrawing substituents (nitrene like).

Because the S_1 state of 1,1-diazene 3 undergoes facile dimerization with S_0 , we thought S_1 might add to alkenes.⁹⁵ (This is the case with nitrene like ground state diazenes with electron delocalizing substituents.)¹ However, neither direct nor sensitized photolysis of 3 in the presence of high concentrations of cis, trans-hexadiene (4M), cis-2-butene (4M), or cis-1-ethoxy-1-butene (4M)⁹⁶ resulted in aziridines or isomerized butenes. Photoaddition of 3 to the alkene yielding an intermediate diradical in which $k_{\text{cleav}} \gg k_{\text{rot}}$ and k_{clos} cannot be ruled out. No observable quenching occurred (< 20%). It is possible that photoaddition will be observed in the photochemistry of less sterically hindered 1,1-diazenes.



For photochemical studies, a degassed, chromatographed solution of 1,1-diazene **2** (0.05M in CFCl_3) was irradiated with visible light at -78°C at $> 500 \text{ nm}$. After 12 h of irradiation at -78°C , the purple color had completely disappeared. Capillary VPC coupled with ^1H NMR spectroscopy (-60°C) revealed three hydrocarbon products **28-30** and tetrazene **32** in a ratio of 1:3. The photoproducts of **2** appear to arise in a manner similar to those of 1,1-diazene **3**: dimerization with S_0 or extrusion of N_2 .



Thermal decomposition of **2** results in the appearance of a fourth hydrocarbon product 1,1,3-trimethylcyclohexane **31**.^{2,61}

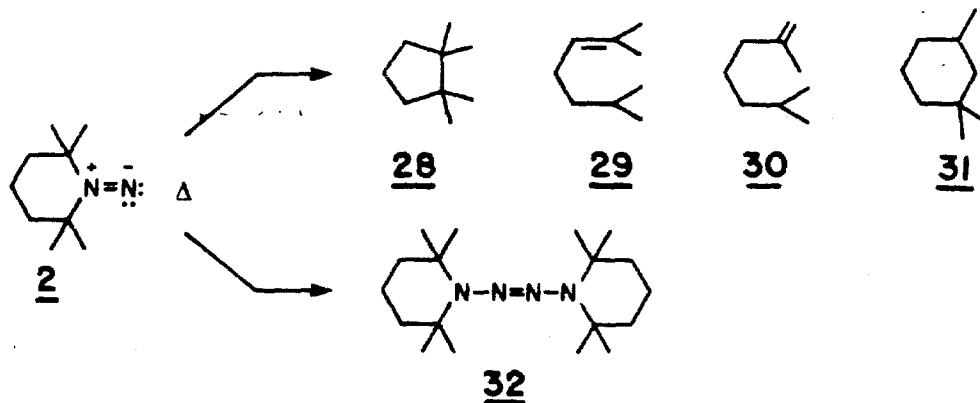
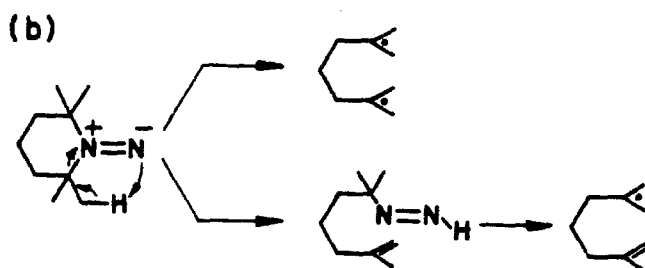
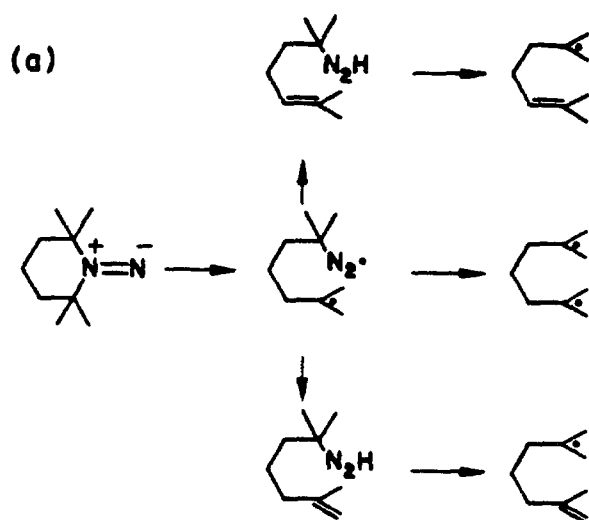


Table XIV - Hydrocarbon Products from 1,1-Diazene 2

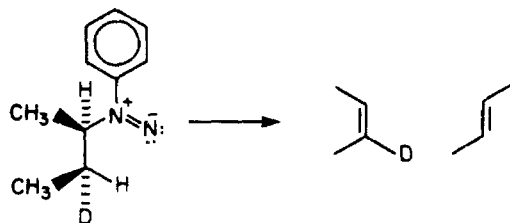
Conditions ^a	28	29	30	31
Thermal, 0°C	24	10	61	5
Thermal, -20°C	24	7	65	4
Direct, h ν , -78°C	29	3	68	0

a) Et₂O

The appearance of the same hydrocarbon products 28-30 in similar ratios from both the thermal and photochemical decomposition of 1,1-diazene 2 suggests a common intermediate. Note that 1,1,3-trimethylcyclohexane is absent in direct photolysis. In earlier studies on the thermal decomposition of 2, Hinsberg^{2,3,61} and Dervan suggested that the appearance of 1,1,3-trimethylcyclohexane raised the issue of two possible competing decomposition pathways for the thermal fragmentation of 2; loss of N₂ to form a 1,5-biradical competing with either stepwise C-N cleavage followed by disproportionation or a concerted intramolecular elimination reaction. Duan and Dervan⁵⁰ have demonstrated the existence of a concerted [2,3]elimination pathway in the decomposition of an acyclic aryl alkyl 1,1-diazene. Their work suggests that 1,1,3-trimethylcyclohexane is the product of a concerted [2,3]



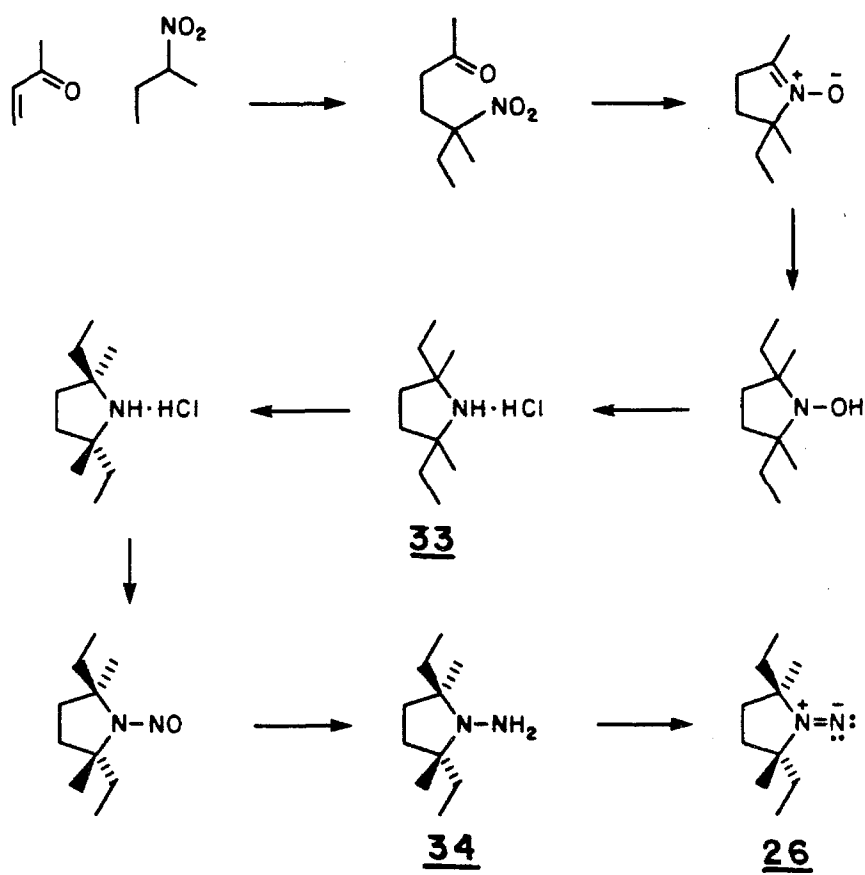
elimination pathway in 2. It seems likely, then, that thermolysis and direct photolysis of 2 proceed largely through a common 1,5-diradical intermediate. The ratio of disproportionation to closure products simply reflects the temperature dependence of each process. The minor (< 15%) concerted elimination pathway in thermolysis is absent in the photochemical decomposition of 2 (symmetry forbidden).



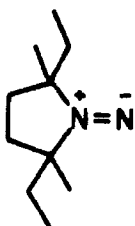
Spin Correlation Effects in the Photodecomposition of dl, -N(2,5-Diethyl-2,5-Dimethylpyrrolidyl)nitrene 26 and the Behavior of the Incipient Biradical

The studies of dl-N(2,5-diethyl-2,5-dimethylpyrrolidyl)nitrene 26 described in this section will enable us to quantitate the deactivation pathways for the 1,1-diazene n, π^* singlet state: fluorescence, internal conversion, intersystem crossing, and chemical reaction. In addition, these studies will provide new insight into the processes controlling intersystem crossing in alkyl diradicals.

A 2/1 mixture of the dl and meso isomers of 2,5-diethyl-2,5-dimethylpyrrolidine was synthesized in four steps from 2-nitrobutane⁹⁷ and methyl vinyl ketone. The dl amine hydrochloride 33 was isolated by fractional recrystallization from isopropanol and identified by partial resolution of the hydrogen tartrate salt followed by conversion to the amine hydrochloride, $[\alpha]_{365}^{20} = +4.80$ ($c = 0.39$, methanol). The dl and meso amine hydrochlorides are distinguishable by 500 MHz ^1H NMR and by 90 MHz ^1H NMR in the presence of a shift reagent, tris-(6,6,7,7,8,8,8-heptafluoro-2,2-dimethyl-3,5-octanedionato)europium. Vapor phase chromatography (VPC) or high pressure liquid chromatography (HPLC) of 2,5-diethyl-2,5-dimethylpyrrolidine, or derivatives thereof (phenylurea, thiophenylurea, nitrosamine, N-amine, acetamide), gave at best marginal separation. Nitrosation of 33 followed by reduction afforded



1-amino-2,5-diethyl-2,5-dimethylpyrrolidine **34** (97% d,l, 3% meso by capillary VPC). The (+)- α -methoxytrifluoromethylphenylacetamide⁹⁸ of the unresolved d,l hydrazine showed two peaks of near equal intensity separated by 12 Hz at -69.5 ppm (relative to CFCl_3) in the ^{19}F NMR and are assigned to the diastereomeric trifluoromethyl groups.



26

Addition of tert-butyl hypochlorite to a stirred solution of hydrazine **34** and triethylamine in anhydrous dimethyl ether at -78°C affords in addition to an insoluble white precipitate (Et_3NHCl), a red solution of 1,1-diazaene **26** which is stable for days at -78°C. Filtration at -78°C, followed by low temperature chromatography (-85°C) on basic alumina and concentration in CFCl_3 yielded a solution of > 98% 1,1-diazaene **26**, < 2% tetrazaene and small amounts of dimethyl ether. Low temperature infrared (-78°C) spectroscopy revealed an absorption at 1630 cm^{-1} which disappeared on warming and is assigned to the $\text{N}=\text{N}$ stretch.

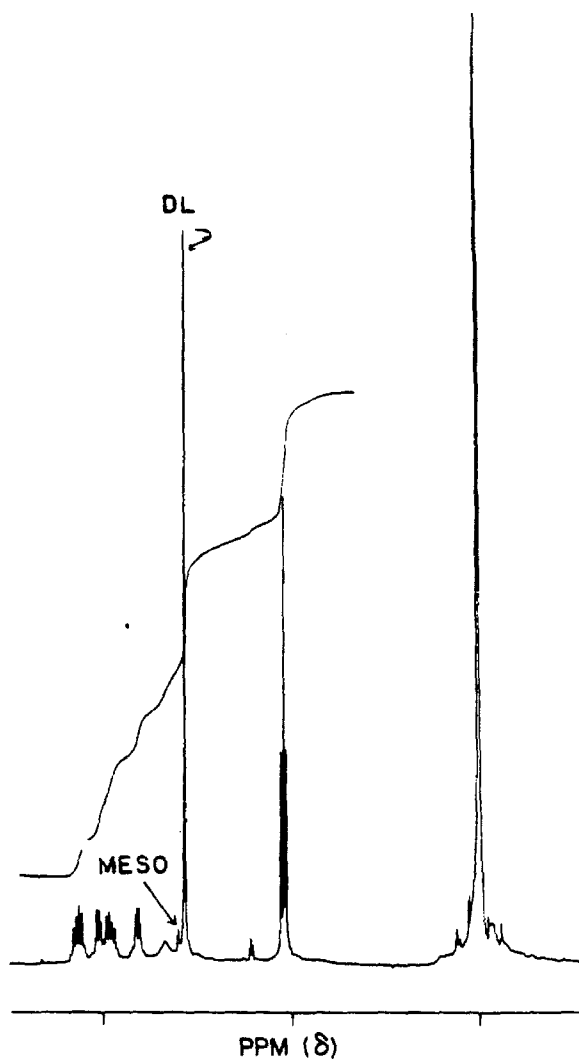


Figure 20. Meso and d,l 33

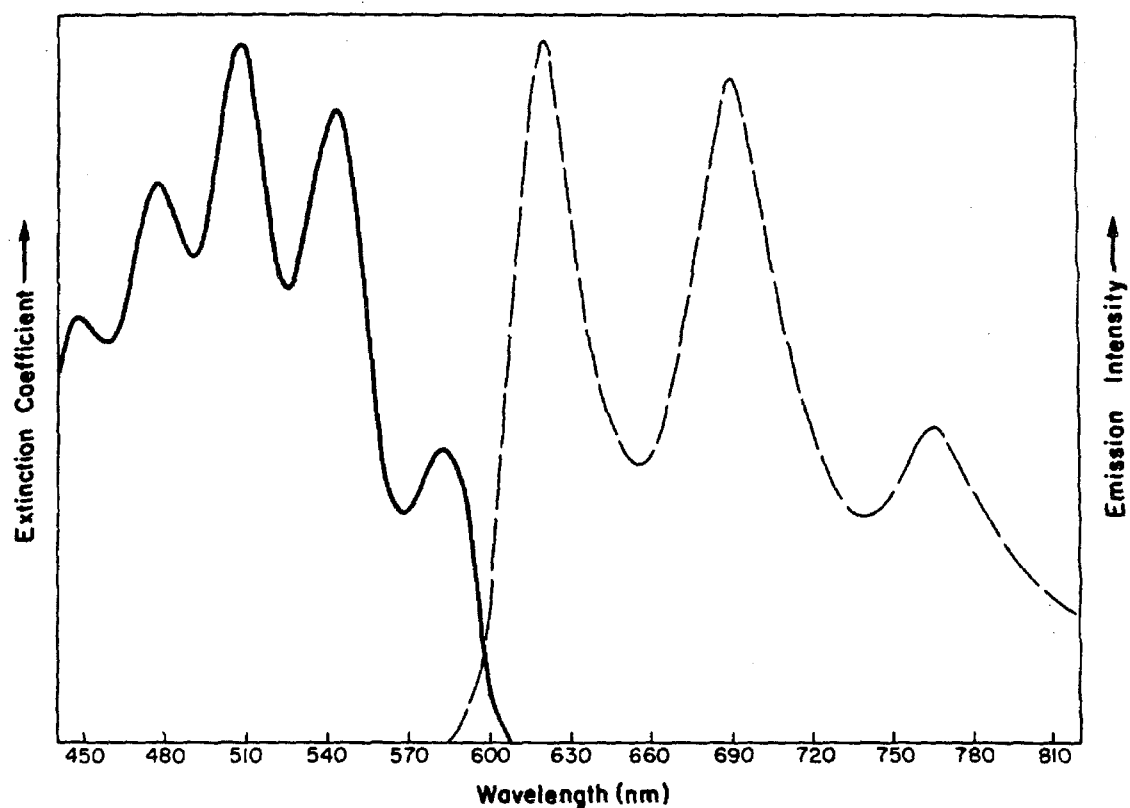
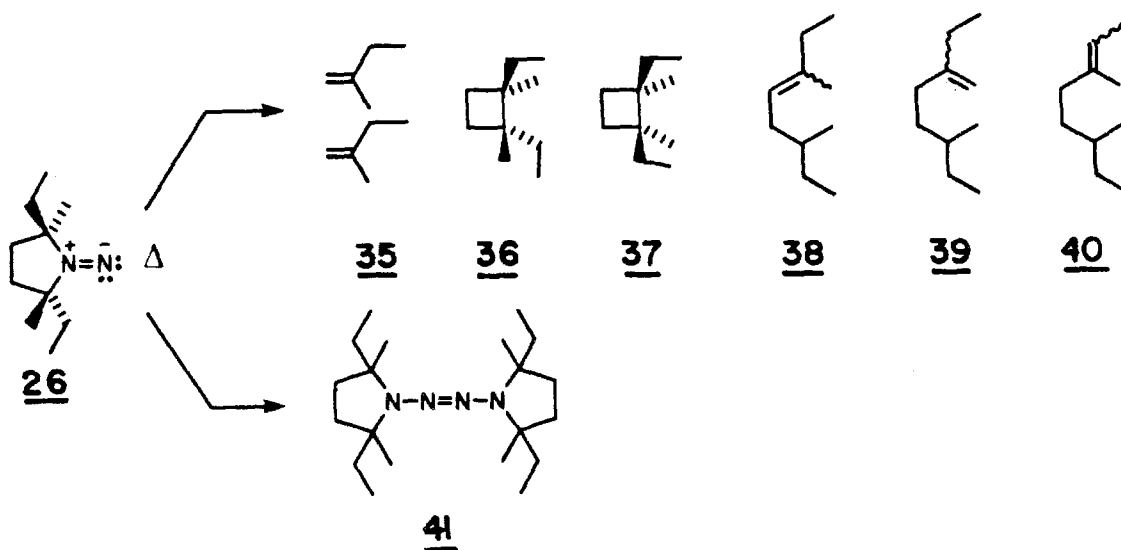


Figure 21 . Absorption spectrum of **26** at -78°C (—). Fluorescence spectrum of **26** at -196°C (---).

The absorption and fluorescence spectra of 1,1-diazene **26** are shown in Figure 21. The absorption spectrum reveals a structured absorption with λ_{max} at 507 nm and a 0-0 band at 568 nm ($\epsilon = 20+2$), CFCl_3 . The vibrational spacing is 1270 cm^{-1} . The emission spectrum has a 0-0 band and λ_{max} at 620 nm (CFCl_3). The spacing between the maxima

at 620 and 690 nm is identical to the vibrational spacing in the infrared spectrum. The shapes of the absorption and emission spectra are different. The fluorescence rate constant (k_F), calculated from the integrated absorption spectrum, is $1 \times 10^5 \text{ sec}^{-1}$. ϕ_F of 1,1-diazene **26** in MTHF is 9×10^{-3} at -196°C . The spectroscopic and photophysical properties of the five membered ring cyclic 1,1-diazene **26** very closely resemble those of **3**.

Thermal decomposition of a degassed chromatographed solution of **26** at 0°C (0.1M, CFCl_3) yielded hydrocarbons **35-40** and tetrazene **41** in a ratio of 20:1. The octenes were identified by VPC coinjection techniques with independently synthesized materials. Tetrazene **41** was synthesized independently by oxygen oxidation of the corresponding





hydrazine 34. Cis- and trans-1,2-diethyl-1,2-dimethylcyclobutane can be separated on a 30 meter capillary SE-54 VPC column. Assignments were made by independent synthesis of the trans isomer, coupled with ^1H NMR and VPC analysis.

The ratio of cleavage/closure products is 0.8 not too different from that found in the thermal fragmentation of 1,1-diazene 3. The retention of stereochemical integrity in the closure product is high (98%), consistent with the behavior expected of a singlet 1,4-biradical with tertiary radical centers; $k(\text{rotation}) \ll k(\text{closure})$.^{67,92} The thermal decomposition of 26 results in a substantially lower yield of tetrazene than that found in the thermal decomposition of 3, reflecting the importance of sterically bulky substituents in slowing dimerization.

Direct and sensitized photolyses of 1,1-diazene 26 were carried out in the manner described for 1,1-diazene 3 and yielded hydrocarbons

35-40 and tetrazene 41. Product distributions from the thermolysis and direct and photosensitized photodecompositions are given in Table XV.

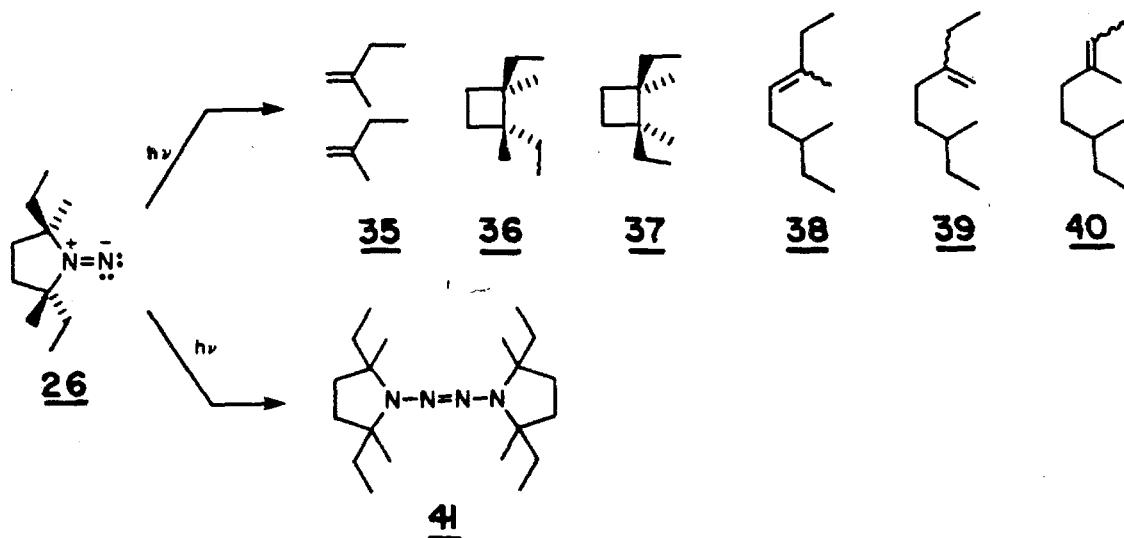
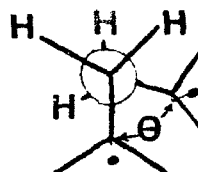
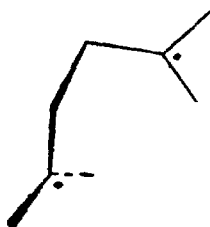
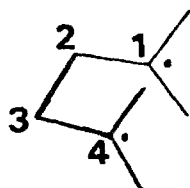
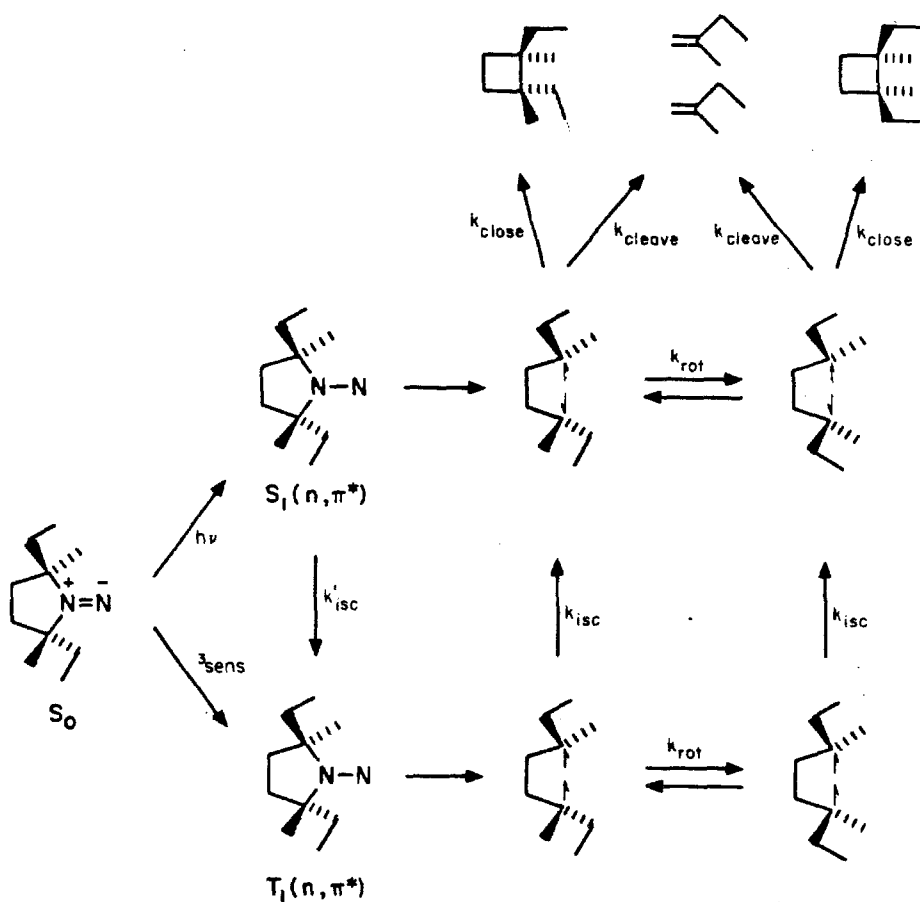


Table XV - Products from 1,1-Diazene 26

Conditions	35	36	37	38-40	41
Thermal, 0°C	44	51	2	3	5
Direct, $h\nu$ -78°C	47	45	2	5	399
Sensitized, $h\nu$ -78°C	73	17	8	2	720

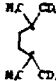
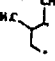
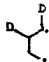
The hydrocarbon product ratios produced by direct irradiation and thermolysis of 1,1-diazeno **26** are quite similar, characterized by cyclobutanes with high retention of configuration and a butene/cyclobutane ratio of approximately 1.0. Triplet sensitized photolysis results in loss of configuration in the cyclobutanes and a butene/cyclobutane ratio of 3. These results can be interpreted in terms of a mechanism similar to that proposed by Bartlett and Porter⁹² for the corresponding 1,2-diazeno. The thermally generated tetrasubstituted singlet biradical is expected to behave in a stereospecific manner. Experiments have demonstrated that rotation about the 1-2 bond in thermally generated tetramethylene diradicals slows with increasing substitution at the radical centers.⁶⁷ This results in $k_{\text{rotation}} \ll k_{\text{closure}}$ for tertiary radical centers.





The Bartlett-Porter mechanism as applied to 1,1-diazene 26. For economy of space we have not drawn all possible conformational isomers about the 2-3 bond in the 1,4-biradical.

Table XVI - Comparison of the Effect of Substitution on $k(\text{rotation})/k(\text{closure})$ for 1,4-Biradicals

		$k(\text{rotation})/$ $k(\text{closure})$	Conditions
	tertiary <u>d,l</u>	< 0.05	425°C/gas ⁹⁹
	secondary <u>cis-</u> <u>trans-</u>	1.4 0.53	439°C/gas ⁶⁴ 439°C/gas
	primary	1.2	439°C/gas ⁶⁴

The triplet biradical, derived from sensitized photodecomposition (Wigner's rule), behaves in a much less stereospecific manner. Closure can occur only in the singlet manifold. If intersystem crossing is rate determining, conformational equilibration results in net formation of partially scrambled cyclobutanes as well as a higher cleavage/closure product ratio. Recent experiments strongly suggest that spin inversion is in fact rate determining in triplet Norrish Type II diradicals produced by ketone photolysis.¹⁰⁰

An alternative mechanism for loss of stereochemical integrity on triplet photolysis, is one bond cleavage from the $T_1(n, \pi^*)$ state of 1,1-diazenes **26** yielding a triplet diazenyl biradical. If rotation in the diazenyl biradical is competitive with cleavage of the C-N bond, one might expect some stereochemical crossover in the cyclobutane products. This mechanism places no constraints on k_{ISC} in the substituted 1,4-biradical. The existence of thermally generated 1-norbornyl and phenyl diazenyl radicals has been demonstrated.¹⁰¹ In addition, recent results suggest that the $T_1(n, \pi^*)$ states of acyclic 1,2-diazenes decompose via a diazenyl radical intermediate whereas the $S_1(n, \pi^*)$

states do not.^{102,103} The decomposition of T_1 via a diazenyl radical implicates different decomposition mechanisms rather than a spin correlation effect (SCE) in a common 1,4-biradical intermediate.

Because direct irradiation of 1,1-diazene **26** affords closure products with high stereospecificity characteristic of singlet 1,4-biradical behavior, we conclude that the (n, π^*) singlet state of **26** (and by extension **3**) is characterized by $k_{ISC} \ll k_{N_2}$. Since $k_{N_2} = 3 \times 10^5 \text{sec}^{-1}$, k_{ISC} must be on the order of 10^4sec^{-1} (from meso/dl cyclobutane ratios). This is one of the lowest n, π^* S_1-T_1 intersystem crossing rates known, consistent with the large 1,1-diazene S_1-T_1 energy gap. In cyclic 1,2-diazenes where $\Delta E_{S_1-T_1}$ is typically 25 kcal, k_{ST} is $\approx 10^6 \text{sec}^{-1}$.^{93a,104}

Table XVII - Stereochemistry of Closure Products

1,1- and 1,2-Diazene	Decomposition Mode	Temp.	% Retention of Configuration
26	Thermal	0a	98
26	Direct $h\nu$	-78a	96
26	Sensitized $h\nu$	-78a	68
27	Thermal ^c	145b	98
27	Direct ^c $h\nu$	25b	97
27	Sensitized ^c $h\nu$	25b	65

a) CFCl_3 . b) benzene. c) reference 92.

Table XVII shows a comparison of the results for the thermal and photochemical decomposition of 1,1-diazene **26** and the corresponding 1,2-isomer **27**. Although the temperatures of photodecomposition differ by 100°C, both diazenes show similar amounts of crossover in the cyclobutane photoproducts.

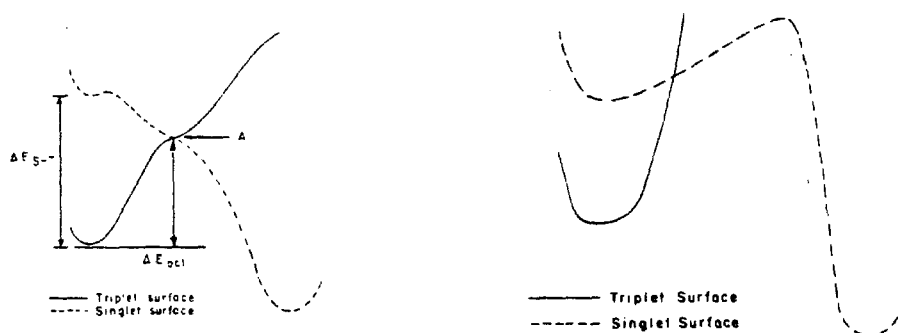


Figure 22. Intersystem crossing may occur concurrent with a molecular motion which leads to curve crossing or via thermal excitation.

If the spin correlation effects in both 1,1-diazene **26** and 1,2-diazene **27** arise via the Bartlett-Porter mechanism, then the temperature insensitivity of the meso/dl cyclobutane ratios demands that $k_{rotation}$ and k_{TS} (the rate of triplet to singlet conversion) have similar E_a values ($E_{rot} = E_{TS} + 0.32$ kcal). Furthermore, since the meso/dl cyclobutane ratio is approximately 2, rotation and triplet to singlet conversion have similar A factors, $\log A_{rot} = \log A_{TS} - 0.44$. Rotational A factors for biradicals are not known, but $\log A$ is calculated to be 11.5 for rotation about tertiary radical centers.^{33a} If we use this A factor, then triplet to singlet conversion has an A

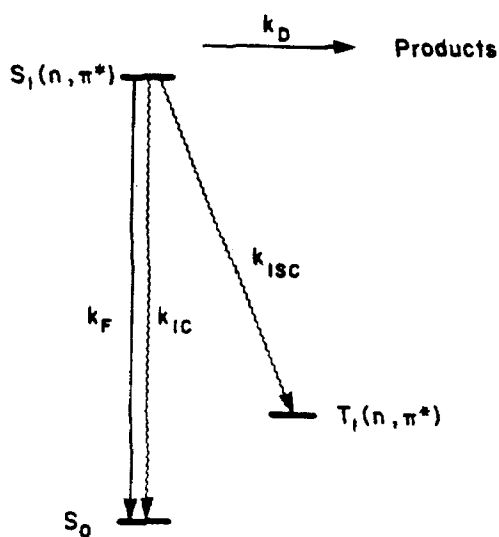
factor of 10^{12} . In any case, it is unlikely that the A factor for triplet to singlet conversion will be less than 10^{10} . The net result is that the triplet lifetime in the substituted tetramethylene diradical is not controlled by a spin inversion process (spin orbit coupling or hyperfine coupling)¹⁰⁵ since A factors of such processes are in the range 10^4 - 10^8 , not 10^{12} . Instead, it is likely that a conformational barrier to biradical intersystem crossing is rate determining. Unfortunately, there are no good estimates of E_a 's for rotation around radical centers. This value would enable us to determine the triplet diradical lifetime.

Lifetimes of Norrish Type II carbonyl derived triplet biradicals are in the range 10^{-5} to 10^{-6} sec and are virtually temperature independent.¹⁰⁰ Temperature independence implies that the E_a for triplet to singlet conversion is <2 kcal/mole. Such a value in the alkyl diradical, coupled with $\log A = 12$, affords a triplet biradical lifetime of $< 10^{-10}$ sec, extremely low in light of the distance between the radical centers. Lifetimes of 10^{-6} to 10^{-7} sec result in an $E_a \sim 7$ kcal/mole for triplet to singlet conversion, which does not lead to temperature independence. Thus it appears that alkyl triplet 1,4-diradicals may behave quite differently than triplet Norrish Type II 1,4-diradicals. Alternatively either **26** or **27** may be decomposing via a diazenyl radical in the triplet state.

Summary

The demonstration of an SCE in the decomposition of 1,1-diazene **26** enables us to define the deactivation pathways for the n, π^* singlet state of **3**: $k_{IC} = 2 \times 10^8 \text{ sec}^{-1}$ (-78°C), $k_F = 3 \times 10^5 \text{ sec}^{-1}$; $k_{DIM} = 8 \times$

10^7 sec^{-1} (-78°C); $k_{\text{N}_2} = 3 \times 10^5 \text{ sec}^{-1}$ (-78°C) and $k_{\text{ISC}} \ll 3 \times 10^5 \text{ sec}^{-1}$ ($\approx 10^4 \text{ sec}^{-1}$). The lifetime of the S_1 state is determined by a fast internal conversion rate. This rate is consistent with the relatively small S_1-S_0 energy gap of 50 kcal. The intersystem crossing rate, k_{ISC} , is one of the lowest known for $n, \pi^* S_1$ to T_1 conversions, reflecting the large S_1-T_1 energy separation. $\Delta E_{S_1-T_1}$ is a consequence of the unique excited state electronic structures of the diazene, in which the n, π^* excitation is largely localized on the terminal amine. The fast bimolecular rate constant for S_0+S_1 dimerization (k_{DIM}) again reflects the nitrene like character of the terminal nitrogen in S_1 . The rate of nitrogen extrusion from S_1 , k_{N_2} , extrapolated to 25°C , is roughly the same as k_{N_2} in the corresponding 1,2-diazene n, π^* singlet state. This is not too surprising since important factors which contribute to make $E_a(1,1\text{-diazene}) < E_a(1,2\text{-diazene})$ in the ground states are lacking in the n, π^* states. Finally, the fluorescence rate constant is that expected for a symmetry forbidden n, π^* transition. The triplet n, π^* state of 1,1-dialkyldiazene reacts by a bimolecular pathway, dimerization with S_0 , and by unimolecular extrusion of N_2 . Attempts to observe T_1 by ESR or optical spectroscopy were unsuccessful. The sensitization experiments place $E(T_1)$ below 31 kcal/mole.



$E(S_1)$		47-50 kcal (CH_2Cl_2)
$E(T_1)$	<	31 kcal
k_F		$3 \times 10^5 \text{ sec}^{-1}$
k_{IC}		$2 \times 10^8 \text{ sec}^{-1}$ (-78°C)
k_{N_2}		$3 \times 10^5 \text{ sec}^{-1}$ (-78°C)
k_{DIM}		$8 \times 10^7 \text{ mol}^{-1} \text{ sec}^{-1}$ (-78°C)
k_{ISC}	<<	k_{N_2} or $\sim 10^4 \text{ sec}^{-1}$

EXPERIMENTAL

Low Temperature Spectroscopic Cells⁶¹ and Glassware

The IR and UV-VIS cells were designed by Hinsberg⁶¹ for use in conjunction with an Air Products WMX-1A Vacuum Shroud and LC-1-110 Cyro-Tip Refrigerator. The windows for the vacuum shroud are sodium chloride (purchased from International Crystal Laboratories) for IR spectroscopy and Suprasil I (ground to size from blanks purchased from Amersil, Inc.) for UV-VIS spectroscopy. Samples are introduced into the cells through 18 gauge Teflon tubing (purchased from Alpha Wire Corp.) by applying suction with a syringe.

The cell body of the UV-VIS spectroscopic cell is constructed from OFHC copper, with stainless steel tubing soldered to it. The body is nickel-plated and has a thermocouple well with set screw. The cell windows are Suprasil I and were ground to size from blanks purchased from Amersil, Inc. The seals between the windows and the body are made with Viton O-rings. The cell path length is 10.0 millimeters, the volume is approximately four milliliters.

The cell body of the IR cell is OFHC copper with stainless steel tubing soldered in place. The cell windows are cesium bromide (purchased from International Crystal Laboratories).

Low temperature filtration funnels and chromatography columns were constructed in the Caltech Glassblowing Shops.

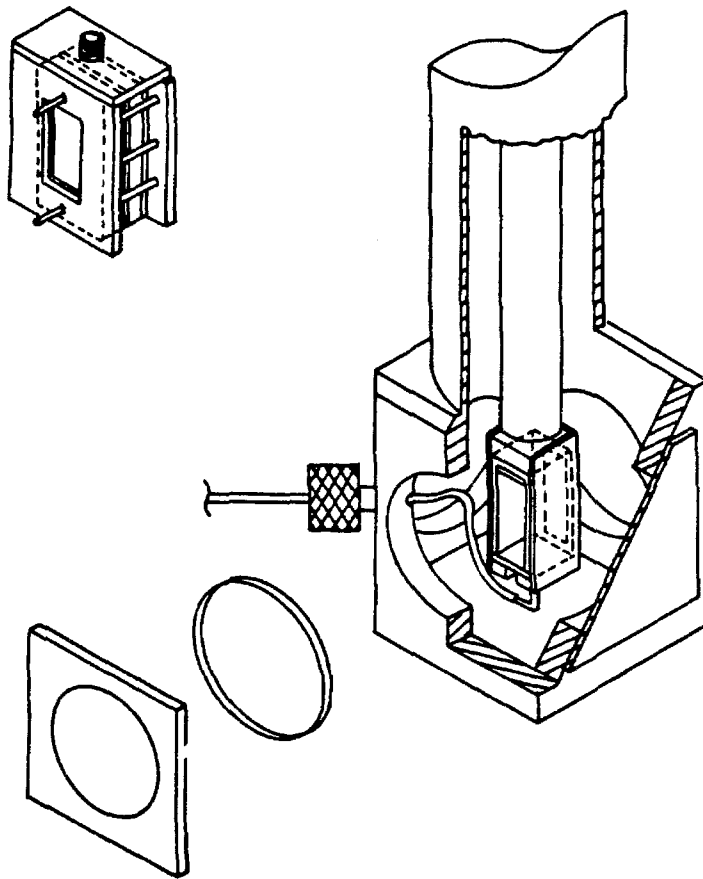


Figure 23. Low temperature spectroscopic cells and shroud.⁶¹

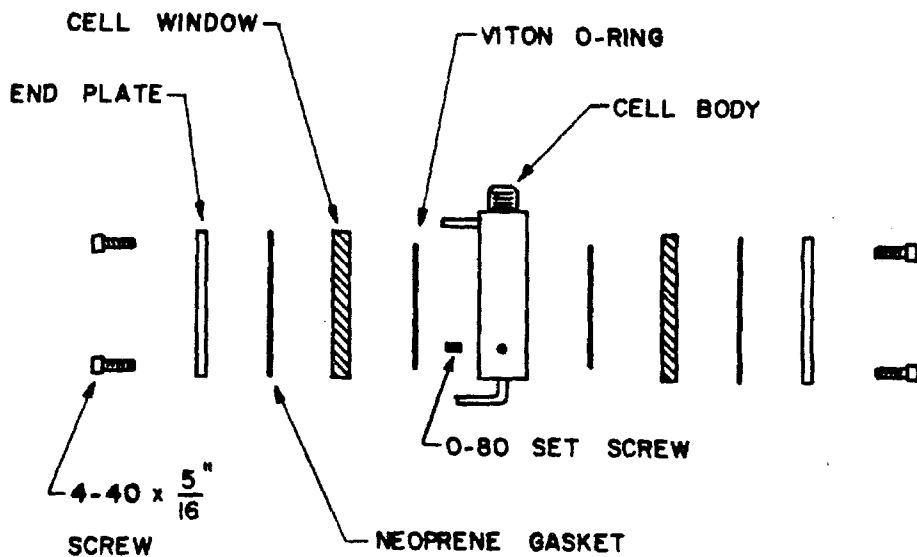


Figure 24: Low temperature UV-VIS spectroscopic cell.⁶¹

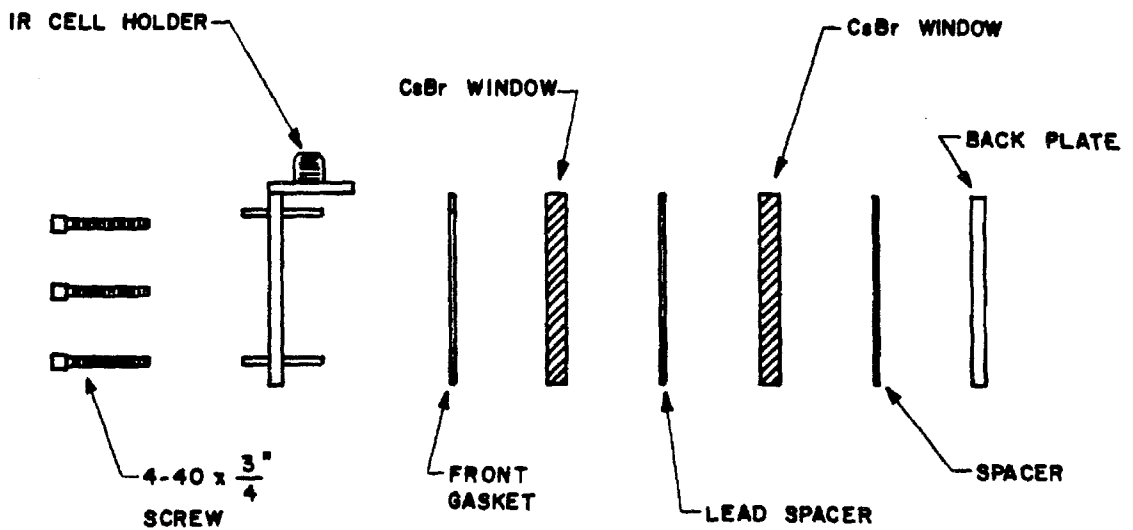
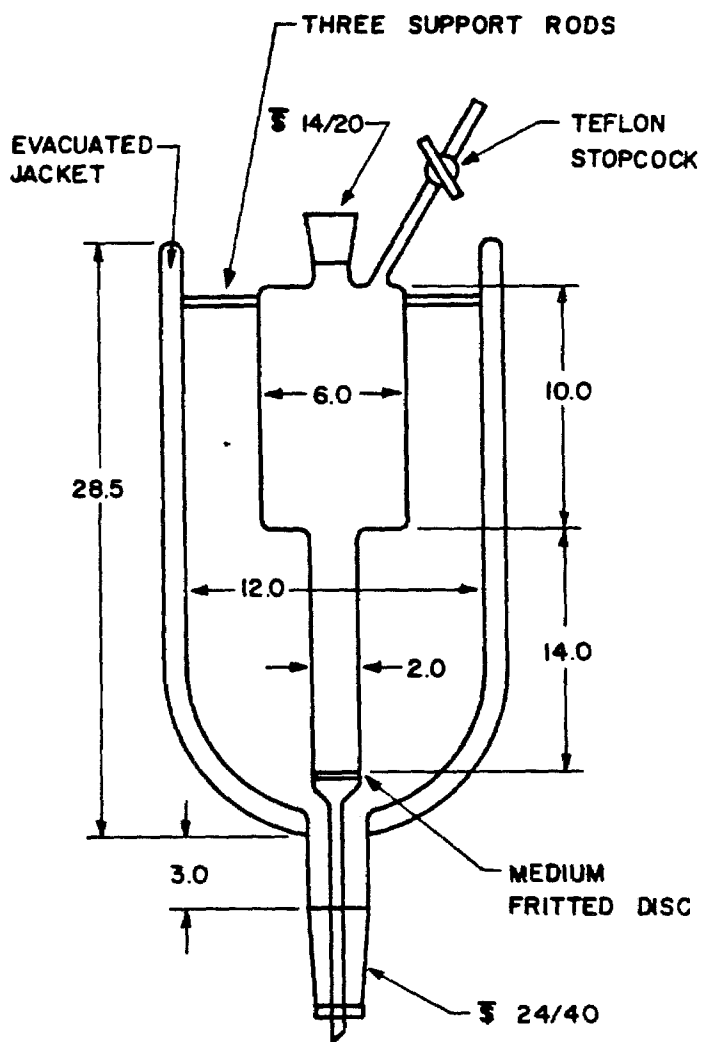
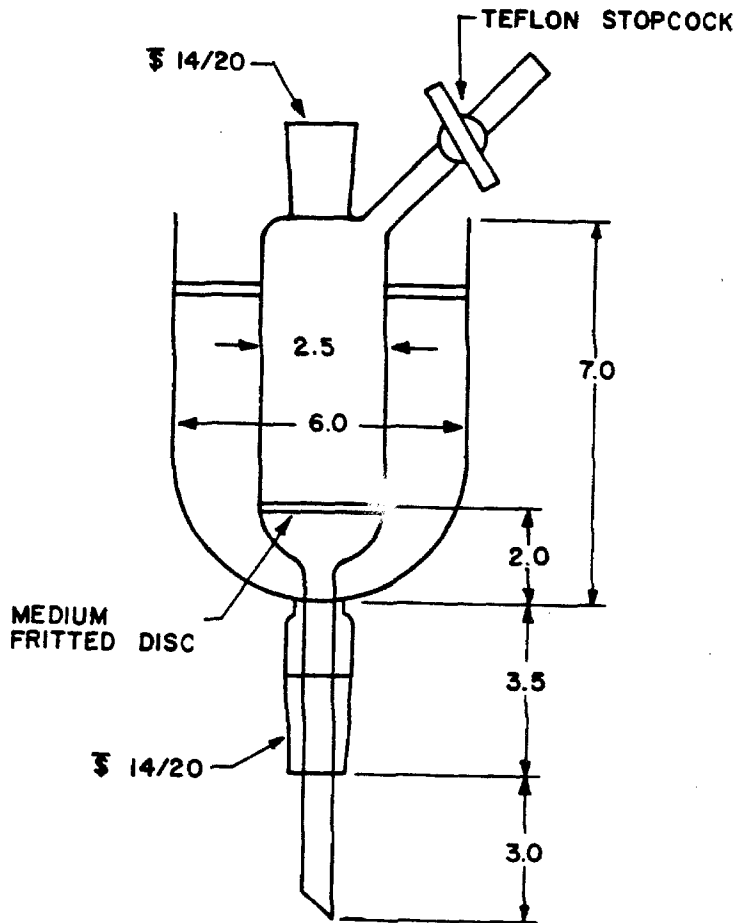


Figure 25: Low temperature IR spectroscopic cell.⁶¹



DIMENSIONS IN CM

Figure 26: Low temperature chromatography column.



DIMENSIONS IN CM

Figure 27: Low temperature filtration funnel.

Synthesis and Procedures

Melting points were determined using a Thomas Hoover Melting Point Apparatus and are uncorrected. Infrared spectra were recorded on a Perkin Elmer 257 Infrared Spectrophotometer. Proton nuclear magnetic resonance (NMR) spectra were obtained on a Varian EM-390, Jeol FX-90, or Bruker 500 Spectrometer. Chemical shifts are reported as parts per million (ppm) downfield from tetramethylsilane in δ units and coupling constants are in Hertz (Hz). Electronic spectra were obtained using a Cary 14 or Varian 219 Spectrophotometer. ESR spectra were recorded using a Varian Associates E-line Spectrometer equipped with an Air Products and Chemicals Helitran LTD-3-110 liquid helium transfer apparatus. The emission spectra were recorded with the assistance of members of Professor H. B. Gray's group at Caltech using a noncommercial spectrophotometer with a 250-W xenon source and Hamamatsu R-406 and R-955 PMTS. Fluorescence lifetimes were measured with the assistance of Professor A. Zewail's group at Caltech using a noncommercial apparatus consisting of a nitrogen pumped dye laser (0.3 cm^{-1} bandwidth, 10-15 nsec pulse width) and IP28 PMT.

For analytical vapor phase chromatography (VPC), a Hewlett Packard 5700A gas chromatograph equipped with a flame ionization detector and nitrogen carrier gas was used. The 0.125 in. packed stainless steel columns used in this instrument are listed in Table XVIII. Quantitative VPC analysis was accomplished using a Hewlett-Packard 3370A electronic digital integrator. A Hewlett Packard 5800 Capillary Gas Chromatograph equipped with flame ionization detector and a Hewlett Packard 5880 series electronic integrator were also used;

hydrogen/helium was used as carrier gas. The 0.25 mm packed fused silica columns used are listed in Table XVIII. For preparative VPC, a Varian 920 instrument equipped with a thermal conductivity detector and helium carried gas was used. The 0.375 in. packed aluminum columns used are listed in Table XVIII. Detector response for hydrocarbons are assumed to be 1.0 relative to n-octane. Quantitative analysis of all other compounds were corrected for detector response.

Table XVIII

Designation	Description
Penrwalt 223	10' x 1/8" stainless steel; 28% Penrwalt 223 on 80/100 Chrom R
Penrwalt 223	10' x 1/4" glass, 28% Penrwalt 223 on 80/100 Chrom R
Carbowax 400	10' x 1/8" stainless steel; 10% Carbowax 400 on 100/120 Chrom P A/W DMCS
ββ	20' x 1/8" stainless steel; 10% ββ -oxydipropionitrile on 100/120 Chrom P A/W DMCS
ββ	10' x 3/8" aluminum; 25% ββ -oxydipropionitrile on 50/80 Chrom P
SF-96	10' x 3/8" aluminum; 25% SF-96 on 45/60 Chrom A
SF-96	10' x 1/8" stainless steel; 10% SF-96 on SF-96 on 100/120 Chrom P A/W
SE-54	SE-54, capillary fused silica, 30M x 0.25 mm
Carbowax 20M	Carbowax 20M, capillary fused silica, 15M x 0.25 mm

Dibutyl ether and isopropanol were distilled from sodium. Ethyl

ether and 2-methyltetrahydrofuran were distilled from sodium benzophenone ketyl. Triethylamine was distilled from barium oxide. Chloroform and fluorotrichloromethane were distilled from phosphorous pentoxide and passed through a short column of basic alumina. Deuteriochloroform used for obtaining 1,1-diazene NMR spectra was passed through a short column of basic alumina. Propane and dimethyl ether used in low temperature chromatography were dried over 4A molecular sieves. Hexane was washed with concentrated sulfuric acid, saturated sodium bicarbonate, saturated sodium chloride solution, dried (CaCl_2) and distilled from calcium hydride or lithium aluminum hydride. t-Butyl hypochlorite was washed with 10% sodium carbonate, water, dried (CaCl_2) and distilled under nitrogen. 1-Amino-2,2,6,6-tetramethylpiperidine, 1-amino-2,5-diethyl-2,5-dimethylpyrrolidine and, 1-amino-2,2,5,5-tetramethylpyrrolidine were always purified by preparative VPC (Pennwalt 223) prior to use.

Mass spectra were recorded on a Dupont 24-492B Mass Spectrometer. Combustion analyses were performed at Galbraith Laboratories, Knoxville, Tennessee. Unless otherwise indicated reactions were carried out under a positive pressure of dry nitrogen.

~~5-Methyl-5-nitrohexane-2-one~~ - A modification of the procedure of Schechter et al.⁵⁴ was used. To a stirred refluxing solution of 132 g (1.48 mole) 2-nitropropane and 10 mls Triton B in 150 mls diethylether was added 100 g (1.43 mole) of methyl vinyl ketone over a three hour period. The mixture was stirred at reflux for an additional 15 h, cooled, and acidified with 10% HCl solution. The ethereal layer was separated, washed twice with water, once with a saturated sodium

chloride solution, and dried (Na_2SO_4). The ethereal solution was then concentrated and distilled giving 197 g (95%) of a yellow oil,

5-methyl-5-nitrohexan-2-one: bp $125-127^\circ\text{C}$ at 10 Torr (lit. $123-125^\circ\text{C}$ at 10 Torr);⁵⁴ IR (CCl_4): 2987, 1727, 1460, 1390, 1360 cm^{-1} . NMR (CDCl_3) δ 2.1 (s, 3H), 2.4-2.1 (m, 4H), 1.5 ppm (s, 6H).

2,2,5-Trimethyl- Δ_1 -pyrroline N-oxide - A modification of the procedure of Lunt⁵⁵ was used. 200 g 5-Methyl-5-nitrohexan-2-one (1.26 mole), 78 g ammonium chloride (1.47 mole), and 2000 ml water was heated with mechanical stirring to 65°C . 170 g Zinc dust (3.9 mole) was then added in portions over 30 min, maintaining the temperature at $65-70^\circ\text{C}$. The mixture was stirred two additional hours at 65°C , cooled and filtered. The aqueous filtrate was acidified with 10% HCl solution, concentrated to 500 ml, made basic with NaOH, and extracted (8 x 300 ml) with methylene chloride. The methylene chloride extracts were combined, dried (Na_2SO_4), and concentrated. The resulting oil was distilled giving 125 g (70%) of a pale yellow oil, 2,2,5-trimethyl- Δ_1 -pyrroline N-oxide: bp $66-67^\circ\text{C}$ at 0.15 Torr (lit. 67°C at 0.15 Torr);⁵⁵ IR (CCl_4): 3440, 2985, 1608, 1461, 1390, 1370 cm^{-1} . NMR (CDCl_3) δ 2.6 (t, 2H, $J=8\text{Hz}$), 2.0 (s, 3H), 2.0 (t, 2H, $J=7.5\text{Hz}$), 1.4 ppm (s, 6H).

1-Hydroxy-2,2,5,5-Tetramethylpyrrolidine - To a Grignard reagent prepared in the usual way from 121 g methyl iodide (1.1 mole) and 27 g magnesium in 500 ml ether was added with stirring a solution of 100 g 2,2,5-trimethyl- Δ_1 -pyrroline oxide (0.8 mole) in 400 ml dry ether at such a rate that the mixture refluxed gently. After addition was complete the mixture was refluxed for 24 h, cooled to 0°C , and a solution of 118 g ammonium chloride in 500 ml water carefully added.

After stirring for 30 min the ether layer was separated and the aqueous layer extracted with ether (5 x 200). The combined ether extracts were dried (Na_2SO_4), solvent removed and the residue distilled to give 55 g (50%) of a colorless oil, 1-hydroxy-2,2,5,5-tetramethylpyrrolidine: bp $79-81^\circ\text{C}$ at 20 Torr (lit. $78-80^\circ\text{C}$ at 20 Torr);⁵⁵ IR (CCl_4): 3505, 2980, 1460, 1382, 1368 cm^{-1} . NMR (CDCl_3) 6.9 (s, 1H), 1.6 (s, 4H), 1.2 ppm (s, 12H).

2,2,5,5-Tetramethylpyrrolidine Hydrochloride - A mixture of 24 g 1-hydroxy-2,2,5,5-tetramethylpyrrolidine (0.17 mole) in 200 ml methanol was hydrogenated with 2 g of Raney nickel catalyst on a Parr rocker at 26°C and 50 lb/in² H_2 . The filtered reaction mixture was acidified with ethereal hydrogen chloride and solvent evaporated to give 28 g of a crystalline precipitate. Recrystallization from isopropanol/ether yielded 26 g (95%) 2,2,5,5-tetramethylpyrrolidine hydrochloride: mp $308-310^\circ\text{C}$ (lit. $310-311^\circ\text{C}$);⁵⁵ IR (CCl_4): 3345, 2920, 1460, 1380, 1370 cm^{-1} . NMR (CDCl_3) δ 8.3 (s, 1H), 2.1 (s, 4H), 1.5 ppm (s, 12H).

Preparation of Raney-Nickel Catalyst

25 g Raney Nickel alloy was added in portions with stirring to 100 ml 25% aqueous sodium hydroxide solution, maintaining the temperature below 40°C . After the addition was complete and hydrogen evolution slowed, the mixture was heated to $90-95^\circ\text{C}$ for 90 min. After cooling to room temperature, the aqueous layer was decanted, another 100 ml 25% aqueous sodium hydroxide solution added, and the mixture heated to 90°C for another hour. After cooling, the aqueous layer was decanted, the Raney-Nickel washed (2 x 100 ml) with distilled water followed by overnight washing with distilled water. The aqueous layer

was decanted and the Raney-Nickel washed (3 x 100 ml) with absolute ethanol. The Raney-Nickel was stored under ethanol.

1-Nitroso-2,2,5,5-Tetramethylpyrrolidine - To a solution of 8g (0.051 mole) of 2,2,5,5-tetramethylpyrrolidine hydrochloride in 100 ml water at 85°C was added slowly with stirring 15.3 g (0.22 mole) of sodium nitrite in 50 ml water. The reaction temperature was maintained at 85°C for 72 h during which time a yellow oil formed. After cooling to room temperature, 30 ml ethyl ether was added to the reaction mixture and the layers were separated. The aqueous layer was extracted twice with ether. The combined ethereal extracts were washed with 10% HCl solution, saturated sodium bicarbonate solution, and saturated sodium chloride solution. The ethereal extract was dried (Na_2SO_4) and concentrated affording 6.9 g (90%) of 1-nitroso-2,2,5,5-tetramethylpyrrolidine. This was further purified for analytical samples by preparative VPC (Pennwalt 223, 2200): mp 51-52°C; IR (CCl_4): 2930, 1460, 1375, 1365 cm^{-1} . NMR (CDCl_3) δ 1.90 (t, 4H, $J=3.5\text{Hz}$), 1.6 (s, 6H), 1.45 ppm (s, 6H). Anal. Calcd. for $\text{C}_8\text{H}_{16}\text{N}_2\text{O}$: C, 61.15; H, 10.32; N, 17.93. Found: C, 61.37; H, 10.50; N, 17.69.

1-Amino-2,2,5,5-Tetramethylpyrrolidine - A slurry of 2.2 g (0.05 mole) of lithium aluminum hydride in 70 ml 6:1 n-butyl ether/diethylether under N_2 was heated with distillation of solvent until the internal temperature reached 100°C. A solution of 5 g (0.032 mole) of 1-nitroso-2,2,5,5-tetramethylpyrrolidine in 20 ml n-butyl ether was then added cautiously over 1 h, never allowing the temperature to rise above 105°C. Heating was continued for 4 h, the reaction mixture was cooled to 0°C and hydrolyzed by careful addition of a large excess of water.

The hydrolyzed mixture was transferred to a separatory funnel and the layers separated. The aqueous layer was extracted twice with ether and the combined organic extracts were extracted three times with 10% HCl solution. The combined acid extracts were made strongly basic with 20% sodium hydroxide solution and were extracted three times with ether. The ethereal extracts were combined and washed with 100 ml of saturated sodium chloride solution. The ethereal extracts were dried (Na_2SO_4) and concentrated affording a colorless oil. This oil was further purified by distillation under reduced pressure at 25°C followed by preparative VPC (Pennwalt 223, 60°C) affording 2.5 g (34%) of 1-amino-2,2,5,5-tetramethylpyrrolidine: IR (film) 3350, 3220, 2950, 2930, 1370, 1355 cm^{-1} . NMR (CDCl_3) δ 2.8 (s, 2H), 1.6 (s, 4H), 1.03 ppm (s, 12H). This hydrazine compound is air-sensitive. Benzamide: Anal. Calcd. for $\text{C}_{15}\text{H}_{22}\text{N}_2\text{O}$: C, 73.13; H, 9.00; N, 11.37. Found: C, 73.07; H, 9.03; N, 11.14.

1,1-Azo-2,2,5,5-Tetramethylpyrrolidine - 250 mg (1.75 mmol) of 1-amino-2,2,5,5-tetramethylpyrrolidine was stirred under an oxygen atmosphere for 24 h. The resulting white crystalline solid was further purified by heating to 50°C (0.05 Torr) for 3 h, to yield 191 mg (78%) of 1,1-azo-2,2,5,5-tetramethylpyrrolidine: mp $62-63^\circ\text{C}$. IR (CHCl_3) 1540, 1460, 1375, 1360 cm^{-1} . NMR (CDCl_3) δ 1.7 (s, 8H), 1.3 ppm (s, 24H); UV (2,2,5-trimethylpentane) 300 (8600), 254 nm (3300). Anal. Calcd. for $\text{C}_{16}\text{H}_{32}\text{N}_4$: C, 68.52; H, 11.50; N, 19.97. Found: C, 68.30; H, 11.35; N, 19.88.

1-Nitroso-2,2,6,6-Tetramethylpiperidine⁶¹ - A modification of the procedure of Overberger and coworkers was used.⁵⁶ A solution of

0.8M HCl was prepared by addition of 14 ml concentrated hydrochloric acid to 200 ml water and placed in a three-necked 1 l round-bottom flask equipped with magnetic stirrer, reflux condenser, addition funnel and thermometer. To this was added slowly with cooling 23.7 gm (0.152 mole) of distilled 2,2,6,6-tetramethylpiperidine. The reaction mixture was heated to 75°C and a solution of 42.1 g (0.61 mole) sodium nitrite in 150 ml water was added over 30 min. Heating was continued for 96 h during which time a yellow oil formed. After cooling to room temperature 100 ml ethyl ether was added to the reaction mixture and the layers were separated. The aqueous layer was extracted twice with ether. The combined ethereal extracts were washed with 100 ml 10% HCl solution, saturated sodium bicarbonate solution, and saturated sodium chloride solution. The ethereal extracts were dried (Na_2SO_4), concentrated, and distilled affording 25.1 g (89%) of 1-nitroso-2,2,6,6-tetramethylpiperidine: bp 114–117°C at 15 Torr (lit. 91–92°C at 12 Torr);⁵⁶ IR (CCl_4): 2925, 1455, 1375, 1360 cm^{-1} . NMR (CDCl_3) δ 1.90–1.50 (m, 6H), 1.64 (s, 6H), 1.40 ppm (s, 6H).

1-Amino-2,2,6,6-Tetramethylpiperidine⁶¹ – A modification of the procedure of Roberts and Ingold was used.⁵⁷ A slurry of 5.0 g (0.13 mole) of lithium aluminum hydride in 150 ml 1:1 ethyl ether/n-butyl ether was stirred in a 500 ml three-necked round-bottomed flask equipped with addition funnel, magnetic stirrer, thermometer, and reflux condenser fitted with a still head. To this was added dropwise a solution of 12.5 g (0.071 mole) 1-nitroso-2,2,6,6-tetramethylpiperidine in 25 ml ethyl ether. After stirring for an additional 30 mins, solvent

was distilled until the internal temperature reached 95°C. Heating was continued for 4 h, at which time the reaction mixture was cooled to 0°C and hydrolyzed by careful addition of a large excess of water. The layers were separated and the aqueous layer was extracted with ether. The combined organic extracts were extracted with 10% HCl solution. The combined acid extracts were made strongly basic with 20% sodium hydroxide solution and were extracted with ether. These ethereal extracts were dried (Na_2SO_4), concentrated and distilled affording 9.1 g (86%) of 1-amino-2,2,6,6-tetramethylpiperidine (95% pure by VPC, PerkinElmer 223, 180°C): bp 82-85°C at 20 Torr (lit.⁵⁷ 80-83°C at 20-21 Torr); IR (film) 3350, 3250, 2960, 2925, 1370, 1360 cm^{-1} ; NMR (CDCl_3) 2.8 (s, 2H), 1.50 (s, 6H), 1.06 ppm (s, 12H).

1-Amino-(^{15}N)-2,2,5,5-Tetramethylpyrrolidine - To a solution of 2 g (0.013 mole) 2,2,5,5-tetramethylpyrrolidine in 25 ml of water at 85°C was added slowly with stirring 2 g (0.03 mole) $\text{Na}^{15}\text{NO}_2$ (97.2 atom %, Prochem) in 15 ml water. The reaction temperature was maintained at 85°C for 72 h during which time a yellow oil formed. After cooling to room temperature, 5 ml ether was added to the reaction mixture and the layers were separated. The aqueous layer was extracted with ether. The combined ethereal extracts were washed with 10% HCl solution, saturated sodium bicarbonate solution, and saturated sodium chloride solution. The dried (Na_2SO_4) ethereal extracts were concentrated giving 1.5 g (80%) of 1-nitroso-(^{15}N)-2,2,5,5-tetramethylpyrrolidine (coinjects on PerkinElmer 223 with unlabeled material). 1.5 g (0.01 mole) Labeled nitrosamine was dissolved in 7 ml n-butyl ether and cautiously added to a slurry of 0.7 g lithium aluminum hydride in 20 ml 6:1 n-butyl

ether/ethyl ether at 100°C. Heating was continued for four hours, at which time the reaction mixture was cooled and worked up in a similar manner to the unlabeled hydrazine. The crude hydrazine was purified by high vacuum distillation at room temperature followed by VPC (Penwalt 223, 160°C) to yield 500 mg (23%) of 1-amino-(¹⁵N)-2,2,5,5-tetramethylpyrrolidine (coinjects with unlabeled compound on Penwalt 223, 160°C).

3,3,6,6-Tetramethyl-1,2-diazacyclohexene⁶³ - 40 g 2,5-Diamino-2,5-dimethylhexane (0.14 mole) and 2 g sodium tungstate dihydrate, were dissolved in 800 ml distilled water and cooled while 63 g of a 30% hydrogen peroxide solution was added slowly. The rate of addition was such that the reaction temperature never rose above 30°C. The solution was stirred for one hour and then extracted with methylene chloride. The combined methylene chlorided extracts were washed with 2N HCl and with water. After removing the chloroform under reduced pressure, the solution was filtered to remove the 3,3,6,6-tetramethyl-1,2-diazacyclohexene-N-oxide. The residue was distilled yielding 17 g bp 48-50 (4.2 Torr) of a mixture of starting material and product. This solution was again washed with 2N HCl and water. After drying (Na₂SO₄) and removing all solvents under reduced pressure, 3,3,6,6-tetramethyl-1,2-diazacyclohexene was further purified by preparative VPC (SF-96, inj. = 110°C, column = 100°C, det = 110°C): IR (CDCl₄): 2990, 1565, 1455, 1380, 1370, 1340 cm⁻¹; NMR (CDCl₃) 1.5 (s,4H), 1.3 ppm (s,12H), lit.⁶³ NMR (CDCl₃) δ 1.45 (s,4H), 1.25 ppm (s,12H).

1,1,2,2-Tetramethylcyclobutane - 0.5 g 3,3,6,6-Tetramethyl-1,2-diazacyclohexene was placed in a Pyrex seal-off tube and degassed three

times by freeze-pump-thaw cycles at less than 0.05 mm Hg. The tube was sealed invacuo and heated for 14 h at 145°C. Preparative VPC (SF-96, 50°C) yielded 0.2 g (40%) 1,1,2,2-tetramethylcyclobutane; IR (CCl₄) 3000, 1460, 1300, 1220, 860 cm⁻¹. NMR (CDCl₃) δ 1.6 (s, 4H), 0.95 ppm (s, 12H). The mass spectrum showed a parent peak of 112.125 with a base peak at 56.

5-Ethyl-5-nitrohexan-2-one - To a refluxing solution of 180 g (1.75 mole) of 2-nitrobutane⁹⁶ and 13 mls Triton B in 250 ml of ether was added 123 g (1.75 mole) methyl vinyl ketone over a three hour period. The mixture was stirred at reflux for an additional 15 hrs, cooled, and acidified with a 10% HCl solution. The ethereal layer was separated, washed twice with water, saturated sodium chloride solution, and dried (Na₂SO₄). The ethereal extracts were concentrated and distilled affording 280 g (95%) of a pale yellow oil, 5-ethyl-5-nitrohexane-2-one: bp 111-113°C at 2.5 Torr; IR (CCl₄): 2985, 1725, 1536, 1460, 1390, 1355 cm⁻¹; NMR (CDCl₃): δ 2.6-2.1 (m, 4H), 2.1-1.7 (m, 2H), 2.1 (s, 3H), 1.5 (s, 3H), 0.85 ppm (t, 3H, J=6Hz). Anal. Calcd. for C₈H₁₅NO₃: C, 55.47; H, 8.74; N, 8.08. Found: C, 55.55; H, 8.65; N, 8.04.

2,5-Dimethyl-2-Ethyl-1-Pyrroline Oxide - 5-Ethyl-5-nitrohexan-2-one (200g, 1.16 mole) and ammonium chloride (77 g, 1.45 mol) in 2 l water were heated to 65°C with mechanical stirring. Zinc dust (117 g, 2.7 mol) was added in portions over 30 min maintaining the temperature of the reaction mixture at 65-70°C. The mixture was stirred two additional hours at 65°C, cooled and filtered. The aqueous filtrate was acidified with dilute HCl, concentrated to 500 ml, made basic with

sodium hydroxide, and extracted (8x100 ml) with methylene chloride. The methylene chloride extracts were combined, dried (Na_2SO_4), and concentrated. The resulting oil was distilled affording 114 g (71%) of a pale yellow oil, 2,5-dimethyl-2-ethyl-1-pyrroline oxide: bp 77-78°C at 0.25 Torr; IR (CCl_4): 3440, 2980, 1603, 1460, 1395, 1370 cm^{-1} ; NMR (CDCl_3): δ 2.5 (t, 2H, J=8Hz), 2.0 (s, 3H), 2.1-1.5 (m, 4H), 1.4 (s, 3H), 0.85 ppm (t, 3H, J=7Hz). Anal. Calcd. for $\text{C}_8\text{H}_{15}\text{NO}$: C, 67.96; H, 10.72; N, 9.92. Found: C, 67.90; H, 10.59; N, 9.94.

1-Hydroxy-2,5-Diethyl-2,5-Dimethylpyrrolidine - To a Grignard reagent prepared in the usual way from 120 g (1.1 mol) ethyl bromide and 27 g (1.1 mol) magnesium turnings in 500 ml ether was added with mechanical stirring a solution of 100 g (0.71 mol) of 2,5-dimethyl-2-ethyl-1-pyrroline oxide in 400 ml ether at such a rate that the mixture refluxed gently. After addition was complete, the mixture was refluxed for 24 hr, cooled to 0°C and a solution of 145 g ammonium chloride in 600 ml water was added slowly. After stirring an additional 30 mins, the ether layer was separated and the aqueous layer extracted with ether. The combined ethereal extracts were dried (Na_2SO_4), concentrated, and distilled affording 50 g (52%) of a colorless oil, 1-hydroxy-2,5-diethyl-2,5-dimethylpyrrolidine: bp 83-85°C at 1.2 Torr; IR (film) 3500, 2980, 1465, 1380, 1370 cm^{-1} ; NMR (CDCl_3): δ 6.9 (s, 1H), 1.8-1.2 (m, 8H), 1.1 (s, 6H), 0.85 ppm (t, 6H, J=7Hz). Anal. Calcd. for $\text{C}_{10}\text{H}_{21}\text{NO}$: C, 70.10; H, 12.38; N, 8.17. Found: C, 70.04; H, 12.09; N, 8.16.

2,5-Diethyl-2,5-Dimethylpyrrolidine Hydrochloride - A mixture of 25 g (0.18 mol) of 1-hydroxy-2,5-diethyl-2,5-dimethylpyrrolidine and 2 g

of Raney-Nickel in 200 ml methanol was hydrogenated on a Parr rocker at 26°C and 50 lb/in² H₂. The filtered reaction mixture was acidified with ethereal hydrogen chloride and the solvent removed to give 30 g of a brownish-white crystalline precipitate. Recrystallization from isopropanol/ether yielded 28 g (95%) 2,5-diethyl-2,5-dimethylpyrrolidine hydrochloride : mp 200-205°C; IR (CCl₄): 2930, 2710, 1460, 1390 cm⁻¹; NMR (CDCl₃) δ 9.3 (s,1H); 2.2-1.8 (m,8H); 1.6 (s,6H); 1.05 ppm (t,6H). The amine hydrochloride was converted to 2,5-diethyl-2,5-dimethylpyrrolidine by dissolving in a 25% aqueous sodium hydroxide solution, extracting the resulting oil with ether, drying the ethereal extracts, and concentrating. Further purification by preparative VPC (Penwalt, 180°) afforded 2,5-diethyl-2,5-dimethylpyrrolidine (>99%): IR (film) 3350, 2915, 1460, 1378, 1370 cm⁻¹; NMR (CDCl₃) δ 1.7-1.2 (m,8H), 1.0 (s,6H), 1.8 ppm (t,6H,J=7Hz). Anal. Calcd. for C₁₀H₂₁N: C, 77.34; H, 13.63; N, 9.02. Found: C, 77.60; H, 13.58; N, 8.99.

1-Nitroso-2,5-Diethyl-2,5-Dimethylpyrrolidine - To a stirred solution of 8 g (0.044 mol) of 2,5-diethyl-2,5-dimethylpyrrolidine hydrochloride in 100 ml of water at 85°C was slowly added a solution of 15.6 g (0.23 mol) sodium nitrite in 50 ml of water. The reaction temperature was maintained at 85°C for 48 hrs during which time a yellow oil formed. The reaction mixture was cooled, 30 ml ether was added, and the layers were separated. The aqueous layer was extracted twice with ether. The combined ethereal extracts were washed with 10% HCl solution, and saturated sodium chloride solution. The ethereal extracts were dried (Na₂SO₄) and concentrated affording 7.0 g (92%) of a yellow

oil, 1-nitroso-2,5-diethyl-2,5-dimethylpyrrolidine. This was further purified by VPC (Penwalt, 220°C). IR (CCl₄): 2930, 1470, 1380, 1370 cm⁻¹; NMR (CDCl₃): δ 2.1-1.5 (m, 8H), 1.45 (s, 3H), 1.35 (s, 3H), 0.85 (t, 3H, J=8Hz), 0.75 ppm (t, 3H, J=8Hz). Anal. Calcd. for C₁₀H₂₀N₂O: C, 65.17; H, 10.94; N, 15.20. Found: C, 65.03; H, 10.91; N, 15.34.

1-Amino-2,5-Diethyl-2,5-Dimethylpyrrolidine - A slurry of 2.2g (0.05 mol) of lithium aluminum hydride in 70 ml 6:1 n-butyl ether/diethyl ether was heated under N₂ with distillation of solvent until the internal temperature reached 105°C. A solution of 5g (0.027 mole) 1-nitroso-2,5-diethyl-2,5-dimethylpyrrolidine in 20 ml n-butyl ether was then cautiously added over one hour never allowing the temperature to rise above 110°C. The temperature was maintained at 95°C for an additional four hours, the reaction mixture cooled to 0°C, and hydrolyzed by careful addition of a large excess of water. The layers were separated and the aqueous layer was extracted twice with ether. The combined organic extracts were extracted three times with 10% HCl solution. The combined acid extracts were made strongly basic with 20% sodium hydroxide solution and were extracted three times with ether. The ethereal extracts were combined and washed with saturated sodium chloride solution. The ethereal extracts were dried (Na₂SO₄) and concentrated affording a colorless oil. This oil was further purified by distillation under reduced pressure at 25°C, followed by preparative VPC (Penwalt, 180°C) affording 3 g (45%) 1-amino-2,5-diethyl-2,5-dimethylpyrrolidine : IR (CCl₄): 3350, 3230, 2970, 1460, 1380, 1365 cm⁻¹; NMR (CDCl₃): δ 2.65 (s, 2H), 1.70-1.20 (m, 8H), 1.0 (s, 6H), 0.85 ppm (t, 3H, J=8Hz). This hydrazine is air sensitive. Benzamide: Anal.

Calcd. for $C_{17}H_{26}N_2O$: C, 74.41; H, 9.55; N, 10.02. Found: C, 74.67; H, 9.32; N, 9.96.

1,1'-Azo-2,5-Diethyl-2,5-Dimethylpyrrolidine - 1-Amino-2,5-diethyl-2,5-dimethylpyrrolidine (250 mg, 0.74 mmol) was stirred under an oxygen atmosphere for 24 hrs. The resulting colorless oil was warmed at 40°C at 0.05 Torr for 24 hr to yield 42 mg (17%) of a white crystalline solid; mp 47-49°C; IR (film) 2960, 1465, 1378, 1367 cm^{-1} ; NMR (CDCl_3): 1.9-1.25 (m, 8H) 1.15 (s, 6H), 0.75 ppm (t, 6H, $J=7\text{Hz}$); UV (2,2,5-trimethylpentane) 303 (9780), 254 nm (2130). Anal. Calcd. for $C_{20}H_{40}N_4$: C, 71.35; H, 12.0; N, 16.64. Found: C, 71.39; H, 11.86; N, 16.65.

d,l-1-Amino-2,5-Diethyl-2,5-Dimethylpyrrolidine - The crude amine hydrochloride was recrystallized from isopropanol (-20°C) to separate the meso and d,l isomers. In a typical experiment, 70 g of the amine hydrochloride was dissolved in 400 ml isopropanol. Approximately 35 g of d,l enriched amine hydrochloride crystallized out after 12 h at -20°C. Recrystallization was repeated eight times until the d,l isomer was obtained in 97% isomeric purity (the d,l and meso isomers are distinguishable by 500 MHz ^1H NMR). The d,l-2,5-diethyl-2,5-dimethylpyrrolidine hydrochloride was converted to d,l-1-amino-2,5-diethyl-2,5-dimethylpyrrolidine by the methods described above. Capillary VPC (Carbowax 20M, 60°C) indicated the hydrazine was 97% d,l, 3% meso.

Resolution of d,l-2,5-Diethyl-2,5-Dimethylpyrrolidine - The d,l amine hydrochloride was converted to the amine by methods described above and purified by preparative VPC (Pennwalt, 160°C). Addition of

1 g of pure amine to a refluxing solution of 1.1 g d-tartaric acid, (7.3 mmol), in 15 ml isopropanol gave on prolonged cooling 1 g of white precipitate. A second recrystallization yielded approximately 0.5 g of crystals. These crystals were dissolved in 10 ml of 20% aqueous potassium hydroxide and extracted with three 10 ml portions of ether. The ether solution was then dried (Na_2SO_4) and concentrated. The amine was collected by VPC (Penwalt, 160°C). A methanolic solution of the amine hydrochloride was obtained by titrating the amine with hydrogen chloride. The amine hydrochloride had the following rotations ($[\alpha]_{365}^{20} = 4.80$, $[\alpha]_{589}^{20} = 0.78$ ($c = 0.39$, methanol). The assignment of the d,l isomer was confirmed by reaction of racemic d,l-1-amino-3,5-diethyl-2,5-dimethylpyrrolidine with (+)-methoxy- α -trifluorophenylacetyl chloride by the method of Dale and Mosher.⁹⁸ ¹⁹F NMR revealed two singlets separated by 12 Hz centered at -69.5 ppm (relative to CFCl_3) corresponding to the diastereomeric trifluoromethyl groups.

trans-1,2-Divinyl-1,2-Dimethylcyclobutane - 100 g Freshly distilled isoprene was placed in a Pyrex seal-off tube with 12 g of benzophenone and degassed twice by freeze-pump-thaw cycles at 0.05 mm Hg. The tube was sealed in vacuo and irradiated for 120 h with a 450 watt Hanovia medium pressure lamp. Distillation of the resulting solution at 4 Torr (bp 28-45°C) gave 50 g of product containing about 20% trans-1,2,-divinyl-1,2-dimethylcyclobutane, VPC, (Carbowax; 90°C). The isomers were separated by distillation through a teflon spinning band column at 16 Torr. Five fractions were collected, the first two coming off at 41°, the last three which showed impurities due to higher

boiling isomers distilled at 42-44°C. The first two fractions were used in the next step (99% purity - 1.0 g); IR (CCl₄): 3150, 3025, 1645, 1460, 910, 680 cm⁻¹. NMR (CDCl₃) δ 6.1-4.7 (m,6H); 2.3-1.3 (m,4H); 1.0 ppm (s,6H).

trans-1,2-Diethyl-1,2-Dimethylcyclobutane - A solution of 1 g trans-1,2-divinyl-1,2-dimethylcyclobutane in 60 ml glacial acetic acid was hydrogenated at 25°C at atmospheric pressure in the presence of 0.1 g platinum oxide. The solution was diluted with water and extracted with pentane. The combined pentane extracts were washed with water, dried (Na₂SO₄) and concentrated. The resulting oil was purified by VPC (SF-95; 120°C) yielding 0.8 g (80%) of trans-1,2-diethyl-1,2-dimethylcyclobutane which was shown by proton NMR and by IR to be identical with trans-1,2-diethyl-1,2-dimethylcyclobutane reported by Bartlett and Porter.⁹² IR (film) 2990, 1460, 1365 cm⁻¹. NMR (CCl₄) δ 1.7-1.2 (m,8H), 1.02 (s,6H), 0.9-0.6 ppm (t,6H,J=8Hz).

1-Bromo-3-methylpentane - 25 g (0.24 mole) 3-Methylpentan-1-ol was cooled under N₂ to 0°C and 28 g (0.1 mole) phosphorous tribromide was slowly added with stirring at such a rate as to keep the temperature below 0°C. After addition was complete, the cooling bath was removed and the solution was allowed to stand overnight at room temperature. Crude product was distilled from the flask (55° at 200 Torr). The distillate was cooled to 0°C, washed with cold concentrated sulfuric acid, washed with anhydrous potassium carbonate, and redistilled affording 47 g (75%) of a colorless oil 1-bromo-3-methylpentane: bp 88-90°C at 758 mm (lit. 88.5-90.5°C at 756 mm);¹⁰⁶ NMR (CDCl₃) δ 3.4 (t,2H,J=7Hz), 1.8-1.0 (m,5H), 1.8 ppm (m,6H).

3,6-Dimethyl-octan-3-ol - To a Grignard solution prepared in the usual way from 25 g (0.15 mole) 1-bromo-3-methylpentane and 3.6 g (0.15 mole) magnesium turnings in 80 ml anhydrous ether was added with stirring 11 g (0.15 mole) 2-butanone in 10 ml ether at such a rate that the mixture refluxed gently. After addition was complete, the solution was allowed to stir an additional 30 min and hydrolyzed by pouring it into 50 ml of cracked ice and 10 g ammonium chloride in 20 ml water. The ether layer was separated and the aqueous layer extracted with ether. The combined ethereal extracts were dried (Na_2SO_4), concentrated, and distilled affording 30 g (67%) of a colorless oil, 3,6-dimethyl-octan-3-ol: bp $87-88^\circ\text{C}$ at 10 Torr; (lit. bp 195°C , 760 Torr).¹⁰⁷ NMR (CDCl_3) δ 1.7-1.2 (m, 10H), 1.2 (s, 3H), 1.10-0.8 ppm (m, 9H).

3,6-Dimethyl-2-octene, 3,6-Dimethyl-3-octene, and 2-Ethyl-5-methyl-1-heptene - 30 g 3,6-Dimethyloctan-3-ol and 10 ml 85% phosphoric acid were mixed and the solution heated at reduced pressure (100 Torr) with distillation until the stillhead temperature reached 80°C . The distillate was washed with 20 ml saturated sodium chloride, and dried (MgSO_4). Preparative VPC (Carbowax 20M, 100°C) afforded a mixture of cis and trans-3,6-dimethyl-2-octene and a mixture of cis and trans-3,6-dimethyl-3-octene; cis and trans-3,6-dimethyl-2-octene: IR (CCl_4) 2960, 1682, 1475, 1380, 820 cm^{-1} ; NMR (CDCl_3) δ 5.2 (m, 1H), 2.9 (m, 2H), 1.55 (s, 3H), 1.50 (m, 3H), 1.25 (m, 5H), 0.8 ppm (m, 6H); cis and trans-3,6-dimethyl-3-octene: IR (CCl_4) 2960, 1680, 1460, 1380, 825 cm^{-1} ; NMR (CDCl_3) δ 5.1 (m, 1H), 1.9 (m, 4H), 1.6 (s, 3H), 1.25 (m, 3H), 0.9 ppm (m, 9H). 2-Ethyl-5-methyl-1-heptene was made via an alternate route.

To a Grignard made in the usual manner from 90 g (1 mole) 2-chlorobutane and 23 g (1 mole) magnesium turnings in 300 ml ether was slowly added 28 g (0.33 mole) ethyl vinyl ketone in 200 ml ether with stirring. 1 g of cuprous chloride was added in 7 portions during the addition of the ketone. After 2 h this mixture was added to 600 ml of 15% aqueous HCl and extracted with ether. The combined ether extracts were washed with saturated sodium bicarbonate solution, water, and dried (Na_2SO_4). The product was then added dropwise to methylene triphenylphosphorane in 200 ml Et_2O prepared in the usual manner from 35.7 g triphenylmethylphosphonium bromide. The solution turned colorless and a white precipitate formed. The mixture was refluxed 12 h, cooled, filtered, and the precipitate washed with ether. The combined ether extracts were dried (Na_2SO_4), concentrated, and purified by VPC (Carbowax 20M, 100°C): IR (CCl_4) 2980, 1652, 1480, 1385, 1370, 890 cm^{-1} . NMR (CDCl_3) δ 4.65 (s, 2H), 1.9 (m, 4H), 1.3 (m, 6H), 0.95 ppm (m, 9H). An equimolar mixture of the $\text{C}_{10}\text{H}_{20}$ isomers was submitted for elemental analysis. Anal. calcd. for $\text{C}_{10}\text{H}_{20}$: C, 85.60; H, 14.39. Found: C, 85.67; H, 14.21. Hydrogenation of this mixture (Pt/H_2 , 1 atm, 25°C) yielded one alkane by VPC (SE-96, 100°C); NMR (CDCl_3) 1.5-1.0 (m, 10H), 0.85 ppm (m, 12H). Relative retention times of 3,6-dimethyl-2-octene, 3,6-dimethyl-3-octene, and 2-ethyl-6-methyl-1-heptene (SE-54, 35°C) by capillary VPC are 7.44, 7.88, and 8.69, respectively.

2,2,5,5-Tetramethylsulfolane - 10 g (0.09 mole) 2,5-Dimethyl-2,4-hexadiene, 100 mg pyrogallol, 100 mg n-butylammonium perchlorate, and 15 ml ether were placed in a Pyrex seal-off tube. 36 g of SO_2 was

added under nitrogen at -78°C and the solution was then degassed three times by freeze-pump-thaw cycles at 0.05 mm Hg. The tube was sealed in vacuo and heated for 12 h at 100°C . The tubes were opened and the crude product purified by column chromatography (silica gel, benzene).

Removal of solvent yielded 3.1 g (20%) of a colorless oil. This oil was added to 50 ml ethyl acetate and 100 mg of platinum oxide and hydrogenated on a Parr rocker at 50 lb/in² at room temperature.

Filtration, followed by removal of solvent afforded a yellow oil that was further purified by VPC (SF-96; 240°C) yielding 2 g (overall 13%) 2,2,5,5-tetramethylsulfolane: IR (CCl_4) 2960, 1460, 1310, 1250, 1130, 1115 cm^{-1} ; NMR (CDCl_3) δ 2.6-1.9 (m, 4H), 1.2-0.9 ppm (m, 12H); the parent peak in a high resolution mass spectrum was 176.087 with a base peak of 112.

Preparation of Nickel Peroxide (NiO_x)⁵⁸

To 65 g nickelous sulfate in 180 ml water was added dropwise with stirring a solution of 21 g sodium hydroxide in 180 ml 5% sodium hypochlorite solution. This solution was stirred for 20 min, filtered, the black solid was washed with water, and dried at reduced pressure in a dessicator. The black NiO_x was then stirred for 20 min in 150 ml 5% sodium hypochlorite, filtered, washed exhaustively with water and dried in a dessicator. Nickel peroxide prepared in this manner had an activity of 4.0×10^{-3} g atom of oxygen/g of nickel peroxide.

General Procedure for Generation and Purification of 1,1-Diazenes

All apparatus must be base-washed and thoroughly dried. Into an argon purged 25 ml flask was placed 1.75 mmol of the appropriate 1,1-dialkylhydrazine. The flask was cooled to -78°C , 12-15 ml of dry

methyl ether was added, followed by 1.25 mmol triethylamine. With rapid stirring, 1.6 mmol *t*-butylhypochlorite was added dropwise over 15 min down the side of the cooled flask. Color appeared almost immediately and was fully developed within 10 mins. The reaction mixture was stirred one hour at -78°C and then transferred via 18 gauge teflon tubing to an argon purged jacketed filter funnel precooled to -78°C . The mixture was filtered under vacuum into a 25 ml three neck flask precooled to -78°C and equipped with serum cap and gas inlet tube. The solution was then concentrated to 2-3 ml for chromatography.

Deactivated alumina was prepared by washing 150g of Woelm Activity I neutral alumina three times with 150 ml 20% sodium hydroxide solution and decanting. After washing three times with 150 ml distilled water, the alumina was washed three times with methanol and dried 12 hrs at 350°C .

A jacketed low temperature chromatography column was equipped with a 200 ml three neck round bottom flask (with serum cap, gas inlet and 3-5g potassium carbonate). The column was charged with 30g deactivated basic alumina and capped. After purging the column with argon, the jacket was filled with acetone and cooled to -88°C by addition of liquid nitrogen with stirring. The column was wetted and rinsed through with 40 ml of dry propane (cooled to -78°C), added by means of a double ended needle. The concentrated 1,1-diazene solution was carefully placed on the column via a double-ended needle and allowed to percolate onto the adsorbent. Elution was begun with 2:3 dimethyl ether/propane using a positive pressure of argon at the column head to maintain a drip rate of 1-2 drops/sec. When the colored band reached

the bottom of the column, elution was halted by releasing the argon pressure. The collection flask was opened to a positive argon pressure and the forerun withdrawn via a double-ended needle into an evacuated flask cooled to -78°C . Elution was resumed until two-thirds of the colored band had been collected. This colored solution was drawn off into a precooled (-78°C), argon purged 100 ml round bottom flask equipped with serum cap argon/vacuum inlet, 3-5 mls solvent and 3-5g potassium carbonate. The propane/methyl ether was then removed under reduced pressure and argon admitted to the flask, leaving a concentrated diazene solution. This procedure afforded 1,1-diazenes 3 and 26 with $\leq 2\%$ tetrazene and small amounts of dimethyl ether. 1,1-Diazene 2 contained 20-40% amino-2,2,6,6-tetramethylpiperidine, 5-10% tetrazene and small amounts of dimethyl ether. Not all chromatographies gave consistent results, therefore aliquots of all samples were checked by low temperature ^1H NMR (-60°C) prior to use.

Generation of the 1,1-Diazene with Nickel Peroxide - To 20 ml anhydrous dimethyl ether, cooled to -78°C , was added 1.75 mmol of the appropriate hydrazine via syringe. To this solution, was added, with vigorous stirring, 2g nickel peroxide through a solid addition funnel. The reaction mixture was stirred at -78°C for 1 h and purified as described above. 1,1-Diazene generated in this manner has a half life of 48 h at -78°C .

Spectroscopy

Visible Absorption Spectroscopy - Typically 0.6-1.5 mmol of the appropriate hydrazine was oxidized with *t*-butyl hypochlorite in the manner described above. The solution was filtered at -78°C through a

jacketed frit into 4-6 ml of the desired precooled solvent and concentrated. Dry argon was admitted to the flask and 1,1-diazene solution was drawn into a low temperature UV-VIS cell (-78°C) and the spectrum recorded at -78°C.

Infrared Spectroscopy - Typically 0.6-1.5 mmol of the appropriate hydrazine was oxidized with *t*-butyl hypochlorite as described above. The resulting solution was filtered at -78°C through a jacketed frit and then concentrated into 2 ml of spectrograde dichloromethane which had been previously passed through a short column of basic alumina. Dry argon was admitted to the flask, the sample was drawn into a low temperature IR cell (-78°C), and the spectrum recorded at -78°C. The sample was then removed from the cell, allowed to decolorize at 25°C, recooled to -78°C, drawn into the cell and the spectrum recorded.

Determination of the Extinction Coefficient - Approximately 1.5 mmoles of the appropriate hydrazine was oxidized and purified by low temperature chromatography. The resulting solution was concentrated in 3 ml of deuteriochloroform. The flask was flushed with dry argon and the solution transferred via teflon tubing to a graduated test tube at -78°C. To 1.6 ml of this solution was added 25.4 mg of dichloromethane. The concentration of 1,1-diazene was determined by proton NMR analysis at -78°C. To the remaining 1.4 ml of this solution was added sufficient dry ethyl ether to give a volume of 4.5 ml. The visible absorption spectrum of this solution then allowed calculation of the molar extinction coefficient.

Nuclear Magnetic Resonance Spectroscopy - Approximately 1.5 mmol

of the appropriate hydrazine was oxidized and the resulting solution purified by low temperature chromatography and concentrated into 5 ml of deuteriochloroform which had previously been passed through a short column of basic alumina. Dry argon was admitted to the flask and the 1,1-diazene solution transferred to a capped graduated test tube at -78°C . Dichloromethane was then added to this solution as an internal standard. The 1,1-diazene solutions were frozen in liquid N_2 until use, at which time approximately 0.3 ml of the thawed solutions were transferred via 18 gauge teflon tubing under positive argon pressure into 5 mm NMR tubes (-78°C) equipped with serum caps. Spectra were recorded on either a Varian EM-390 or Jeol FX-90 NMR spectrometer at -60°C .

Unimolecular Decomposition Kinetics - Solutions for studying the decomposition kinetics of the 1,1-diazenes were prepared in the following manner. Typically 200 mg of the hydrazine was oxidized and the resulting solution purified by low temperature chromatography and concentrated in 25-50 ml of freshly distilled ethyl ether, n-hexane, or tetrahydrofuran chilled to -78°C and containing $50\ \mu\text{l}$ of triethylamine. Kinetic measurements were done in a low temperature spectroscopic cell with temperature determined to the nearest 0.2°C by means of an iron constantan thermocouple embedded in the cell body. The cell was cooled by circulating methanol from a low temperature circulating bath through the cell's coolant well.⁶² The outer cell windows were wrapped with heating tape in order to prevent water condensation during extended kinetic runs. A typical kinetics run was carried out in the following manner: the spectroscopic cell was flushed four times and filled with

freshly distilled solvent. The cell was cooled to the desired temperature, solvent expelled with an argon filled syringe and the chromatographed 1,1-diazene then drawn into the cell. The absorbance of 3 was monitored at 497 nm as a function of time. All data prior to temperature equilibration were discarded. Typically the reaction was followed through 10 half lives and the reported rate constants are derived by conventional linear least squares analysis. In order to confirm a first order process, rate constants for 1,1-diazene decompositions were determined for two different concentrations and in all cases the values were identical within experimental error.

Bimolecular Decomposition Kinetics - Solutions for studying the decomposition kinetics were prepared in the following manner. 500 mg of the hydrazine was oxidized and purified by low temperature chromatography and concentrated in approximately 2.5 ml of deuteriochloroform which had been passed through a short column of basic alumina. The concentrated solution was transferred via 18 gauge teflon tubing to a graduate test tube at -78°C . 25 Mg of triethylamine and 25 mg of dichloromethane were added as an internal standard. Approximately 0.3 ml of the 1,1-diazene solution was transferred into a base washed argon purged NMR tube at -78°C . The tube was then transferred to a precooled Jeol FX-90 NMR probe and after a five minute equilibration period data collection was begun. Disappearance of 1,1-diazenes 2 and 3 was monitored by integrating the 2.15 and 2.32 peaks, respectively, relative to the methylene protons of triethylamine at discrete time intervals preprogrammed into a kinetics program on the Jeol FX-90 NMR spectrometer. The triethylamine concentration could be calculated and

agreed with an independent measurement relative to the second dichloromethane standard. The reported rate constants are derived by conventional linear least squares analysis. Temperatures were calibrated by measuring methanol chemical shift vs. temperature.

Emission Spectroscopy and Determination of Photochemical Parameters

Approximately 1.5 mmol of the appropriate hydrazine was oxidized, filtered, chromatographed, and concentrated into 5-10 mls of solvent. Dry argon was admitted to the flask and 0.3 ml of the 1,1-diazene solution transferred via 18 guage teflon tubing into an argon purged 5 mm NMR tube precooled to -78°C . For emission spectroscopy, the sample tubes were then placed in a jacketed liquid nitrogen dewar at -196°C and the spectra were recorded using a noncommercial spectrophotometer in Professor H.B. Gray's group at Caltech. Excitation wavelength was 520 nm, using a 250 watt mercury-xenon source and Hamamatsu R406 PMT. Response factors for the R406 PMT are 0.775 (500 nm), 0.835 (550 nm), 0.82 (600 nm), 0.785 (650 nm), 0.76 (700 nm), 0.58 (750 nm), 0.440 (800 nm), 0.325 (860 nm), and 0.235 (900 nm). No emission (phosphorescence) was present other than fluorescence from 500 to 1100 nm (R406). Saturated azulene and benzophenone solutions of 3 at -78°C were prepared by transferring 3 into NMR tubes containing an excess of sensitizer. Emission spectroscopy of these solutions at -196°C again revealed no emission signals from 600 nm to 1100 nm (R406) other than fluorescence. Samples for quantum yield determinations were prepared by dilution of a degassed chromatographed solution of 1,1-diazene (CFCl_3) 1/10 in the appropriate degassed solvent (argon purged). Concentrations were determined by

measuring the absorbance of 4 ml aliquots of 1,1-diazene solutions. Fluorescence quantum yields in 2-methyltetrahydrofuran were determined at -196°C by comparing the corrected integrated emission band of the 1,1-diazene with that of rubrene ($\phi_f=1$),⁸⁰ using an excitation wavelength of 480 nm. All other ϕ_f were determined relative to 3 in 2-methyltetrahydrofuran. Lifetimes of similarly prepared 1,1-diazene solutions were measured by the single photon counting technique using a noncommercial instrument made available by Professor A. Zewail's group at Caltech. We are grateful to William Lambert for assistance in these experiments.

Samples for ESR experiments were prepared as described above using both 2-methyltetrahydrofuran and cyclohexane as solvents. Solutions of 1,1-diazene (0.05 M) and 1,1-diazene (0.05 M) saturated with either azulene or benzophenone were irradiated at 10°K and 88°K with a 250 W mercury-xenon lamp filtered through water and Pyrex (9.234 GHz). The only feature in the spectrum is a strong doublet absorption at 3300g which increases with time, presumably due to tetrazene decomposition. Solutions of tetrazene under the same conditions yield the same result.

Samples for determination of ϕ_D were prepared as described above and introduced into the precooled (-78°C) low temperature UV-VIS cell. The absorbance spectrum was then recorded. The cell was then irradiated with a 1000-W xenon lamp using water, Pyrex, and Corning filters CS3-70 and CS4-96. Transmitted light and incident light were measured using a Scientech laser Power Meter (Model 360001). Initial concentrations of 1,1-diazene were 0.05-0.1M and photolyses were carried out to 5%

conversion as determined by absorbance spectra. ϕ_D for 2,3-diazabicyclo[2.2.1]hept-2-ene determined by this method is 0.9, close to the literature value of 1.0.⁶⁶

Products from the Thermal Decompositions of 1,1-Diazenes 3 and 26

The appropriate hydrazine (1.5 mm) was oxidized with t-butyl hypochlorite, filtered, chromatographed, and concentrated in 3 ml of solvent containing 50 μ l of $CDCl_3$. The solution was then transferred via a double-ended needle to a graduated test tube sealed with a serum cap. Approximately 0.3 ml of this solution was transferred to an NMR tube ($-78^\circ C$) containing 50 μ l of CD_2Cl_2 . The concentration of 1,1-diazene was determined by low temperature 1H -NMR (0.01-0.05 M). The sample was then pyrolyzed at $0^\circ C$, $-10^\circ C$, or $-20^\circ C$, recooled and analyzed by 1H -NMR. The only thermolysis products were hydrocarbons and tetrazene. 150 μ l aliquots of the remaining stock solution were placed in 5 mm x 100 mm basewashed Pyrex tubes (capped with serum caps, thoroughly flushed with dry nitrogen, and precooled to $-78^\circ C$). The samples were pyrolyzed at the appropriate temperature until completely decolorized, cooled to $-78^\circ C$, and analyzed by VPC with a precooled syringe. Four hydrocarbon products were found when 3 was decomposed. Relative retention times the decomposition products are (Carbowax 400, $25^\circ C$): 2-methylpropene (1.0), 1,1,2,2-tetramethylcyclobutane (3.0), 2,5-dimethyl-1-hexene (4.71), and 2,5-dimethyl-2-hexene (4.85). Typical yields were 20-30%. The 1,2-diazene 25 was shown to be absent by comparison with authentic material (SF 96, $110^\circ C$). 2-Methyl-1-propene was identified by coinjection of an authentic sample (Matheson). Preparative VPC ($\beta\beta$, $30^\circ C$) afforded a sample whose NMR was identical to

authentic 2-methyl-1-propene: NMR (CDCl_3) 4.75 (s, 2H), 1.8 ppm (m, 6H). Tetramethylcyclobutane was also identified by coinjection of an authentic sample. Preparative VPC (Carbowax 400, 30°C) afforded a sample whose NMR was identical to authentic tetramethylcyclobutane: NMR (CDCl_3) δ 1.6 (s, 4H), 0.95 ppm (s, 12H). 2,5-Dimethyl-1-hexene and 2,5-dimethyl-2-hexene were identified by coinjection with authentic materials (Chemsampco).

Seven products were found when 1,1-diazene **26** (65% d,l 35% meso) was decomposed thermally or photochemically in CFCl_3 . Relative retention times for the hydrocarbon products by capillary (SE 54, 30°C) VPC are 2-methylbutene (0.63), trans-1,2-diethyl-1,2-dimethylcyclobutane (6.35), cis-1,2-diethyl-1,2-dimethylcyclobutane (6.60), cis and trans-3,6-dimethyl-3-octene/2-ethyl-5-methyl-1-heptene (7.44, 7.48), and cis and trans-3,6-dimethyl-2-octene (9.30). The 2-methylbutene/(trans + cis-1,2-diethyl-1,2-dimethylcyclobutane) ratio was determined independently by 0.125 in. analytical VPC (Carbowax 400, 80°C). 2-Methyl-1-butene was identified by coinjection of an authentic sample (Matheson). Preparative VPC (β 30°C) afforded a sample whose NMR was identical to that of authentic 2-methyl-1-butene (Matheson). NMR (CDCl_3): δ 4.7 (s, 2H), 2.0 (m, 2H) 1.7 (s, 3H), 1.05 ppm (t, 3H). cis- and trans-1,2-Diethyl-1,2-dimethyl cyclobutanes eluted as one peak on a 0.125 in. Carbowax 400 column (80°C). The retention time was identical to that of an authentic sample of trans-1,2-diethyl-1,2-dimethyl cyclobutane. Preparative VPC (SF-96, 80°C) revealed the presence of both cis and trans isomers by comparison of NMR to literature values,⁹² NMR (CCL_4): δ 1.7 -1.2 (m, 8H), 1.02 (s, trans, 6H),

0.98 (s,cis,6H), 0.75 ppm (t,6H,J=7Hz). The mass spectrum reveals a parent peak at 140.15 with a base peak, $m/e=70$. The cis and trans cyclobutanes could be separated on a 30 meter SE-54 fused silica capillary VPC column (35°C). Assignment of stereochemistry was made by coinjection of authentic trans-1,2-diethyl-1,2-dimethylcyclobutane. Cis and trans-3,6-Dimethyl-3-octene and 2-ethyl-5-methyl-1-heptene eluted together on a 0.125 in. Carbowax 20M column (80°C). Preparative VPC (Carbowax 20M, 100°C) revealed the presence of 38 and 39 and were identified by comparison of the NMR spectra to authentic samples. 3,6-Dimethyl-2-octene 40 was separable from 38 and 39 and identified by comparison of the NMR spectrum to authentic material. The alkenes could not be further separated by capillary VPC on either 30M SE-54 or 50M Carbowax. Coinjection techniques on 30M SE-54 verified the assignments of these alkenes. 38, 39 and 40 eluted as one peak on SF-96 (100°C) affording a sample whose elemental agreed with the formula $C_{10}H_{20}$. Anal. Calcd. for $C_{10}H_{20}$: C, 85.60; H, 14.39. Found: C, 85.67; H, 14.21. Hydrogenation of this mixture in a manner similar to that described for trans-1,2-divinyl-1,2-dimethylcyclobutane yielded one alkane (SF-96, 120°C) NMR ($CDCl_3$): δ 1.5-1.0 (m,10H), 0.85 ppm (m,12H). Tetrazene was identified by 1H -NMR.

Photodecompositions of 1,1- and 1,2-Diazenes - A degassed chromatographed solution of the appropriate 1,1- or 1,2-diazene (0.02-0.05 M, $CFCl_3$) was sealed in base-washed, argon purged, precooled (-78°C) 5 mm NMR tubes. Sensitizers (0.02-0.05 M final concentration) were added to the tubes before addition of 1,1-diazene. In all photochemical decompositions two identical samples were prepared, one

was photolyzed at -78°C and the other remained in the dark at -78°C . ^1H NMR spectra (-60°C) were taken before and after photolysis to insure that all decomposition of diazene arose from photolysis. In addition, the 1,1-diazenees were shown to be stable to partial photodecomposition. Photolyses were carried out at -78°C (hexane, dry ice) in an evacuated quartz dewar. For direct photolyses of 1,1-diazene 3 and 26 a water filter, Pyrex filter and two Corning glass filters CS-370 and CS4-96 were used (466-610 nm). For sensitized photolyses of 3 and 26, a water filter, Pyrex filter, and Corning glass filter CS2-59 (>608 nm) were used. For direct studies on 1,1-diazene 2, Corning filter CS-251 was used. For sensitized photolysis, 3 and 26 were irradiated in the absence of azulene at >608 nm and shown to be photostable. All solutions were photolyzed with a 1000 W xenon arc lamp until the diazene had completely decomposed. Tetrazene/hydrocarbon ratios were determined by ^1H NMR (-60°C). Hydrocarbon ratios were determined by a combination of 0.125 analytical VPC and capillary VPC. Solutions of 1,2-diazene (0.02 M) were degassed by three freeze pump thaw cycles in 5 mm NMR tubes and sealed. Photolysis were carried out at -78°C (hexane/dry ice) in an evacuated quartz dewar using a water filter, Pyrex filter, and WF-335 Schott filter (>330 nm). Photolysis were halted at approximately 50% completion and analyzed in a manner identical to that of 3. Triplet sensitized photolyses were done in an identical manner using 0.05M thioxanthone as a sensitizer. Solvents are listed in text.

References

1. For reviews of 1,1-diazenes, see: (a) Lemal, D.M. in "Nitrenes," Lwowski, W., ed., Interscience, New York, N.Y., 1970, Chapter 10; (b) Ioffe, B.V.; Kuznetsov, M.A. Russ. Chem. Rev., **1972**, 41, 131; (c) Lwowski, W. in "Reactive Intermediates," Jones, M. and Moss, R. eds., Wiley, New York, N.Y. 1978, Chapter 6; (d) Lwowski, W. in "Reactive Intermediates," Vol. 2, Jones, M.; Moss, R., eds., Wiley, New York, 1981.
2. (a) Hinsberg, W.D.; Dervan, P.B. J. Am. Chem. Soc. **1978**, 100, 1608; (b) Hinsberg, W.D.; Dervan, P.B. J. Am. Chem. Soc. **1979**, 101, 6142.
3. (a) Schultz, P.G.; Dervan, P.B. J. Am. Chem. Soc. **1980**, 102, 878; (b) Schultz, P.G.; Dervan, P.B. J. Am. Chem. Soc. **1981**, 103, 1563; (c) Hinsberg, W.D.; Schultz, P.G.; Dervan, P.B. J. Am. Chem. Soc. **1982**, 104, 766; (d) Schultz, P.G.; Dervan, P.B. J. Am. Chem. Soc. **1982**, 104, 6660.
4. Parsons, C.A.; Dykstra, C.E. J. Chem. Phys. **1979**, 71, 3025.
5. Casewit, C.; Goddard, W.A. J. Am. Chem. Soc. **1980**, 102, 4057.
6. Lehn, J.M.; Munsch, B. Theoret. Chim. Acta. **1978**, 12, 91.
7. Schaad, L.J.; Kinser, H.B. J. Phys. Chem. **1969**, 73, 1901.
8. Wong, D.P.; Fink, W.H.; Allen, L.C. J. Chem. Phys. **1970**, 52, 6291.
9. Radom, L.; Hehre, W.J.; Pople, J.A. J. Am. Chem. Soc. **1971**, 93, 289.
10. Baird, N.C.; Swenson, J.R. Can. J. Chem. **1969**, 51, 3097.
11. Hariharan, P.C.; Pople, J.A. Theoret. Chim. Acta. **1973**, 28, 213.

12. Baird, N.C.; Barr, R.F. Can. J. Chem. **1973**, 51, 3303.
13. Wagniere, G. Theoret. Chim. Acta. **1973**, 31, 269.
14. Merenyi, G.; Wettermark, G.; Roos, B. Chem. Phys. **1978**, 1, 340.
15. Vasadevan, K.; Peyerimhoff, S.D.; Buenker, R.J.; Kammer, W.E. Chem. Phys. **1975**, 7, 187.
16. Winter, N.W.; Pitzer, R.M. J. Chem. Phys. **1975**, 62, 1269.
17. Ahlrichs, R.; Staemmler, V. Chem. Phys. Lett. **1976**, 37, 77.
18. Howell, J.M.; Kirschenbaum, L.J. J. Am. Chem. Soc. **1976**, 98, 877.
19. Camp, R.N.; Epstein, I.R.; Steel, C. J. Am. Chem. Soc. **1977**, 99, 2453.
20. Cimiraglia, R.; Riera, J.M.; Tomasi, J. Theoret. Chim. Acta. **1977**, 46, 22.
21. Peric, M.; Buenker, R.J.; Peyerimhoff, S.D. Can. J. Chem. **1977**, 55, 1533.
22. Shanke, P.N. Chem. Phys. Lett. **1977**, 47, 259.
23. Baird, N.D.; Wernette, D.A. Can. J. Chem. **1977**, 55, 350.
24. Davis, J.H.; Goddard, W.A. J. Am. Chem. Soc. **1977**, 99, 7111.
25. Pople, J.A.; Krishnan, R.; Schlegel, H.B.; Binkley, J.S. Int. J. Quant. Chem. **1978**, 14, 545.
26. Talaty, E.R.; Schwartz, A.K.; Simons, G. J. Am. Chem. Soc. **1975**, 97, 972.
27. Ditchfield, R.; Del Bene, J.E.; Pople, J.A. J. Am. Chem. Soc. **1972**, 94, 703.
28. Lathon, W.A.; Curtiss, L.A.; Hehre, W.J.; Lisle, J.B.; Pople, J.A. Prog. Phys. Org. Chem. **1974**, 11, 175.

29. Pasto, D.J.; Chipman, D.M. J. Am. Chem. Soc. **1979**, 101, 2290.
30. Carlotti, M.; Johns, J.W.C.; Tromfetti, A. Can. J. Phys. **1974**, 52, 340.
31. Swalen, J.D.; Ibers, J.A. J. Chem. Phys. **1962**, 36, 914.
32. "JANAF Thermochemical Tables", NSRDS-NBS-37 U.S. Government Printing Office, Washington, D.C., 1970.
33. (a) Benson, S.W. Thermochemical Kinetics," 2nd ed., Wiley, New York, N.Y. 1976; (b) Benson, S.W.; O'Neal, H.E. "Kinetic Data on Gas Phase Unimolecular Reactions," HSRDS-NBS No. 21, 1970, p. 448.
34. Benson, S.W.; O'Neal, H.E. Natl. Stand. Ref. Data Ser., Natl. Bur. Stand. **1979**, 21, 31.
35. Foner, S.N.; Hudson, R.L. J. Chem. Phys. **1978**, 68, 3162.
36. For example, Baumgarten, H.E.; Wittman, W.F.; Lehmann, G.J. J. Heteroc. Chem. **1969**, 6, 333.
37. For example, Bhatnagar, I.; George, M.V. J. Org. Chem. **1968**, 33, 2407.
38. For example, Atkinson, R.S.; Rees, C.W. Chem. Comm. **1967**, 1230.
39. For example, Urry, W.H.; Kruse, H.W.; McBride, W.R. J. Am. Chem. Soc. **1957**, 79, 6568.
40. For example, Overberger, C.G.; Lombardino, J.G.; Hiskey, R.G. J. Am. Chem. Soc. **1957**, 79, 6430.
41. For example (a) Carpino, I.A. J. Am. Chem. Soc. **1957**, 79, 4427; (b) Lemal, D.M.; Rave, T.W.; McGregor, S.D. J. Am. Chem. Soc. **1964**, 86, 2395; (c) Dervan, P.B.; Uyehara, T. J. Am. Chem. Soc. **1979**, 101, 2076.

42. (a) Anderson, D.J.; Gilchrist, T.L.; Horwell, D.C.; Rees, C.W.; Yelland, M. Chem. Comm. **1969**, 146; (b) Rees, C. W.; Yelland, M. Chem. Comm. **1969**, 377.
43. Busch, M.; Weiss, B. Chem. Ber. **1900**, 33, 2701.
44. For a review of one bond vs. two bond scission in 1,2-diazenes see: Engel, P.S. Chem. Rev. **1980**, 80, 99.
45. Lemal, D.M.; McGregor, S.D. J. Am. Chem. Soc. **1966**, 88, 1335.
46. Lichter, R.L., Ph.D. Thesis, University of Wisconsin, Madison, 1967, as quoted in reference 1.
47. Lemal, D.M.; Menger, F.; Coats, E.A. J. Am. Chem. Soc. **1964**, 86, 2395.
48. Adams, D.J.C.; Bradbury, S.; Howell, D.C.; Keating, M.; Rees, C.W.; Storr, R.C. Chem. Comm. **1971**, 828.
49. Baldwin, J.E.; Brown, J.E.; Hofle, G. J. Am. Chem. Soc. **1971**, 93, 788.
50. Duan, D.C.; Dervan, P.B. J. Org. Chem. **1983**, 48, 970.
51. a) McBride, W.; Kruse, H.W. J. Am. Chem. Soc. **1957**, 79, 572.
b) McBride, W.; Bens, E. J. Am. Chem. Soc. **1959**, 81, 5546.
52. Anderson, D.J.; Gilchrist, T.L.; Rees, C.W. Chem. Comm. **1971**, 800.
53. (a) Atkinson, R.S.; Rees, C.W. Chem. Comm. **1967**, 1230; (b) Atkinson, R.S.; Rees, C.W. J. Chem. Soc. (C) **1969**, 772.
54. Schecter, H.; Ley, D.E.; Zeldin, L. J. Am. Chem. Soc. **1952**, 74, 3664.
55. Lunt, E. Proc. Int. Symp. Nitro. Compounds **1964**, **1963**, 291.
56. Overberger, C.G.; Lombardino, J.G.; Hiskey, R.G. J. Am. Chem. Soc. **1957**, 79, 6430.
57. Roberts, J.R.; Ingold, K.U. J. Am. Chem. Soc. **1974**, 96, 3949.

58. Nakagawa, K.; Konaka, R.; Nakata, T. J. Org. Chem. **1962**, 27, 1597.
59. For a discussion on the origins of solvent-induced shifts,
see: Huberfield, P.; Lux, M.S.; Rosen, D. J. Am. Chem. Soc. **1977**,
99, 6828.
60. Calvert, J.G.; Pitts, J.N. "Photochemistry," Wiley, New York,
N.Y., 1966, p. 257.
61. Hinsberg, W.D., Ph.D. Thesis, California Institute of Technology,
1980, Pasadena, California.
62. Silverstein, R.M., et al. "Spectrometric Identification of Organic
Compounds," Wiley, New York, N.Y., 1974.
63. Greene, F.D.; Gilbert, K.E. J. Org. Chem. **1975**, 40, 1409.
64. (a) Dervan, P.B.; Uyehara, T.; Santilli, D.S. J. Am. Chem. Soc.
1979, 101, 2069; (b) Dervan, P.B.; Santilli, D.S. J. Am. Chem.
Soc. **1980**, 102, 3863.
65. Reichardt, C. Angew. Chem. Int. Ed. Engl. **1965**, 4, 29.
66. Engel, P.S.; Hayes, R.A.; Keifer, L.; Szilagyi, S.; Timberlake,
J.W. J. Am. Chem. Soc. **1978**, 100, 1876.
67. See Dervan, P.B.; Dougherty, D.A. in "Diradicals," Borden, W.,
ed., Wiley, New York, N.Y., 1982, Chapter 3.
68. See: (a) Bergman, R. in "Free Radicals," Vol. I., Kochi, J., ed.,
Wiley, New York, N.Y., 1973, Chapter 5; (b) Berson, J.A. in
"Rearrangements in the Ground and Excited States," Vol. I.,
de Mayo, P. ed., Academic Press, New York, 1980.
69. Morrell, M.L.; Vincow, G. J. Am. Chem. Soc. **1969**, 91, 6389.
70. Dervan, P.B.; Squillacote, M.E.; Lahti, P.M.; Sylwester, A.P.;
Roberts, J.D. J. Am. Chem. Soc. **1981**, 103, 1120.

71. For reviews of ketone photochemistry, see (a) Srinivasan, R. Adv. in Photochem. **1963**, 1, 83; (b) Dalton, J.C.; Turro, N.J. Ann. Rev. Phys. Chem. **1970**, 21, 499; (c) Wagner, P.J.; Hammond, G.S. Adv. Photochem. **1968**, 5, 168; (d) Turro, N.J. "Modern Molecular Photochemistry," Benjamin/Cummings, Menlo Park, Calif. 1978; (e) Wagner, P. in "Rearrangements in the Ground and Excited States," Vol. II, de Mayo, P. ed., Academic Press, New York, 1981.
72. Herzberg, G. "Electronic Spectra and Electronic Structure of Polyatomic Molecules," Van Nostrand, N.J., 1966.
73. For a review of formaldehyde photochemistry see: Gelbart, W.M.; Elert, M.L.; Heller, D.F. Chem. Rev. **1980**, 80, 403.
74. Harding, L.B.; Goddard, W.A. J. Am. Chem. Soc. **1975**, 97, 6293.
75. (a) Robinson, G.W.; Frosch, R.P. J. Chem. Phys. **1963**, 38, 1187; ibid. **1962**, 37, 1962; (b) Dexter, D.L.; Fowlere, W.B. ibid **1967**, 47, 1379.
76. Siebrand, W. J. Chem. Phys. **1967**, 47, 2411.
77. Halpern, A.; Ware, W.R. J. Chem. Phys. **1970**, 53, 1969.
78. Borkman, R.F. Molec. Photochem. **1972**, 4, 453.
79. (a) Perrin, F. J. Phys. Radium. **1962**, 7, 390; (b) Berlman, I.B. Molec. Crystals **1968**, 4, 157.
80. Parker, C.A. "Photoluminescence in Solutions," Elseview, New York, N.Y. 1968.
81. Mirbach, M.J.; Kon-Chang, L.; Mirbach, M.F.; Cherry, W.R.; Turro, N.J.; Engle, P.S. J. Am. Chem. Soc. **1978**, 100, 5122.
82. Weiss, D.S.; Chapman, O.L. Organic Photochemistry **1973**, 3, 197.

83. Ippen, E.P.; Shank, C.V.; Woerner, R.L. Chem. Phys. Lett. **1976**, 44, 76.
84. Turro, N.J.; et al. Tetrahedron Lett. **1978**, 555.
85. Wasserman, E. Prog. Phys. Org. Chem. **1971**, 8, 319.
86. Zittel, P.F.; Ellison, G.B.; O'Neil, S.V.; Herbst, E.; Laneberger, W.C.; Reinhardt, W.P. J. Am. Chem. Soc. **1976**, 98, 3731.
87. Reichen, W. Chem. Rev. **1978**, 78, 569.
88. O'Neal, H.E.; Larson, C.W. J. Phys. Chem. **1969**, 73, 1011.
89. (a) Wagner, P.J.; Spoerke, R.W. J. Am. Chem. Soc. **1969**, 91, 4437;
(b) Dalton, J.C.; et al. J. Am. Chem. Soc. **1971**, 93, 7213.
90. Assuming an A factor of 10^{13} and E_a of 80 kcal/mole.
91. (a) Renzepis, P.M. Chem. Phys. Lett. **1969**, 3717; (b) Kerkstroeter, W.G. J. Am. Chem. Soc. **1975**, 97, 4161.
92. (a) Bartlett, P.D.; Porter, N.A. J. Am. Chem. Soc. **1968**, 90, 5317;
(b) Porter, N.A., Ph.D. Thesis, Harvard University, Cambridge, Mass., 1969.
93. For a discussion of spin correlation effects see: (a) Engel, P.S. Chem. Rev. **1980**, 80, 99; (b) Bergman, R.G. in "Free Radicals," Kochi, J., ed., Wiley, New York, N.Y., 1973, Chapter 5.
94. For a review of photoreduction mechanisms, see: (a) Sciano, J.C. J. Photochem. **1973/74**, 2, 81; (b) Wagner, P.J. Topics in Current Chemistry **1976**, 66 1, and reference 71.

95. For reviews of ketone photocycloaddition reactions, see: (a) Arnold, D.R. Adv. Photochem. **1968**, 6, 301; (b) Dalton, J.C.; Turro, N.J. Ann. Rev. Phys. Chem. **1970**, 71, 499.
96. Synthesized by the method of McElvain, S.M.; Stammer, C.H. J. Am. Chem. Soc. **1951**, 73, 915.
97. Kornblum, N.; Larson, H.O.; Blackwood, K.K.; Mooberry, O.D.; Oliveto, E.P.; Grahan, G.E. J. Am. Chem. Soc. **1956**, 78, 1497.
98. Dale, A.D.; Mosher, H.S. J. Am. Chem. Soc. **1973**, 95, 512.
99. Berson, J.A.; Tompkins, D.C.; Jones, G. J. Am. Chem. Soc. **1970**, 92, 5799.
100. Spin inversion is held to be rate determining in 1,4-biradicals from ketone photolysis. (a) Small, R.D., Jr.; Scaiano, J.C. J. Phys. Chem. **1977**, 81, 2126; (b) Closs, G.L. Adv. Magn. Reson. **1974**, 7, 157; (c) Doubleday, C., Jr. Chem. Phys. Lett. **1981**, 77, 131; (d) Scaiano, J.C. Tetrahedron **1982**, 38, 819.
101. Porter, N.A.; Dubay, G.R.; Green, J.G. J. Am. Chem. Soc. **1978**, 100, 920.
102. Engel, P.S.; Bishop, D.J.; Page, M.A. J. Am. Chem. Soc. **1978**, 100, 7009.
103. Both energy-localized (n, π^*) states and vibrationally excited ground states have been postulated in the photodecomposition of the isomeric 1,2-diazenes. See: Engel, P.S. Chem. Rev. **1980**, 80, 99.

104. Solomon, B.S.; Thomas, T.F.; Steel, C. J. Am. Chem. Soc. **1968**, 90, 2449.
105. (a) Salem, L.; Rowland, C. Angew. Chem. Int. Ed. Engl. **1972**, 11, 92; (b) Turro, N.J. in "Diradicals," Borden, W., ed., Wiley, New York, N.Y., 1982, Chapter 6.
106. Olivier, R. Chem. Ber. **1936**, 55, 1034.

CHAPTER II

Design of Sequence Specific DNA Cleaving Molecules

INTRODUCTION

The sequence specific recognition of nucleic acids by proteins and small molecules is important in the regulation of many biological processes. The binding event is, in many cases, followed by chemical modification of the DNA at or near the recognition site. Such interactions are exemplified by the bacterial restriction endonucleases which produce double strand cleavage adjacent to specific four to six base pair nucleotide sequences.¹ The ability of these enzymes to cleave duplex DNA into unique fragments makes possible DNA sequencing, gene isolation, chromosome analysis and recombinant DNA methodology.

I describe here studies aimed at defining those elements necessary for the design of synthetic double strand DNA cleaving molecules with defined target sequences and binding sites sizes.²⁻⁶ This work has also resulted in a direct method, "DNA affinity cleaving", for determining the binding site locations and sizes of small molecules on DNA.^{3,6}

Restriction Endonucleases

DNA restriction endonucleases and modification methylases are strain specific prokaryotic enzymes responsible for the host-specific barriers to interstrain transfer of DNA.¹ The strain specific modification enzymes catalyze methyl transfer from S-adenosyl-L-methionine (AdoMet) to the cellular DNA sequences recognized by the endonuclease. Thus cellular DNA is rendered resistant to attack by the endogeneous restriction enzyme by virtue of methylated recognition sites, whereas foreign DNA is rapidly hydrolyzed.

Three classes of restriction endonucleases have been

characterized, Type I, Type II, and Type III.⁷ The Type I enzymes are typified by the strain B and K E.coli enzymes, Eco B and Eco K. Restriction and modification activities reside in a multifunctional complex ($\sim 5 \times 10^5$ daltons) consisting of three polypeptide chains, the (restriction), β (methylation and restriction) and γ (sequence recognition) chains.^{7,8} In vitro restriction depends on the presence of ATP, AdoMet and a divalent cation. The γ subunit recognizes a specific seven base pair recognition site, but DNA cleavage occurs over a 1000 base pair region. Double strand cleavage is the result of two independent binding and single strand cleavage events.^{9a} The 5' termini may have an unusual structure.^{9b} Methyl transfer by the Type I enzyme complex is to the recognition site and requires only AdoMet, with ATP and divalent cation being stimulatory.

The Type III restriction and modification enzymes are similar to and slightly simpler than the Type I enzymes.^{7b} The restriction and modification activities are contained in a multifunctional complex composed of two distinct peptide subunits. DNA cleavage requires only the presence of ATP and Mg^{++} , S-adenosyl-L-methionine is not required. Unlike the Type I enzymes, DNA cleavage occurs near the DNA binding sites. Methyl transfer requires AdoMet, with ATP and Mg^{++} being stimulatory.

The most numerous and useful restriction enzymes are the Type II restriction endonucleases.^{1,9} These enzymes are relatively small ($2 \times 10^4 - 5 \times 10^4$ daltons) with simple cofactor requirements: Mg^{++} for restriction and AdoMet for methyl transfer. The restriction and methylation activities reside in distinct (and separable) polypeptide

chains and act on nucleotides near to or in the recognition sequence. Type II restriction enzyme recognition sequences vary from four to six base pairs corresponding to expected frequencies of occurrence of one per 136 base pairs and one per 2080 base pairs, respectively.¹⁰ With few exceptions these sequences have two-fold rotational symmetry with strand scission occurring at sites symmetric to the rotational axis. To date 398 restriction nucleases have been isolated, affording a minimum of 91 specificities.^{1c} There are 186 endonucleases with six base pair recognition sequences, 38 enzymes with five base pair requirements, and 84 enzymes which bind four base pairs. The properties of Type II restriction endonucleases isolated to date have recently been tabulated.^{1c}

The study of the structures and mechanisms of Type II enzymes is still at an early stage. Only a few endonucleases have been purified to homogeneity.¹¹⁻¹³ Perhaps the best characterized enzyme is Eco RI, which exists in solution as a mixture of dimers and tetramers.^{11,14} The Eco RI methylase has also been isolated and purified to homogeneity.^{15,16} Both enzymes recognize the sequence 5'-GAATTC-3'. Surprisingly, although these two enzymes have the same sequence recognition requirements they do not have a great degree of sequence homology, differ in reactivity to sulfhydryl reagents, do not cross react immunologically, and differ substantially in reactions with glycosylated T4 DNA.⁸ In fact the DNA-protein interactions, which lead to identical sequence recognition, are thought to differ considerably, the endonuclease (dimer) interactions having twofold symmetry while the modification enzyme binds asymmetrically as the monomer.^{8,1e} X-ray

diffraction studies on the Eco RI endonuclease and an Eco RI-DNA cocrystal are in progress.^{17,18}

The kinetics of Eco RI cleavage have been investigated by Modrich.^{11,16} The dimeric form of the enzyme is catalytically active and the reaction follows Michaelis-Menten kinetics.^{11,15,19} The intermediacy of single stranded DNA depends

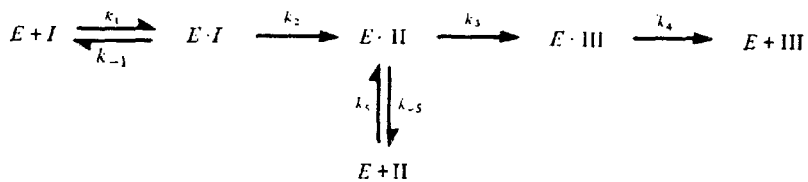


Figure 1. Proposed mechanism of cleavage of unmodified DNA by Eco RI endonuclease, I, II, and III represent, respectively, an intact Eco RI sequence; an intermediate species which contains a strand scission in only one strand of the Eco RI sequence; and a site which has suffered double strand cleavage.
 $k_2 \geq 40 \text{ min}^{-1}$ at 30°C , $k_3 = 14 \text{ min}^{-1}$,
 $k_{\text{cat}} = 1 \text{ min}.$

on temperature and reaction conditions. At 37°C the majority of double strand scissions are introduced without dissociation of the E·II intermediate. The turnover number, k_{cat} , for Eco RI is 0.7 min^{-1} and appears to be limited by dissociation of the Michaelis complex.^{11,16}

The restriction reaction results in the hydrolysis of two phosphodiester bonds and affords 3' hydroxyl and 5' phosphate termini. The molecular details of the phosphodiester cleavage reaction are unknown but may be similar in nature to those of staphylococcal nuclease, a Ca^{2+} dependent DNase of 16,800 daltons. A mechanism of action has been proposed for this enzyme based on a 1.5 Å crystal structure of an enzyme - thymidine 3',5'-biphosphate-calcium ion complex.²¹

Available evidence suggests that the presence of an unmodified recognition sequence is sufficient for enzymatic cleavage of DNA. However, the efficiency of DNA cleavage appears to be affected not only by the recognition sequence, but also by DNA regions outside the specific site. These effects are reflected in altered K_m s.^{15,20} The specificity of several Type II systems can be relaxed by changing reaction conditions.²²⁻²⁴ The specificity of highly purified Eco RI endonuclease is reduced at elevated pH and low ionic strength, or in the presence of Mn^{2+} , from a hexanucleotide to tetranucleotide recognition sequence.²² In addition Eco RI restriction has been relaxed to single strand cleavage.²⁵ The endonucleases, in general, do not cleave single stranded DNA or RNA.^{1,8}

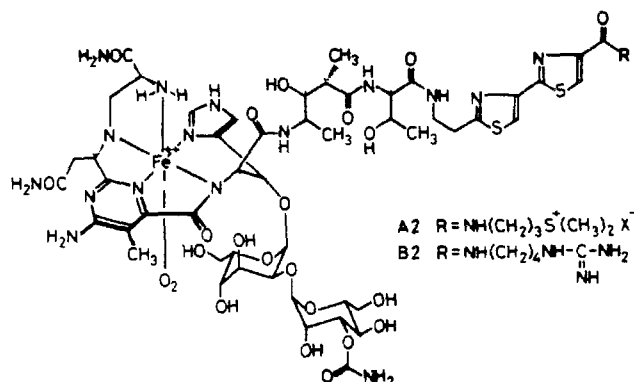
It has been suggested that Eco RI locates its recognition site by nonspecific DNA binding with directed diffusion along the

helix.^{20b,26} The affinity of Eco RI for its recognition site is 10^4 to 10^6 times greater than for nonspecific sequences.²⁷ DNA modification studies have revealed the major contact points of the Eco RI-DNA interaction. Included are the guanine N(7)²⁸ and adenine NH₂(6)²⁹ and N(3),²⁸ representing major and minor groove contacts. Although data point to a dimeric symmetric recognition mechanism, little else is known about the protein-DNA interactions. One might imagine these interactions are similar to those of the lac, cro and λ repressors, oligomeric DNA binding proteins with symmetric recognition sequences.³⁰⁻⁴²

In summary, although substantial information is available concerning the mode of interaction of restriction enzymes with DNA, understanding of the molecular mechanisms of phosphodiester hydrolysis, sequence discrimination and protein-DNA specific binding is at an early stage. We have therefore turned our attention to simpler DNA recognition elements and cleaving functions.

Experimental Strategy

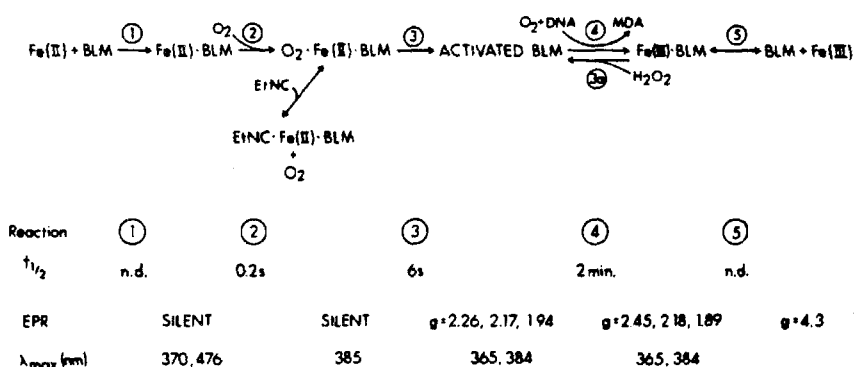
The sequence specific DNA cleaving molecules described here are bifunctional molecules, incorporating a chemically reactive moiety and a sequence specific DNA binding molecule. The design of these molecules was inspired by the naturally occurring antitumor antibiotic bleomycin,⁴³ which cleaves DNA at a two base pair recognition site in a reaction dependent on Fe(II) and O₂. Bleomycin consists of a DNA binding moiety which is believed to include the terminal amine, aminoethyl bithiazole and threonine residues, linked to the glycolated



The proposed structure for bleomycin-Fe(II) complex

pseudotetrapeptide A metal binding ligand. Some evidence suggests that the bithiazole may bind DNA by intercalation.⁴⁴ Bleomycin-Fe(II) cleaves DNA at the pyrimidine of a two base pair 5'-GT-3' or 5'-GC-3'^{45,46} site. It has not been determined what role if any the metal chelating ligand plays in DNA binding/specificity. A crystal structure of the BLM-Fe(II):DNA complex is lacking and our understanding of the recognition elements critical to the two base pair 5'-G-pyrimidine binding are not known.

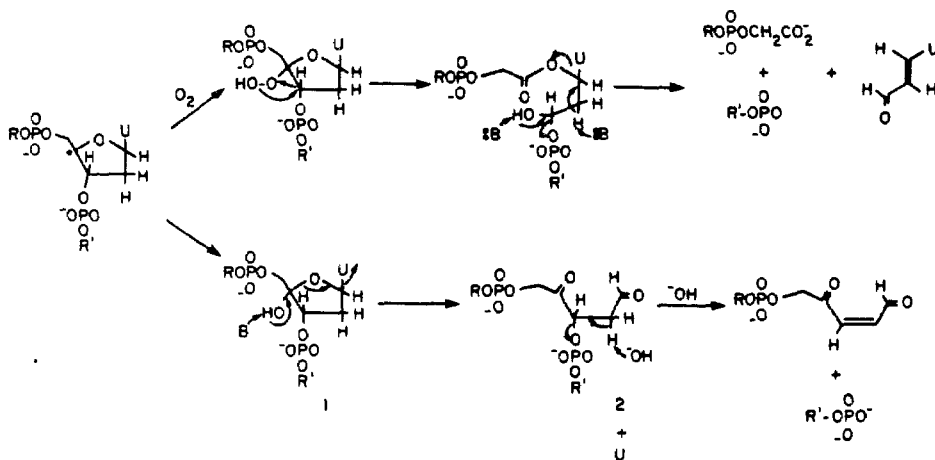
Peisach and coworkers have characterized the steps leading to the activated bleomycin complex.⁴⁷ Both oxygen activation of ferrous bleomycin and



H₂O₂ activation of ferric bleomycin lead to the activated complex. The nature of the actual Fe species involved in DNA cleavage is still unknown, but may be similar to that in horse metmyoglobin oxidations.⁴⁸



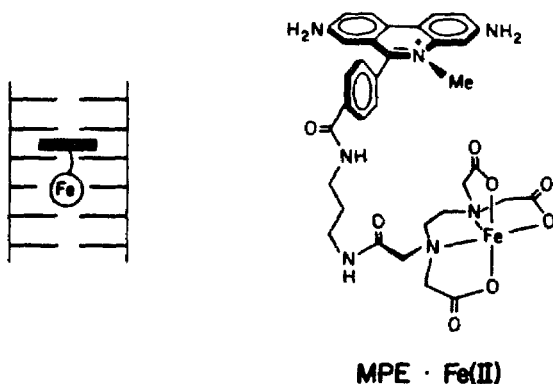
Oxygen dependent single and double strand DNA cleavage results in a terminal 5'-phosphate, terminal 3'-phosphoglycolate and base propenal.⁴⁹ In the absence of oxygen, bleomycin produces alkali labile sites, and free base release.⁴⁹ The following mechanism has been proposed and is supported by tritium labelling experiments.⁵⁰



Degradation is initiated by abstraction of the ribose C₄-H followed by a

partitioning of the 4' radical center between hydroperoxide and hydroxyl formation.

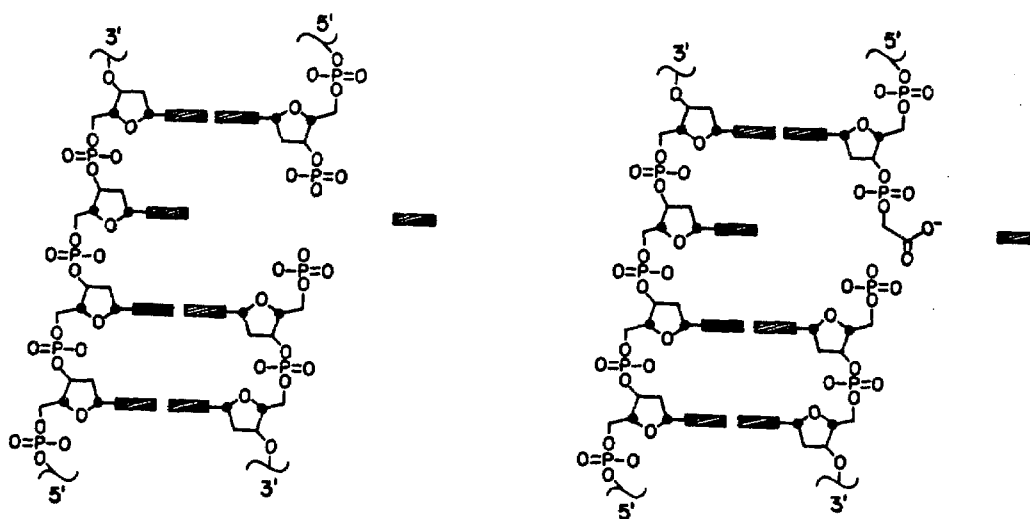
In an effort to mimic the oxidative degradation of DNA by bleomycin, Hertzberg and Dervan recently synthesized methidiumpropyl-EDTA, (**MPE**) which has the metal chelator, EDTA, tethered to the DNA intercalator methidium.⁵¹



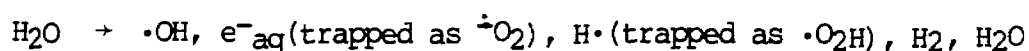
In the presence of Fe(II), oxygen, and a reducing source (dithiothreitol), **MPE** single strand cleaves DNA at efficiencies comparable to those of bleomycin cleavage. **MPE**·Fe(II) cleaves DNA in a nonsequence specific manner consistent with spectrophotometric binding studies that indicate ethidium has no overall base composition specificity.⁵² Consequently, the inhibition of **MPE**·Fe(II) cleavage on drug protected regions of DNA can be analyzed by high resolution gel electrophoresis and provides a rapid, direct method for determining the binding sites of drugs on DNA.⁵³ Because **MPE**·Fe(II) cleaves DNA more uniformly than does DNase I, **MPE**·Fe(II) footprinting provides more

detailed information on small molecule binding than does DNase I footprinting.⁵⁴ The drugs distamycin, netropsin, actinomycin, olivomycin, mithramycin, and chromomycin have been footprinted with $\text{MPE} \cdot \text{Fe(II)}$, to date.⁵³

Unlike bleomycin, $\text{MPE} \cdot \text{Fe(II)}$ strand scission leads to stoichiometric free base release.⁵⁵ The 5' DNA terminus is a phosphoryl group, while the 3' termini are a mixture of phosphoryl groups and phosphoglycolates, suggesting two different cleavage mechanisms.⁵⁵ The remaining deoxyribose degradation products have not yet been identified. The composition of the 3' ends is the same as that found with



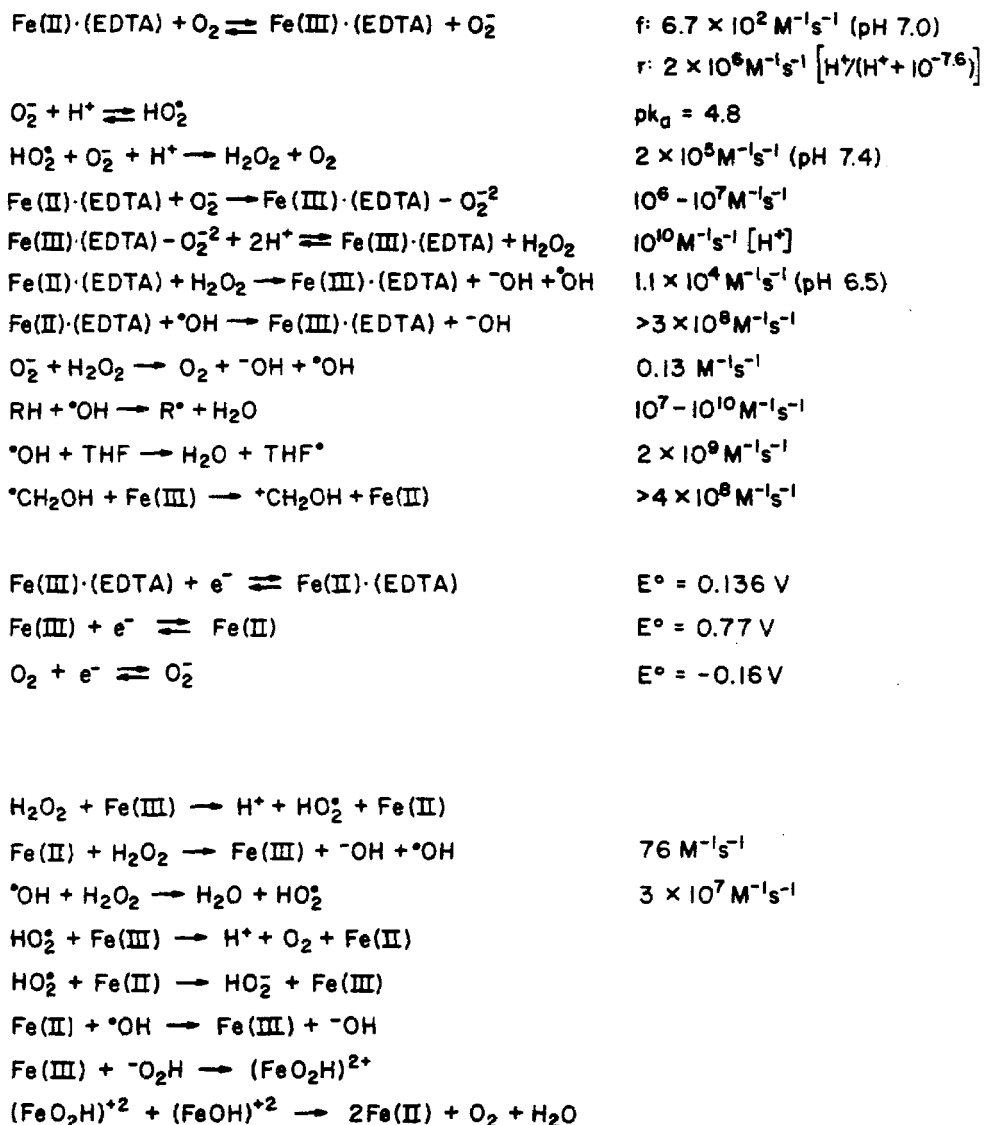
$\text{EDTA} \cdot \text{Fe(II)}$ ⁵⁵ or γ irradiation induced DNA degradation.⁵⁶ Both γ irradiation⁵⁷ and $\text{EDTA} \cdot \text{Fe(II)}$ ⁵⁸ are known to produce $\cdot\text{OH}$ radical. γ Irradiation decomposes water to high energy species:⁵⁹



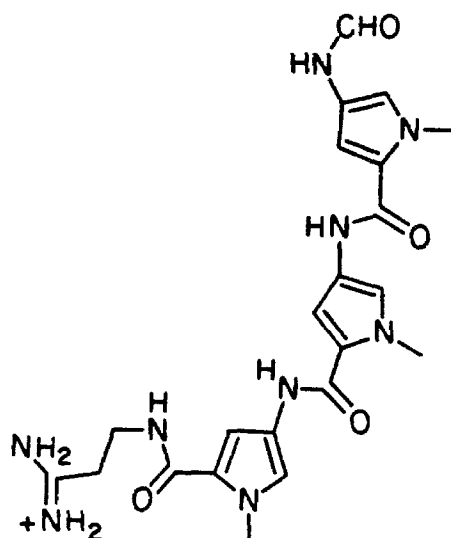
Chain reaction mechanisms involving hydroxyl radicals are well established for aqueous Fe(II) and EDTA·Fe(II) oxidations.⁶¹ Evidence includes kinetic analyses, spin trapping and ESR experiments, and product analyses.^{60,61,63} The similarity of products from **MPE**·Fe(II) cleavage and hydroxyl radical mediated DNA cleavage suggest the intermediacy of ·OH in the **MPE**·Fe(II) strand scission reactions.

From the finding of Hertzberg and Dervan that attachment of EDTA·Fe(II) to the intercalator, methidium, results in an efficient DNA cleaving molecule, we investigated the attachment of EDTA to sequence specific DNA binding molecules. We chose distamycin A, an oligopeptide which hydrogen bonds to the minor groove of DNA with a preference for A+T sequences.

Scheme I62



Distamycin A⁶⁴ is obtained from Streptomyces distallicus and is a biologically active inhibitor of bacterial, viral, and cellular systems. It is known that distamycin competes with E.coli RNA polymerase for the specific promotor sequences on DNA, thereby inhibiting DNA-dependent RNA synthesis.⁶⁵

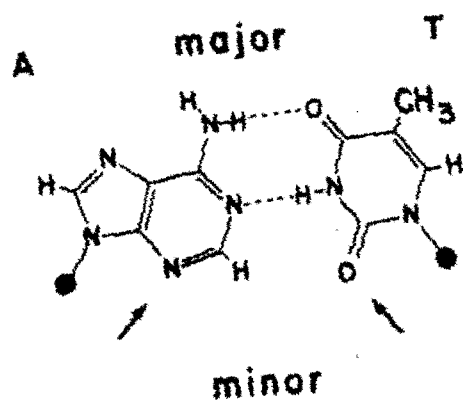
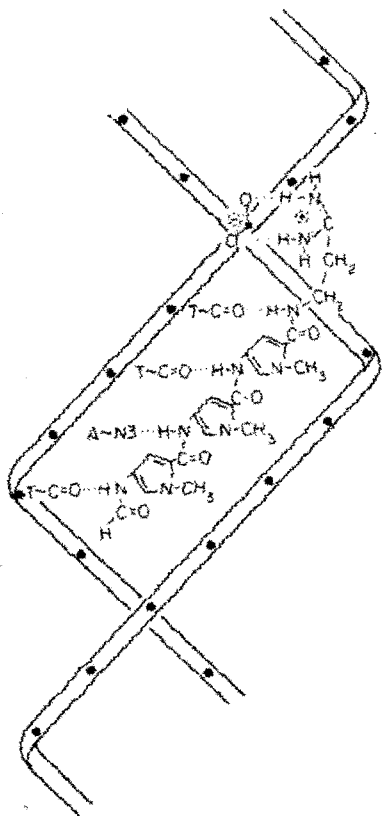


Distomycin A

Distamycin binding to DNA is characterized by marked elevation of the thermal denaturation temperature T_m , metachromic UV shifts, and induced circular dichroism.⁶⁶ Binding constants have been obtained from sedimentation dialysis⁶⁷ assays and binding experiments with [formyl-¹⁴C] distamycin A:⁶⁸ $2.4 \times 10^9 \text{ M}^{-1}$ and $5 \times 10^5 \text{ M}^{-1}$ for the strong and weak sites, respectively. Fluorescent quenching experiments of dansyldistamycin analogs revealed that each pyrrolecarboxamide group increases the binding free energy 2 kcal/mole for poly(dA)·poly(dT) and 0.95 kcal/mole for poly(dG)·poly(dC).⁶⁹ (The binding enthalpy of

netropsin, a two pyrrole carboxamide analog of distamycin, is -10.7 kcal/mole, ΔS is positive.^{70c}) These results are consistent with DNA-drug hydrogen bonding interactions resulting in displacement of bound water. Distamycin binds tightly to poly(dA)·poly(dT), poly(dA-dT) and poly(dI)·poly(dC), but not to poly(dG)·poly(dC), poly(dG-dC), single stranded DNA or RNA.^{66,69,70} Recently, using **MPE**·Fe(II) footprinting, Van Dyke and Dervan have demonstrated that distamycin binds A+T sites on heterogeneous DNA.⁵³

Distamycin does not affect the supercoiling of DNA at levels of binding up to saturation,^{66b,c,67} ruling out intercalative binding. Magnetic circular dichroism⁷¹ and NMR experiments⁷² exclude the occurrence of large distortions of the base pairs or the helical conformation on distamycin binding. A crystal structure of netropsin⁷³ has been obtained (a 1.7 Å netropsin DNA cocrystal is now being analyzed). This information together with NMR evidence⁷² and model building^{66,70} suggests the following DNA-distamycin structure. The amide nitrogens of the antibiotic are situated in the minor groove of right-handed B DNA so as to engage in hydrogen bonding interactions with the O(2) atoms of thymine or N(3) of adenine. Electrostatic interactions between the amidine function and phosphates are necessary for binding. Steric interactions between N(2) of guanine and distamycin prevent binding to G-C base pairs.^{66b} This model is supported by methylation studies,⁷⁴ glycosylated phage DNA binding studies,⁷⁵ and flow dichroism studies.⁷⁶

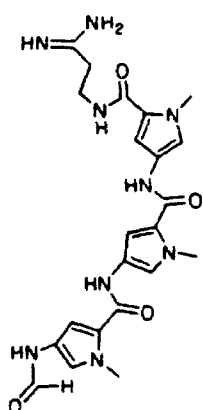


RESULTS AND DISCUSSION

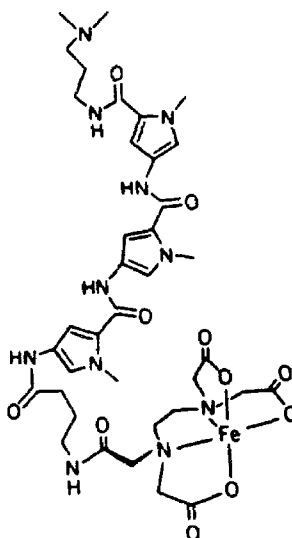
Design of Sequence Specific DNA Cleaving Molecules. Distamycin-EDTA (DE)

Synthesis

Data in the literature suggests that the formyl group of distamycin does not interact with DNA⁷⁷, but that the



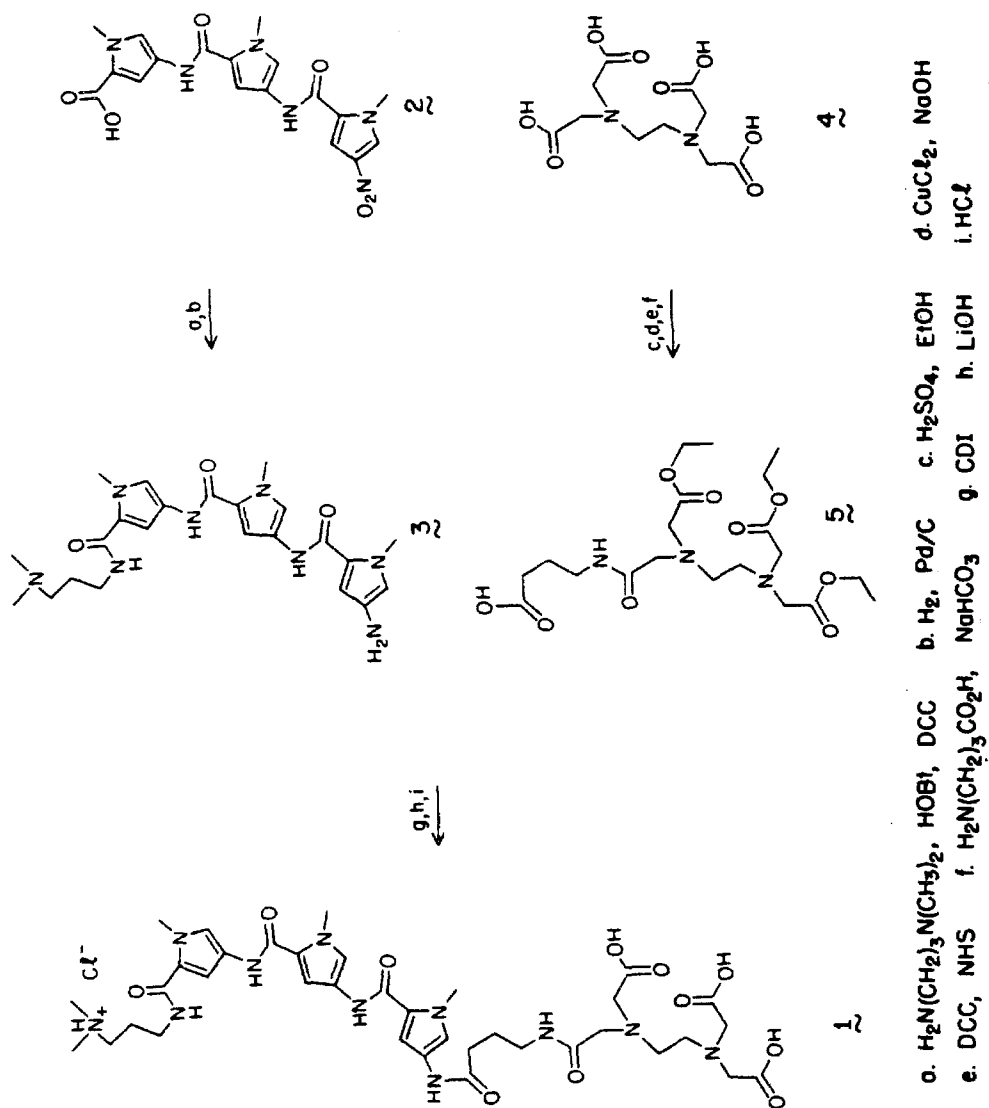
D



DE · Fe(II)

amidine group is required for DNA binding.⁶⁶ The EDTA was therefore initially tethered to the amino terminus of the N-methyl pyrrole oligopeptide in order to minimize interference with electrostatic binding interactions. Nitro acid 2 is a known compound readily available in eight steps from N-methylpyrrole-2-carboxylic acid.⁷⁸ Modifications of the literature synthetic methodology afforded 2 in an overall yield of 30%. The terminal amidine was replaced by dimethyl

Synthetic Scheme

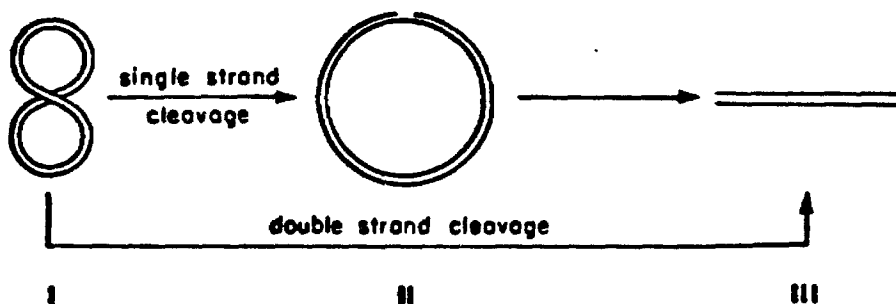


amine in order to simplify synthetic and chromatographic manipulations. The DE-Fe(II) analog with a terminal amidine does not differ in its cleavage efficiency or specificity from 1. EDTA-Fe(II) was linked to the peptide via a four carbon tether in order to avoid perturbations on the distamycin minor groove binding geometry which might arise from close EDTA-DNA contacts.

The N-hydroxybenzotriazole ester⁷⁹ of nitro acid 2 was condensed with 3-dimethylaminopropylamine. Subsequent reduction of the nitro group (hydrogen over 5% Pd/C, DMF) afforded diamine 3. 3 was condensed with the imidazolid⁸⁰ of the triethyl ester 5, available in four steps from EDTA.⁸¹ Hydrolysis (0.25M aq LiOH) and acidification gave 1. DE was chromatographed on silica gel (230-400 mesh) with ammonia/ethanol, and was further purified by supporting it on Amberlite XAD-2, washing with 5% aqueous disodium EDTA, distilled water and eluting with methanol.

Cleavage Efficiency

The cleavage of DNA by DE-Fe(II) was followed by monitoring the conversion of supercoiled (form I) pBR-322 plasmid DNA⁹¹ to open circular (II) and linear forms (III)⁸² (nondenaturing 1% agarose gel electrophoresis/ethidium bromide staining).



The introduction of one single strand break converts form I to II. The introduction of a second single strand break within 16 base pairs of an existing single strand break converts form II to III.⁸³ The cleavage of DNA by DE•Fe(II)/DTT was examined at two DNA concentrations, 10⁻³M bp and 10⁻⁵M bp (Table I).

Table I - Cleavage of pBR-322 Plasmid in the Presence of DTT^a

Reagent	conc. M	% Form			DNA conc. (bp)	Reagent/ bp
		I	II	III		
EDTA•Fe(II)	10 ⁻⁶	94	6	0	10 ⁻⁵	10 ⁻¹
MPE•Fe(II)	10 ⁻⁷	0	98	2	10 ⁻⁵	10 ⁻²
bleomycin• Fe(II)	10 ⁻⁷	0	43	57	10 ⁻⁵	10 ⁻²
DE•Fe(II)	10 ⁻³	0	75	25	10 ⁻⁵	10 ²
DE•Fe(II)	10 ⁻⁴	0	85	15	10 ⁻⁵	10 ¹
DE•Fe(II)	10 ⁻⁵	0	90	10	10 ⁻⁵	1
DE•Fe(II)	10 ⁻⁶	32	68	0	10 ⁻⁵	10 ⁻¹
DE•Fe(II)	10 ⁻⁷	74	26	0	10 ⁻⁵	10 ⁻²
MPE•Fe(II)	10 ⁻⁵	0	95	5	10 ⁻³	10 ⁻²
DE•Fe(II)	10 ⁻⁴	0	85	15	10 ⁻³	10 ⁻¹
DE•Fe(II)	10 ⁻⁵	1	95	4	10 ⁻³	10 ⁻²
DE•Fe(II)	10 ⁻⁷	50	50	0	10 ⁻³	10 ⁻⁴
DE•Fe(II)	10 ⁻⁸	60	40	0	10 ⁻³	10 ⁻⁵

- a) Form I pBR-322 reagent, buffer (40 mM Tris-base, 5 mM NaOAc, pH 7.9) and dithiothreitol (5 mM) were allowed to react at 25°C for 30 min. Forms I-III were analyzed with agarose gel electrophoresis and quantitated after ethidium bromide staining by densitometry.

DE·Fe(II) cleaves DNA efficiently at 10^{-6} M concentrations in the presence of O_2 and dithiothreitol. The efficiency of **DE**·Fe(II) cleavage (single strand cleavage/total **DE**·Fe(II) concentration) is less than that of **MPE**·Fe(II). Both increased specificity (fewer binding sites) and a decreased binding constant of **DE**·Fe(II) relative to **MPE**·Fe(II) would account for this observation.

The increase in **DE**·Fe(II) cleavage efficiency with increasing DNA concentration (10^{-5} to 10^{-3} M bp) suggests that the ratio of the DE_{bound}/DE_{free} is higher at 10^{-3} M bp than 10^{-5} M bp. From the Scatchard relationship:

$$r/c = K(n-r)$$

(where r = drug bound/base pair, c = drug free, K = binding constant and n = apparent binding site concentration/base pair), it is apparent that only when the apparent binding site concentration is on the order of K^{-1} is $DE_{bound}/DE_{free} \geq 1$. Therefore the large increase in cleavage efficiency at 10^{-3} M bp versus 10^{-5} M bp suggests that a high percentage of the total **DE** is bound at 10^{-3} M bp and consequently, K^{-1} is close to the apparent binding site concentration. If the number of **DE**·Fe(II) binding sites on DNA is 100 (page 154) then $K^{-1} \sim 10^{-3} \times 100/4362 \sim 2 \times 10^{-5}$ and $K \sim 5 \times 10^4$. Although the efficiency of **DE**·Fe(II) cleavage differs at 10^{-3} and 10^{-5} M bp, the form II/form III ratio does not. The reason for this is that although DE_{bound}/DE_{free} differ, the percentage of apparent sites bound does not.

Since the binding constant of distamycin to A-T regions is approximately $10^9 M^{-1}$ ⁶⁸ and that of dansyl distamycin to poly(dA)·poly(dT) is $5 \times 10^7 M^{-1}$,⁶⁹ a binding constant of **DE**·Fe(II) $\leq 10^5 M^{-1}$

represents a significant decrease in binding affinity. Attachment of EDTA·Fe(II) to methidium doesn't significantly reduce its binding constant as evidenced by the fact that MPE·Ni(II) has a binding constant of $1.3 \times 10^5 \text{ M}^{-1}$, not too different than that of ethidium.⁵² Tethering EDTA·Fe(II) to a groove binder may, however, lead to severe steric interactions between the EDTA·Fe(II) complex and DNA, with a concomitant decrease in binding affinity. In addition DE might be forming nonbinding dimers in solution as a result of a hydrogen bonding interactions coupled with reversible $[\text{EDTA} \cdot \text{FeOFe} \cdot \text{EDTA}]^{-286}$ formation (a pyrrole dipeptide distamycin analog binds strongly to itself in crystals).⁸⁷ Unfortunately the binding constant of DE·Ni(II) which should approximate the K value for the active form of DE·Fe(II) is difficult to obtain due to the instability of the oligopeptide.

The average number of single strand scissions per DNA molecule, S, can be calculated from a Poisson distribution where P_n is the fraction

$$P_n = (S^n/n!)e^{-S} \quad (1)$$

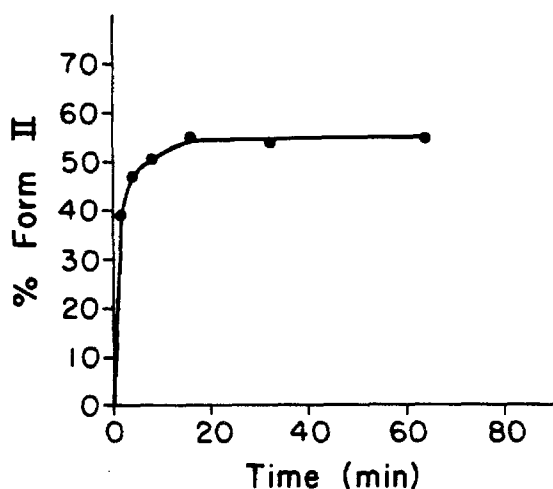
of molecules that have n nicks each.⁸ It is assumed here that the probability of a second strand scission is independent of the first scission. When only forms I and II DNA are present (1) simplifies to

$$S = -\ln(f_I)$$

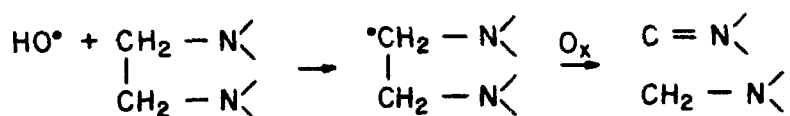
where f is the fraction of form I DNA's. A minimum boundary on S is one per every form I to form II event. The cleavage efficiency of the EDTA·Fe(II) moiety can therefore be approximated from the data in Table

I. At $10^{-3}M$ bp and $10^{-7}M$ DE•Fe(II), the cleavage efficiency E is $900 \leq E \leq 1100$. Clearly then, DE•Fe(II) is catalytic with a minimum of nine turnovers per DE•Fe(II). The catalytic efficiency is sensitive to DE•Fe(II) concentration and DNA concentration. At low [DNA], less EDTA•Fe(II) is localized on the DNA and E should be low ($E = 1\%$ at $10^{-5}M$ base pairs and $10^{-7}M$ DE•Fe(II).)

The cleavage reaction is complete within 15 minutes ($10^{-5}M$ bp, $10^{-6}M$ DE). Addition of DTT to the reaction mixture after 30 minutes



does not result in reactivation of DE•Fe(II). Inactivation of DE•Fe(II) may be due to hydroxyl radical degradation of EDTA. The rate constant for this reaction has been determined, $2.76 \times 10^9 \text{ l M}^{-1}\text{s}^{-1}$,^{62b} and should be



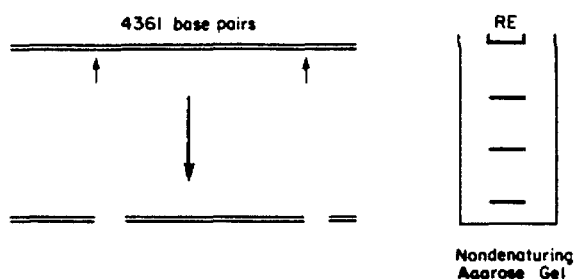
competitive with abstraction of C-H from a deoxyribose. Presumably, then the catalytic properties of $\text{DE}\cdot\text{Fe(II)}$ could be improved with more resistant chelators.

Double Strand Cleavage

The ability of $\text{DE}\cdot\text{Fe(II)}/\text{DTT}$ to sequence specifically double strand cleave DNA was assayed on linear pBR-322 DNA (4362 base pairs)⁹¹ at 10^{-3}M base pairs where nonspecific cleavage due to free $\text{DE}\cdot\text{Fe(II)}$ in solution is minimized.

Supercoiled pBR-322 was linearized with the restriction endonuclease, SalI, and purified by two ethanol precipitations. $\text{DE}\cdot\text{Fe(II)}$ was then allowed to react with linear DNA at a series of concentrations and the reactions were analyzed by 1% agarose gel electrophoresis with ethidium bromide staining. Figure 2 shows the result of $\text{DE}\cdot\text{Fe(II)}$ cleavage of linear pBR-322 (10^{-3}M bp). $\text{DE}\cdot\text{Fe(II)}$ double strand cleaves pBR-322 into discrete fragments. The large number of fragments produced is consistent with a relatively large number of binding sites on the DNA. Note that the molecular weights of the fragments do not sum to 4362, indicating partial digest of the DNA. As the DE/bp ratio increases, the specificity further decreases, presumably reflecting cleavage at less preferred binding sites. Therefore the double strand cleavage specificity of $\text{DE}\cdot\text{Fe(II)}$ is not absolute and depends on the ratio of reagent/base pairs.

Double strand cleavage may result from two single strand cleavage sites within 16 base pairs⁸³ of one another or by cleavage on opposite strands at one binding site. Furthermore, opposite strand cleavage at one binding site may result from one binding event and more



than one cleavage event or dissociation followed by specific reassociation and cleavage at the same site. At present we cannot rigorously distinguish these possibilities. The data in Table I and the graph of strand scission as a function of time indicate that double strand cleavage is a function of the amount of form II DNA and is relatively independent of the amount of form I DNA. The amount of form II DNA at $10^{-7}M$ $DE \cdot Fe(II)$ and $10^{-3}M$ bp is nine times the amount of $DE \cdot Fe(II)$ present, indicating that $DE \cdot Fe(II)$ dissociates from the DNA after cleavage. These results argue against a catalytic recycling of $EDTA \cdot Fe(II)$ while bound to one site.

Double strand cleavage may arise by the following kinetic scheme:

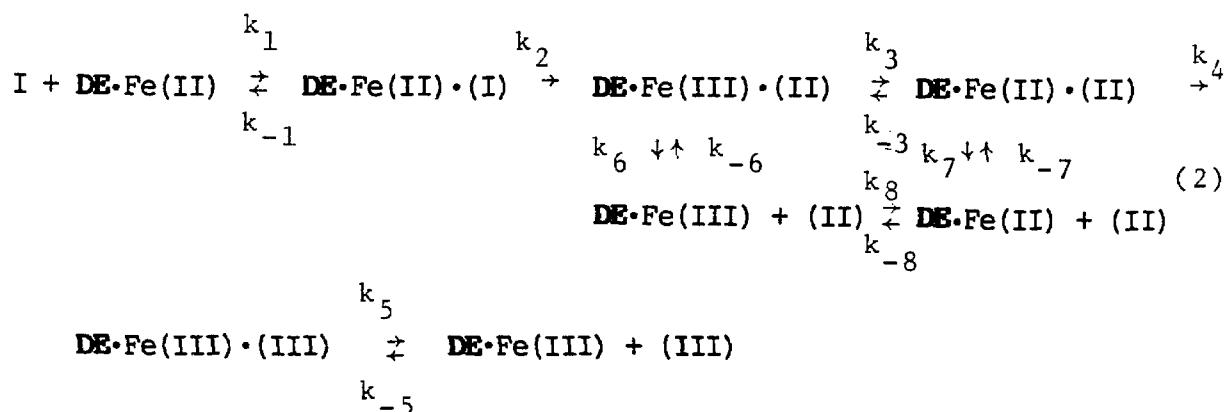
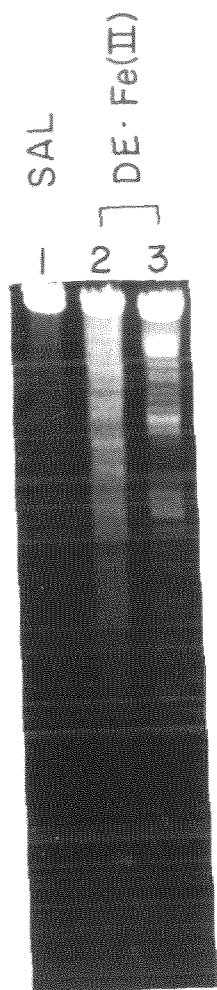


Figure 2. Agarose gel. Lanes 1,2,3: 10^{-3} M bp pBR-322, SalI digest. Lane 2: DE·Fe(II), 10^{-4} M; Lane 3: DE·Fe(II), 10^{-5} M. Buffer is 40 mM Tris Base, 5 mM NaOAc, pH 7.9; DTT is 5 mM; reaction time is 1.5 h.



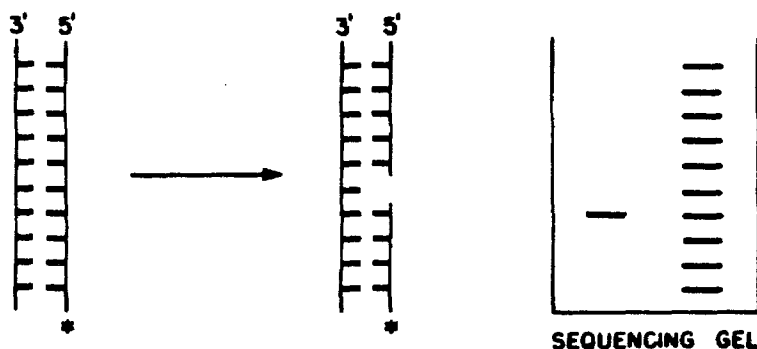
The ratio of single strand cleavage should then follow Michaelis-Menten kinetics

$$1/v = (1/n) K_m / V_{max} + 1/V_{max}$$

where $1/n$ is binding site concentration, K_M is the Michaelis constant, and V is reaction velocity.^{16,89} Finally, note that double strand cleavage does not occur at $10^{-5}M$ bp and $10^{-4}M$ or $10^{-5}M$ DE-Fe(II).

Cleavage Specificity

The specificity of DE-Fe(II) single strand cleavage was examined on three ^{32}P end labeled pBR-322⁹¹ restriction fragments: a 516 base pair Eco RI-Rsa I fragment (3847-4363); a 167 base pair Eco RI-Rsa I fragment (0-167); and a 381 base pair Bam HI-Eco RI (0-381) fragment. The 167 and 516 base pair fragments were labeled separately with ^{32}P on the 5' and 3' termini^{90,92,93} of the Eco RI site, the 381 base pair fragment was labeled on the 5' and 3' termini of the Bam HI site. The



end labeled fragments were reacted with **DE**·Fe(II)/DTT for 1 hr at 37°C. In addition, **MPE**·Fe(II)/DTT was reacted with the DNA with and without prior equilibration (30 min) of distamycin. The samples were then frozen, lyophilized, suspended in formamide and electrophoresed on a high resolution 0.4 mm, 8% polyacrylamide/50% urea gel capable of resolving DNA fragments differing in length by one nucleotide. The autoradiograms of the gels were analyzed by densitometry at 500 nm and cleavage efficiencies were correlated with peak area. The autoradiograms of the gels and the resulting histograms are shown in Figures 3-7. Arrows correspond to cleavage resulting in the release of the indicated base.

The **MPE**·Fe(II) lanes show a uniform DNA cleavage pattern indicative of relatively non-sequence specific cleavage. Note that **MPE**·Fe(II) cleaves least efficiently in those areas where **DE**·Fe(II) and distamycin bind. The cleavage patterns of **DE**·Fe(II), on the other hand, show a considerable degree of sequence specificity. Each cleavage site is composed of three to five strand scissions centered around a minimum of three AT base pairs. This A+T site is assigned as the **DE**·Fe(II) binding site. Increasing the **DE**·Fe(II)/base pair ratio results in the appearance of new cleavage sites which presumably have a lower binding affinity for **DE**·Fe(II). (Figures 7,8)

The three to five strand scissions on each side of the **DE**·Fe(II) binding site may reflect multiple binding modes of the oligopeptide, such as sliding one to two base pairs within the site. Data in the literature suggest that the formation of a long lived distamycin-DNA complex follows the association and dissociation of short lived low

Figure 3. Autoradiogram of high resolution denaturing gel. Lanes 1,3,5, and 7 are 3' end labeled 381 bp fragment; Lanes 2,4,6, and 8 are 5' end labeled 381 bp fragment. Lanes 1,2: Maxam Gilbert G reactions; Lanes 3,4: **MPE**·Fe(II), 5×10^{-6} M; Lanes 5,6: **DE**·Fe(II), 1×10^{-5} M; Lanes 7,8: distamycin 1×10^{-5} M, **MPE**·Fe(II) 5×10^{-6} M. All reactions are > 600 cpm 32 P end-labeled 381 bp fragment, made up to 10^{-4} M bp DNA with sonicated calf thymus DNA in 40 mM Tris base, pH 7.9, 5 mM NaOAc; 1 mM DTT.

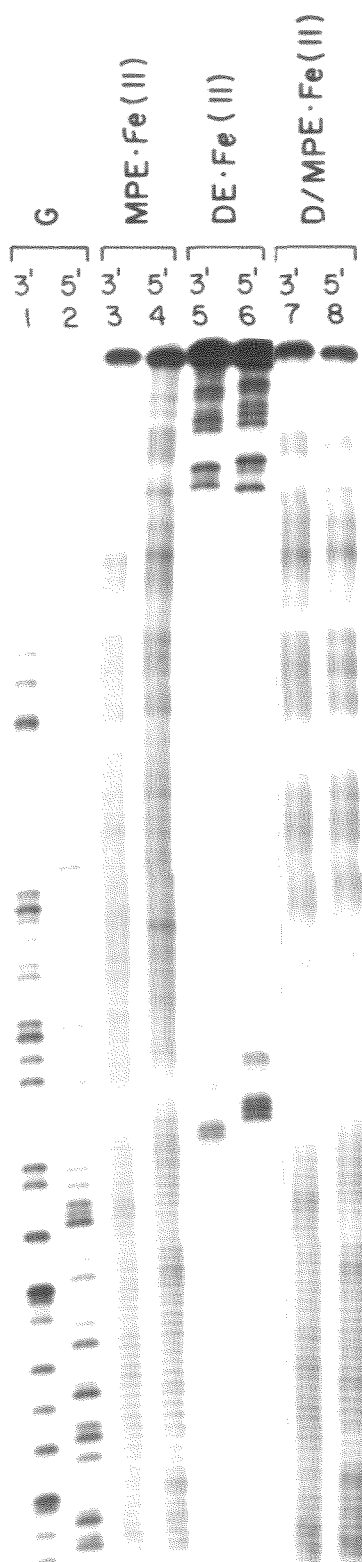


Figure 4. Autoradiogram of high resolution denaturing gel.
Lanes 1,3,5, and 7 are 3' end labeled 516 bp fragment;
Lanes 2,4,6, and 8 are 5' end labeled 516 bp fragment.
Lanes 1,2: Maxam-Gilbert G reaction; Lanes 3,4:
MPE·Fe(II), $5 \times 10^{-6}\text{M}$; Lanes 5,6: **DE**·Fe(II), $1 \times 10^{-5}\text{M}$;
Lanes 7,8: distamycin $1 \times 10^{-5}\text{M}$, **MPE** $5 \times 10^{-6}\text{M}$.

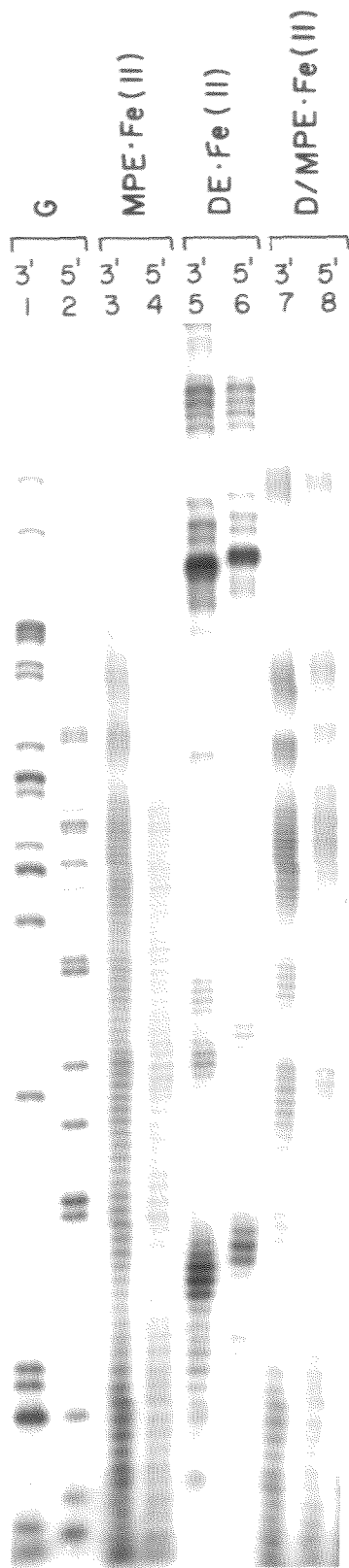
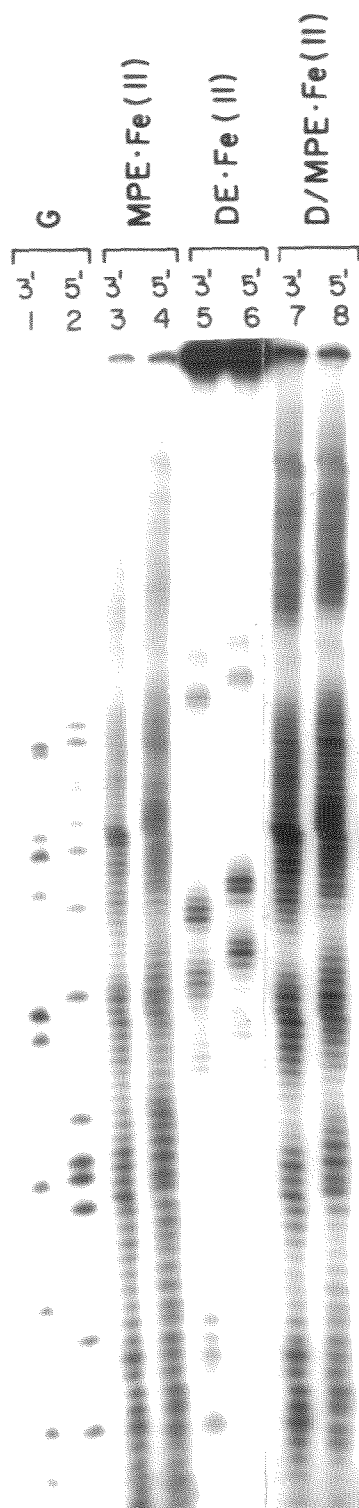


Figure 5. Autoradiogram of high resolution denaturing gel.
Lanes 1,3,5, and 7 are 3' end labeled 167 bp fragment;
Lanes 2,4,6, and 8 are 5' end labeled 167 bp fragment.
Lanes 1,2: Maxam-Gilbert G reaction; Lanes 3,4:
MPE·Fe(II), 5×10^{-6} M; Lanes 5,6: **DE**·Fe(II), 1×10^{-5} M;
Lanes 7,8: distamycin 1×10^{-5} M, **MPE** 5×10^{-6} M.



DE·Fe(II) 167

32p 5' ATAAGCTTTAAATGCGGTAGTTTATCACAGTTAAATTGCTAAACGCAGTCAGGCACCGTGTATGAAATCTAACAATCC
3' TATTCGAAATTACGCCATCAAAATAGTGTCAATTTAAACGATTGCGTCAGTCCGTGGCACATACCTTTAGATTGTTAGG

D/MPE·Fe(II) 167

32p 5' ATAAGCTTTAAATGCGGTAGTTTATCACAGTTAAATTGCTAAACGCAGTCAGGCACCGTGTATGAAATCTAACAATCC
3' TATTCGAAATTACGCCATCAAAATAGTGTCAATTTAAACGATTGCGTCAGTCCGTGGCACATACCTTTAGATTGTTAGG

MPE·Fe(II) 167

32p 5' ATAAGCTTTAAATGCGGTAGTTTATCACAGTTAAATTGCTAAACGCAGTCAGGCACCGTGTATGAAATCTAACAATCC
3' TATTCGAAATTACGCCATCAAAATAGTGTCAATTTAAACGATTGCGTCAGTCCGTGGCACATACCTTTAGATTGTTAGG

Figure 6. Histogram of DE·Fe(II) cleavage patterns and distamycin/MPE·Fe(II) inhibition patterns.

DE·Fe(II) 516

32p 5' ATACGCCCTATTTTATAGGTTAATGTCATGATAATAATGGTTTCTTAGACGTCAGGTGGCACCTTTTCGGGGAAATGTGCGCGGAA
3' TATGCGGATAAAAATATCCAAATTACAGTACTATTATACCAAAGAATCTGCAGTCCACCGTGAAAAGCCCTTTACACGCGCCTT

D/MPE·Fe(II) 516

32p 5' ATACGCCCTATTTTATAGGTTAATGTCATGATAATAATGGTTTCTTAGACGTCAGGTGGCACCTTTTCGGGGAAATGTGCGCGGAA
3' TATGCGGATAAAAATATCCAAATTACAGTACTATTATACCAAAGAATCTGCAGTCCACCGTGAAAAGCCCTTTACACGCGCCTT

MPE·Fe(II) 516

32p 5' ATACGCCCTATTTTATAGGTTAATGTCATGATAATAATGGTTTCTTAGACGTCAGGTGGCACCTTTTCGGGGAAATGTGCGCGGAA
3' TATGCGGATAAAAATATCCAAATTACAGTACTATTATACCAAAGAATCTGCAGTCCACCGTGAAAAGCCCTTTACACGCGCCTT

DE·Fe(II) 381

32P 5' GGCGGCCAAAGCGGTCGGACAGTGCTCCGAGAACGGGTGCGCATAGAAAATTGCATCAACGCATATAGCGCTAGC 3'
3' CCGCCGGTTTCGCCAGCCTGTCACGAGGCTCTTGCCACACGCGTATCTTTAAACGTAGTTGCGTATATCGCGATCG 5'

D/MPE·Fe(II) 381

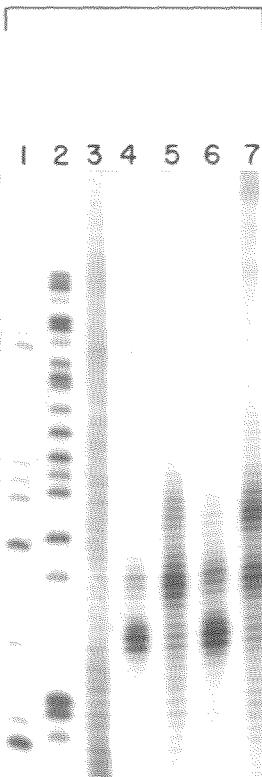
32P 5' GGCGGCCAAAGCGGTCGGACAGTGCTCCGAGAACGGGTGCGCATAGAAAATTGCATCAACGCATATAGCGCTAGC 3'
3' CCGCCGGTTTCGCCAGCCTGTCACGAGGCTCTTGCCACACGCGTATCTTTAAACGTAGTTGCGTATATCGCGATCG 5'

MPE·Fe(II) 381

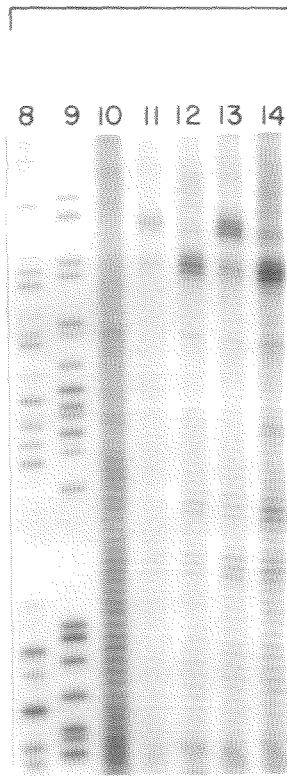
32P 5' GGCGGCCAAAGCGGTCGGACAGTGCTCCGAGAACGGGTGCGCATAGAAAATTGCATCAACGCATATAGCGCTAGC 3'
3' CCGCCGGTTTCGCCAGCCTGTCACGAGGCTCTTGCCACACGCGTATCTTTAAACGTAGTTGCGTATATCGCGATCG 5'

Figure 7. Effect of concentration on cleavage patterns.
Lanes 1,8,15: Bleomycin·Fe(II) $4 \times 10^{-6}\text{M}$
Lanes 2,9,16: Maxam-Gilbert G reaction; Lanes
3,10,17: **MPE**·Fe(II) $1 \times 10^{-5}\text{M}$; Lanes
4,11,18: **DE**·Fe(II) $1.25 \times 10^{-5}\text{M}$; Lanes
5,12,19: **ED**·Fe(II) $1.25 \times 10^{-5}\text{M}$; Lanes
6,13,20: **DE**·Fe(II) $5 \times 10^{-5}\text{M}$; Lanes
7,14,21: **ED**·Fe(II) $5 \times 10^{-5}\text{M}$. All reactions
are made up to 10^{-4}M bp DNA with sonicated calf
thymus DNA in 10 mM Tris·HCl, pH 7.8, 50 mM
NaCl, 1 mM DTT. Base pairs shown from bottom to
top: 77-146 (167 fragment) 68-146 (279 fragment)
77-176 (fragment).

167



279



381

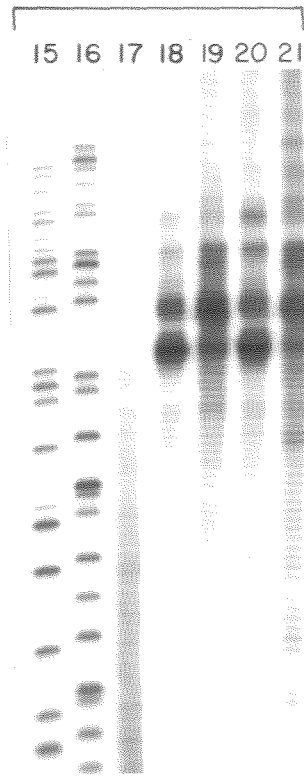


Figure 8. Histogram of the autoradiograms of the Maxam-Gilbert gels. Shown are DNA fragments 167 bp, lanes 4 and 5; 279 bp, lanes 13 and 14; and 381 bp, lanes 18 and 19.

167 bp fragment

80 90 100 110 120 130 140
 5' AGGCACCGTGATGAAATCTAACAATCCCCTCATCGTCAATCCTCGGCACCGGTACCCCTGGATGCTGTAGGC
 32p 3' TCCGTGGCACATACCTTAGATTGTTAGGGGAGTAGCAGTAGGAGCCGTGGCAGTGGGACCTACGACATCCG
 DE·Fe (II) ↑↑ ↑
 ED·Fe (II) ... ↑↑↑↑↑

279 bp fragment

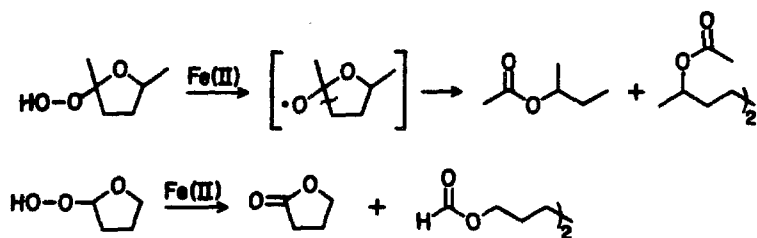
80 90 100 110 120 130 140
 5' ATCACCAGTGGGGAAGATCGGGCTCGCCACTTCGGGGCTCATGAGCGCTTGTTCGGCGTGGGTATGGTGG
 32p 3' TAGTGGCTACCCCTTCTAGCCCCGAGCGGTGAAGCCCCGAGTACTCGCGAACAAGCCGACCCATACCACC
 DE·Fe (II) ... ↑↑↑↑↑
 ED·Fe (II) ...

381 bp fragment

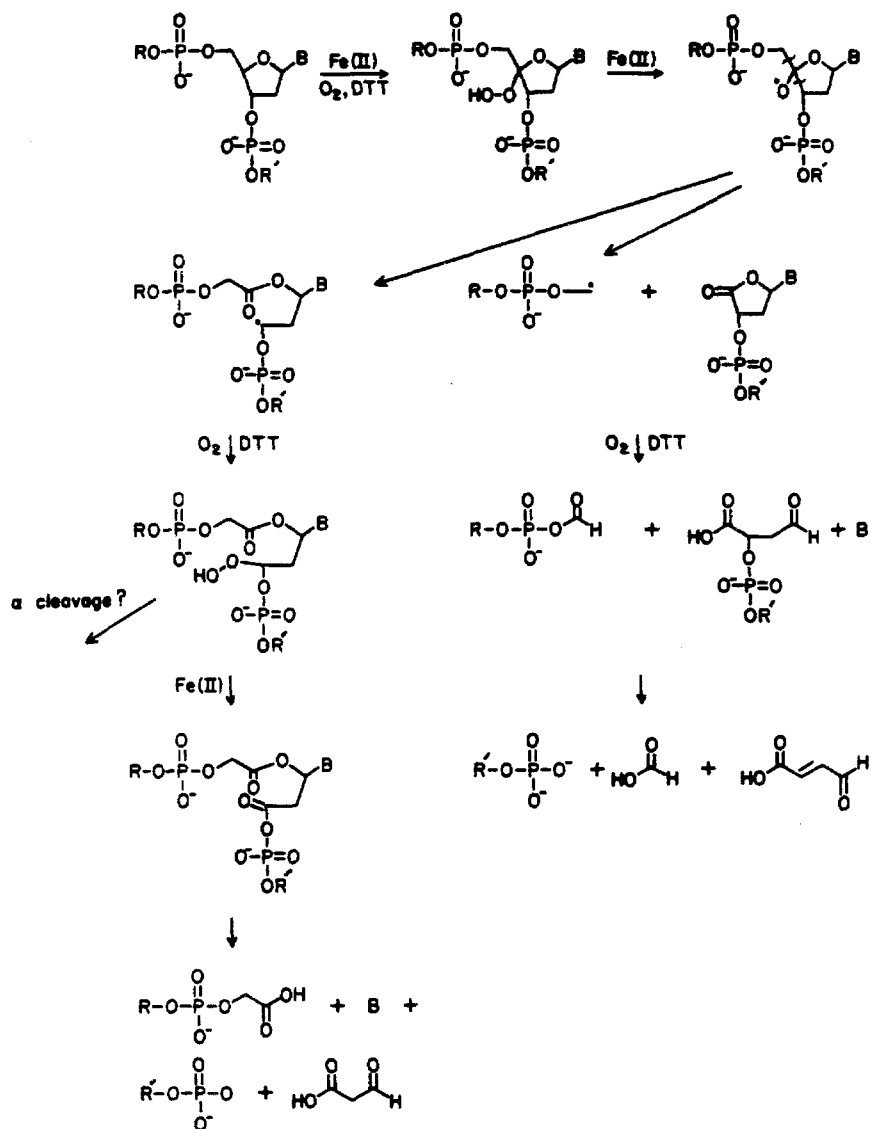
80 90 100 110 120 130 140 150 160 170
 5' CGGCGGCCAAAGCGGTCGGACAGTGCCTCCGAGAACGGGTGCGCATAGAAAATTGCATCAACGCAATATAGCGCTAGCAGCACGCCCATAGTGACTGGCGATGC
 32p 3' GCCGCCGGTTTCGCCAGCCCTGTACGAGGCTCTTGCCCCACGCGTATCTTTAACGTAGTTGCGTATATCGCCGATCGTCGTGCGGTATCACTGACCGCTACG
 DE·Fe (II) ↑↑↑↑↑ ↑↑↑
 ED·Fe (II) ↑↑↑ ↑↑↑↑

specificity complexes. Alternatively, the multiple strand scission may result from the generation of a diffusible hydroxyl radical at some average position of the EDTA·Fe(II) complex. The DNA termini produced by DE·Fe(II) cleavage are consistent with the later interpretation.

The DNA terminal end groups can be analyzed by examining a DE·Fe(II) cleavage site on a 3' and 5' ³²P end-labeled 192 base pair NDE I-Hae III restriction fragment labeled at the NDE site. The DNA 3' termini migrate with the MPE·Fe(II) generated phosphoryl and phosphoglycolate termini and occur in approximately a 1:1 ratio. The 5' DNA termini migrate with the MPE·Fe(II) generated phosphoryl termini.⁵⁵ These results suggest that DE·Fe(II), MPE·Fe(II), Fe(II)/H₂O₂, and γ irradiation⁵⁵⁻⁵⁸ mediated DNA scission occur via a common mechanism, hydroxyl radical attack on the backbone deoxyribose. A plausible mechanism is outlined in Scheme III.⁹⁴ This mechanism is based upon the products obtained from reaction of 2,5-dimethyl-2-hydroperoxytetrahydrofuran^{94a} and 2-hydroperoxytetrahydrofuran^{94b} with aqueous Fe(II).



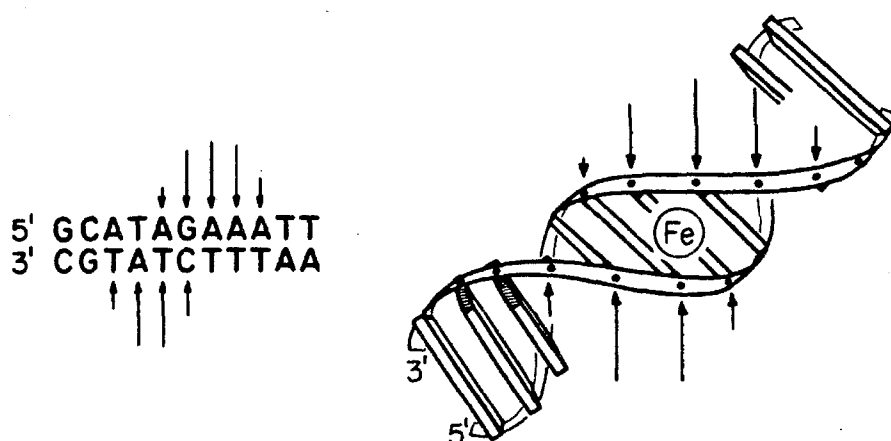
Scheme II



The strand scission pattern becomes less intense in the presence of radical scavengers (1M DTT) but does not change in shape. Finally it would be of interest to examine the cleavage pattern produced by iodosylbenzene **DE**·Fe(II) activation.

Because strand scission produces both 3' and 5' phosphates, the ends of a double strand scission may be ligatable. Exonuclease III⁹⁰ catalyzes the 3'→5' removal of 5' nucleotides and has a 3' phosphatase activity. Use of exonuclease III followed by DNA polymerase and dNTP should produce a family of blunt end DNA's which can be ligated by T4-DNA ligase.⁹⁰ Alternatively nuclease Bal 31 can be substituted for Exo III. This sequence can be tested easily on an isolated **DE**·Fe(II), **PSE**·Fe(II), or **BED**·Fe(II) cleavage site.

The multiple strand scissions produced by **DE**·Fe(II) are asymmetric on opposite strands and shifted to the 3' end. The reason for this shift is apparent if we examine a model of right handed B DNA with EDTA·Fe(II) site specifically placed in the minor groove. The bases proximal to EDTA·Fe(II) are to its 3' side. Consequently, we can interpret the asymmetric multiple cleavage bands surrounding **DE**·Fe(II) as resulting from generation of a diffusible reactive species at the average position of the tethered EDTA·Fe(II) in the minor groove. As a result, the attached DNA binding unit can be positioned on the DNA.



The lifetime of the reactive diffusive species can be estimated if one ignores the helicity of the DNA. The approximate distance traveled, x , is 10^8 Å, so from diffusion theory, $10^6 t = 2Dx^2 = 3 \times 10^{-10}$ sec for a value of $D = 1.5 \times 10^{-5} \text{ cm}^2 \text{ sec}^{-1}$ (aqueous 0.01M salt solution).¹⁰⁷ The observed decomposition rate is then $3 \times 10^9 \text{ sec}^{-1}$. Note, however, that the helical nature of DNA alters the accessibility of the sugars to hydroxyl radical. Therefore the pattern of 3 to 5 strand scissions may not be the result of the diffusive species' lifetime but is more likely due to geometrical constraints of B DNA. The minimum lifetime of the reactive species is then $3 \times 10^{-10} \text{ sec}^{-1}$.

A model relating cleavage patterns to the $\text{DE} \cdot \text{Fe(II)}$ binding site is illustrated in Figure 9 for the 5'-AAATT-3' 381 bp fragment site.

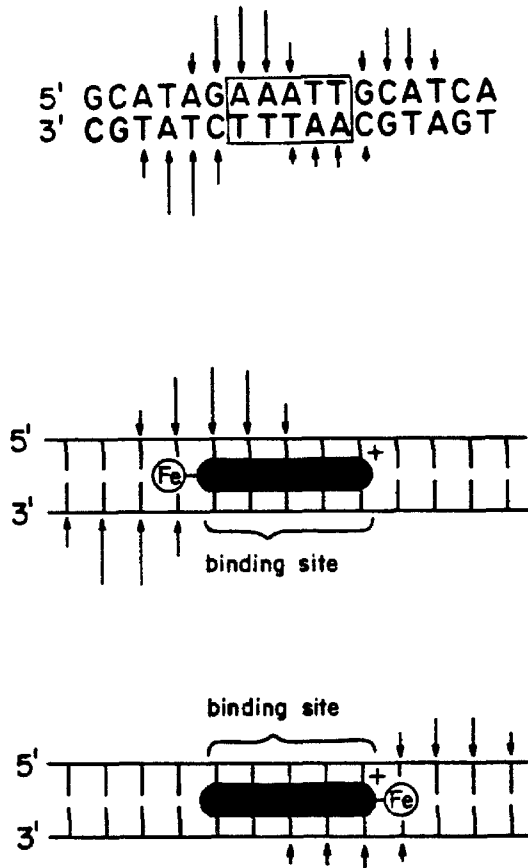
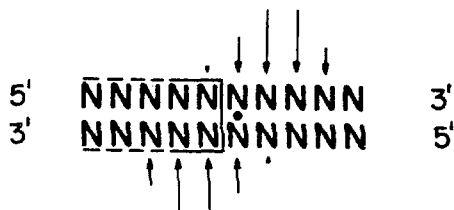


Figure 9. DE·Fe(II) binding sites for major and minor orientations on the 381 bp fragment.

The binding site boundary is located 1.0 base pairs from the average EDTA·Fe(II) position. This assignment is consistent with distances derived from CPK space filling models. An "average" DE·Fe(II) cleavage site compiled from histograms in Figure 5 is illustrated below.



The fact that multiple strand scissions are located on both sides of the A+T distamycin binding site, indicates that DE·Fe(II) can assume two orientations in the minor groove. The preferred orientation of the tripeptide is reflected by the more intense of the two cleavage sites. In the case of the 5'-AAATT-3' site above, the major tripeptide orientation occurs with the amino terminus to the 5' end.

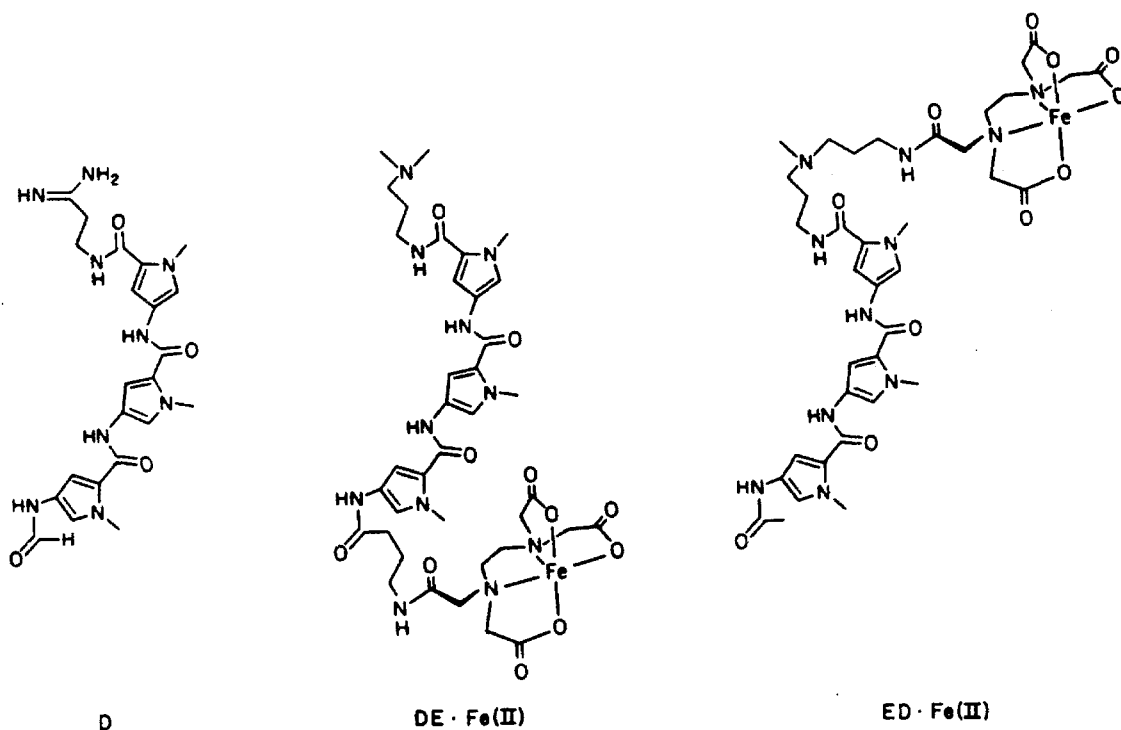
Assignment of tripeptide binding sites from DE cleavage patterns on the 167, 381, and 516 base pair fragments results in a five base pair distamycin binding site in all cases (see Figure 15, page 190). We will see later that these binding sites are identical to those derived from distamycin/MPE·Fe(II) inhibition patterns and can be interpreted in terms of four carboxamide hydrogen bonding interactions with the DNA. It is important to note that in deriving a five base pair binding site it has been assumed that the major and minor orientations of DE·Fe(II) bind the same site. In order to verify this assumption, EDTA-distamycin (ED) 6 has been synthesized, in which the EDTA is tethered to the

carboxy terminus of the tripeptide. Comparison of the cleavage patterns produced by **ED** and **DE** will fix the location of the amino and carboxy termini for one orientation of the tripeptide in the minor groove. This analysis should confirm the **DE**·Fe(II) binding model and thereby precisely define binding site location, size and drug orientation for distamycin.

EDTA-Distamycin (ED)

Synthesis

EDTA-Distamycin 6, an analog of **DE**, has the metal chelator, EDTA, tethered to the carboxy terminus of the N-methylpyrrole.



oligopeptide.³ The amino terminus of the oligopeptide was acetylated so as to maintain as much similarity to **DE** as possible. **EDTA** was linked to the tripeptide via 3,3'-diamino-N-methyldipropylamine. Although **EDTA** is fairly remote from the binding region of the molecule the location of the positive amino group is preserved.

The imidazolidine⁸⁰ of nitro acid **278** was condensed with an excess of 3,3'-diamino-N-methyldipropylamine to afford nitro amine **8**. **8** was condensed with the imidazolidine of triethyl ester **9**,⁸¹ available in two steps from **EDTA**, affording the nitro triester **10**. Reduction (hydrogen over 5% Pd/C, DMF) of the nitro group, acetylation, hydrolysis of the resulting triester (0.25M aq LiOH) and acidification yielded **6**. **ED (6)** was purified by chromatography on silica gel (230-400 mesh) with ammonia/methanol, followed by chromatography on Amberlite XAD-2.

Cleavage Efficiency

ED·Fe(II) cleaves supercoiled pBR-322 plasmid DNA more efficiently than **DE**·Fe(II), but at concentrations an order of magnitude higher than required for equivalent **MPE**·Fe(II) cleavage (Table II).

Scheme III

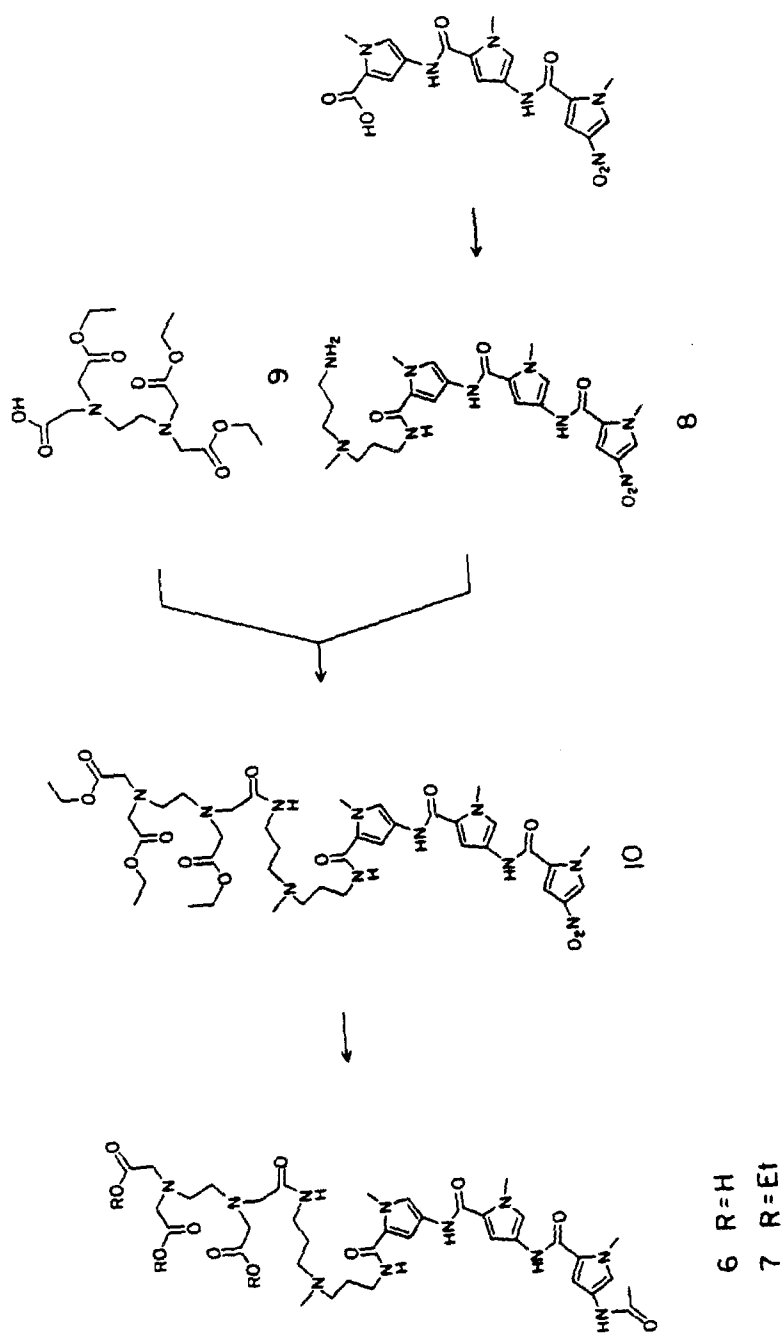


Table II - Cleavage of pBR-322 Plasmid in the Presence of DTTa

Reagent	conc. M	% Form			DNA conc. M	Reagent/ bp
		I	II	III		
MPE •Fe(II)	10 ⁻⁷	0	91	9	10 ⁻⁵	10 ⁻²
ED •Fe(II)	10 ⁻⁴	0	15	85	10 ⁻⁵	10 ¹
ED •Fe(II)	10 ⁻⁵	0	91	9	10 ⁻⁵	1
ED •Fe(II)	10 ⁻⁶	23	76	1	10 ⁻⁵	10 ⁻¹
ED •Fe(II)	10 ⁻⁷	74	26	0	10 ⁻⁵	10 ⁻²
MPE •Fe(II)	10 ⁻⁵	0	95	5	10 ⁻³	10 ⁻²
ED •Fe(II)	10 ⁻⁴	0	20	80	10 ⁻³	10 ⁻¹
ED •Fe(II)	10 ⁻⁵	0	90	10	10 ⁻³	10 ⁻²

a) Form I pBR-322, reagent, buffer (40 mM Tris Base, 5 mM NaOAc, pH 7.9) and dithiothreitol (5 mM) were allowed to react at 25°C for 1 h. Forms I-III were analyzed by agarose gel electrophoresis and quantitated after ethidium bromide staining by densitometry.

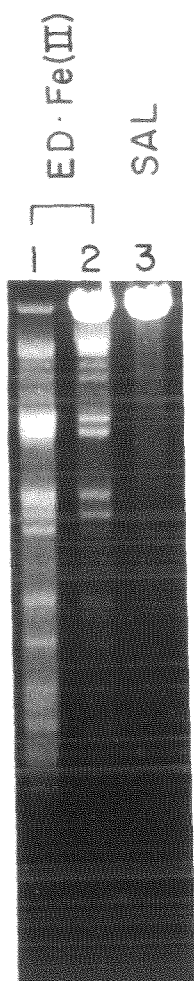
The reason for the increased efficiency of **ED**•Fe(II) cleavage relative to **DE**•Fe(II) cleavage is not clear. The **EDTA**•Fe(II) complex may interfere less with the tripeptide DNA binding geometry in **ED**•Fe(II) than in **DE**•Fe(II) due to increased linker length. As was the case with **DE**•Fe(II) the relative amounts of forms I, II, and III DNA are similar at fixed **ED**•Fe(II) concentration and variable DNA concentration suggesting that strand scission is proportional to drug bound. Cleavage of DNA by **ED**•Fe(II) is complete within 15 minutes.

Double Strand Cleavage

Double strand cleavage of DNA by **ED**•Fe(II) was examined on linear pBR-322 DNA (Sal I digest, 10⁻³M base pair) in the manner described previously for **DE**•Fe(II) (Figure 10). **ED**•Fe(II) double strand cleaves pBR-322 into discrete fragments. The specificity of **ED**•Fe(II) cleavage (10⁻⁵M) is similar to that of **DE**•Fe(II) cleavage (10⁻⁵M). Again cleavage specificity is a function of the **ED**•Fe(II)/base pair

ratio. At higher binding ratios less preferred sites are bound and the cleavage specificity decreases. The positions of the major **ED**·Fe(II) cleavage sites are 4.2, 3.3, 3.2, 2.6, and 2.4 ± 0.1 kb⁹¹ (based on **P5E**·Fe(II) cleavage pattern analysis, page 209). These are 5'-Tn-3' regions of DNA,⁹¹ consistent with a binding preference of the pyrrole tripeptide for poly(dT)·poly(dA) DNA.⁶⁶⁻⁷⁰ The double strand cleavage patterns of **ED**·Fe(II) were also examined at 5×10^{-5} M bp and 10^{-4} M and 10^{-5} M **ED**·Fe(II). The patterns produced at these **ED**·Fe(II) concentrations were identical to those produced at the same **ED**·Fe(II) concentrations at 10^{-3} M base pairs suggesting that both reagent efficiency and specificity depend on reagent bound and not free reagent in solution.

Figure 10 - Agarose gel. Lanes 1,2,3 10^{-3} M bp, pBR-322, Sal I digest. Lane 1: **ED**·Fe(II), 10^{-4} M; Lane 2: **ED**·Fe(II), 10^{-5} M. Buffer is 40 mM Tris Base, 5 mM NaOAc, pH 7.9; DTT is 5 mM; reaction time is 1.5 h.



Cleavage Specificity

The cleavage specificity of **ED**·Fe(II) was examined on 5' and 3'^{90,92,93} end labeled 516, 381 and 167 bp restriction fragments of pBR-322⁹¹ in a manner identical to that described for **DE**·Fe(II). The autoradiograms and corresponding histograms of the **ED**·Fe(II) cleavage patterns are presented in Figures 11-13. It is apparent from the histograms that both **ED**·Fe(II) and **DE**·Fe(II) cleave DNA adjacent to the same A+T sites.

DNA Affinity Cleaving with **ED**·Fe(II) and **DE**·Fe(II)

Let us examine in detail the cleavage patterns produced by **DE**·Fe(II) and **ED**·Fe(II) on the 381 base pair fragment. The **DE**·Fe(II) and **ED**·Fe(II) cleavage sites are centered around 5'-AAATT-3'. Recall that the carboxyl terminus of the tripeptide is defined by the cleavage pattern produced by **ED**·Fe(II) and the amino terminus by the cleavage pattern produced by **DE**·Fe(II). For **DE**·Fe(II), the major cleavage site is on the 3' end of this sequence whereas for **ED**·Fe(II) it is on the 5' end.



Figure 11. Autoradiograms of high resolution gels. Lanes 1,3: 5' end labeled DNA. Lanes 2,4: 3' end labeled DNA. a) 516 base pair fragment, b) 167 base pair fragment. Lanes 1,2: Maxam Gilbert G reactions. Lanes 3,4: $\text{ED}\cdot\text{Fe(II)}$, $1 \times 10^{-5}\text{M}$. All reactions are $> 600 \text{ cpm } ^{32}\text{P}$ end labeled restriction fragments made up to 10^{-4}M base pairs with sonicated calf thymus DNA.

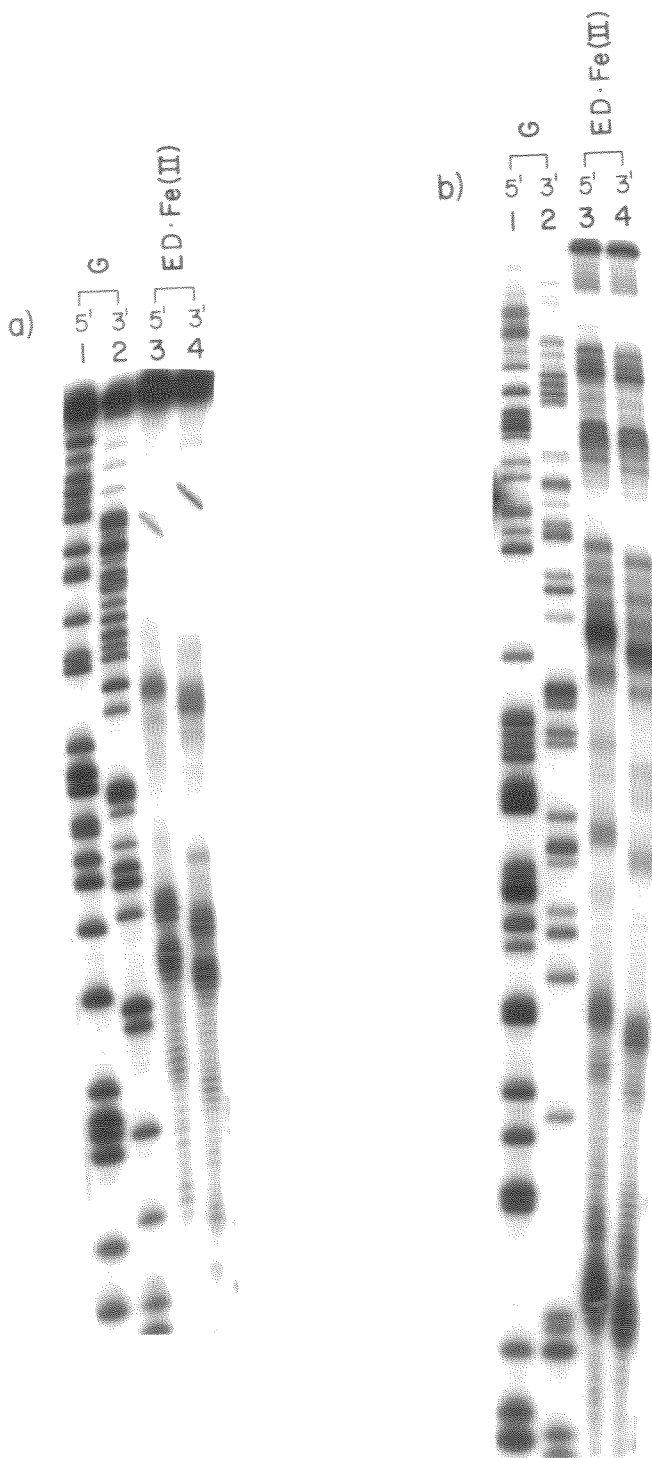
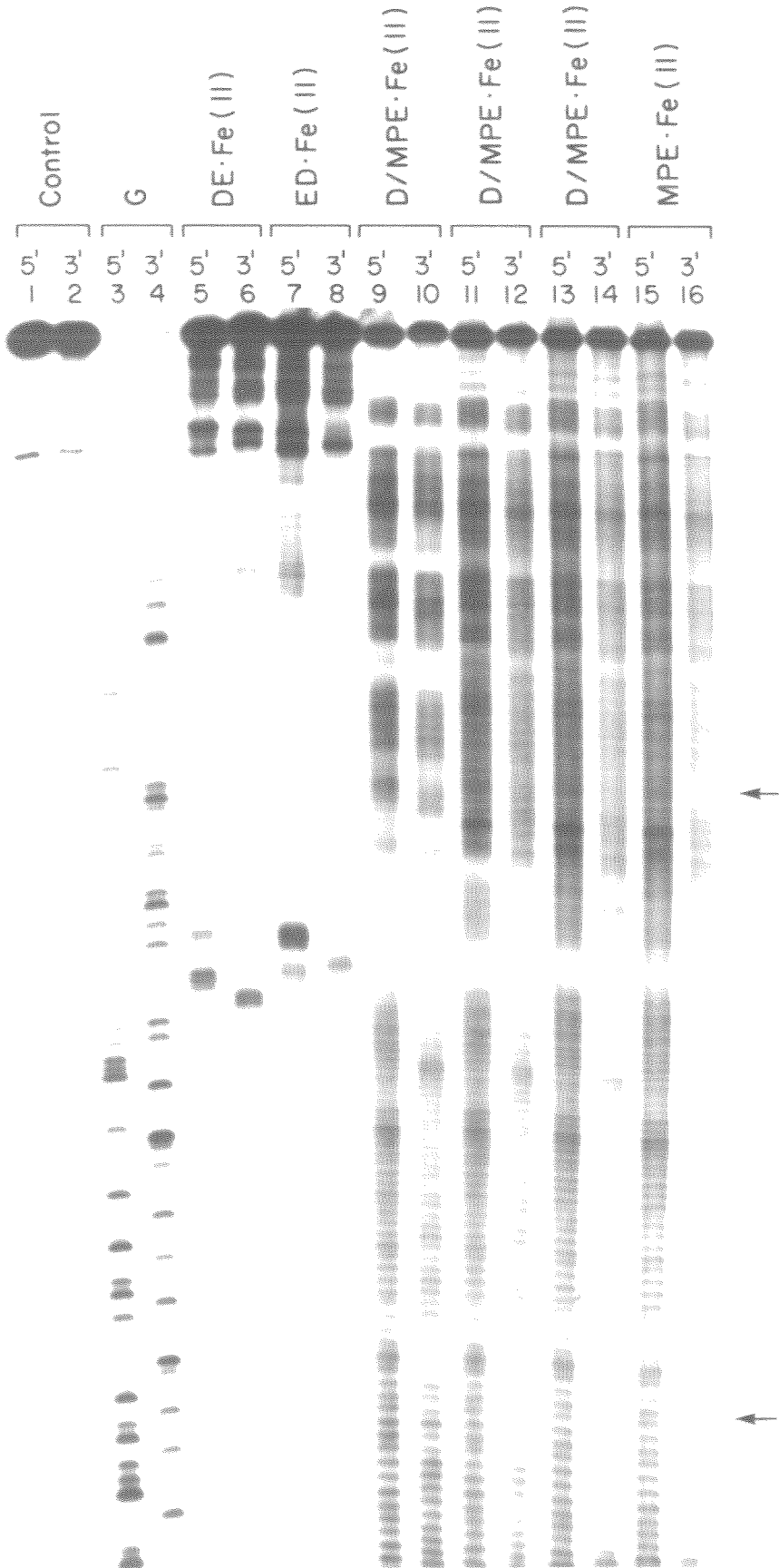


Figure 12. Autoradiogram of high resolution denaturing gel. Lanes 1,3,5,7,9,11,13, and 15 are 5' end-labeled 381 bp fragment; Lanes 2,4,6,8,10,12,14, and 16 are 3' end-labeled 381 bp fragment; Lanes 1,2: intact 381 bp fragment; Lanes 3,4: Maxam-Gilbert G reactions; Lanes 5,6: **DE**·Fe(II) $1.25 \times 10^{-5}\text{M}$; Lanes 7,8: **ED**·Fe(II) $1.25 \times 10^{-5}\text{M}$; Lanes 9,10: Distamycin $2.5 \times 10^{-5}\text{M}$, **MPE** $1 \times 10^{-5}\text{M}$; Lanes 11,12: Distamycin $1.25 \times 10^{-6}\text{M}$, **MPE** $1 \times 10^{-5}\text{M}$; Lanes 15,16: **MPE** $1 \times 10^{-5}\text{M}$. All reactions are $> 600 \text{ cpm } ^{32}\text{P}$ end-labeled 381 fragment, made up to 10^{-4}M bp with sonicated calf thymus DNA. Distamycin is pre-equilibrated with DNA for 30 minutes.



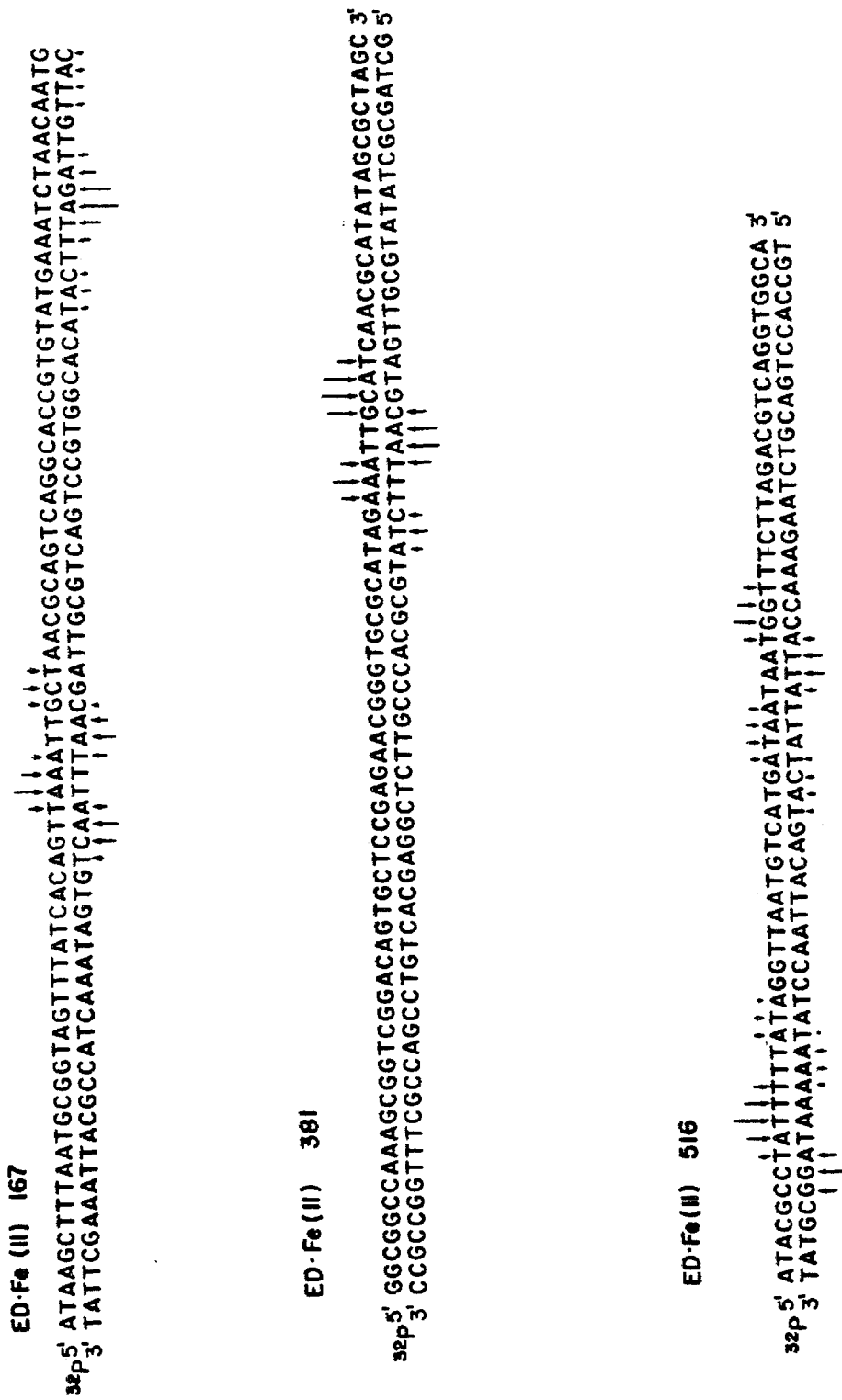
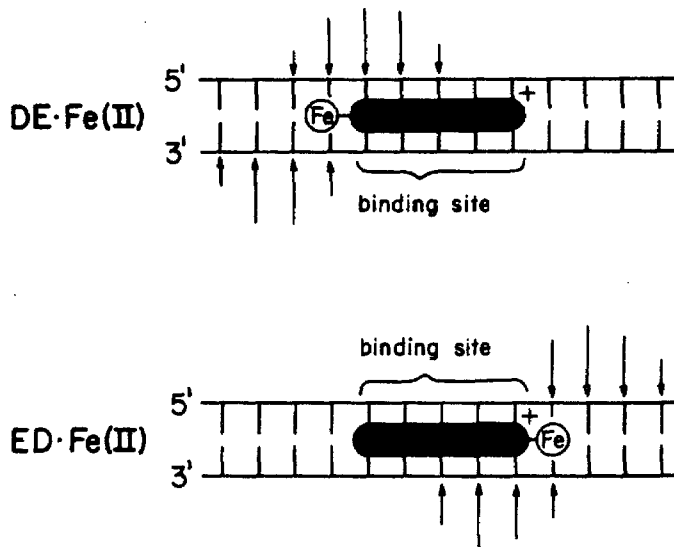


Figure 13. Histograms of ED·Fe(II) cleavage patterns.

Therefore the major orientation of the N-methylpyrrole tripeptide binds the five base pair 5'-AAATT-3' sequence with the amino terminus position to the 5' side.



The binding sites for the major and minor orientations of the tripeptide binding unit on the 381 base pair fragment are illustrated in Figure 14. The site for the minor orientation of the tripeptide unit is 5'-AAATT-3', with the amino terminus at the 3' end of the A rich strand. The binding sites for the major and minor orientations both encompass the same five base pairs. Importantly, this five base pair site is identical to that derived earlier from analysis of the **DE·Fe(II)** cleavage pattern.

A general model relating the average **ED·Fe(II)** cleavage pattern (compiled from the histograms in Figure 13) to the tripeptide binding site is illustrated below.

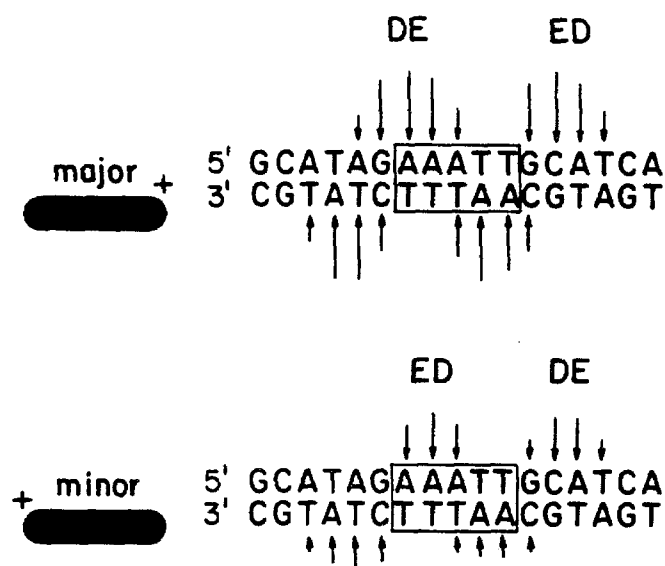


Figure 14. Binding sites for the major and minor orientations of the tripeptide unit on the 381 base pair restriction fragment. The major orientation site is defined by the major cleavage patterns from **DE**·Fe(II) and **ED**·Fe(II). Similarly, the minor orientation site is determined by the minor cleavage bands.

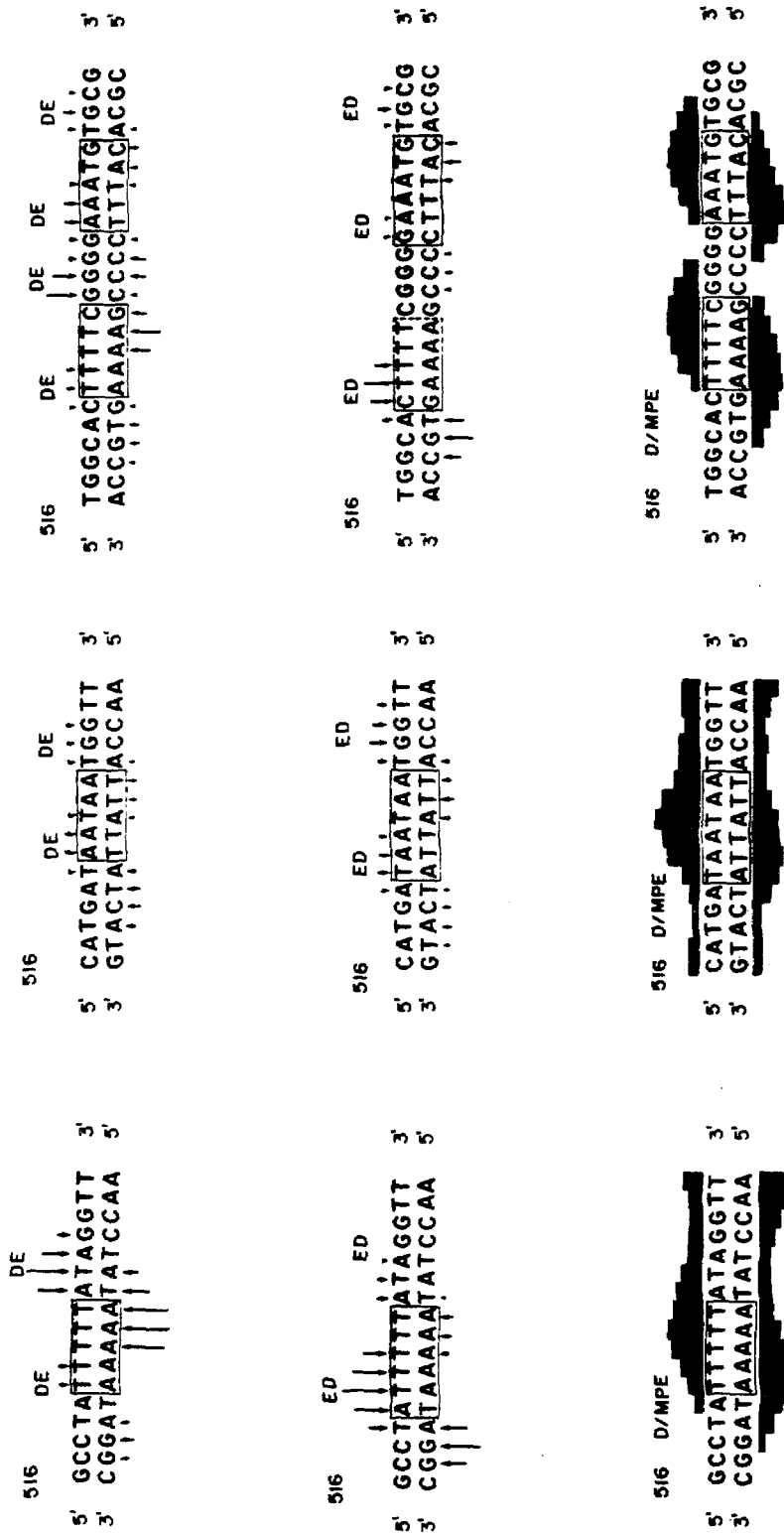


Figure 15. Binding sites for the major and minor orientations of DE•Fe(II) and ED•Fe(II). Distamycin/MPE•Fe(II) inhibition patterns are included.

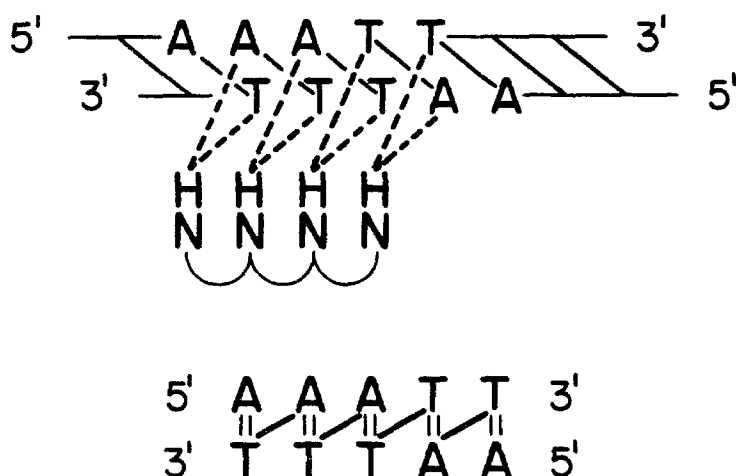
The average EDTA·Fe(II) position is located slightly nearer the binding site for ED·Fe(II) than DE·Fe(II). This may be due to the ability of the longer linker to "reach back" toward the binding site.

The major and minor DE·Fe(II) and ED·Fe(II) binding sites can now be assigned for all cleavage patterns on the 167, 381, and 516 base pair fragments (Figure 15). From these data a general picture of the DE·Fe(II) and ED·Fe(II) DNA binding interactions can be composed. DE·Fe(II) and ED·Fe(II) bind to a five base pair sequence. Predominant cleavage by DE·Fe(II) and ED·Fe(II) occurs at 5'XXTT-3', where X = A or T. There are 27 such binding sites on 4362 bp pBR-322 plasmid DNA. The major orientation places the amino terminus of distamycin at the 3' end of this sequence. Note that the sequence 5'-TTTX-3', where X = A or T, is a poor cleavage site. Consistent with this, the orientation preference of DE·Fe(II) and ED·Fe(II) at the 3'-TTTT-5' 516 bp site is the largest observed. The strongest tripeptide DNA binding interactions must therefore occur between the carboxamides closest to the peptide's amino terminus and the 3' thymines. Distamycin binding studies have shown that homopolymer poly(dC)·poly(dG) binds distamycin poorly.⁶⁶ It has also been demonstrated that the binding constant of a fluorescent dansyl distamycin analog for poly(dAT)·poly(dAT) is one fourth that for poly(dA)·poly(dT).⁶⁹ Our results are consistent with both observations.

Note that attachment of EDTA·Fe(II) to either the carboxy or amino terminus of the N-methylpyrrole tripeptide does not in general alter the tripeptide binding site on the DNA. (Figure 13) Furthermore, the orientation bias of the N-methylpyrrole tripeptide binding unit is the same for ED·Fe(II) and DE·Fe(II). This is somewhat surprising since

the orientation preference reflects < 1 kcal/mole difference in binding interactions. EDTA-Fe(II) attachment therefore appears to have little effect on the specificity of N-methylpyrrole carboxamide oligopeptide DNA binding. Presumably then, the binding sites of DE-Fe(II) and ED-Fe(II) are the same as those of the antibiotic distamycin A - DE-Fe(II) and ED-Fe(II) function as "affinity cleaving reagents", locating the distamycin binding sites on heterogeneous duplex DNA.

Consequently a model for the binding of distamycin to the minor groove of B DNA can be postulated based on the cleavage patterns of DE and ED. Distamycin is centered in the groove in order to minimize steric interactions. Hydrogen bonding may then occur between



the carboxamide NH's and N(3) of adenine or O(2) of thymine on adjacent base pairs. Hydrogen bonding to O(2) should be favored due to better lone pair orientation (thymine O(2) protrudes 0.5 \AA more from the

helical axis than adenine N(3)). The N(2) of guanine provides a steric barrier to hydrogen bonding resulting in distamycin's A+T preference. Alternating A+T base pairs remove a thymine O(2)-carboxamide hydrogen bond from every other base pair consistent with the preference of **DE** and **ED** for 5'-T_n-3'. Steric interactions between C(2)H of the pyrroles and N(2)H of adenine may account for the 3'-5' directional bias. However, it is not clear from this model why 3'-TTTXX-5' is a better binding site than 3'-XXTTT-5'.

Finally evidence in the literature suggests that distamycin A binding may be conformationally dependent.⁹⁵ On changing from 60% ethanol to 80% ethanol (5 x 10⁻⁴M salt), conditions known to induce a B → A helical transition,⁹⁶ distamycin binding is severely reduced.^{95a} In addition distamycin binds strongly to poly(dA)·poly(dT) but binding to poly(rA)·poly(dT) and poly(rA)·poly(rU) (A conformation) is diminished.^{96b,c} It may therefore be possible to use **DE**·Fe(II)/**ED**·Fe(II) cleavage to probe the conformational properties of heterogeneous DNA. For example, the RNA polymerase promoter sites in the lac operon are A+T rich.^{37,96,97} Furthermore it has been suggested that a B-A conformational transition may be necessary for transcription.⁹⁷ Cleavage of the lac operon by **DE**·Fe(II) in the presence or absence of RNA polymerase or catabolite regulator protein (CAP)⁹⁷ might reveal conformational changes in the DNA.

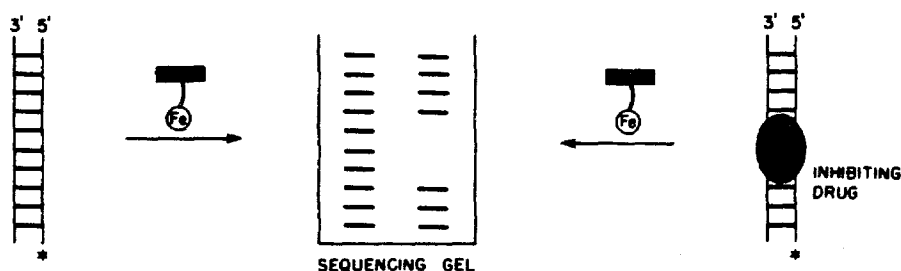
The general strategy of attaching cleaving functions (in this case a chelated metal capable of redox chemistry) to DNA binding molecules may be a general direct method for determining the binding site and binding orientation of small molecules on DNA. (Recently it

has been shown that attachment of ^{125}I to Hoechst 33258 allows mapping of the drug's binding site on DNA by analysis of single strand cleavage patterns.)⁹⁸ One can imagine that the DNA affinity cleavage method is extendable to larger DNA binding molecules including peptides and DNA binding proteins. A method exists in the literature for derivatizing the basic amino groups of proteins with the metal chelator diethylene triamine pentaacetic acid dianhydride.⁹⁹

Comparison of Affinity Cleaving with $\text{MPE}\cdot\text{Fe(II)}$ Footprinting

Let us now compare the binding sites of distamycin determined by the affinity cleaving method with the $\text{MPE}\cdot\text{Fe(II)}$ DNA inhibition⁵³ patterns produced by distamycin (Figures 8 and 15).

The $\text{MPE}\cdot\text{Fe(II)}$ cleavage inhibition patterns produced by distamycin are shown in the gel autoradiograms and histograms in Figures 3-7. A $\text{MPE}\cdot\text{Fe(II)}$ /base pair ratio of 0.05 results in partial strand scission of the end labeled restriction fragment. The light regions of reduced $\text{MPE}\cdot\text{Fe(II)}$ cleavage are interpreted as resulting from the presence of bound drugs.⁵³



A histogram of **MPE**·Fe(II) inhibition patterns produced by distamycin in the region of base pairs 229-262 of the 381 bp fragment (drug/bp = 0.1) is shown in Figure 16.

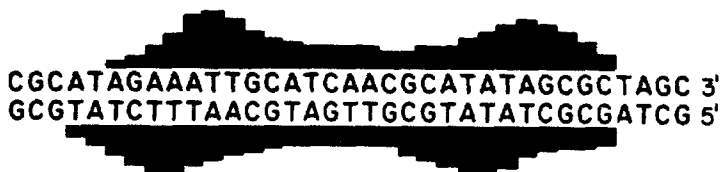


Figure 16 - Histogram of distamycin inhibition patterns on opposite strands of 381 bp fragment.

The extent of **MPE**·Fe(II) cleavage inhibition is represented by the bar height over each base pair. Two major A+T rich distamycin binding sites are present. In addition **MPE**·Fe(II) is inhibited to some extent in the 11 base pair region between the sites. This suggests that the binding of distamycin to DNA may produce a change in the DNA five to ten base pairs away which effects methidium binding.¹³ Krylov⁶⁹ and Crothers¹⁰⁰ have both presented evidence suggesting that the binding of distamycin to DNA alters the state of DNA. The evidence includes: cooperativity in distamycin binding (fluorescence and phase partition binding assays);^{69,100} changes in DNA length up to a maximum of $14 \text{ \AA}^0/\text{drug}$ at $r = 0.03$ (electric dichroism);¹⁰⁰ and a reduction in ethidium binding

affinity to calf thymus DNA at $r_{\text{distamycin}} = 0.03$ as well as a change in ethidium intercalation geometry at $r_{\text{distamycin}} = 0.03$.¹⁰⁰ Note that **MPE**•Fe(II) is also slightly inhibited in some A+T rich regions without bound distamycin. This may reflect some G-C or conformational specificity in methidium binding.

The **DE**•Fe(II)/**ED**•Fe(II) cleavage patterns provide a model for accurately interpreting **MPE**•Fe(II) footprints. A distamycin/**MPE** inhibition pattern (distamycin/bp = 0.1, 167 bp fragment) is illustrated in Figure 17. The corresponding **DE**•Fe(II) cleavage patterns are shown for comparison. The **MPE**•Fe(II) inhibition patterns are centered around the distamycin binding sites. In addition the inhibition patterns are asymmetric on opposite strands and shifted to the 3' ends. The extent of inhibition at each base pair is complementary to the cleavage produced at that base pair by an **EDTA**•Fe(II) whose average position is n

base pairs distant. By using the cleavage pattern produced by $\text{DE} \cdot \text{Fe(II)}$ we can determine the boundaries of the distamycin binding site. Two assumptions are made: 1) the cleavage pattern produced by the average position of a distamycin linked $\text{EDTA} \cdot \text{Fe(II)}$ is the same as that produced by the average position of a methidium linked $\text{EDTA} \cdot \text{Fe(II)}$ (substantial differences are required to alter the model appreciably); 2) the closest $\text{MPE} \cdot \text{Fe(II)}$ intercalation site is one base pair removed from the distamycin binding site. By summing the cleavage patterns produced by an $\text{EDTA} \cdot \text{Fe(II)}$ placed at each of the bases adjacent to a distamycin binding site we get the calculated inhibition pattern illustrated in Figure 19. Inhibition reaches > 50% its maximum value 2 base pairs into the binding site in the 5' direction and 2 base pairs out of the binding site in the 3' direction. Consequently the 5' strand is underprotected by one base pair and the 3' strand is overprotected by two base pairs. The agreement between the experimental inhibition pattern and that predicted by the model is good. The model suggests

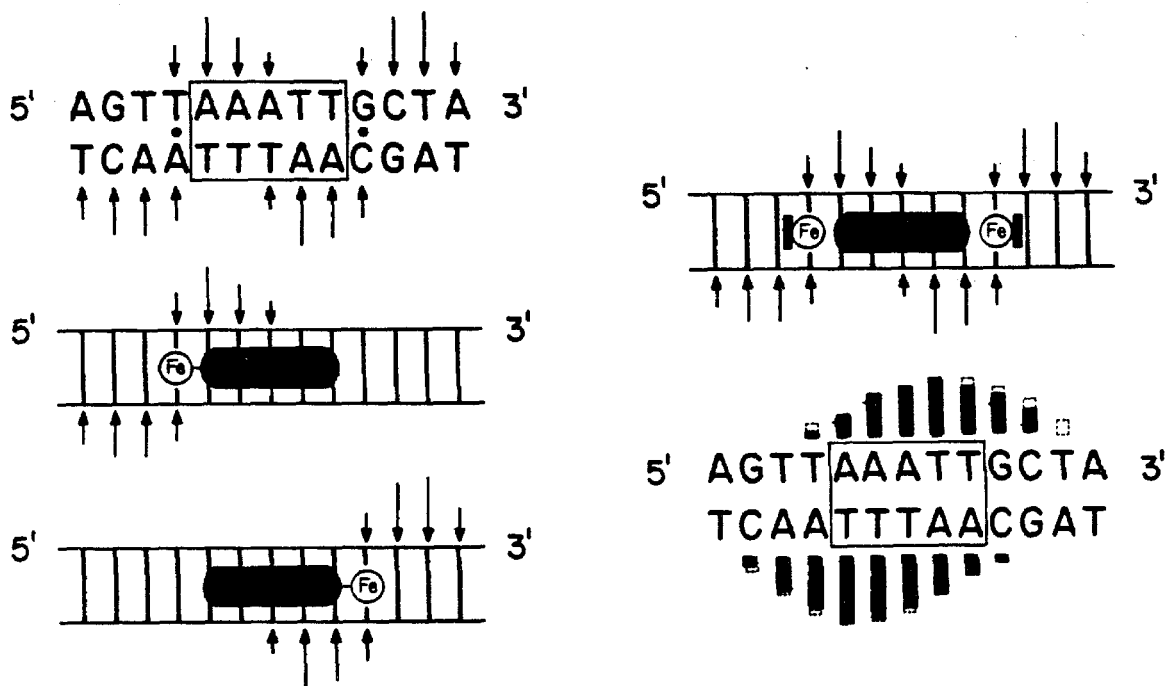


Figure 17. Distamycin/**MPE**·Fe(II) inhibition patterns and **DE**·Fe(II) cleavage patterns on the 167 bp fragment. Calculated inhibition pattern —.

that if a small molecule could be footprinted, or a DNA cleaving molecule synthesized, which binds to left handed Z DNA, the asymmetry of the cleavage patterns might distinguish the conformations of DNA.

By using the average **EDTA**·Fe(II) cleavage pattern determined from **DE**·Fe(II), **ED**·Fe(II), **P5E**·Fe(II), **EBD**·Fe(II) and **BED**·Fe(II) cleavage sites, a general model for footprints can be proposed (Figure 19). Again inhibition reaches > 50% its maximum value two base pairs into the binding site on the 5' strand and two base pairs out of the

binding site on the 3' end. This model agrees well with that proposed earlier by Van Dyke and Dervan.⁵³

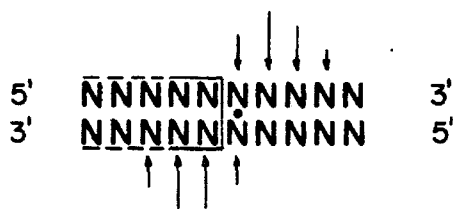


Figure 18 - The average cleavage pattern around EDTA·Fe(II) in the minor groove of right-handed DNA - determined from DE·Fe(II), ED·Fe(II), PSE·Fe(II), EBD·Fe(II) and BED·Fe(II) cleavage sites.

Application of the footprinting model to the MPE·Fe(II) inhibition patterns produced by distamycin on the 167, 381, and 516 base pair fragment affords the distamycin binding sites boxed in Figure 20. The distamycin binding sites are in most cases five base pairs in size and occur in A+T rich regions of the DNA. Few GC base pairs are present in the distamycin binding sites. The experimental inhibition patterns agree well with those predicted by our models.

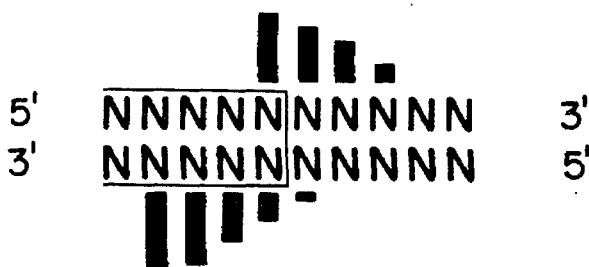


Figure 19 - Model of a "calculated" footprint.

Examination of Figures 13 and 14 reveals that the binding sites produced by **DE**·Fe(II) and **ED**·Fe(II) are identical in almost every case to the distamycin footprints at the same locations (Table III). The correspondence between **DE**·Fe(II), **ED**·Fe(II) and distamycin binding sites demonstrates that EDTA attachment or bound **MPE**·Fe(II) does not significantly perturb the recognition or binding interactions of the N-methylpyrroletripeptide with DNA. In regions of DNA where the drug binding sites are less than 10 base pairs apart, it becomes difficult to precisely determine the binding site size by footprinting due to the high degree of **MPE**·Fe(II) inhibition produced between the sites. bound drug. At similar pyrrole tripeptide/bp ratios (0.1), footprinting reveals more distamycin binding sites than revealed by **DE**·Fe(II) and **ED**·Fe(II) cleavage. Increasing **DE**·Fe(II)/**ED**·Fe(II) concentration relative to distamycin concentration increases the correspondence between the footprints and **DE** cleavage patterns (figure 7). Increasing the concentration of distamycin results in an increase in the relative number of sites protected from **MPE**·Fe(II) cleavage (see Figure 12). A number of factors could contribute to the variation in the number of sites detected by the two methods. EDTA attachment may reduce the tripeptide binding constant due to a net reduction of the nonspecific electrostatic binding of **DE**·Fe(II) and **ED**·Fe(II) as well as nonspecific steric interactions of EDTA·Fe(II) with the DNA. Furthermore since we expect **DE** cleavage to follow Michaelis Menten kinetics, the extent of cleavage at each site is also dependent on the cleavage and reactivation rates of the EDTA·Fe(II) moiety (page 154). However the binding of **MPE**·Fe(II) to DNA could also alter the affinity of individual distamycin binding sites on DNA. Therefore, although the sensitivities of the two

methods for detecting individual sites may vary, it is not clear whether this is due to an allosteric effect associated with **MPE** or the binding/cleavage properties of **DE**.

In summary, DNA affinity cleavage patterns^{3,6} and **MPE**·Fe(II) inhibition patterns⁵³ have been used to determine the binding sites of polypyrrole peptides on heterogeneous duplex DNA. Both techniques yield similar binding site locations and sizes indicating that each technique locates small molecule binding sites on DNA accurately. Affinity cleaving allows precise binding details to be determined such as major orientation preferences, whereas footprinting does not afford such detailed information. The two techniques differ in sensitivity in detecting individual distamycin binding sites. Affinity cleaving studies require the attachment of EDTA to the DNA binding moiety, and are therefore not as easily done and not as general as **MPE**·Fe(II) footprinting. Both techniques provide a direct method for determining drug binding sites on DNA and should be valuable tools in future studies of small molecule, peptide, and protein DNA binding.

Table III - Common Sites for **DE**·Fe(II) and D^a

<u>DNA Fragment</u>	<u>DE·Fe(II) sites</u>	<u>S</u>	<u>D/MPE·Fe(II) sites</u>	<u>S</u>
167	AAATT	5	AAATT	5
	AAATC	5	AAATC	5
381	AAATT	5	AAATT	5
516	TTTTT	5	TTTTT	5
	AATAA (ω) ^b	5	TAATAA	6
	TTTTC (ω)	5	TTTTC	5
	AAATG (ω)	5	AAATG	5

a) 5' to 3', b) (ω) is a weak site

D/MPE·Fe(II) 167

32p 5' ATAAGC TTTAA TGC GG T AG TTT ATC ACAG TTA AAT T GCT AAC GCAG TCAG GCAC CGT GTAT GAAATCTAACAATCC
3' TATTCGAAATACGCCATCAATAGTGTCAATTTAACGATTGCGTCAGTCCGTGGCACATACCTTAGATTGTTAGG

D/MPE·Fe(II) 381

32p 5' GCGGGCCAAAGCGGTCCGACAGTGCTCCGAGAACGGGTGCGCATAGAAATTCATCAACGCATATAGCGCTAGC 3'
3' CCGCGGTTTCGCCAGCCTGTCAGGAGCTCTTGCCACGCGTATCTTTAACGTTGCGTATATCGCGATCG 5'

D/MPE·Fe(II) 516

32p 5' ATACGCCCTATTTTATAGGTTAATGTCATGATAATAATGGTTTCTTAGACGTCAGGTGGCACITTCGGGAAATGTGCGCGGAA
3' TATGCGGATAAAAATATCCAAATTACAGTACTATTATTACCAAGAATCTGCAGTCCACCGTGAAAAGCCCCITTTACACGCGCCTT

Figure 20. Distamycin footprints with binding sites boxed.

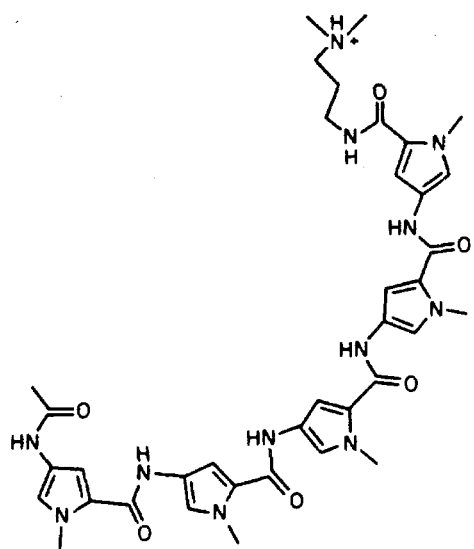
Penta-N-Methylpyrrole carboxamide-EDTA (P5E)

DE·Fe(II) and **ED**·Fe(II) double strand cleave pBR-322 at high binding densities and/or high DNA concentrations. Although cleavage is sequence dependent, the frequency of double strand scissions is high. The question arises whether a DNA binding molecule with increased specific base pair interactions would double strand cleave DNA with higher sequence specificity and at lower binding densities.

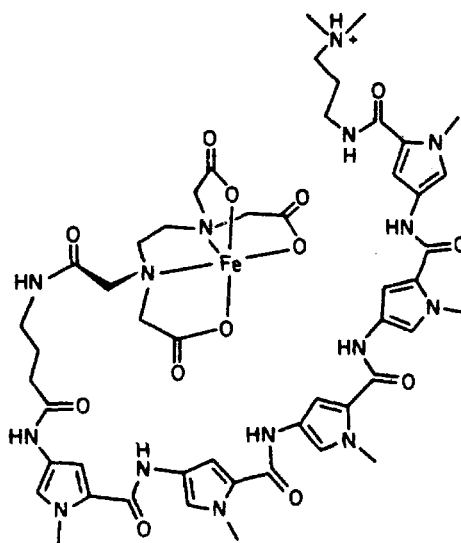
To test this hypothesis we synthesized the distamycin-EDTA·Fe(II) homolog, penta-N-methylpyrrole carboxamide-EDTA (**P5E**·Fe(II)). It has been previously demonstrated¹⁰¹ that the complex of DNA with a pentapeptide distamycin homolog is characterized by higher melting temperatures (T_m) and higher ellipticity (ϕ) than the distamycin DNA complex. These data as well as the binding studies of Krylov⁶⁹ mentioned earlier, suggested that **P5E** might bind tightly enough to DNA to cleave both strands sequentially. Alternatively higher binding specificity (relative to **DE**) might allow **P5E** to bind a site, cleave, dissociate and rebind and cleave the same site with high probability. Recall that restriction enzymes double strand cleave DNA by both mechanisms, depending on reaction conditions.

Synthesis

The synthesis of **P5E** is analogous to that of **DE**. Nitro amine **11** was converted to **13** by additional hydrogenation/coupling sequences. The remaining synthetic steps and purifications were identical to those described for **DE**·Fe(II) (Scheme IV). Acetylation of the reduced nitro amine, **13**, afforded **P5**. This derivative was synthesized for footprinting purposes.



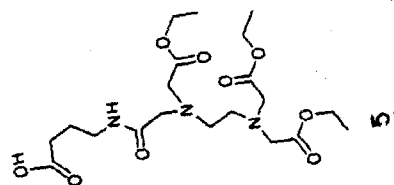
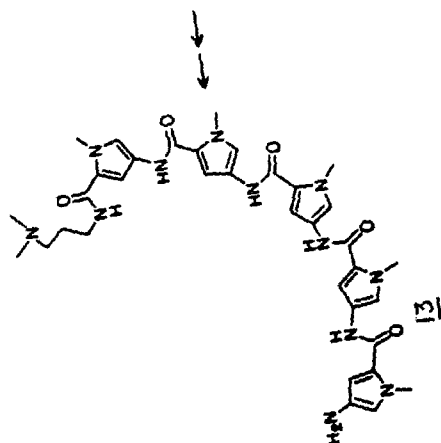
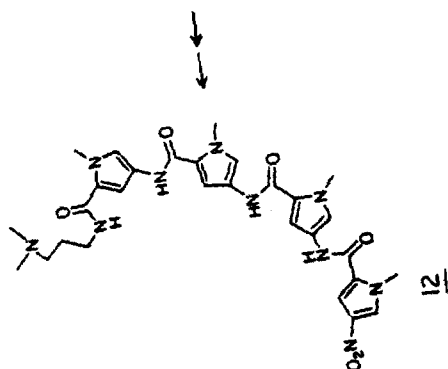
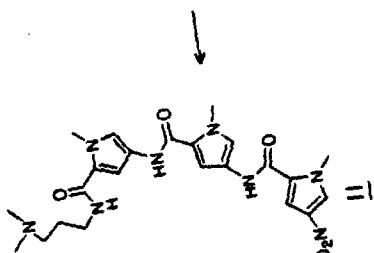
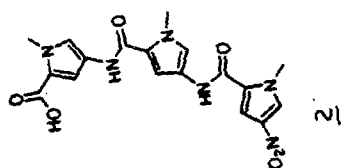
P5E



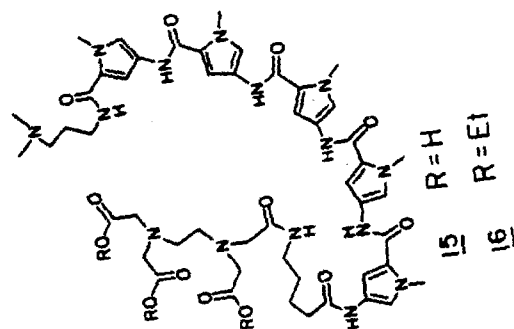
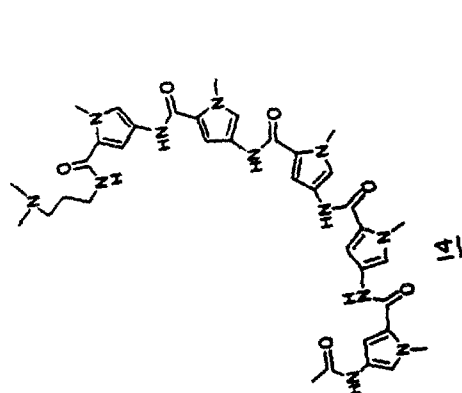
P5E · Fe (II)

Cleavage Efficiency

In the presence of O_2 and DTT (5 mM), 10 nanomolar P5E-Fe(II) cleaves supercoiled pBR-322 DNA (10 μ M base pairs) to afford 48% form I, 47% form II, and 5% form III DNA. Unlike DE-Fe(II), P5E-Fe(II) requires preequilibration (37°C, 1 hr) with the DNA before initiation of cleavage with DTT for optimum efficiency. Presumably formation of the final one or two hydrogen bonding interactions is kinetically slow or requires a substantial breathing motion of the helix.



Scheme IV



R = H
R = Et

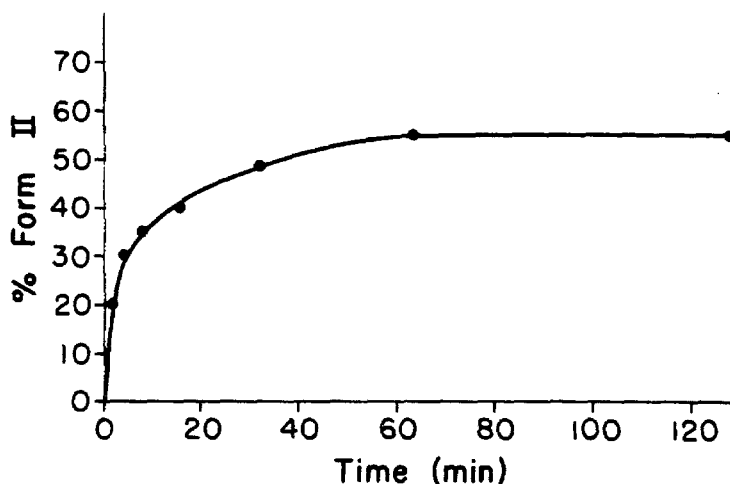
Table IV - Cleavage of pBR-322 Plasmid DNA in the Presence of DTTa

Reagent	conc. M	% Form			DNA conc. M	Reagent/ bp
		I	II	III		
MPE ·Fe(II)	10 ⁻⁷	0	98	2	10 ⁻⁵	10 ⁻²
DE ·Fe(II)	10 ⁻⁶	32	68	0	10 ⁻⁵	10 ⁻¹
P5E ·Fe(II)	10 ⁻⁷	3	59	38	10 ⁻⁵	10 ⁻²
P5E ·Fe(II)	10 ⁻⁸	48	47	5	10 ⁻⁵	10 ⁻³
P5E ·Fe(II)	10 ⁻⁹	84	16	0	10 ⁻⁵	10 ⁻⁴
P5E ·Fe(II)	10 ^{-8b}	90	10	0	10 ⁻⁵	10 ⁻³
MPE ·Fe(II)	10 ⁻⁵	0	95	5	10 ⁻³	10 ⁻²
P5E ·Fe(II)	10 ⁻⁵	0	0	100 ^c	10 ⁻³	10 ⁻²
P5E ·Fe(II)	10 ⁻⁶	0	80	20	10 ⁻³	10 ⁻³
P5E ·Fe(II)	10 ⁻⁷	12	85	2	10 ⁻³	10 ⁻⁴
P5E ·Fe(II)	10 ⁻⁸	60	40	0	10 ⁻³	10 ⁻⁵

a) All reactions run to completion. **P5E** was preequilibrated with DNA at 37°C for 1 hr. b) no preequilibration c) linear DNA fragments < 4362 bp.

P5E·Fe(II) cleaves DNA (10⁻⁵M bp) to afford the same relative amounts of forms I, II and III DNA at two orders of magnitude lower concentration than **DE**·Fe(II). This result is consistent with an increased **P5E**·Fe(II) binding constant due to two additional hydrogen bonding interactions. Consequently, the amount of bound **P5E**·Fe(II) is higher at any given DNA concentration than the amount of bound **DE**·Fe(II). The efficiency of **P5E**·Fe(II) at 10⁻⁸M **P5E** and 10⁻³M base pairs is 1100% (based on Poisson distribution) representing a minimum of 11 turnovers. The cleavage efficiency of **P5E**·Fe(II) at 10⁻⁸M **P5E** and 10⁻⁵M base pairs is 20% indicating that at 10⁻⁵M DNA substantial amounts of **P5E** is unbound. Keep in mind that 10⁻⁵M bp is not the actual **P5E** binding site concentration.

Cleavage of DNA by **P5E**·Fe(II) is complete after two hours, considerably longer than the reaction time of **DE**·Fe(II) with DNA.



Inactivation of the catalyst by OH^- may occur more slowly when $\text{EDTA}\cdot\text{Fe(II)}$ is bound to DNA than when free in solution. Further addition of DTT to the reaction mixture after two hours did not result in additional cleavage, consistent with catalyst degradation.

The effect of inhibitors on $\text{PSE}\cdot\text{Fe(II)}$ cleavage was examined (Table IV). Addition of Fe(II) to PSE in the presence of the strong metal chelator desferrioxamine resulted in no cleavage. Addition of Fe(II) to $\text{PSE}\cdot\text{Ni(II)}$ resulted in only slight DNA cleavage. Ni(II) is known to form stable complexes with EDTA and presumably competes effectively with Fe(II) for the chelation site on PSE^{102} . Fe(II) is therefore essential to the cleavage reaction.

Table IV - Inhibition Studies

Inhibitor	conc.	% Form			
		M	I	II	III
none	—		5	95	0
Desferrioxamine	0.05		92	8	0
Ni(II)	0.01		98	2	0
DTT	1 M		92	8	0
DMSO	0.8M		92	8	0
catalase	100 ^b		95	5	0

a) pBR-322 plasmid DNA (10^{-5} M bp), P5E (2.5×10^{-6} M) and inhibitor were combined in buffer, then Fe(II) (2.5×10^{-6} M) was added. b) Concentration in $\mu\text{g/ml}$.

The presence of catalase in the reaction reduces cleavage substantially, suggesting that H_2O_2 is important for cleavage. Furthermore, the hydroxyl radical traps DMSO (0.8M) and DTT (1M) strongly inhibited the P5E cleavage reactions. These results are consistent with the mechanism proposed earlier for EDTA·Fe(II) DNA cleavage.

Double Strand Cleavage

The ability of P5E·Fe(II)/DTT to sequence specifically double strand cleave DNA was assayed on linear pBR-322 plasmid DNA (4362 base pairs⁹¹). Supercoiled pBR-322 was linearized with a series of restriction enzymes and purified by ethanol precipitation. P5E·Fe(II) was then allowed to react with the linear DNA's (50 μM bp) at a series of concentrations and the reactions were analyzed by 1% agarose gel electrophoresis with ethidium bromide staining. Figure 21 shows the result of P5E·Fe(II)/DTT cleavage of Eco RI and Sal I linearized DNA's. P5E·Fe(II) double strand cleaves pBR-322 into discrete fragments at P5E·Fe(II)/base pair ratios, b , ≤ 0.01 . At $b = 0.01$, the position of

eight dominant cleavage sites have been mapped from an analysis of the cleavage patterns produced by **P5E**·Fe(II)/DTT on Eco RI, Sal I, Nde I, Ava I, Hind II and Ava I, Taq I, and Rsa I linearized pBR-322 fragments (Table V).

The cleavage sites of **P5E**·Fe(II) were located by digesting pBR-322 with a series of restriction enzymes, reacting these digests with **P5E**·Fe(II), and measuring the lengths of the resulting fragments produced. The restriction enzymes used, the cleavage site of the restriction enzyme, and the fragment sizes produced by reaction with **P5E**·Fe(II) are listed in Table VA. The assignment of the **P5E** cleavage sites was confirmed by assaying the disappearance of restriction enzyme fragments on reaction with **P5E**·Fe(II). The restriction enzymes used, the fragments these enzymes produced with pBR-322 and the absence of restriction fragments on **P5E**·Fe(II) digest are noted in Table VB.

Major double strand cleavage sites ($b = 0.01$) are centered at 4.3, 4.2, 3.3, and 3.2 kilobases (kb) and minor sites at 2.6, 2.4, 2.0, and 1.8 ± 0.1 kb. These sites are all located in regions of pBR-322 with sequences corresponding to $5'-T_n-3'$ where $n \geq 5$.⁹¹ Furthermore, these are the only regions of pBR-322 with such sequences.⁹¹ Therefore it appears that **P5E**·Fe(II) has a high propensity to double strand cleave poly(dA)·poly(dT) sequences. This is consistent with the model proposed earlier for the distamycin DNA complex. Note, however, that the molecular weights of the fragments do not sum to 4362, indicating that we are observing partial digests of the DNA. At high **P5E**·Fe(II)/base pair ratios the intensity of the major cleavage sites diminishes and a near continuum of smaller DNA fragments appears. Presumably at $b > 0.05$, **P5E**·Fe(II) begins to cleave at the less preferred **P5E**·Fe(II) binding sites producing a larger number of smaller sized fragments.

Table V - Restriction Mapping of **P5E·Fe(II)** Sites

A

<u>Eco RI</u> (0) ^a	<u>Sal I</u> (650)	<u>Nde</u> (2297)	<u>Ava I</u> (424)
4250	3700	2500	1900
3400	3650	2300	1700
3250	2550	1100	1550
2700	2700	1000	1450
2450	2000		
2050	1850		
1850	1400		
	1200		

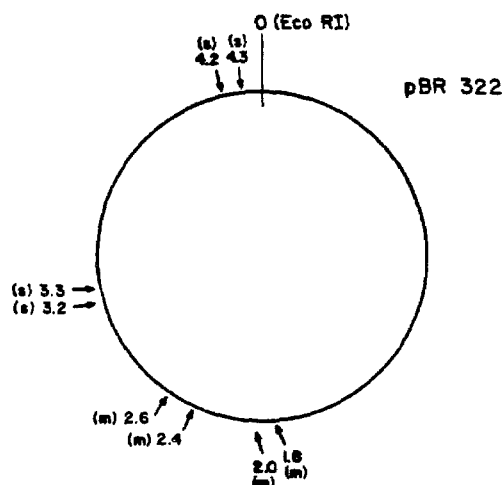
Hind III/Ava I (652,1424,3908) Form I pBR-322

1900	3600
1700	3450
700	700
650	650

B

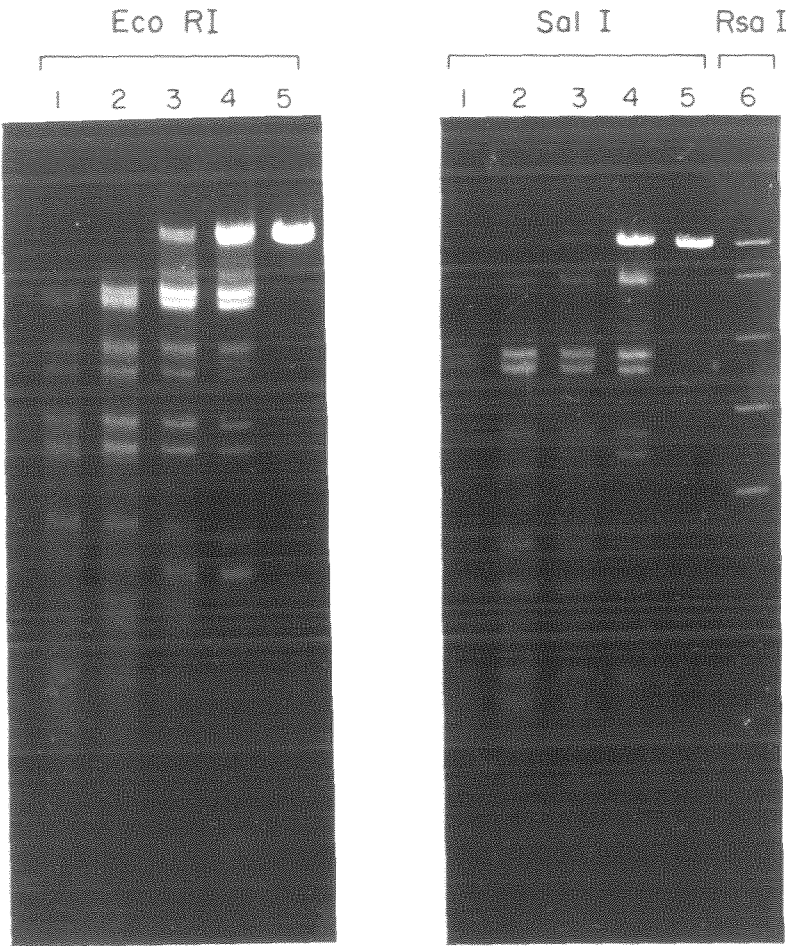
<u>Rsa I</u> ^b	<u>Taq I</u> ^b
p(165-2282)	(24- 399)
-(2282-3847)	(339- 651)
-(3487- 165)	(651-1267)
	p(1267-2574)
	-(2574-4018)
	-(4018- 24)

a) location of restriction enzyme cleavage site on pBR-322 b) - represents the disappearance of the indicated fragment on reaction with **P5E·Fe(II)**, p represents partial disappearance.



Cleavage Sites of **P5E·Fe(II)**; s (strong), m (moderate)

Figure 21. Nondenaturing agarose gel. Lanes 1,2,3,4,5: Eco RI pBR 322 digest 50 μ M bp; Lanes 6,7,8,9,10: Sal I digest; Lane 11, partial Rsa I digest; Lanes 1 and 6: 5 μ M P5E-Fe(II); Lanes 2 and 7: 1 μ M P5E-Fe(II); Lanes 3 and 8: 0.5 μ M P5E-Fe(II); Lanes 4 and 9: 0.25 μ M P5E-Fe(II). P5E-Fe(II) was allowed to preequilibrate for 1 hr (37°C) with DNA in 40 mM Tris Base, 5 mM NaOAc, pH 7.9 buffer. DTT was 5 mM.



The specificity of **P5E**·Fe(II) double strand cleavage at low binding densities is substantially greater than that of **DE**·Fe(II) and **ED**·Fe(II). The two additional carboxamide hydrogen bonding interactions therefore not only increase the binding constant of **P5E**·Fe(II) but preferentially increase the binding constant to poly(dA)·poly(dT) DNA.

At 10^{-3} M base pairs and 10^{-8} M **P5E** there exists more form II DNA than **P5E**·Fe(II) in solution indicating that the **P5E**·Fe(II) DNA complex dissociates. In addition the plot of strand scission versus time reveals that double strand cleavage is dependent on the concentration of form II DNA not form I. These results suggest that **P5E**·Fe(II) double strand cleaves DNA by site specifically rebinding and cleaving single strand cleaved form II DNA. The mechanism of double strand cleavage of DNA by **P5E**·Fe(II) is therefore consistent with equation (2) (page 151). For **P5E**·Fe(II) we might expect the rate of reactivation of **P5E**·Fe(II), k_3 , to become more competitive with the rate of dissociation of **P5E**·Fe(II) from the DNA.¹⁰⁸

The specificity of **P5E**·Fe(II) double strand cleavage is invariant to salt concentration in the 10 to 200 mM range. 1M NaCl inhibits double strand cleavage altogether, probably by reducing electrostatic binding interactions. These results are consistent with data in the literature indicating that netropsin binding (CD) to poly(dA·dT) is independent of salt from 20 to 300 mM NaCl.⁶⁴

Cleavage Specificity

P5E·Fe(II) single strand cleavage was examined on the 3' and 5' ³²P end-labeled^{90,92,93} 167, 381 and 516 base pair restriction fragments

using high resolution denaturing gel electrophoresis. The autoradiograms and resulting histograms are illustrated in Figures 22-25. For comparison, the **P5/MPE**·Fe(II) inhibition patterns, distamycin/**MPE**·Fe(II) inhibition patterns and **DE**·Fe(II) cleavage patterns are also shown.

A model relating the average **EDTA**·Fe(II) position to the **P5E**·Fe(II) binding site is illustrated in Figure 26 (based on the average **P5E**·Fe(II) cleavage pattern).

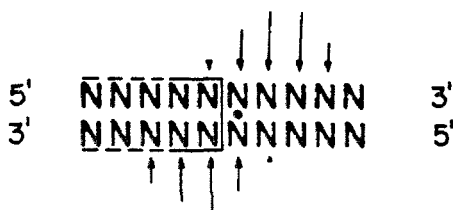


Figure 26. Relationship between average **EDTA**·Fe(II) position and the **P5E**·Fe(II) binding site.

Note the similarity of the average **P5E**·Fe(II) cleavage pattern to that of **DE**·Fe(II). The **P5E**·Fe(II) binding sites and **P5/MPE**·Fe(II) inhibition sites have been assigned in Figure 25. In assigning the **P5E**·Fe(II) binding site it has been assumed that the major and minor orientations bind the same site. This has been shown to be the case for **DE**·Fe(II) cleavage.

Figure 22 - Autoradiogram of high resolution denaturing gel.
Lanes 1,3,5,7,9,11 are 3' end labeled 516 bp fragment.
Lanes 2,4,6,8,10,12 are 5' end labeled 516 bp fragment.
Lanes 1,2: Maxam Gilbert G reactions; Lanes 3,4:
MPE·Fe(II), 5×10^{-6} M; Lanes 5,6: **DE**·Fe(II),
 1×10^{-5} M; Lanes 7,8: **PSE**·Fe(II), 2×10^{-6} M;
Lanes 9,10: distamycin 1×10^{-5} M, **MPE**·Fe(II)
 5×10^{-6} M; Lanes 11,12: **P5** 4×10^{-6} M,
MPE·Fe(II) 5×10^{-6} M. All reactions are > 600 cpm
 32 P end labeled 516 bp fragment, made up to 10^{-4} M
bp with sonicated calf thymus DNA in 40 mM Tris
base, pH 7.9, 5 mM NaOAc; 1 mM DTT.

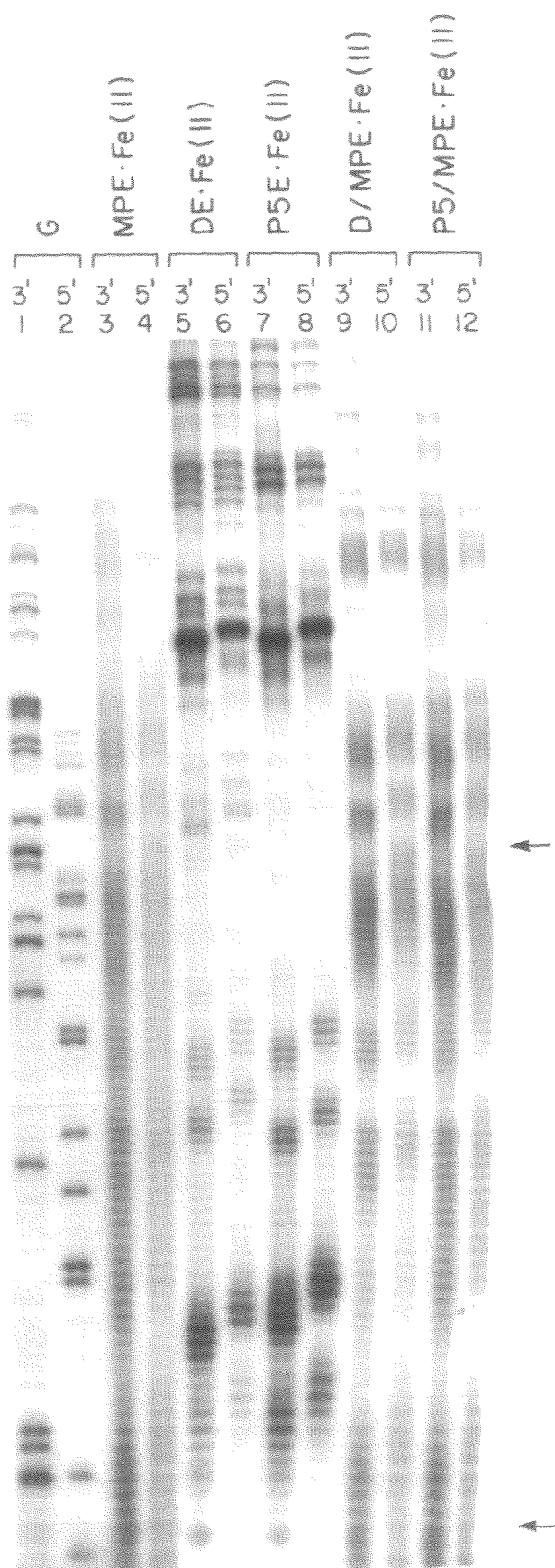


Figure 23 - Autoradiogram of high resolution denaturing gel.

Lanes 1,3,5,7,9,11 are 3' end labeled 381 bp fragment.
Lanes 2,4,6,8,10,12 are 5' end labeled 381 bp fragment.

Lanes 1,2: Maxam Gilbert G reactions; Lanes 3,4:

MPE·Fe(II), 5×10^{-6} M; Lanes 5,6: **DE**·Fe(II),

1×10^{-5} M; Lanes 7,8: **P5E**·Fe(II), 2×10^{-6} M;

Lanes 9,10: distamycin 1×10^{-5} M, **MPE**·Fe(II)

5×10^{-6} M; Lanes 11,12: **P5** 4×10^{-6} M,

MPE·Fe(II) 5×10^{-6} M.

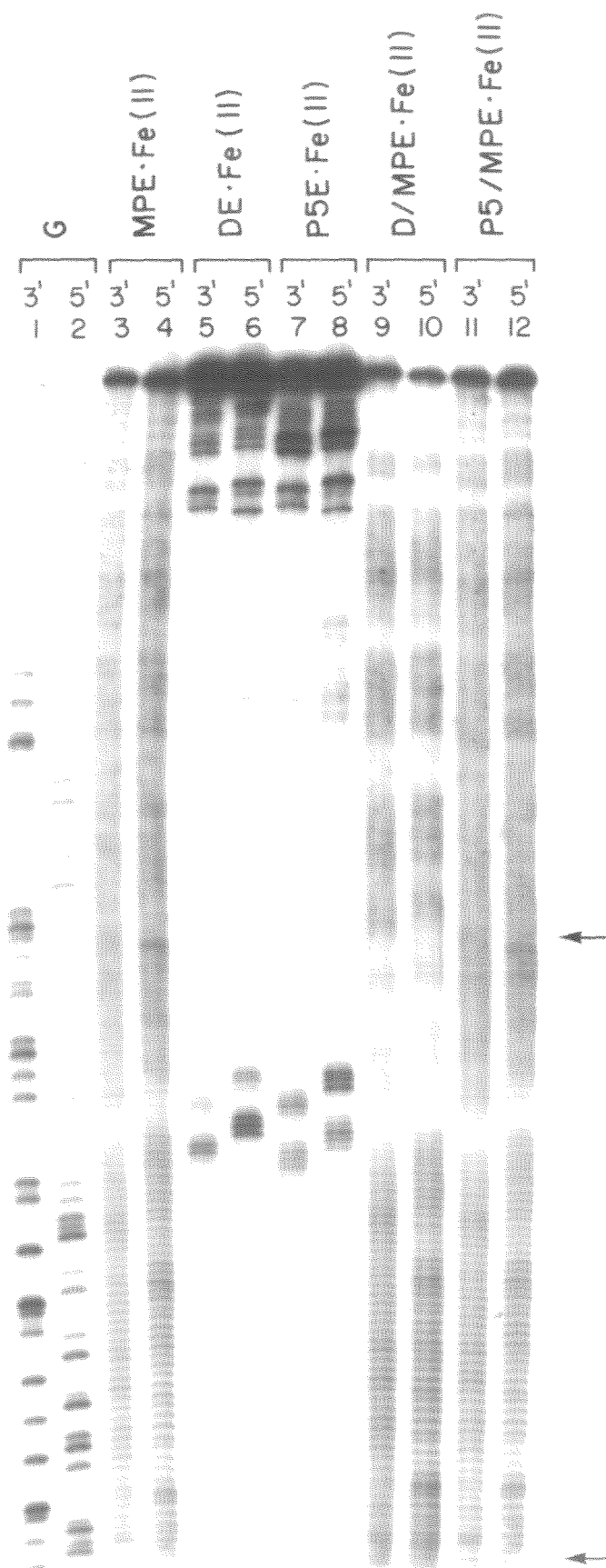
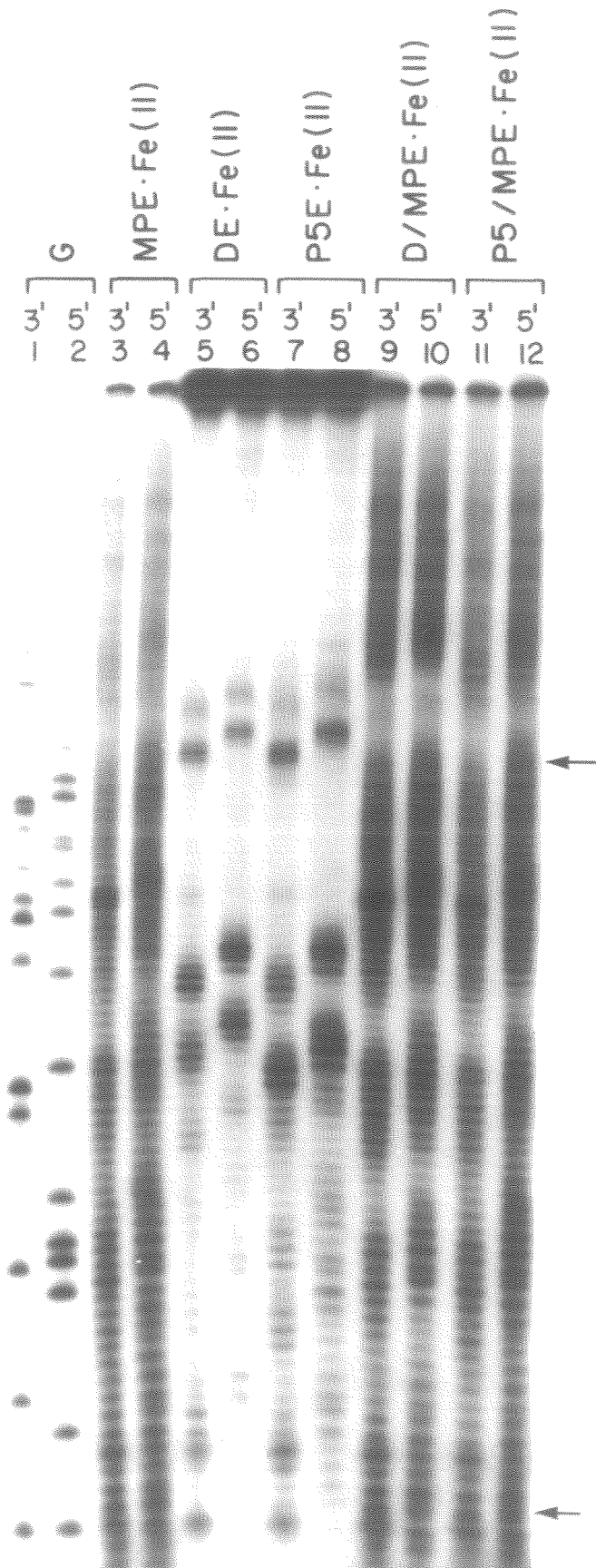
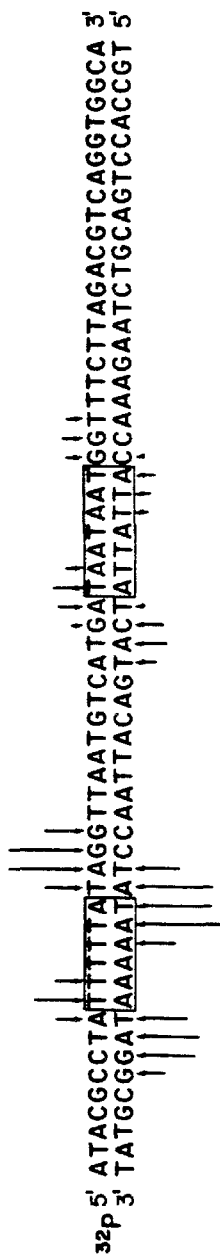


Figure 24 - Autoradiogram of high resolution denaturing gel.
Lanes 1,3,5,7,9,11 are 3' end labeled 167 bp fragment.
Lanes 2,4,6,8,10,12 are 5' end labeled 167 bp fragment.
Lanes 1,2: Maxam Gilbert G reactions; Lanes 3,4:
MPE·Fe(II), 5×10^{-6} M; Lanes 5,6: **DE**·Fe(II),
 1×10^{-5} M; Lanes 7,8: **PSE**·Fe(II), 2×10^{-6} M;
Lanes 9,10: distamycin 1×10^{-5} M, **MPE**·Fe(II)
 5×10^{-6} M; Lanes 11,12: **PS** 4×10^{-6} M,
MPE·Fe(II) 5×10^{-6} M.



P5E·Fe(II) 516



P5/MPE·Fe(II) 516



Figure 25 - Histograms of P5E·Fe(II) cleavage patterns and P5/MPE·Fe(II) inhibition patterns - binding site is boxed.

P5E·Fe(II) 381

32p 5' GCGGGCCAAAGCGGTTCGGACAGTGCTCCGAGAACGGGTGCGCATAGAAATTCGCATCAACGCATATAGCGCTAGC 3'
3' CCGCCGGTTTCGCCAGCCTGTCACGAGGCTCTTGCCCAACGCGTATCTTTAAACGTAAGTTGCGTATATCGCGATCG 5'

P5/MPE·Fe(II) 381

32p 5' GCGGGCCAAAGCGGTTCGGACAGTGCTCCGAGAACGGGTGCGCATAGAAATTCGCATCAACGCATATAGCGCTAGC 3'
3' CCGCCGGTTTCGCCAGCCTGTCACGAGGCTCTTGCCCAACGCGTATCTTTAAACGTAAGTTGCGTATATCGCGATCG 5'

P5E·Fe(II) 167

32p 5' ATAAGCTTTAAATGCGGTAGTTTATCACAGTTAAATTGCTAAACCCAGTCAGGCACCGTG 3'
3' TATTCGAAATTACGCCATCAAAATAGTGTCAATTTAAACGATTGCGTCAGTCCGTGGCAC 5'

P5/MPE·Fe(II) 167

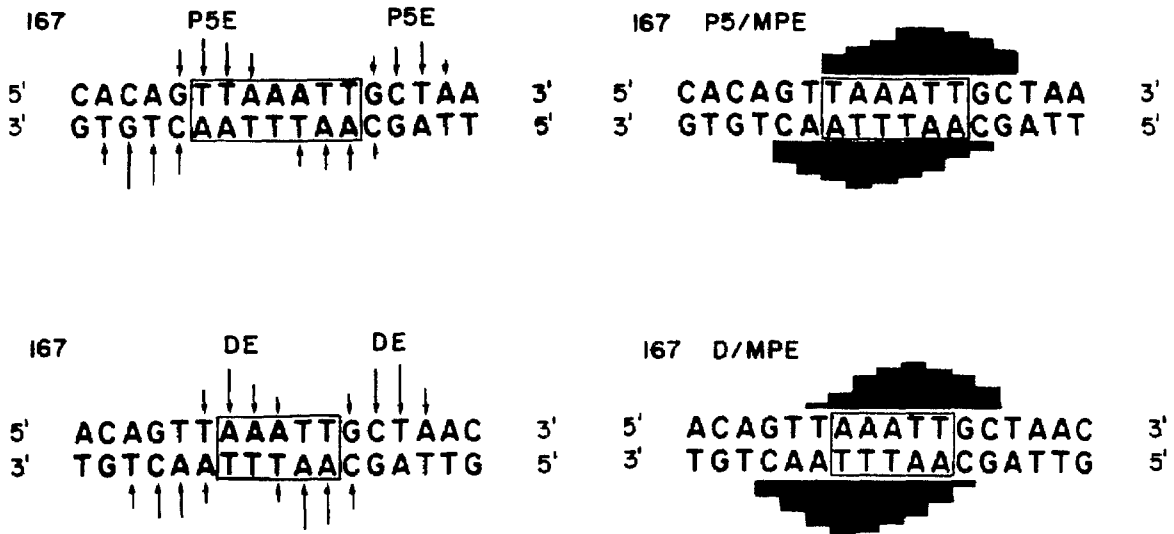
32p 5' ATAAGCTTTAAATGCGGTAGTTTATCACAGTTAAATTGCTAAACGCAGTCAGGCACCGTG 3'
3' TATTCGAAATTACGCCATCAAAATAGTGTCAATTTAAACGATTGCGTCAGTCCGTGGCAC 5'

The 5'-TTTTTA-3' **P5E**·Fe(II) site on the 516 base pair fragment (bp 4322-4328) has been assigned to the 4.3 kb double strand cleavage site. The intensity of cleavage at this site supports our hypothesis that 5'-T_n-3' is the preferred binding sequence of poly-N-methylpyrrole carboxamides. The major binding orientation places the amino terminus at the 3' end of the 5'-TTTTTA-3' sequence (the same orientation preference as **DE**·Fe(II)). The **P5E**·Fe(II) binding sites cover six to seven base pairs, consistent with the addition of two additional N-methylpyrrole carboxamides to **DE**·Fe(II) (Table VI). A comparison of the **DE**·Fe(II) and **P5E**·Fe(II) cleavage sites on the 167 bp fragment is illustrated below.

Table VI - Cleavage Sites of **P5E**·Fe(II) vs. **DE**·Fe(II)^a

<u>DNA Fragment</u>	<u>P5E·Fe(II)</u>	<u>S</u>	<u>DE·Fe(II)</u>	<u>S</u>
167	TTAAATT	7	AAATT	5
381	AGAAATT	7	AAATT	5
516	TTTTTA	6	TTTTT	5
	TAATAAT	7	AATAA	5

a) 5'-3'



Footprinting of **P5** reveals more pentapeptide binding sites than does the affinity cleaving. Recall that this was also the case with **DE**·Fe(II) and distamycin.

Table VII - Common Sites for **P5E**·Fe(II) and **P5^a**

DNA Fragment	P5E ·Fe(II)	S	P5/MPE ·Fe(II)	S
167	TTAAATT	7	TAAATT	6
381	AGAAATT	7	AGAAATT	7
516	TTTTTA	6	TTTTTA	6
	TAATAAT	7	TAATAAT	7

a) 5'-3'

The correspondence between the **P5/MPE**·Fe(II) inhibition patterns and **P5E**·Fe(II) cleavage sites is high. The increase in the pentapyrrole peptide's binding constant increases the sensitivity of the affinity cleavage assay. The binding site location and size of the common **P5E**·Fe(II) cleavage and **P5/MPE**·Fe(II) inhibition sites are identical with the exception of the 5'-TTAAATT-3' site where there is a one base pair discrepancy (Table VI). This fact further validates the utility of both affinity cleaving and **MPE**·Fe(II) footprinting for determining small

molecule binding sites on heterogenous DNA. Note also, that the model for assigning footprints works well for P5. The 3' strand is overprotected by 2 base pairs and the 5' strand underprotected by 1 base pair. Again, increasing the P5E·Fe(II)/base pair ratio results in the appearance of minor P5E·Fe(II) cleavage sites.

P5E·Fe(II) double strand cleaves DNA with a preference for 5'-T_n-3' (n ≥ 5) sites. There are 16 such sites on pBR-322 DNA all located at or near the major and minor double strand cleavage sites. Only one restriction endonuclease cleaves A+T sites, Aha III, which cleaves 5'-TTTAAA-3'. Because regions preceding genes tend to be rich in A+T sequences, e.g. promotor and control regions, P5E·Fe(II) may be of use in studies of gene structure and in gene isolation. P5E·Fe(II) may also allow the isolation of important regions of DNA's that are inaccessible by ordinary restriction enzymes, such as the expression linked region in Trypanosomes. Because of its small size, P5E·Fe(II) should be of value in studies of packaged DNA. Preliminary data obtained by Sutton and Dervan show that P5E·Fe(II) cleaves packaged λ DNA. Cleavage of free λ DNA occurs predominantly in the 20-22 kb region and the 42-44 kb regions. Cleavage of packaged DNA appears to be nonspecific. Finally, P5E·Fe(II) cleaves DNA under a wide variety of conditions, unlike the restriction enzymes where cleavage is typically limited to narrow salt, temperature, and pH ranges.

Bis(distamycin-EDTA) (BED) and EDTA-bisdistamycin (EBD)

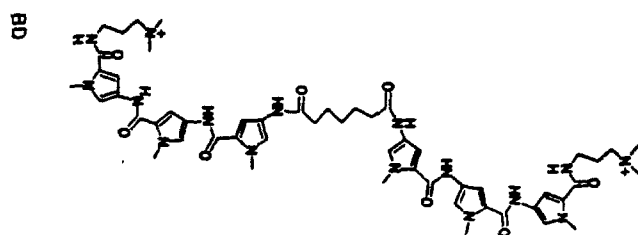
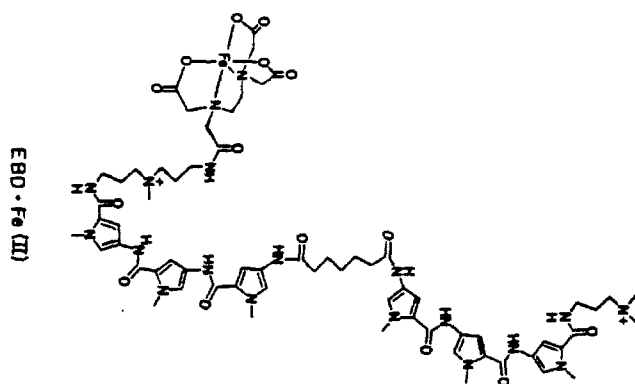
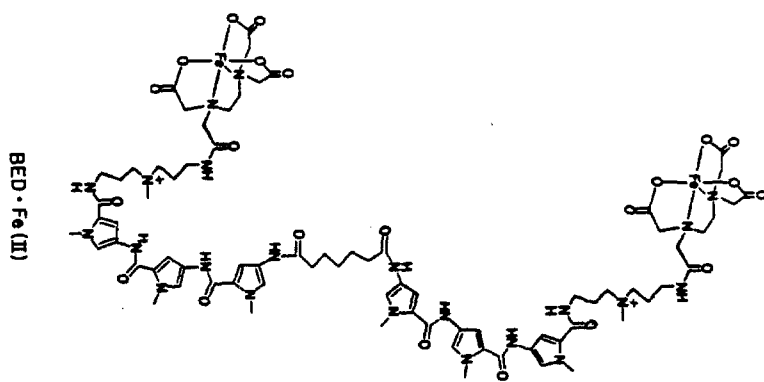
Recall that the restriction enzyme Eco RI is active as a dimer, binds to a symmetric recognition sequence and cleaves symmetrically about the sequence's symmetry axis.¹ We therefore asked the question

whether a more general approach to a more efficient sequence specific double strand cleaving molecule would entail dimerization of two monomeric DNA cleaving reagents with like or dissimilar specificities. In order to test this approach we decided to dimerize **ED**·Fe(II), (affording **BED**·Fe(II) **17**) since the properties of this monomeric cleaving reagent have already been characterized. For comparative purposes, the bisdistamycin binding unit tethered to one EDTA (**EBD** **18**) and bisdistamycin (**BD** **19**) itself were also synthesized.

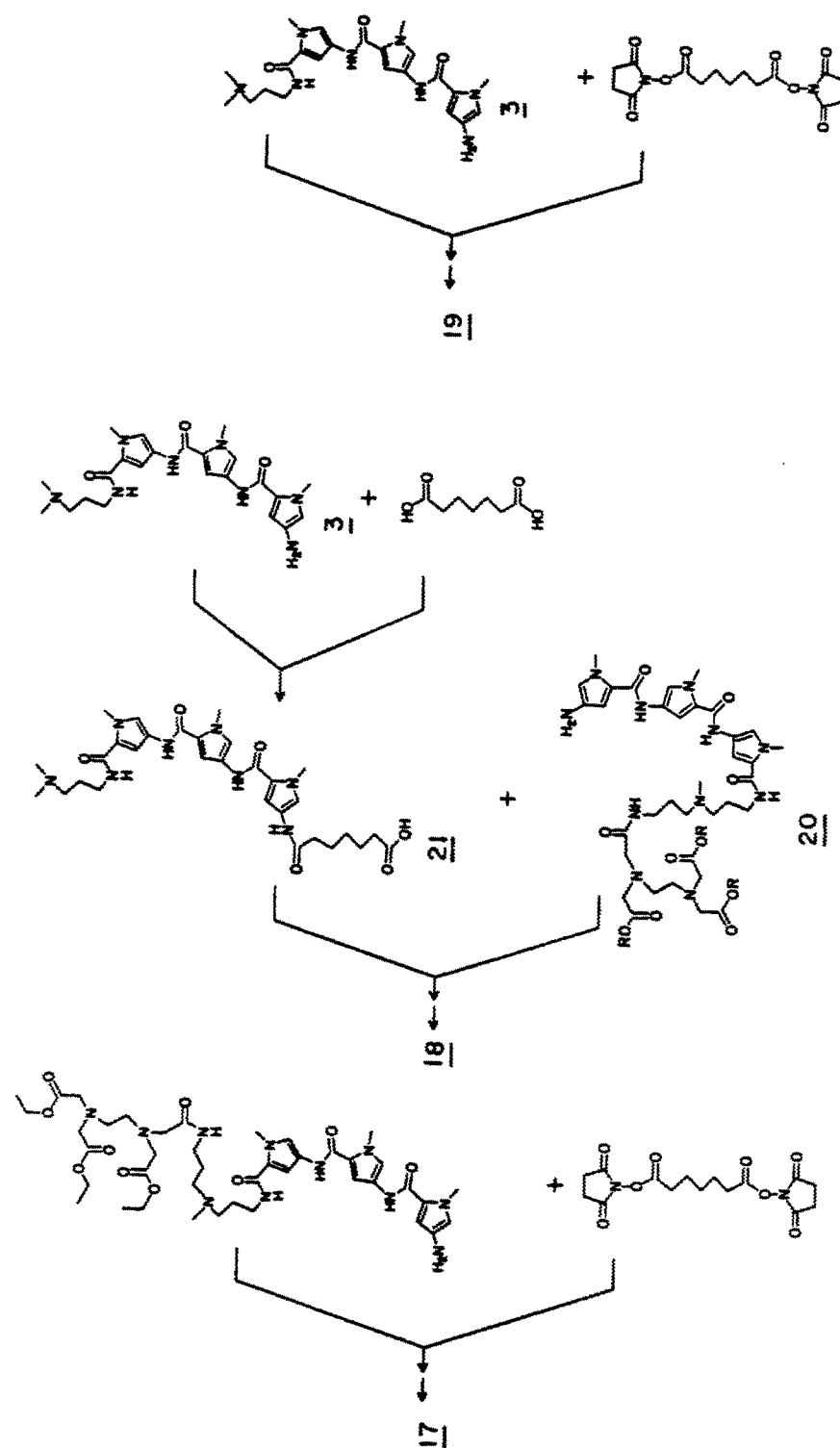
Bisnetropsin¹⁰³ derivatives have already been characterized. Netropsins were linked in antiparallel and parallel orientations via the di-N-hydroxysuccinimide ester of hexane dicarboxylic acid (C₆), octane dicarboxylic acid (C₈) and dodecane dicarboxylic acid (C₁₂). Circular dichroism titrations indicated that both ligands of the bis netropsin derivative (C₆) bind the DNA and that they occupy 10 base pairs (netropsin occupies 5, C₆ occupies 10, C₁₂ occupies 11).¹⁰³ Competition between DNA binding of the C₆ dimer and a fluorescent netropsin analog afforded a binding constant of the C₆ dimer to poly(dA)·poly(dT) ≥ 100 times the monomer binding constant (5×10^6).¹⁰³

Synthesis

Based on the above results, **ED**·Fe(II) was dimerized via a seven carbon heptane dicarboxylic acid linker to afford **BED**. Molecular model building suggests that the monomeric binding units of **BED**·Fe(II), **EBD**, and **BD** can bind the same or opposite strands without an intervening unbound base pair. These dimers all contain distamycin linked in an antiparallel fashion at the amino terminus; it will be of interest in the future to synthesize and characterize the two other dimers,



Scheme IV



antiparallel at the carboxy terminus and parallel head to tail linked.

Condensation of the di-N-hydroxysuccinimide^{81b} ester of heptanedioic acid with two equivalents of amine **22** afforded the ester of **BED**. Subsequent hydrolysis with 0.25M lithium hydroxide, followed by acidification and flash chromatography on silica gel (ammonia/methanol) yielded **BED**. **BED** was rendered metal free by supporting it on Amberlite XAD-2 and washing with aqueous Na₂EDTA, deionized water, and eluting with methanol. Condensation of diamine **3** with an excess of the mono-imidazolidine⁸⁰ of heptanedioic acid afforded the amino acid **21**. Formation of the imidazolidine of **21**, followed by condensation with **20** yielded the triethyl ester of **BED**. Hydrolysis, acidification, and purification as described above afforded **EBD** (Scheme IV). Condensation of the diamine **3** with the di-N-hydroxysuccinimide ester of heptanedioic acid afforded **BD**.

Cleavage Efficiency

At 1.0 nanomolar concentrations, **BED**·2Fe(II) and **EBD**·Fe(II) efficiently cleave DNA (10 μ M) in the presence of O₂ and DTT, almost three orders of magnitude lower concentration than that required for efficient **ED**·Fe(II) cleavage. This result is consistent with the increase in carboxamide hydrogen bonding interactions leading to an increase in the binding constant and as a result, the ratio of reagent bound/reagent free.

Attachment of two EDTA's (**BED**·2Fe(II)) versus one (**EBD**·Fe(II)) results in a substantial increase in the relative amounts of linear DNA at drug concentrations at or above 10⁻⁸M (Table VII). The difference in the ratios of form II/form III DNA between **EBD**·Fe(II) and **BED**·2Fe(II)

($\geq 10^{-8}M$) is consistent with a contribution from a double strand cleavage - one binding event pathway for **BED**·2Fe(II). Both EDTA·Fe(II) complexes must be cleaving the DNA on opposite strands in some fraction of the **BED** binding events.

Table VII - Cleavage of pBR-322 Plasmid in the Presence of DTTa

Reagent	conc. M	% Form			Reagent/ bp
		I	II	III	
MPE	10^{-7}	43	57	0	10^{-2}
ED ·Fe(II)	10^{-5}	0	80	20	1
ED ·Fe(II)	10^{-6}	10	85	5	10^{-1}
EBD ·Fe(II)	10^{-7}	0	66	34	10^{-2}
EBD ·Fe(II)	10^{-8}	0	81	19	10^{-3}
EBD ·Fe(II)	5×10^{-9}	18	68	14	5×10^{-3}
EBD ·Fe(II)	10^{-9}	43	48	9	10^{-4}
BED ·Fe(II)	10^{-7}	0	17	53(30) ^b	10^{-2}
BED ·Fe(II)	10^{-8}	9	54	36	10^{-3}
BED ·Fe(II)	5×10^{-9}	24	59	17	5×10^{-3}
BED ·Fe(II)	10^{-9}	48	42	10	10^{-4}

a) Form I pBR-322 ($10^{-5}M$ bp), reagent, buffer (40 mM Tris base, 5 mM NaOAc, pH 7.8) and DTT (5 mM) were allowed to react at 25°C for one hour and quenched. In all cases reactions were carried to completion. Forms I, II, and III were analyzed by agarose gel electrophoresis and quantitated by densitometry after ethidium bromide staining.

b) Smaller M.W. linear DNA.

At concentrations below $10^{-8}M$, the relative amounts of double strand cleavage by **BED**·Fe(II) and **EBD**·Fe(II) are similar. Such behavior implies that cleavage at low reagent concentrations is determined by a bimolecular event not depending on the binding moiety but on the attached EDTA, such as reactivation of an oxidized inactive iron moiety or dissociation and reassociation of the ferrous (ferric) EDTA complex.¹⁰¹ Consequently, at reagent concentrations below $10^{-8}M$, the

relative concentration of **BED**·Fe(II) with two active **EDTA**·Fe(II) complexes is very small.

The ratio of form III/form II DNA for both **BED**·Fe(II) and **EBD**·Fe(II) is higher than for **DE**·Fe(II), **ED**·Fe(II), and even **P5E**·Fe(II). This result suggests that the rate of reactivation, k_3 , (equation (2), page 151) of bound **BED**·2Fe(II)/**EBD**·Fe(II) may be competitive with dissociation of the reagent DNA complex, k_8 . The dependence of the production of form III DNA on form II and form I DNA present should be determined on an isolated site as a function of time.

The cleavage reactions of **BED**·2Fe(II) and **EBD**·Fe(II) are complete in 2 h, behavior similar to that obtained with **P5E**·Fe(II). Again this can be interpreted as bound DNA scavenging $\dot{\text{O}}\text{H}$ and thereby reducing the rate of bound reagent inactivation relative to the rate of inactivation of free reagent in solution. Finally preequilibration of the dimers with DNA before initiation of cleavage had no effect on the reaction efficiency.

Double Strand Cleavage

The ability of **BED**·2Fe(II) and **EBD**·Fe(II) to sequence specifically double strand cleave DNA was assayed on linear pBR-322 plasmid DNA⁹¹ (4362 base pairs) in the manner previously described. The fragments produced by **BED**·2Fe(II), **EBD**·Fe(II) cleavage of linearized pBR-322 (Eco RI or Sal I) are illustrated in Figure 26. Both dimers double strand cleave DNA into discrete fragments at reagent/bp ratios of 5×10^{-3} and 1.2×10^{-3} . At binding ratios of 5×10^{-3} the positions of the two major cleavage sites of **BED**·2Fe(II) and **EBD**·Fe(II) were located at 4200 and 3300 base pairs. The restriction endonuclease

Aha III (5'-TTTAAA) cleaves pBR-322 at 3233, 3252, and 3944 base pairs. It is apparent from Figure 26 that **EBD**·Fe(II) has a specificity similar to **BED**·2Fe(II) indicating that attachment of two EDTA's versus one has little effect on the sequence specificity of the binding moiety.

BED·2Fe(II) double strand cleavage is more specific than that of **P5E**·Fe(II). The major **P5E**·Fe(II) bands at 3.2 and 4.3 kb have become minor and the minor bands at 2.6, 2.4, 2.0 and 1.8 kb have diminished in intensity,⁹¹ consistent with the additional hydrogen bonding centers in the dimeric reagents. As is the case with **P5E**·Fe(II), the specificity of **BED**·2Fe(II) and **EBD**·Fe(II) decreases at higher reagent binding densities.

Table VIII - Restriction Mapping of **BED**·2Fe(II)

A

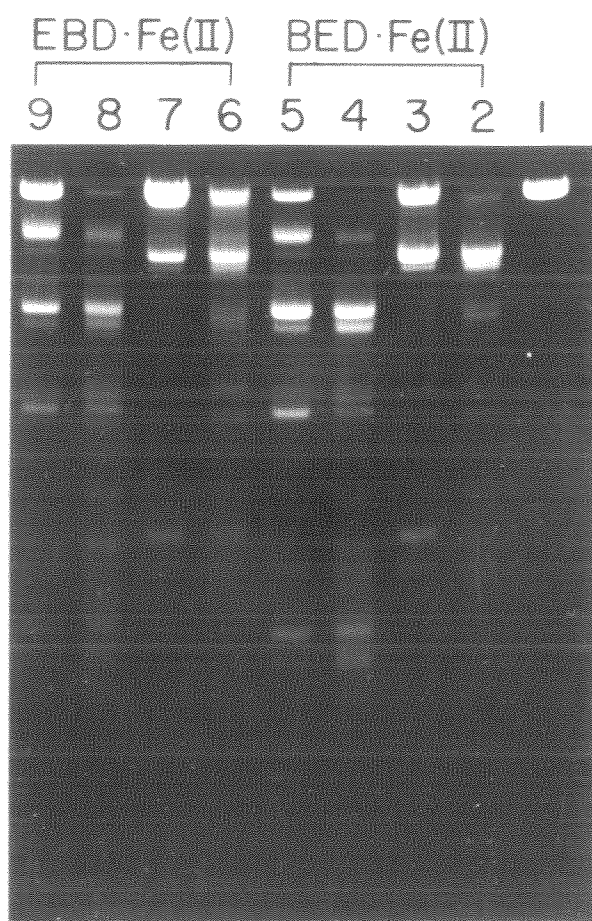
<u>Eco RI</u> (0) ^a	<u>Sal I</u> (650)	<u>Nde I</u> (2297)	<u>Form I</u>
3350	4200 2700	2450 1100	3450

B

<u>Hind/Ava I</u> (652,1424,3908)	<u>Rsa I</u> ^a
1900 (652-1424) -(1424-3908) -(3908- 652)	(165-2282) -(2282-3847) -(3847- 165)

a) location of restriction enzyme cleavage site on pBR-322. b) - represents the disappearance of the indicated fragment on reaction with **P5E**·Fe(II).

Figure 25 - Double strand cleavage of pBR-322 by **BED**·Fe(II), **EBD**·Fe(II) and **PSE**·Fe(II).
Lanes 1,2,3,6,7, and 10 are 50 μ M
base pair Eco RI digest. Lanes 4,5,8,9,11 are 50 μ M
base pair Sal I digest. Lanes 2 and 4: **BED**·2Fe(II),
0.25 μ M; Lanes 3 and 5: **BED**·2Fe(II), 0.06 μ M
Lanes 6 and 8: **EBD**·Fe(II), 0.25 μ M; Lanes 7
and 10: **EBD**·Fe(II), 0.06 μ M; Buffer is 40 mM Tris
base, 5 mM NaOAc, pH 7.9; DTT is 5 mM; reaction time
= 1.5 h.



Cleavage Specificity

The specificity of **BED**·2Fe(II) and **EBD**·Fe(II) single strand cleavage was examined on the 3' and 5' ³²P end-labeled^{90,92,93} 167, 381, and 516 base pair restriction fragments using high resolution denaturing gel electrophoresis. The autoradiograms and resulting histograms of the 381 and 516 bp fragments are shown in Figures 27 - 29. For comparison, the bisdistamycin (**BD**)/**MPE**·Fe(II) inhibition patterns, distamycin/**MPE**·Fe(II) inhibition patterns and **DE**·Fe(II) cleavage patterns are also shown. The model used in assigning the **BED**·Fe(II) and **EBD**·Fe(II) binding sites is illustrated in Figure 30 (based on average **BED**/**EBD** cleavage pattern).

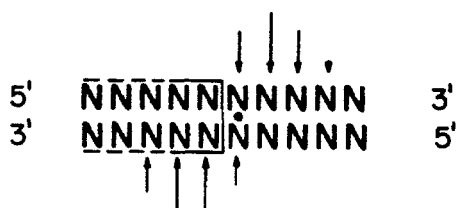


Figure 30. Relationship between average **EDTA**·Fe(II) position and the **BED**·Fe(II)/**EBD**·Fe(II) binding site.

This model is similar to that described earlier for **ED**·Fe(II). Because **BED**·2Fe(II) has a cleaving moiety attached to each terminus, assignment of the cleavage site is unambiguous. Examination of the 516 base pair fragment reveals two **BED**·Fe(II)/**EBD** binding sites. The binding site at base pairs 4320-4328 covers nine base pairs, 5'ATTTTATA-3'. Although this pattern could result from binding and cleavage of one distamycin unit in one orientation at two sites it is more likely that both units are binding a total of nine

Figure 27_ - Autoradiogram of High Resolution Denaturing Gel. Lanes 1,3,5,7,9,11,13 are 3' end labeled 516 bp fragment. Lanes 2,4,6,8,10,12,14 are 5' end-labeled fragment. Lanes 1,2: Maxam-Gilbert G reaction; Lanes 3,4: **MPE**·Fe(II), 5×10^{-6} M; Lanes 5,6: **DE**·Fe(II), 1×10^{-5} M; Lanes 7,8: **EBD**·Fe(II), 1×10^{-6} M; Lanes 9,10: **BED**·Fe(II), 1×10^{-6} M; Lanes 11,12: distamycin 1×10^{-5} M **MPE**·Fe(II) 5×10^{-6} M; Lanes 13,14: **BD** 2.5×10^{-6} M, **MPE**·Fe(II) 5×10^{-6} M. All reactions are > 600 cpm 32 P end labeled 381 bp fragment, made up to 100μ M bp with sonicated calf thymus DNA in 40 mM Tris base, pH 7.8, 5 mM NaOAc; 1 mM DTT.

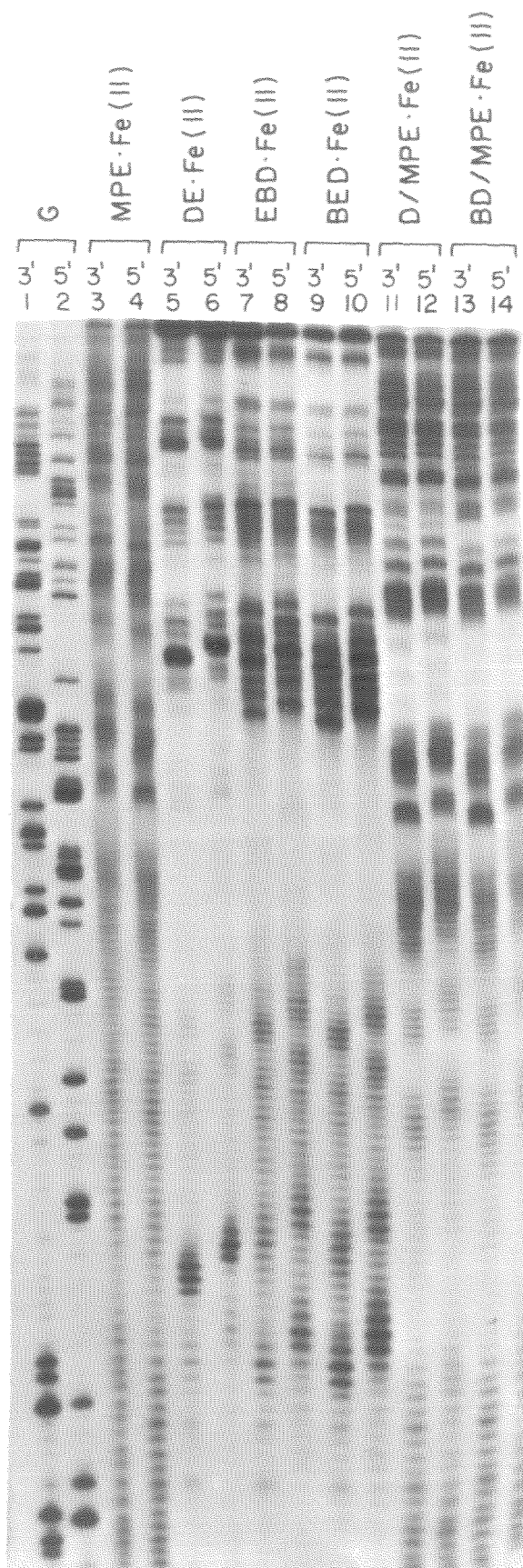
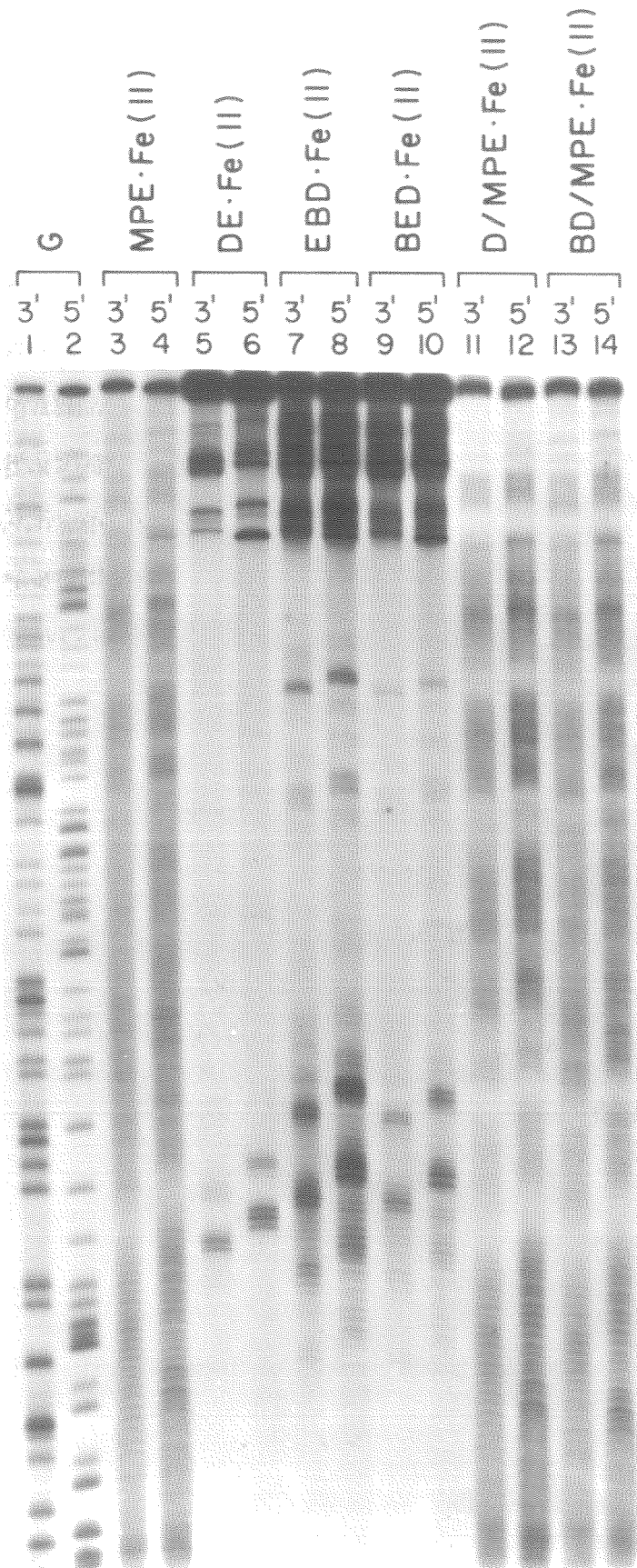


Figure 28_ - Autoradiogram of High Resolution Denaturing Gel. Lanes 1,3,5,7,9,11,13 are 3' end labeled 381 bp fragment. Lanes 2,4,6,8,10,12,14 are 5' end-labeled fragment. Lanes 1,2: Maxam-Gilbert G reaction; Lanes 3,4: **MPE**·Fe(II), 5×10^{-6} M; Lanes 5,6: **DE**·Fe(II), 1×10^{-5} M; Lanes 7,8: **EBD**·Fe(II), 1×10^{-6} M; Lanes 9,10: **BED**·Fe(II), 1×10^{-6} M; Lanes 11,12: distamycin 1×10^{-5} M **MPE**·Fe(II) 5×10^{-6} M; Lanes 13,14: **BD** 2.5×10^{-6} M, **MPE**·Fe(II) 5×10^{-6} M. All reactions are > 600 cpm 32 P end labeled 381 bp fragment, made up to 100μ M bp with sonicated calf thymus DNA in 40 mM Tris base, pH 7.8, 5 mM NaCl; 1 mM DTT.



BED·Fe(II) 516

32p 5' ATACGCCCTATTTTATAGGTTAATGTCATGATTAATAATGGTTTCTTAGACGTCAGGTGGCA 3'
3' TATGCGGATAAAAATATCCCAATTACAGTACTATTATACCAAGAATCTGCAGTCCACCGT 5'

EBD·Fe(II) 516

32p 5' ATACGCCCTATTTTATAGGTTAATGTCATGATTAATAATGGTTTCTTAGACGTCAGGTGGCA 3'
3' TATGCGGATAAAAATATCCCAATTACAGTACTATTATACCAAGAATCTGCAGTCCACCGT 5'

BD/MPE·Fe(II) 516

32p 5' ATACGCCCTATTTTATAGGTTAATGTCATGATTAATAATGGTTTCTTAGACGTCAGGTGGCA 3'
3' TATGCGGATAAAAATATCCCAATTACAGTACTATTATACCAAGAATCTGCAGTCCACCGT 5'

Figure 29 - Histograms of BED·2Fe(II) and EBD·Fe(II) cleavage patterns and BD/MPE·Fe(II) inhibition patterns. Binding site are boxed.

BED·Fe(II) 381

³²P 5' GGC GGCC AAAG CGGT CGG ACAGT GCT CCG AGA AC GGGT GCG CAT AG AAAT TGC ATCAAC GCA TAT AG CGCTAGC 3'
 3' CCG CCGGT TCG CCAGCT GT CAC GAGGCT CT TGCC CAC GCGT ATCT TTAAC GTAGT TGG GTATAT CGCGATCG 5'

EBD·Fe(II) 381

³²P 5' GGC GGCC AAAG CGGT CGG ACAGT GCT CCG AGA AC GGGT GCG CAT AG AAAT TGC ATCAAC GCA TAT AG CGCTAGC 3'
 3' CCG CCGGT TCG CCAGCT GT CAC GAGGCT CT TGCC CAC GCGT ATCT TTAAC GTAGT TGG GTATAT CGCGATCG 5'

BD/MPE·Fe(III) 381

³²P 5' GGC GGCC AAAG CGGT CGG ACAGT GCT CCG AGA AC GGGT GCG CAT AG AAAT TGC ATCAAC GCA TAT AG CGCTAGC 3'
 3' CCG CCGGT TCG CCAGCT GT CAC GAGGCT CT TGCC CAC GCGT ATCT TTAAC GTAGT TGG GTATAT CGCGATCG 5'

base pairs. **BED**·2Fe(II) binds an eight base pair 5'-TAGAAATT-3' site on the 381 bp fragment. If it is assumed that the major and minor orientations of **EBD**·Fe(II) bind identical sites, **EBD**·Fe(II) binds the same sequences as **BED**·2Fe(II). The binding site size is consistent with the model described earlier for distamycin binding. Eight hydrogen bonds can be formed to nine adjacent base pairs resulting in a binding site size of nine bp. The tether is flexible enough to also allow for monomeric binding modes. **BED**·2Fe(II) and **EBD**·Fe(II) bind two binding sites of 4-6 base pairs, 5'-TAATAA-3' and 5'TATA-3'. These sites are similar in size and location to **ED**·Fe(II) binding sites. (Table IX) Presumably sequence specific double strand cleavage occurs at the dimeric binding sites whereas cleavage at the monomeric sites is confined largely to single strand cleavage. The number of cleavage sites is sensitive to **BED**·2Fe(II) and **EBD**·Fe(II) binding densities.

Table IX **BED**·2Fe(II) vs **ED**·Fe(II) Cleavage Sites^a

<u>DNA Fragment</u>	<u>BED·2Fe(II)</u>	<u>S</u>	<u>ED·Fe(II)</u>	<u>S</u>
381	TAGAAATT	8	AAATT	5
516	ATTTTATA	9	ATTTT	6
	TAATAA	6	TAATAA	6

a) 5'-3'

Rigidification of the linker might lead to an increase in specificity by inducing negative binding interactions in the second distamycin unit at the monomeric binding sites. It would also be of interest to examine the effect of parallel versus antiparallel linkage of the tripyrrole units. One might predict that parallel linkage would result in tighter binding to 5'-T_n-3' sites and antiparallel linkage

tighter binding to 5'-T_xA_y-3' sites.

The cleavage bands surrounding the **BED**·2Fe(II) and **ED**·Fe(II) binding sites are of unequal intensity. The more intense cleavage is located adjacent to the base pairs which the dimer and **ED**·Fe(II) binding sites have in common. This result suggests that one distamycin unit of the dimer may be bound more tightly than the second. For example, the intensity of cleavage surrounding the 5'-TAGAAATT-3' site on the 381 bp fragment is considerably more intense to the 3' side. Steric interactions with the NH₂(2) of guanine probably weaken the binding interactions on the 5' side of the binding site. **BED**·Fe(II) has the same intensity pattern and therefore probably the same binding properties.

Footprinting of **P6** reveals the presence of both dimeric and monomeric binding sites. **P6** binds the 5'-TTTTAT-3', 5'ATATAG-3' and 5'-TTCTTA-3' sites on the 516 base pair fragment and the 5'-GAAATT-3' and 5'-ATATAG-3' sites on the 381 bp fragment. Footprinting sites match the affinity cleavage sites within a base pair, with the exception of the 381 5'GAAATT-3' site. This is likely a consequence of the guanine NH₂(2) interposed in the sequence and disrupting hydrogen bonding. Note that the **P6** footprints fit the general model established for distamycin footprints.

Finally, it may be possible to use the strategy outlined above to construct a G+C specific DNA cleaving reagent. Dimerization of a G-C specific DNA binding molecule, such as the dye neutral phenyl red (NPR), may provide a large enough recognition sequence to make possible G+C specific DNA cleavage. A monomeric G-C specific reagent, NPR-EDTA,

cleaves with low sequence specificity, presumably due to the high frequency of G-C sites and the diffuse cleavage pattern of EDTA-Fe(II).¹⁰⁵

Conclusion

Considerable progress has been made in the design and synthesis of double strand sequence specific DNA cleaving molecules. **P5E**-Fe(II), **RED**-Fe(II) and **EBD**-Fe(II) catalytically double strand cleave pBR-322 plasmid DNA at low binding densities to produce a small set of discrete fragments. A general method for the construction of sequence specific double strand cleaving reagents has been demonstrated. By coupling a series of sequence specific DNA binding molecules of similar or diverse specificities and attaching a catalytic cleaving moiety it may be possible to construct artificial restriction enzymes with defined target sequences and low cleavage frequencies (< 1 in 5000). Before this can be accomplished however, absolute specificity, i.e., specificity independent of binding density, and single base scission must be realized.

A direct method, DNA affinity cleaving, has been developed for mapping the locations, binding site sizes, and orientations of small molecules on heterogeneous DNA. This technique may be extendable to peptides and DNA binding proteins. A comparison of DNA affinity cleaving with **MPE**-Fe(II) footprinting has resulted in well defined models for interpretation of cleavage patterns and **MPE**-Fe(II) inhibition patterns.

Experimental

Infrared spectra were recorded on a Beckman 4210 spectrophotometer. Ultraviolet-visible spectra were recorded on a Beckman Model 25 spectrophotometer. ^1H Nuclear magnetic resonance spectra were recorded on a Varian Associates EM-390 (90 MHz) or Bruker WM 500 (500 MHz) spectrometer and are reported in parts per million from tetramethylsilane. Mass spectra were recorded on Kratos MS-50S spectrometer equipped with a SIMS ion source (Cs^+ ion beam). Spectra were recorded at the Bioorganic Biomedical Mass Spectrometry Resource at UC, San Francisco or the Division of Resources and the Middle Atlantic Mass Spectrometry Laboratory at Johns Hopkins University. Gel scans were performed on a Cary 219 spectrophotometer with an Apple microcomputer gel scanning program.

Flash chromatography was performed using EM Reagents Silica Gel 60 (230-400 mesh). Reagent grade chemicals were used without purification unless otherwise stated. Dimethyl formamide was dried over 4A molecular sieves. $\text{N,N}'$ -Carbonyldiimidazole was sublimed under reduced pressure prior to use. Ferrous ammonium sulfate was a Baker Analyzed Reagent. DTT was obtained from Calbiochem. Bleomycin (70% bleomycin A_2 and 30% bleomycin B_2) was generously supplied by Bristol Laboratories. MPE was prepared as previously described.⁵¹ All nonaqueous reactions were run under nitrogen with rigorous exclusion of water unless otherwise noted. Doubly distilled water was used for all biological reactions and dilutions. Aqueous 5'-($\alpha^{32}\text{P}$)dATP, triethylammonium salt, 3000 Ci/mole, was from Amersham and aqueous 3'-($\gamma^{32}\text{P}$)dATP, 5000-9000 Ci/mole, was from ICN. Nucleotide

triphosphates were from Boehringer Mannheim. All enzymes were from New England Biolabs except bacterial alkaline phosphatase and polynucleotide kinase which were from BRL. Calf thymus DNA (Sigma) was sonicated, deproteinized and extensively dialyzed.

N-Methyl-4-nitropyrrole-2-carboxylic acid 22⁷⁸ - 75G (0.60 moles)

N-methylpyrrole-2-carboxylic source acid was dissolved in 500 ml acetic anhydride. The solution was stirred by means of an overhead stirrer at 25°C for 15 min then cooled to -25°C (dry ice/acetone bath at -40°C). 60 ml cold HNO₃ was added slowly with stirring to 200 ml acetic anhydride at 0°C. This solution was added dropwise to the reaction mixture, maintaining the temperature at -25°C. The solution was stirred (-25°C) for 1 h then poured into 750 ml ice and the solution stirred an additional 30 min. The mixture was extracted with dichloromethane, dried, and solvent removed under vacuum. A cold solution of 75 ml H₂SO₄ in 500 ml ethanol was added to the resulting solid and the mixture refluxed for 12 h. 200 ml methanol was removed under reduced pressure, 1000 ml H₂O added, and the mixture was extracted with dichloromethane. The organic layer was dried and evaporated. The residue was dry loaded (150g alumina/CH₂Cl₂) and chromatographed on alumina (activity II, 500g). Elution with petroleum ether:ether (95:5) gave N-methyl-5-nitropyrrole-2-carboxylic acid methyl ester (13g), NMR (CDCl₃): δ 7.1 (d, 1H, J=5Hz), 6.85 (d, 1H, J=5Hz), 4.3 (s, 3H), 3.85 ppm (s, 3H); lit⁷⁸ NMR (CDCl₃) 7.07 (d, 1H, J=4.5Hz), 6.84 (d, 1H, J=4.5Hz), 4.27 (s, 3H), 3.84 ppm (s, 3H).

Elution with petroleum ether:ether (80:20 → 25:75) gave 45g (40%) N-methyl-4-nitropyrrole-5-carboxylic acid methyl ester, NMR (CDCl₃)

δ 7.55 (d, 1H, $J=1.5\text{Hz}$), 7.35 (d, 1H, $J=1.5\text{Hz}$), 4.0 (s, 3H), 3.85 ppm (s, 3H); lit.⁷⁸ NMR (CDCl_3) δ 7.55 (d, 1H, $J=1.5\text{Hz}$), 7.34 (d, 1H, $J=1.5\text{Hz}$), 4.0 (s, 3H), 3.84 (s, 3H).

N-Methyl-4-nitropyrrole-2-carboxylic acid 23⁷⁸ - The methyl ester (30g, 0.16 mole) was suspended in 400 ml ethanol and a solution of NaOH (18g) in 400 ml H_2O was added. The mixture was refluxed for 4 h, cooled, and reduced to 400 ml under vacuum. The mixture was acidified with 6N HCl, and the filtrate was precipitated and washed with water and methanol to afford 26g (95%) N-methyl-4-nitropyrrole-2-carboxylic acid; NMR ($\text{DMSO}-d_6$) δ 8.25 (d, 1H, $J=2\text{Hz}$), 7.25 (d, 1H, $J=2\text{Hz}$), 3.9 ppm (s, 3H).

N-Methyl-4-(N-methyl-4-nitropyrrole-2-carboxylamide)-pyrrole-2-carboxylic acid methyl ester 24⁷⁸ - Nitro ester **22** (15g, 0.08 mole) was dissolved in 150 ml dimethyl formamide and reduced over 5% Pd/C (1g) at atmospheric pressure. The solution was filtered through Celite, the Celite was washed with 20 ml DMF and the combined filtrates added to a solution of 10g NaHCO_3 in 500 ml H_2O . To this solution was added with stirring a mixture of 15g N-methyl-4-nitropyrrole-2-carboxylic acid chloride **25** in 50 ml DMF. (N-methyl-4-nitropyrrole-2-carboxyl chloride was prepared by refluxing one equivalent of N-methyl-4-nitropyrrole-2-carboxylic acid with four equivalents of thionyl chloride for 4 h, followed by removal of excess thionyl chloride under vacuum.) The mixture was stirred overnight, 500 ml H_2O added, and filtered. The product was washed with 10% aqueous NaHCO_3 solution, water, methanol, and dried to afford 20g (80%) of nitro ester **24**; NMR ($\text{DMSO}-d_6$) δ 10.3 (s, 1H), 8.2 (d, 1H, $J=1.5\text{Hz}$), 7.6 (d, 1H, $J=2.0\text{Hz}$), 7.5 (d, 1H, $J=1.5\text{Hz}$), 6.9 (d, 1H, $J=1.5\text{Hz}$), 4.0 (s, 3H), 3.85 (s, 3H), 3.75 ppm (s, 3H); Lit. NMR

(CDCl₃)⁷⁸ δ 9.24 (s,1H), 8.12 (1H), 7.5 (1H), 7.4 (1H), 6.83 (1H), 3.9 (3H), 3.8 (3H), 3.7 ppm (3H).

~~N-Methyl-4-[N-methyl-4(N-methyl-4-nitropyrrole-2-carboxamide)-~~

~~pyrrole-2-carboxamide]-pyrrole-2-carboxylic acid methyl ester 25~~⁷⁸ - A

solution of methyl ester **22** (20g, 0.065 moles) in 300 ml DMF was reduced over Pd/C (1g) at atmospheric pressure. The solution was filtered through Celite, the Celite washed with 20 ml DMF and the combined solutions added with stirring to 6.5g NaHCO₃ in 1500 ml H₂O. 12G of the acid chloride **25** was immediately added and the solution stirred overnight. The precipitate was filtered, washed with aqueous sodium bicarbonate, water, methanol, and dried to afford 15g (53%) **26**; NMR

(DMSO-d₆) δ 10.35 (s,1H), 10 (s,1H), 8.2 (d,1H,J=1.5Hz), 7.6

(d,1H,J=1.5Hz), 7.5 (d,1H,J=1.5Hz), 7.25 (d,1H,J=1.5Hz), 7.05

(d,1H,J=1.5Hz), 6.9 (d,1H,J=1.5Hz), 4.0 (s,3H), 3.85 (s,3H), 3.83

(s,3H), 3.75 ppm (s,3H); Lit NMR⁷⁸: δ 10.27 (s,1H), 9.95 (s,1H), 8.12

(d,1H), 7.57 (d,1H), 7.46 (d,1H), 7.26 (d,1H), 7.05 (d,1H), 6.89 (d,1H),

3.96 (s,3H), 3.86 (s,3H), 3.85 (s,3H), 3.72 ppm (s,3H).

~~N-Methyl-4-[N-methyl-4(N-methyl-4-nitropyrrole-2-carboxamide)-~~

~~pyrrole-2-carboxamide]-pyrrole-2-carboxylic acid 27~~⁸ - A solution of 15g

(0.035 moles) nitro ester **26** was suspended in 400 ml ethanol. A

solution of 12g NaOH in 400 ml H₂O was added and the mixture was

refluxed for 4 h. The solution was cooled, filtered, and reduced to 500

ml under vacuum. The filtrate was acidified with 6N HCl, and the

resulting precipitate was filtered, washed with water, methanol, and

dried to afford 13g (90%) nitro acid **2**; IR (KBr) 1690, 1650, 1600,

1565, 1530, 1500, 1310, 1215, 1110 cm⁻¹; NMR (DMSO-d₆) δ 3.84 (s,3H),

3.87 (s,3H), 3.97 (s,3H), 6.85 (d,1H,J=1.5Hz), 7.1 (d,1H,J=1.5Hz), 7.25 (d,1H,J=1.5Hz), 7.26 (d,1H,J=1.5Hz), 7.45 (d,1H,J=1.5Hz), 7.65 (d,1H,J=1.5Hz), 8.2 (d,1H,J=1.5Hz), 9.95 (s,1H), 10.35 (s,1H); UV (H₂O) 391 nm (35,600), 236; Lit.⁷⁸ (DMSO-d₆) δ 9.65 (s,1H), 9.48 (s,1H), 8.97 (s,1H), 7.51 (s,1H), 7.30 (s,1H), 7.19 (s,1H), 7.01 (s,1H), 6.82 (s,1H), 3.92, 3.82 (9H); IR⁷⁸ (KBr) 1700, 1660 cm⁻¹.

~~N-Methyl-4-[N-methyl-4(N-methyl-4-nitropyrrole-2-carboxamide)-pyrrole-2-carboxamide]-pyrrole-2-carboxamide-dimethylpropylamine 11~~⁷⁸ -

To a solution of 2.5g (6.0 mmol) nitro acid 5, 0.68g (6.6 mmol) 3-dimethylaminopropylamine, and 0.89g (6.6 mmol) N-hydroxybenzotriazole⁷⁹ in 10 mL dimethylformamide was added with stirring at 0°C 1.36g (6.6 mmol) dicyclohexylcarbodiimide. The solution was stirred at 0°C for 1h and 25°C for 12h. The dimethylformamide was removed under high vacuum at 35°C, and the residue was triturated with ether 3 times. The residue was then purified by flash chromatography on silica gel with 3% concentrated aqueous ammonia in methanol to give 2.1g (70%) of nitro amine 11: IR(KBr) 3130, 2950, 1638, 1580, 1530, 1500, 1308, 1250 cm⁻¹; NMR (DMSO-d₆) δ 1.6 (m,2H), 2.15 (s,6H), 2.28 (t,2H,J=6Hz), 3.2 (m,2H), 3.8 (s,3H), 3.85 (s,3H), 3.95 (s,3H), 6.85 (d,1H,J=1.5Hz), 7.05 (d,1H,J=1.5Hz), 7.2 (d,1H,J=1.5Hz), 7.27 (d,1H,J=1.5Hz), 7.6 (d,1H,J=1.5Hz), 8.05 (t,1H,J=4Hz), 8.15 (d,1H,J=1.5Hz), 9.95 (s,1H), 10.35 (s,1H); UV (H₂O) 286 nm, 238; m/e 499 (M⁺).

EDTA-triethyl ester 9 - To a solution of 10g (0.034 mol) EDTA in 250 mL dry ethanol was added with stirring 1.5 mL of H₂SO₄. The reaction was refluxed for 24h and the solvent was removed. Saturated aqueous sodium bicarbonate (50 ml) was added followed by 250 mL dichloromethane. The

layers were separated and the organic layer was washed three times with saturated aqueous sodium bicarbonate, two times with water, dried (Na_2SO_4), and concentrated to afford 11g (80%) of the crude tetraethylester. The triethyl ester **9** was prepared according to the procedure of Hay and Nolan.⁸¹ To a solution of the unpurified tetraester and 4.6g (0.027 mol) of cupric chloride dihydrate in 500 mL water was added with stirring 1.3g (0.032 mol) of sodium hydroxide in 7 mL water at such a rate as to maintain the pH at ca. 5. The solution was then treated with H_2S and filtered. The filtrate was concentrated and purified by flash chromatography on silica gel with 10% methanol in dichloromethane to yield 9g (90%) of the triethylester **9**: IR (CH_2Cl_2) 3000, 1745, 1380, 1210 cm^{-1} ; NMR (CHCl_3) δ 1.3 (t, 9H, $J = \text{Hz}$), 2.75 (s, 4H), 3.3 (s, 2H), 3.4 (s, 2H), 3.5 (s, 4H), 4.1 (q, 4H, $J = 7\text{Hz}$); m/e 376 (M^+); tlc (silica gel, 10% MeOH in CH_2Cl_2) $R_f = 0.55$.

EDTA-triethylester-linker 5 - To a solution of 5g (0.013 mol)

EDTA-triethylester **9** and 1.52g (0.13 mol) *N*-hydroxysuccinimide^{81b} in 100 mL dioxane was added with stirring 2.7g (0.013 mol) of dicyclohexylcarbodiimide in 20 mL dioxane. The solution was stirred for 12h, filtered, and the filtrate concentrated. This residue was dissolved in 100 mL of dimethoxyethane and added with stirring to a solution of 2g (0.02 mol) of 4-aminobutyric acid and 1.68g (0.02 mol) of sodium bicarbonate in 100 mL water. After 12h the solvent was removed in vacuo and the residue purified by flash chromatography on silica gel with 10% methanol in dichloromethane to give 4g (65%) of **5**: IR (CH_2Cl_2) 3000, 1740, 1665, 1210 cm^{-1} ; NMR ($\text{DMSO}-d_6$) δ 1.19 (t, 9H, $J = 7\text{Hz}$), 1.63 (m, 2), 2.2 (t, 2H, $J = 6\text{Hz}$), 2.7 (t, 2H, $J = 6\text{Hz}$), 3.1 (m, 2H), 3.19 (s, 2H), 3.45

(s,2H), 3.53 (s,4H), 4.08 (m,6H), 8.0 (t,1H); m/e 461 (M^+).

Distamycin-EDTA-triethylester 11 - A solution of 1g (2.0 mmol) of nitro amine 11 in 20 mL dimethylformamide was hydrogenated over 200 mg of 5% palladium on charcoal at 52 psi hydrogen on a Parr rocker for 12h. The mixture was filtered through Celite and the celite was washed with 25 mL DMF affording a solution of the crude amine 3. To a solution of 0.93g (2.0 mmol) acid 10 in 25 mL dimethylformamide was added with stirring 0.36g (2.2 mmol) of N,N'-carbonyldiimidazole in 5 mL dimethylformamide. After 2h, amine 3 was added and the resulting solution was stirred for 12h. Dimethylformamide was removed under high vacuum at 35°C the residue triturated three times with ether and purified by flash chromatography on silica gel with 3% concentrated aqueous ammonia in methanol to yield 0.9g (48%) **27**: IR(KBr) 2940, 1730, 1650, 1570, 1530, 1460, 1430, 1400, 1250, 1200 cm^{-1} ; NMR (DMSO- d_6) δ 1.19 (t,9H,J=7Hz), 1.6 (m,2H), 1.75 (m,2H), 2.13 (s,6H), 2.2 (t,2H,J=7Hz), 2.26 (t,2H,J=7Hz), 2.7 (m,4H), 3.1 (m,2H), 3.2 (m,2H), 3.2 (s,2H), 3.45 (s,2H), 3.55 (s,4H), 3.84 (s,3H), 3.88 (s,3H), 3.90 (s,3H), 4.08 (q,6H,J=7Hz), 6.8 (d,1H), 6.86 (d,1H), 7.0 (d,1H), 7.16 (d,1H), 7.18 (d,1H), 7.22 (d,1H), 8.0 (t,1H), 8.05 (t,1H), 9.8 (t,1H), 9.88 (t,1H), 10.37 (d,1H); UV (H_2O) 298 nm, 234; m/e 912 (M^+).

Distamycin-EDTA 1 - To a solution of 0.25g (0.37 mmol) **27** in 5 mL ethanol was added with stirring 5mL of 0.25M aqueous lithium hydroxide. The resulting solution was stirred for 12h and acidified to pH 4 with 10% aqueous hydrochloric acid. The solvent was removed under vacuum at 35°C, the residue triturated three times with ether and purified by flash chromatography on silica gel with 20% concentrated aqueous ammonia

in ethanol. Final purification was carried out by loading the product dissolved in water on to an Amberlite XAD-2 column and washing with 1 3% aqueous Na_2EDTA and 2 % doubly distilled water. Elution with methanol afforded 0.15g (66%) **1**: IR(KBr): 2960, 1730, 1640, 1565, 1550, 1465, 1435, 1260, 1210, 1105 cm^{-1} ; NMR ($\text{DMSO}-d_6$): δ 1.73 (m,2H), 1.85 (m,2H), 2.3 (t,2H,J=7Hz), 2.72 (s,6H), 3.05 (t,2H,J=7Hz), 3.13 (m,2H), 3.22 (m,2H), 3.4 (,2H,J=6Hz), 3.45 (,2H,J=6Hz), 3.8 (s,3H), 3.82 (s,3H), 3.83 (s,3H), 3.93 (s,4H), 4.04 (s,2H), 4.17 (s,2H), 6.91 (s,1H), 6.93 (s,1H), 7.05 (s,1H), 7.18 (s,1H), 7.22 (s,1H), 7.26 (s,1H), 8.25 (t,1H), 8.86 (t,1H), 9.95 (s,1H), 9.97 (s,1H), 10.15 (s,1H); UV (H_2O): 297 nm (35,600), 236 (29,400); m/e 866 ($\text{C}_{37}\text{H}_{53}\text{N}_{11}\text{O}_{11}\text{K}^+$).

Nitro amine 8 - To a solution of 2.5g (6.0 mmol) nitro acid **2** in 50 mL dimethylformamide was added with stirring 1.07g (6.6 mmol) of N,N'-carbonyldiimidazole in 10 mL dimethylformamide. After 2h, 9.6g (66 mmol) of 3,3'-diamino-N-methyl- dipropylamine was quickly added and the resulting solution was stirred for 12h. The dimethylformamide was removed under high vacuum at 35°C and the residue was triturated three times with ether. The crude product was purified by flash chromatography on silica gel with 12% concentrated aqueous ammonia in methanol to yield 2.3g (68%) of the nitro amine **8**: IR(KBr) 2960, 1640, 1580, 1530, 1311, 1210 cm^{-1} ; NMR ($\text{DMSO}-d_6$) δ 1.46 (m,2H), 1.6 (m,2H), 2.12 (s,3H), 2.33 (t,4H,J=7Hz), 2.55 (s,2H), 3.2 (m,4H), 3.80 (s,3H), 3.86 (s,3H), 3.96 (s,3H), 6.8 (d,1H,J=1.5Hz), 7.04 (d,1H,J=1.5Hz), 7.2 (d,1H,J=1.5Hz), 7.27 (d,1H,J=1.5Hz), 7.6 (d,1H,H=1.5Hz), 8.05 (t,1H,J=6Hz), 8.2 (d,1H,J=1.5Hz), 9.94 (d,1h), 10.3 (d,1h); UV (H_2O) 294 nm, 239; m/e 542 (M^+).

Nitro EDTA-triethylester 10 - To a solution of 1.39g (3.7 mmol) acid **9** in 25 mL dimethylformamide was added with stirring 0.66g (4.07 mmol) of N,N'-carbonyldiimidazole¹⁵ in 5 mL dimethylformamide. After 2h, 2g (3.7 mmol) of nitro-amine **8** was added and the resulting solution was stirred for 12h. Dimethylformamide was removed under high vacuum at 35°C the residue triturated three times with ether and purified by flash chromatography on silica gel with 3% concentrated aqueous ammonia in ethanol to yield 2.5g (75%) of **10**: IR(KBr) 2950, 1735, 1640, 1590, 1525, 1500, 1438, 1400, 1310, 1255, 1210; NMR (DMSO-d₆) δ 1.15 (t, 9H, J=7Hz), 1.55 (m, 2H), 1.6 (m, 2H), 2.12 (s, 3H), 2.7 (m, 4H), 3.12 (m, 2H), 3.18 (s, 2H), 3.20 (m, 2H), 3.44 (s, 2H), 3.5 (s, 4H), 3.8 (s, 3H), 3.86 (s, 3H), 3.97 (s, 3H), 4.05 (q, 6H, J=7Hz), 6.82 (d, 1H, J=1.5Hz), 7.05 (d, 1H, J=1.5Hz), 7.19 (d, 1H, J=1.5Hz), 7.27 (d, 1H, J=1.5Hz), 7.59 (d, 1H, J=1.5Hz), 7.96 (t, 1H, J=7Hz), 8.03 (t, 1H, J=7Hz), 8.18 (d, 1H, J=1.5Hz), 8.56 (d, 1), 8.9 (d, 1); UV (H₂O) 288 nm, 240; m/e 900 (M⁺).

EDTA-Distamycin-triethylester 7 - A solution of 1g (1.11 mmol) **10** in 10 mL dimethylformamide was hydrogenated over 200 mg of 5% palladium on charcoal at 52 psi hydrogen on a Parr rocker for 12h. The mixture was filtered through Celite and the celite was washed with 25 mL DMF to afford the crude amine **28**. To a solution of 0.08g (1.33 mmol) acetic acid in 3 mL dimethylformamide was added with stirring 0.22g (1.33 mmol) of N,N'-carbonyldiimidazole in 3 mL dimethylformamide. After 2h, amine **28** was added and the resulting solution was stirred for 12h. Dimethylformamide was removed under high vacuum at 35°C, the residue triturated three times with ether and purified by flash chromatography

on silica gel with 2% concentrated aqueous ammonia in methanol to yield 0.55g (54%) of **7**: IR(KBr) 2950, 1730, 1650, 1580, 1550, 1535, 1460, 1440, 1400, 1260, 1210 cm^{-1} ; NMR (DMSO- d_6) δ 1.17 (t,9H,J=7Hz), 1.55 (m,2H), 1.6 (m,2H), 1.97 (s,3H), 2.12 (s,3H), 2.28 (m,4H), 2.65 (m,2H), 2.70 (m,2H), 3.12 (m,2H), 3.17 (s,2H), 3.17 (m,2H), 3.44 (s,2H), 3.5 (s,4H), 3.85 (s,3H), 3.88 (s,3H), 3.9 (s,3H), 4.08 (q,6H,J=7Hz), 6.8 (d,1H), 6.84 (d,1H), 6.98 (d,1H), 7.02 (d,1H), 7.14 (d,1H), 7.17 (d,1H), 7.22 (d,1H), 7.62 (d,1H), 7.97 (t,1H,J=7Hz), 8.02 (t,1H,J=7Hz), 9.83 (d,1H), 9.9 (d,1H); UV (H_2O) 304 nm, 235; m/e 912 (M^+).

EDTA-Distamycin 6 - To a solution of 0.25g (0.27 mmol) **7** in 5 mL ethanol was added with stirring 5 mL of 0.25M aqueous lithium hydroxide. The resulting solution was stirred for 12h and acidified to pH 4 with 10% aqueous hydrochloric acid. The solvent was removed under high vacuum at 35°C and the residue purified by flash chromatography on silica gel with 3% concentrated ammonia in methanol to yield 0.17g (75%) of the ammonium salt of **ED 6**: IR (KBr) 2950, 1635, 1580, 1460, 1430, 1400, 1255, 1205, 1105 cm^{-1} ; NMR (D_2O) δ 1.87 (s,3H), 1.9 (m,4H), 2.8 (s,3H), 2.9-3.13 (m,12H), 3.17-3.3 (m,6H), 3.53 (s,3H), 3.57 (s,3H), 3.6 (s,3H), 3.67 (s,2H), 6.42 (d,1H), 6.48 (d,1H), 6.56 (d,1H), 6.8 (d,1H), 6.83 (d,1H), 6.87 (s,1H); UV (H_2O) 303 nm (35,000 est.) 235; m/e 828 (M^+).

4-Nitro-tetra-N-methylpyrrole-carboxamide propyldimethyl amine 12 - A solution of 3g (6.0 mmol) nitro amine **11** in 25 mL dimethylformamide was hydrogenated over 400 mg of 5% palladium on charcoal at 52 psi hydrogen on a Parr rocker for 12 hr. The mixture was filtered through Celite and the celite was washed with 20 mL dimethylformamide to afford the crude amine. 200 mL of water and 0.6g (7.2 mmol) NaHCO_3 were added with

stirring to the filtrate, followed by a solution of 1.35g (7.2 mmol) acid chloride 25 in 10 mL dimethylformamide. The mixture was stirred 12 h, 200 mL water added and filtered. The product was washed with saturated aqueous sodium bicarbonate, water and dried to afford 2.6g (70%) of the nitro amine 12 : IR (KBr) 2950, 1630, 1580, 1530, 1465, 1430, 1308, 1255 cm^{-1} ; NMR ($\text{DMSO}-d_6$) δ 1.6 (m,2H), 2.2 (s,6H), 2.3 (t,2H,J=7Hz), 3.2 (m,2H), 3.8 (s,3H), 3.85 (s,3H), 3.88 (s,3H), 3.95 (s,3H), 6.85 (s,1H), 7.07 (m,2H), 7.2 (s,1H), 7.27 (s,1H), 7.31 (s,1H), 8.05 (t,1H,J=7Hz), 8.1 (s,1H), 9.92 (s,1H), 9.97 (s,1H), 10.03 (s,1H), 10.35 (s,1H); UV (H_2O) 305 nm, 236; m/e 621 (M^+).

4-Nitro-penta-N-methylpyrrole-carboxamide propyldimethyl amine 13 - A solution of 2.6g (4.2 mmol) nitro-tetrapyrrole amine 12 in 40 mL dimethylformamide was hydrogenated over 400 mg of 5% palladium on charcoal at 52 psi hydrogen on a Parr rocker for 12 h. The mixture was filtered through Celite and the celite was washed with 10 mL DMF to afford the crude amine. 200 mL of water and 0.42 g (5.0 mmol) NaHCO_3 were added with stirring to the filtrate, followed by a solution of 0.95g (5.0 mmol) acid chloride 25 in 7 mL dimethylformamide. The mixture was stirred for 12 h and the solvent removed under high vacuum at 35°C. The residue was triturated three times with ether and purified by chromatography on silica gel with 2% concentrated aqueous ammonia (33%) in methanol yielding 1.9g (61%) of nitro amine 13 : IR (KBr) 3350, 2945, 1627, 1580, 1530, 1465, 1435, 1307, 1260, 1110 cm^{-1} ; NMR ($\text{DMSO}-d_6$) δ 1.65 (m,2H), 2.2 (s,6H), 2.3 (t,2H,J=7Hz), 3.2 (m,2H), 3.83 (s,3H), 3.9 (s,3H), 3.91 (s,3H), 3.92 (s,3H), 4.0 (s,3H), 6.85 (s,1H), 7.1 (m,3H), 7.2 (m,3H), 7.27 (m,2H), 7.31 (s,1H), 8.1 (t,1H,J=7Hz), 8.2

(s,1H), 9.92 (s,1H), 9.97 (s,1H), 10.03 (s,1H), 10.35 (s,1H); UV (H₂O) 310 nm, 236; m/e 743 (M⁺).

~~Penta-N-methylpyrrole-carboxamide-EDTA~~ triethyl ester 16 - A solution of 1g (1.35 mmol) nitro amine 13 in 20 mL dimethylformamide was hydrogenated over 200 mg of 5% palladium on charcoal at atmospheric pressure for 24 h. The mixture was filtered through Celite and the celite was washed with 25 mL DMF to afford the crude amine.

To a solution of 0.62g (1.35 mmol) triethylester 5 in 10 mL dimethylformamide was added with stirring 0.24g (1.5 mmol) of N,N'-carbonyldiimidazole in 5 mL dimethylformamide. After 2 h, the reduced nitro compound was added and the resulting solution was stirred for 12 h. Dimethylformamide was removed under high vacuum at 35°C, the residue was triturated three times with ether and purified by flash chromatography on silica gel with 4% concentrated aqueous ammonia (33%) in ethanol to afford 0.6g (40%) of **P5E** ethyl ester 16 : IR (KBr) 2960, 1725, 1650, 1585, 1540, 1470, 1440, 1410, 1260, 1210, 1110 cm⁻¹; NMR (DMSO-d₆) δ 1.2 (t,6H,J=7Hz), 1.65 (m,2H), 1.74 (m,2H), 2.15 (s,6H), 2.2 (m,2H), 2.3 (t,2H,J=7Hz), 2.7 (m,4H), 3.1 (m,2H), 3.2 (m,2H), 3.22 (s,2H), 3.45 (s,2H), 3.50 (s,4H), 3.8 (s,3H), 3.87 (m,12H), 4.07 (m,6H), 6.8 (s,2H), 7.07 (m,3H), 7.2 (s,2H), 7.25 (s,3H), 8.1 (t,1H,H=7Hz), 9.9 (s,1H) 9.95 (s,1H); uv (H₂O) 306 nm, 236; m/e 1156 (M⁺).

~~Penta-N-methylpyrrole caboxamide-EDTA~~ 15 - To a solution of 250 mg (0.23 mmol) **P5E** triethyl ester 16 in 5 mL ethanol was added with stirring 5 mL of 0.25M aqueous lithium hydroxide. The resulting solution was stirred for 12 h and acidified to pH 4 with 10% aqueous hydrochloric acid. The solvent was removed under high vacuum at 35°C and the residue purified

by flash chromatography on silica gel with 4% concentrated aqueous ammonia (33%) in methanol. Final purification was carried out by loading the product dissolved in water, onto an amberlite XAD-2 column and washing with 1 L of 3% aqueous Na₂EDTA and 2L of water. Elution with methanol afforded 0.17 (73%) **P5E 15**: IR (KBr) 2950, 1730, 1640, 1570, 1460, 1438, 1430, 1400, 1252, 1205 cm⁻¹; NMR (DMSO-d₆) δ 1.77 (m, 2H), 1.92 (m, 2H), 2.33 (t, 2H, J=7Hz), 2.75 (s, 6H), 3.08 (m, 2H), 3.2 (m, 2H), 3.24 (m, 2H), 3.3 (m, 2H), 3.35 (m, 2H), 3.8 (s, 3H), 3.87 (m, 12H), 3.98 (s, 2H), 4.1 (s, 2H), 6.95 (m, 2H), 7.1 (m, 3H), 7.2 (s, 1H), 7.22 (s, 1H), 7.32 (s, 3H), 8.2 (s, 1H), 8.65 (s, 1H), 9.97 (m, 4H), 10.05 (s, 1H); UV (H₂O) 310 nm (45,000) 238 nm; m/e 1072 (M⁺).

Penta-N-methylpyrrole-propyldimethyl amine P5 14 - A solution of 250 mg (0.35 mmol) nitro-penta-N-methylpyrrolepropyl dimethyl amine **13** in 20 mL dimethylformamide was hydrogenated over 100 mg of 5% palladium on charcoal at 52 psi hydrogen on a Parr rocker for 12 h. The mixture was filtered through celite yielding the crude amine. The celite was washed with 10 mL DMF.

To a solution of 0.024g (0.40 mmol) acetic acid in 3 mL dimethylformamide was added with stirring 0.065g (0.40 mmol) of N,N'-carbonyldiimidazole in 2 mL dimethylformamide. After 2 h, the crude amine was added and the resulting solution was stirred for 12 h. Dimethylformamide was removed under high vacuum at 35°C, the residue was triturated three times with ether and purified by flash chromatography on silica gel with 5% concentrated aqueous ammonia (33%) in ethanol to yield 150 mg (60%) of **P5 14** : IR (KBr) 2940, 1640, 1580, 1530, 1460, 1430, 1400, 1255, 1200, 1100 cm⁻¹; NMR (DMSO-d₆) δ 1.65 (m, 2H), 2.0

(s,3H), 2.2 (s,6H), 2.3 (t,2H,J=7Hz), 3.2 (m,2H), 3.83 (s,3H), 3.9 (m,12H), 6.85 (s,1H), 6.9 (s,1H), 7.07 (m,3H), 7.15 (s,1H), 7.18 (s,1H), 7.25 (s,3H), 8.10 (t,1H,J=6Hz), 9.85 (s,1H), 9.91 (m,2H), 9.97 (s,2H); UV (H₂O) 312 nm, (45,000)¹⁰¹ 236 nm; m/e 755 (M⁺).

Bisdistamycin 19 - A solution of 0.25g (0.5 mmol) nitro amine 2 in 10 mL dimethylformamide was hydrogenated over 200 mg of 5% palladium on charcoal at 50 psi hydrogen on a Parr rocker for 12 h. The mixture was filtered through Celite affording the crude amine 3. The celite was washed with 10 ml DMF. To this solution was added with stirring 0.09g (0.28 mmol) of di-N-hydroxysuccinimide-heptane dicarboxylic acid 30. The activated diester 30 was prepared as follows. To a solution of 5g (31.0 mmol) pimelic acid and 7.9g (68 mmol) N-hydroxysuccinimide was added with stirring 14g (68 mmol) of dicyclohexylcarbodiimide in 20 ml dioxane. The solution was stirred for 12 h, filtered, concentrated and chromatographed on silica gel with 25% ethyl acetate in dichloromethane to give 8g (72%) activated diester 20; NMR (CDCl₃) δ 2.8 (s,8H), 2.6 (t,2H,J=8Hz), 1.7 ppm (m,6H).

After 12 h DMF was removed from the bisdistamycin under high vacuum at 35°C, the residue was triturated three times with ether and purified by flash chromatography on silica gel with 5% concentrated aqueous ammonia (33%) in methanol affording 0.30g (70%) **BD**: IR (KBr) 3280, 2940, 1640, 1580, 1530, 1460, 1430, 1400, 1250, 1200 cm⁻¹; NMR (DMSO-d₆) δ 1.3 (m,2H), 1.5 (m,8H), 2.1 (s,12H), 2.2 (m,8H), 3.15 (m,4H), 3.8 (s,3H), 3.85 (s,3H), 3.77 (s,3H), 6.8 (d,2H,J=1.65Hz), 6.85 (d,2H,J=1.5Hz), 7.04 (d,2H,J=1.5Hz), 7.15 (m,4H), 7.25 (d,2H,J=1.5Hz), 8.05 (t,2H,J=6Hz), 9.8 (s,2H), 9.9 (s,4H), UV (EtOH) 305 nm, (70,000)¹⁰³

230 nm, m/e 1061 (M^+).

Bis(EDTA-triethylester distamycin) BED-Et₃ - A solution of 0.25g (0.23 mmol) nitro-EDTA triethylester **10** in 10 ml DMF was hydrogenated over 200 mg of 5% Pd/C at 50 psi hydrogen on a Parr rocker for 12 h. The mixture was filtered through celite and the celite was washed with 10 ml DMF. To this solution was added with stirring 0.041g (0.1 mmol) di-N-hydroxysuccinimide heptane dicarboxylic acid **30**. After 12 h, DMF was removed under high vacuum at 35°C, the residue was triturated three times with ether and purified by flash chromatography on silica gel with 35% concentrated aqueous ammonia in methanol to yield 0.2g (80%) **BED-Et₃ 31**: IR (KBr) 3290, 2940, 1735, 1660, 1640, 1580, 1530, 1460, 1430, 1255, 1200 cm^{-1} ; NMR (DMSO- d_6) δ 1.18 (t, 18H, J=8Hz), 1.3 (m, 2H), 1.6 (m, 12H), 2.13 (s, 6H), 2.25 (t, 4H, J=7Hz), 2.3 (m, 8H), 2.68 (m, 4H), 2.73 (m, 4H), 3.13 (m, 4H), 3.18 (m, 4H), 3.2 (m, 4H), 3.5 (m, 4H), 3.59 (m, 8H), 3.8 (s, 6H), 3.86 (s, 6H), 3.97 (s, 6H), 4.05 (m, 12H), 6.82 (d, 2H, J=1.5Hz), 6.86 (d, 2H, J=1.5Hz), 7.05 (d, 2H, J=1.5Hz), 7.18 (d, 2H, J=1.5Hz), 7.20 (d, 2H, J=1.5Hz), 7.23 (d, 2H, J=1.5Hz), 7.96 (s, 2), 8.02 (s, 2H), 9.77 (s, 2H), 9.88 (s, 2H), 10.0 (s, 2H); UV (H₂O) 306 nm, 235 ; m/e 1864 (M^+).

Bis(EDTA-distamycin) BED - To a solution of 0.25g (0.14 mmol) **BED-Et₃ 31** in 5 mL ethanol was added with stirring 5 mL of 0.25M aqueous lithium hydroxide. The resulting solution was stirred for 12 h and acidified to pH 4 with 10% aqueous hydrochloric acid. The solvent was removed under high vacuum at 35°C, the residue was triturated three times with ether and purified by flash chromatography on silica gel with 5% concentrated aqueous ammonia (33%) in methanol. Final purification was carried out by loading the product dissolved in water onto an amberlite XAD-2 column

and washing with 1 l 3% aqueous Na₂EDTA and 2 l doubly distilled water. Elution with methanol afforded 0.15g (62%) **BED 17**; IR (KBr): 3300, 2940, 1740, 1660, 1640, 1570, 1540, 1470, 1440, 1410, 1260 cm⁻¹; NMR (DMSO-d₆): δ 1.25 (m, 2H), 1.65 (m, 4H), 1.9 (m, 8H), 2.3 (t, 4H, J=7Hz), 2.7 (s, 6H), 3.1 (m, 8H), 3.25 (m, 4H), 3.3 (m, 4H), 3.4 (m, 4H), 3.45 (m, 4H), 3.8 (3s, 18H), 3.94 (s, 8H), 4.0 (s, 4H), 4.1 (s, 4H), 6.9 (s, 4H), 7.0 (d, 2H, J=1.5 Hz), 7.17 (d, 2H, J=1.5Hz), 7.20 (d, 2H, J=1.5Hz), 7.23 (d, 2H, J=1.5Hz), 8.2 (s, 2H), 8.83 (s, 2H), 9.95 (3s, 6H); UV (H₂O) 306 (70,000) 10³ 235 nm; m/e 1732 (M⁺).

Dimethylamino tri-N-methylpyrrole heptanoic acid 21 - A solution of 0.5g (1 mmol) nitro amine **2** in 10 ml dimethylformamide was hydrogenated over 200 mg Pd/C at 50 psi hydrogen on a Parr rocker for 12 h. The mixture was filtered through celite and the celite was washed with 10 ml DMF. The combined solution was added with stirring to 2 mmol heptane dicarboxylic acid monoimidazolidine in 10 ml DMF. Heptane dicarboxylic acid monoimidazolidine was synthesized by adding with stirring 0.4g (2 mmol) acyldiimidazole to 1.6g (10 mmol) heptane dicarboxylic acid in 10 ml DMF and stirring an addition 1 h. After 12 h, 10 ml H₂O was added to the reaction mixture, solvent was removed under vacuum at 35°C, the residue was triturated three times with ether and purified by flash chromatography on silica gel with 2% concentrated aqueous ammonia in methanol to afford 0.5g (5%) amino acid **21**; IR (KBr) 3300, 2950, 1660, 1640, 1570, 1530, 1460, 1430, 1400, 1260, 1200 cm⁻¹; NMR (DMSO-d₆) δ 1.3 (m, 2H), 1.4-1.6 (m, 3H), 2.15 (s, 6H), 2.25 (m, 6H), 3.2 (m, 2H), 3.75 (s, 3H), 3.8 (s, 3H), 3.83 (s, 3H), 6.85 (d, 1H, J=1.5Hz), 6.90 (d, 1H, J=1.5Hz), 7.05 (d, 1H, J=1.5Hz), 7.15 (m, 2H), 7.2 (d, 1H, J=1.5Hz),

8.1 (t, 1H, J=6Hz), 9.8 (s, 1H), 9.9 (s, 1H), 9.93 (s, 1H); uv (H₂O) 302 nm, 238 nm; m/e 611 (M⁺).

EDTA bisdistamycin triethylester E(Et₃)BD 33 - 0.37g (0.41 mmol) nitro EDTA triester 10 in 15 ml DMF was hydrogenated over 200 mg Pd/C at 50 psi hydrogen on a Parr rocker for 12 h. This solution was filtered through celite and the celite was washed with 10 ml DMF to afford the crude amine. To 0.25g (0.41 mmol) amino acid 21 in 15 ml dimethylformamide was added with stirring 0.09g (0.49 mmol) acyldiimidazole. After 1 h the crude amine solution was added to the imidazolide with stirring and the resulting solution stirred for 12 h at 25°C. The DMF was removed under vacuum at 35°C, the resulting residue triturated three times with ether and purified by flash chromatography on silica gel with 4.5% concentrated aqueous ammonia in methanol to afford 0.45g (73%) EBD triethyl ester 33: IR (KBr) 3290, 2950, 1740, 1670, 1640, 1590, 1560, 1470, 1440, 1410, 1260, 1210 cm⁻¹; NMR (DMSO-d₆) δ 1.2 (t, 9H, J=7Hz), 1.3 (m, 2H), 1.6 (m, 10H), 2.15 (s, 9H), 2.3 (t, 4H, J=7Hz), 2.35 (m, 6H), 2.7 (m, 4H), 3.15 (m, 2H), 3.2 (m, 6H), 3.5 (s, 4H), 4.6 (s, 2H), 3.85 (s, m3H), 3.9 (s, 3H), 3.92 (s, 3H), 6.85 (s, 1H), 6.87 (s, 1H), 6.9 (s, 2H), 7.06 (s, 2H), 7.15 (s, 2H), 7.17 (s, 2H), 7.23 (s, 2H), 7.95 (t, 1H, J=7Hz), 8.0 (t, 1H, J=7Hz), 8.05 (t, 1H, J=7Hz), 9.85 (s, 2H), 9.95 (s, 2H), 9.96 (s, 2H); UV (EtOH) 303 nm, 235 nm; m/e 1463 (M⁺).

EDTA-bis distamycin - EBD - To a solution of 0.2g (0.14 mmol) triester 33 in 5 ml ethanol was added with stirring 5 ml of 0.25M aqueous lithium hydroxide. The resulting solution was stirred for 12 h and acidified to pH 4 with 10% hydrochloric acid. The solvent was removed under high

vacuum at 35°C and the residue purified by flash chromatography on silica gel with 5% concentrated ammonia hydroxide in methanol. Final purification was carried out by loading the product, dissolved in distilled H₂O onto a nonionic amberlite XAD-2 column and washing, with 1 ℓ 3% aqueous Na₂EDTA and 2 ℓ doubly distilled water. Elution with methanol afforded 0.1g (52%) **EED**: IR (KBr) 3310, 2950, 1730, 1650, 1640, 1560, 1530, 1460, 1430, 1400, 1260, 1200 cm⁻¹; NMR (DMSO-d₆) δ 1.3 (m,2H), 1.65 (m,4H), 1.9 (m,6H), 2.25 (t,4H,J=7Hz), 2.75 (s,9H), 3.05 (m,6H), 3.2 (m,6H), 3.4 (m,4H), 3.9 (3s,9H), 3.95 (s,4H), 4.0 (s,2H), 4.1 (s,2H), 6.9 (s,4H), 7.03 (d,2H,J=1.5Hz), 7.15 (d,2H,J=1.5Hz), 8.3 (s,2H), 8.9 (t,1H,J=7Hz), 9.9 (3s,6H); UV (H₂O) 303 (70,000) 103, 235 nm; m/e 1447 (M⁺) (C 65, H 90, O 16, N 19, Li, Na).

pBR-322 Plasmid Preparation^{90,104}

Cell Growth

The bacterial plasmid pBR-322 was grown in E.Coli strain HB 101. The following solutions are necessary (Vogel Bonner Minimal Media)

(I) 5g MgSO₄·H₂O

50g Citric acid

250g K₂HPO₄ (anhyd)

56.1g Na₂HPO₄·7H₂O

27.6g (NH₄)₂HPO₄

and 335 ml H₂O (millipore filtered) pH 7.0

(II) 40g anhydrous D glucose and d.d. H₂O (millipore)
to 200 ml

In each of 6 2 ℓ broth flasks add 10 ml (I) 25 mg thymine and 1g

Casamino acids and 500 ml dd H₂O (millipore filtered). In 1 50 ml flask add 1 ml (I), 2.5 mg thymine and 100 mg Casamino acids. Autoclave broth flasks and glucose solution separately. Let cool and add 20 ml (II) to 500 ml broths and 2 ml (II) to 50 ml broth. Also add 1 ml 25 mg/ml ampicillin sodium salt solution and 1 ml thiamine (1 mg/ml) to 500 ml broth, and 100 μ l ampicillin and 100 μ l Thiamine to 50 ml broth. Ampicillin and thiamine solutions should be filtered sterilized (Swinnex 45 μ M).

Innoculate 50 ml broth with a single bacterial colony of E. Coli HB 101. The single colony was isolated by streaking⁹⁰ V.B. salt plates with bacteria from an E.Coli HB101 stab obtained from Professor J. Campbell at Caltech.

V.B. Minimal Salt Plates

III 20 ml I and 280 ml dd H₂O (millipore filtered)

IV 15 gm Agar and 680 ml H₂O in 680 ml H₂O

Autoclave III and IV separately. At 50°C mix III, IV, 20 ml II and 1 ml Thiamine (1 mg/ml). Also add 1 ml of 25 mg/ml ampicillin and 0.5 ml of 12.5 mg/ml tetracycline hydrochloride solution (50% v/v ethanol, water filter sterilized through Swinnex (45 μ M))). Add 30-35 ml per 85 mm autoclaved petri dish.

Incubate 50 ml starter broth on a shaker at 37°C for 24 h. Innoculate 500 ml broth flasks with 5 ml of starter broth and grow at 37°C on a shaker to an absorbance of 0.4-0.5 at 600 nm (\sim 4 h). Add 1

ml/500 ml broth a 100 mg/ml chloromycetin sodium succinate solution (Parker Davis, filter sterilize through Swinnex 45 μ M). Grow for 20 additional hours at 37°C on a shaker (A = 1.7). Harvest cells by centrifugation at 8,000 rpm for 10 min at 4°C in a Sorvel centrifuge (500 ml bottles). Be sure bottles are sealed with O-ring. After spin, drain off supernatant.

Lysis

Lysis Solution:

- (I) 25g Sucrose
10 ml 0.5M Tris Base, pH 8.0
dilute to 100 ml total with dd H₂O cool I to 0°C
- (II) 0.2g lysozyme
5 ml 0.5M Tris Base, pH 8.0
5 ml dd H₂O cool II to 0°C
- (III) 4.65g Na₂EDTA in 50 ml H₂O
adjust pH to 8.0 with 1N NaOH cool III to 0°C
- (IV) 10 ml Triton X-100
20 ml 0.5M Tris Base pH 8.0
25 ml solution (III)
45 ml dd H₂O cool IV to 0°C

Note pH > 8.0 required for lysozyme

Resuspend cells in each bottle in 6 ml solution I and transfer to 250 ml baker. Wash bottle with additional 2 ml of I. Cool the combined suspensions to 0°C, add 10 ml (II) and incubate 5 min at 0°C.

Add 20 ml (III) and incubate at 0°C for 15 min. Add 75 ml (IV) and incubate at 0°C for 15 min. Pour solution into centrifuge tube and spin at 40K, 70 Ti Rotor, for 1 h. Remove supernatant and discard precipitate.

Ethidium Bromide Centrifugation

Add 1g of cesium chloride/ml of DNA solution. Add 0.8 ml of ethidium bromide (10 mg/ml H₂O) solution for every 10 ml of cesium chloride solution. Mix. Final density should be 1.55g/ml. Spin at 20°C at 45,000 rpm in Ti 70 rotor for 36 h. Separate closed circular plasmid DNA⁹⁰ by suction using Gilson peristaltic pump. DNA can be visualized under UV light (excessive exposure nicks DNA). Add to this solution cesium chloride/ethidium bromide solution (d = 1.55) to a total volume of 32 ml. Spin on Ti-70 rotor at 20°C for 36 additional hours and separate supercoiled DNA. Extract⁹⁰ DNA solution with an equal volume of n-butanol saturated H₂O 4-6 times. Dialyze⁹⁰ the clear aqueous phase against TE buffer 4 times and against RB two times (TE is 10 mM Tris HCl, pH 8.0, 1 mM EDTA; RB is 10 mM Tris HCl, pH 7.9, 40 mM NaCl). 45.45 µg/ml = 1 absorbance unit.⁹⁰

Calf Thymus Preparation

100 mg Calf thymus was dissolved in 18 ml 10 mM aqueous NaCl. The solution was deoxygenated by purging with N₂ 15 min at 0°C. The solution was then sonicated at 0°C with a microtip probe three times for 30 sec each time. Cool 1 min at 0°C between sonication. The solution was then deoxygenated a second time, and sonicated three additional times. The sonicated DNA was phenol⁹⁰ extracted two times, ether extracted three times, and ether removed under a stream of air. The

solution was filtered through Swinnex HA, a two times, ether extracted three times, and ether removed under stream of air. The solution was filtered through Swinnex HA, $45.45 \mu\text{g/ml} = 1$ absorbance unit.

³²P End-labeled Restriction Fragments

3' End-labeling Procedure^{90,92,93}

10 μg of pBR-322 (100 $\mu\text{g/ml}$) was digested with the appropriate restriction enzyme⁹⁰ under the prescribed reaction conditions (BRL). Complete digestion was assayed by electrophoresis of an aliquot on a 1% agarose mini-gel⁹⁰ with ethidium bromide staining. (An initial Eco RI digest, followed by end-labeling and a final Rsa I digest affords the 167 and 516 bp fragments. An initial Bam HI digest, followed by end labeling and a final Eco RI/Sal I digest affords the 381 (381-0 bp) and 279 bp fragments.) The digested DNA was ethanol precipitated,⁹⁰ ethanol washed, and dried (3 min/high vacuum). The DNA was then dissolved in 20 μl

H₂O and 5 μl 66 mM DTT solution, and 5 μl 60 mM Tris HCl (pH 7.4), 60 mM NaCl, 66 mM MgCl₂ buffer added. The solution was made 1 mM in dTTP, dCTP, dGTP (Bam HI site) or 1 mM in dTTP (Eco RI site) by addition of 1 μl of a 50 mM, pH 7.0 (buffered with 0.05M Tris Base⁹⁰) dNTP solution.

10 μl (100 μCi) of a 3000 Ci/mole (10 mCi/ml) 5'-($\alpha^{32}\text{P}$)dATP triethylammonium salt was then added followed by 25 units of the Klenow fragment of E.Coli polymerase I. After 30 min at 25°C, 1 μl of 50 mM dATP, dCTP, dGTP, dTTP solutions was added to the Bam HI labeled DNA and 1 μl of 50 mM dATP and dTTP solutions to the Eco RI labeled DNA. After 10 additional minutes at 25°C, 10 μl 100 mM Na₂EDTA was added and the reactions were ethanol precipitated two times, washed, and dried (3 min, high vacuum). The end labeled DNA was then dissolved in 50 μl of the

appropriate endonuclease buffer and digested to afford the final end labeled fragments. 5 μ l of gel loading buffer was added (0.25% bromophenol blue, 0.25% xylene cyanol and 25% Ficoll (400) in H₂O) and the end labeled fragments were separated on a 5% 1/30 crosslinked acrylamide gel at 240 V.^{90,92,93} After the bromophenol blue reached the bottom, the gel was autoradiographed⁹⁰ using Kodak X-Omat AR film (2 min exposure). The individual bands were then located and removed and incubated in 0.75 ml elution buffer (0.5M NH₄OAc, 10 mM MgCl₂, 1 mM EDTA, 0.10% SDS) for 36 h at 35°C. The resulting solutions were filtered through 45 μ M Swinnex, the appropriate amount of sonicated calf thymus DNA added, and the solutions were ethanol precipitated twice, ethanol washed, and dried (3 min, high vacuum). Final specific activities were typically > 2.5 mRN/hr/ 1 Maxam Gilbert G reactions were carried out as described in the literature.⁹² The base pair fragment labeled at the Nde site was isolated by digesting 10 μ g pBR-322 with Nde I, end labeling, and digesting a second time with Hae III.

5'-End Labeling

10 μ g of 100 μ g/ml pBR-322 plasmid DNA was digested with Eco RI or Bam HI. The reactions were ethanol precipitated, ethanol washed, and dried. The digested DNA was then dissolved in 100 μ l RXB buffer (40 mM Tris Base, 5 mM NaOAc, pH 7.8). 1000 units (0.5 μ l) of bacterial alkaline phosphatase was then added and the reaction incubated at 65°C for 1 h. The solution was cooled to 25°C, phenol extracted⁹⁰ three times (1v/1v) and ether extracted three times (2v/1v). The DNA was then ethanol precipitated two times, ethanol washed, and dried. The DNA was dissolved in 30 μ l H₂O and 5 μ l kinase buffer (10x = 500 mM Tris HCl (pH

7.6), 100 mM MgCl₂, 10 mM spermidine, 10 mM Na₂EDTA) and 5 1 60 mM DTT added. 5 μ l (1 mCi) of 9000 Ci/mmole 3'-(γ ³²P)dATP (\sim 0.2 mCi/ μ l) was added followed by 20 units T4 polynucleotide kinase. The reaction was incubated at 37°C for 1 h, ethanol precipitated twice, ethanol washed, and dried. The end-labeled DNA was then digested and isolated as described above. The base pair fragment labeled at the Nde site was prepared by digesting 10 μ g pBR-322 with Nde, end labeling, and digesting a second time with Hae III.

Gel Electrophoresis

Agarose gel electrophoresis was carried out in the usual manner⁹⁰ using 5 mm thick gels, 19 x 16 glass plates and a Watson vertical gel apparatus. Gel buffer consisted of 40 mM Tris Base (pH 7.8 with HOAc), 5 mM NaOAc and 10 mM Na₂EDTA. Loading buffer was 0.25% bromophenol blue, 10% Ficoll (400) in H₂O. Gels were electrophoresed at 120v until bromophenol blue ran to bottom. Gels were stained with ethidium bromide (0.5 mg/ml) destained and photographed under long wave length irradiation using Polaroid type 55 positive/negative land film. The negative film was scanned at 485 nm using a Varian 219 spectrophotometer, Varian gel scanner and an Apple gel scanning program. Forms I, II, and III DNA were correlated to peak areas. Gels were corrected for form II DNA and corrected for the decreased stainability of form I DNA (1.22).⁵¹ Agarose mini gels were run in the usual manner⁹⁰ at 80V using RXB buffer.

Polyacrylamide nondenaturing gels were run in the usual manner using 2 mM 5% acrylamide, 1/30 crosslinked gels on 19 x 16 glass plates

and a Watson vertical gel apparatus. Gel buffer (TBE) consisted of 100 mM Tris base, 100 mM boric acid and 10 mM Na₂EDTA, pH 8.0. Gels were preelectrophoresed 0.5 h, samples loaded and electrophoresed at 240V until bromophenol blue ran to bottom.

Polyacrylamide denaturing gels were run in the usual manner^{90,92} using 0.4 mm thick 8% acrylamide, 1/20 crosslinked, 50% urea 34 x 40 cm slab gels and a BRL model 30 electrophoresis apparatus. Gel buffer was TBE and loading buffer was 0.1% bromophenol blue, 50% formamide and 50% 2 x TBE buffer. Samples were denatured for 2 min at 90°C, immediately cooled to 0°C, and after 2 min loaded onto the gel. Gels were preelectrophoresed for 1 h, samples loaded, and electrophoresed at 1500V until bromophenol blue reached the bottom or for twice this time.

Autoradiography was carried out at -50°C with or without the use of an intensification screen and Kodak X-Omat AR film. An 8 x 10 positive of the original autoradiogram was scanned at 485 nm using a Varian 219 spectrophotometer, gel scanner, and an Apple gel scanning program. Peak area was correlated to cleavage intensity.

High resolution polyacrylamide denaturing gels were run as described above. Gels were 0.4 mm 20% acrylamide, 1/30 crosslinked 50% urea 40 cm slab gels. Gels were run at 1500V.

Cleavage Reactions

Cleavage of Supercoiled pBR-322 DNA

All reactions were carried out using freshly prepared dithiothreitol, reagent, and ferrous ammonium sulfate stock solutions. Extinction coefficients used were DE (305 nm ϵ = 35,000), ED (300 nm, ϵ = 35,000), P5E (313 nm, ϵ = 45,000), BED (300 nm, ϵ = 70,000), EBD (300

nm, $\epsilon = 70,000$). Reagents were characterized by UV spectroscopy immediately prior to use.

Reactions were run in 10 μ l total volume: 2 μ l 50 μ M or 5 mM form I pBR-322, 2 μ l 5 x reaction buffer (1x = 40 mM Tris base pH 7.9, 10 mM NaOAc) and 4 μ l of a 5x reagent-Fe(II) solution were equilibrated at 37°C for 5 min (DE, ED, BED, EBD) or 60 min (P5E). P5E-Fe(II) cleavage was equivalent when equilibrated 60 min at 37°C or 3 min at 65°C. The reagent-Fe(II) complex was made by mixing aqueous 1-5 mM reagent and 1-5 mM aqueous ferrous ammonium sulfate, equilibrating at 25°C for 3 min and diluting to the desired concentration in H₂O. To the reagent-Fe(II) - DNA solution was added 2 μ l 25 mM aqueous DTT, the reaction vortexed, spun down and incubated at 25°C in the presence of air for 2 h.

2 μ l of agarose gel loading buffer was then added and the reaction mixture loaded on an agarose gel (10 μ l for 10 μ M bp, 1.5 μ l for 1 mM bp). These conditions were found to give optimum cleavage. For inhibition studies, reactions were identical except reagent and inhibitor were preequilibrated for 5 min before addition of Fe(II) and no DTT was used. The control (reagent/no inhibition) reactions were run without preequilibrating reagent and Fe(II). For time course studies, reactions were run as described above on a 10x scale.

10 μ l aliquots were quenched at intervals in 10 μ l 100 mM Na₂EDTA and immediately vortexed, spin down, and frozen at -78°C. Loading buffer was added, the solutions were thawed and immediately loaded. Controls show that no additional cleavage occurs after freezing, thawing and loading the samples.

Cleavage of Linear pBR-322 DNA

Supercoiled DNA (100 $\mu\text{g/ml}$) was digested by Eco RI, Sal I, Ava I, Ava I + Hind II, Nde I, Rsa I or Taq I under the appropriate reaction conditions (BRL). The DNA was then ethanol precipitated, ethanol washed, and dried for 3 min under high vacuum. The DNA was then diluted to 250 μM or 5 mM. Cleavage reactions were carried out in the manner described above. Reagent cleaved DNA and starting linear DNA's were run on 1% agarose gels. The enzyme digested fragments were used as molecular weight markers and DNA size determined by plotting \log_{10} nucleotide pairs versus distance migrated (cm). Plots were linear in the 3700-1000 bp range.

Salt effects on cleavage specificity were determined by adding to 2 μl 250 μM DNA and 1 μl 10x reaction buffer, 1 μl 10M, 1M or 100 mM NaCl solution. Reactions were then carried out as described above. Time course studies on the cleavage reaction were carried out as described above.

Cleavage of End-labeled Restriction Fragments

The cleavage reactions were run with > 600 cpm of ^{32}P end labeled restriction fragments per cleavage reaction. A stock solution of ^{32}P end labeled DNA was made up to a total concentration of 250 M with sonicated calf thymus DNA. Total reaction volumes were 15 μl . 6 μl 250 μM DNA stock solution, 3 μl 5x reaction buffer (1x = 40 mM Tris base, pH 7.9, 10 mM NaOAc) and 4 μl of a 7.5x reagent-Fe(II) solution were equilibrated at 37°C for 5 min (DE, ED, BED, EBD) or 60 min (P5E). P5E-Fe(II) cleavage was equivalent when equilibrated at 37°C for 60 min or at 65°C for 3 min.

Reagent-Fe(II) complexes were made as described above. To the reagent-Fe(II)-DNA solution was added 2 μ l of 7.5 mM aqueous DTT, the reaction vortexed, spun down, and incubated at 25°C for 2 h in the presence of air. The reactions were then frozen (-78°C, 5 min), lyophilized (~30 min) and 5 μ l formamide loading buffer added. The reactions were vortexed, spun down, heated to 90°C for 2 min, cooled to 0°C for 2 min and loaded on a denaturing acrylamide/urea gel.

MPE-Fe(II) footprinting reactions were run in a similar manner. 6 μ l 250 μ M DNA, 1 μ l 15x reaction buffer, and 2 μ l 7.5x aqueous distamycin, P5, or BD solutions were mixed and equilibrated 60 min at 37°C.

Cleavage was initiated by adding 4 μ l of a 7.5x aqueous MPE-Fe(II) solution followed by 2 μ l 7.5 mM aqueous DTT. 1-5 mM aqueous MPE and 1-5 mM aqueous ferrous ammonium sulfate solutions were mixed, equilibrated at 25°C for 3 min and diluted to the desired concentration.

References

1. a) Smith, H.O. Science **1979**, 205, 455. b) Malcolm, A.D.B. in "Genetic Engineering", ed. Williamson, R., Academic Press, New York, p. 129, c) Roberts, R.J. Nucleic Acids Res. **1983**, 11, R135. d) Wells, R.D.; Klein, R.D.; Singleton, C.K. in "The Enzymes", ed. Boyer, H., Academic Press, New York, 1981, p. 157. e) Modrich, P. CRC Critical Reviews in Biochemistry **1982**, 13 288.
2. Schultz, P.G.; Taylor, J.S.; Dervan, P.B. J. Amer. Chem. Soc. **1982**, 104, 6861.
3. Taylor, J.S.; Schultz, P.G.; Dervan, P.B. Tet. Symposium in Print on Bioorganic Studies on Receptor Sites **1983**, in press.
4. Schultz, P.G.; Dervan, P.B. Proc. Natl. Acad. Sci. USA **1983**, in press.
5. Schultz, P.G.; Dervan, P.B. J. Amer. Chem. Soc. **1983**, in press.
6. Schultz, P.G.; Dervan, P.B. Biomolecular Structure and Dynamics **1983**, in press.
7. a) Boyer, H.W. Ann. Rev. Microbiol. **1971**, 25, 153. b) Yuen, R. Ann. Rev. Biochem. **1981**, 50, 285.
8. Modrich, P. Quart. Rev. Biophys. **1979**, 12, 315.
9. a) Linn, S.; Lautenberger, J.A.; Eskin, B.; Lackey, D. Fedn. Proc. **1974**, 33, 1128. b) Murray, N.E.; Batten, P.L.; Murray, K. J. Mol. Biol. **1973**, 81, 395.
10. The number of unique recognition sites for a sequence of double stranded DNA containing n bases, where n is odd is $4^{n/2}$. The number of recognition sites for n bases where n is even is $(4^{n/2}) + (4^{n/2}/2)$. The total number of sites for n consecu-

tive A+T bp is 2^n .

11. Modrich, P.; Zabel, D. J. Biol. Chem. **1976**, 251, 5866.
12. Yoo, O.J.; Agarwal, K.L. J. Biol. Chem. **1980**, 255, 6455.
13. Herman, G.E., Ph.D. Thesis, Duke University, 1981.
14. Rubin, R.A.; Modrich, P. in "Methods in Enzymology, Nucleic Acids and Protein Synthesis", Part H, ed. K. Grossman, K. Moldave, New York, Academic Press.
15. Greene, P.J.; Poonian, M.S.; Nussbaum, A.L.; Tobias, L.; Garfin, D.E.; Boyer, H.W.; Goodman, H.M. J. Molec. Biol. **1975**, 99, 237.
16. a) Rubin, R.A.; Modrich, P. J. Biol. Chem. **1977**, 252, 7265.
b) Rubin, R.A.; Modrich, P. Nucl. Acids Res. **1978**, 5, 2991.
17. Young, T.S.; Kim, S.H.; Modrich, P.; Beth, A.; Ernest, J. J. Mol. Biol. **1981**, 145, 607.
18. Rosenberg, J.M.; Dickerson, R.E.; Greene, P.J.; Boyer, H.W. J. Molec. Biol. **1978**, 122, 241.
19. Berkner, K.L.; Folk, W.R. J. Biol. Chem. **1977**, 252, 3185.
20. a) Forsblum, S.; Rigler, R.; Ehenberg, M.; Peterson, U.; Philipson, L. Nucl. Acids Res. **1976**, 3, 3255. b) Richter, P.H.; Eigen, M. Biophys. Chem. **1974**, 2, 255.
21. Cotton, F.A.; Hazen, E.E.; Legg, M.J. Proc. Natl. Acad. Sci. USA **1979**, 76, 2551.
22. Polisky, B.; Greene, P.; Garfin, D.E.; McCarthy, B.J.; Goodman, H.M.; Boyer, H.W. Proc. Natl. Acad. Sci. USA **1975**, 72, 3310.
23. Hsu, M.; Berg, P. Biochemistry **1978**, 17, 131.
24. Woodbury, C.P.; Hagenbuchle, O. Fedn. Proc. **1979**, 38, 780.
25. Bishop, J.O. J. Mol. Biol. **1979**, 128, 545.

26. Schrammes, R.; Richter, P.H. Biophys. Chem. **1978**, 8, 135.
27. a) Jack, W.E.; Rubin, R.A.; Kim, S.H.; Modrich, P. in "Gene Amplification and Analysis", Chirikjian, J.G., ed., Elsevier, 1980, 165.
b) Rosenberg, J.M.; Boyer, H.W.; Greene, ibid, 131.
28. Lu, A-L.; Jack, W.E.; Modrich, P. J. Biol. Chem. **1981**, 256, 13200.
29. Bugalczyk, A.; Hedgpeth, J.; Boyer, H.W.; Goodman, H.M. Biochemistry, **1974**, 13, 503.
30. Anderson, W.F.; Ohlendorf, D.H.; Takeda, Y.; Matthews, B.W. Nature **1981**, 290, 754.
31. Pabo, C.; Krovatin, W.; Jeffrey, A.; Sauer, R.T. Nature **1982**, 298, 441.
32. Pabo, C.; Lewis, M. Nature, **1982**, 298, 443.
33. McKay, D.B.; Steitz, T.A. Nature, **1981**, 290, 744.
34. Matthews, B.W.; Ohlendorf, D.H.; Anderson, W.F.; Takeda, Y. Proc. Natl. Acad. Sci. USA, **1982**, 74, 1428.
35. O'Neill, M.C.; Amass, K.; DeCrombrughe, B. Proc. Natl. Acad. Sci. USA **1981**, 78, 2213.
36. Caruthers, M.H. Acc. Chem. Res. **1980**, 13, 155.
37. Von Hippel, P.H. in "Biological Regulation and Development", Goldberger, R.F., ed., Plenum, 1979, p. 279.
38. Nelson, H.C.M.; Hecht, M.H.; Sauer, R.T. "Symposia on Quantitative Biology", Vol. 1, 1982, Cold Spring Harbor, 441.
39. Kim, R.; Kim, S-H. ibid, 1982, 451.
40. Johnson, A.D.; Poteete, R.A.; Lauer, G.; Sauer, R.T.; Ackers, G.K.; Ptashne, M. Nature, **1981**, 294.
41. Ptashne, M., et al. Cell, **1980**, 19, 1.

42. Johnson, A.; Meyer, B.J.; Ptashne, M. Proc. Natl. Acad. Sci. USA **1978**, 75, 1783.
43. For reviews see: a) "Bleomycin, Biochemical and Biological Aspects", Hecht, S.M., ed., Springer Verlag, New York, 1979.
b) Burger, R.M.; Peisach, J.; Horwitz, S.B. Life Sciences **1981**, 28, 715.
44. Povirk, L.F.; Hogan, M.; Dattagupta, N. Biochemistry **1979**, 18, 96.
45. D'Andrea, A.D.; Haseltine, W.A. Proc. Natl. Acad. Sci. USA **1978**, 75, 3608.
46. Takeshita, M.; Grollman, A.P.; Ohtsubo, E.; Ohtsubo, H. Proc. Natl. Acad. Sci. USA **1978**, 75, 5983.
47. Burger, R.M.; Peisach, J.; Horwitz, S.B. J. Biol. Chem. **1981**, 256, 11636.
48. Clore, G.M.; Lane, A.M.; Holloway, M.R. Inorg. Chim. Acta **1980**, 46, 139.
49. a) Giloni, L.; Takeshita, M.; Johnson, F.; Iden, C.; Grollman, A. J. Biol. Chem. **1981**, 256, 8608. b) Burger, R.M.; Berkowitz, A.R.; Peisach, J.; Horowitz, S.B. J. Biol. Chem. **1980**, 255, 11832.
c) Burger, R.M.; Peisach, J.; Horwitz, S.B. J. Biol. Chem. **1982**, 256, 11636.
50. Wu, J.C.; Kozarich, J.W.; Stubbe, J. J. Biol. Chem. **1983**, 258, 4694.
51. Hertzberg, R.P.; Dervan, P.B. J. Amer. Chem. Soc. **1982**, 104, 313.
52. a) Waring, M.J. J. Mol. Biol. **1965**, 13, 269; LePecq, J.-B.; Paoletti, C. J. Mol. Biol. **1967**, 27, 87. b) Muller, W.; Crothers, D.M. Eur. J. Biochim. **1975**, 54, 267. c) Bresloff, J.L.;

- Crothers, D.M. Biochemistry **1981**, 20, 3457. See also d)
- Kastrup, R.V.; Young, M.A.; Krugh, T.R. Biochemistry **1978**, 17, 4885.
53. For a description of **MPE**-Fe(II) footprinting see a) Van Dyke, M.W.; Hertzberg, R.P.; Dervan, P.B. Proc. Natl. Acad. Sci. USA **1982**, 79, 5470. b) Van Dyke, M.W.; Dervan, P.B. Symposia on Quantitative Biology, Cold Spring Harbor, **1982**, 47, 347.
54. Van Dyke, M.W.; Dervan, P.B. Nucleic Acids Res. **1983**, in press.
55. Hertzberg, R.H.; Dervan, R.B. Biochemistry, **1984**, submitted.
56. Henner, W.D.; Grunberg, S.M.; Haseltine, W.A. J. Biol. Chem. **1982**, 257, 11750.
57. Scholes, G. in "Effects of Ionizing Radiation on DNA", Hutterman, J., et al. eds., Vol. 27, 1978, Springer Verlag p. 153.
58. McCord, J.M.; Day, E.D. Febs Lett. **1978**, 86, 139.
59. Ward, J.F.; Urist, M.M. Int. J. Radiat. Biol. **1967**, 12, 209.
60. a) Groves, J.T.; McClusky, G.A. in "Biochemical and Clinical Aspects of Oxygen", Academic Press, 1979, p. 277. b) Groves, J.T. "Metal Ion Activation of Dioxygen", Spiro, T.G., ed., Wiley, New York, 1980.
61. a) Walling, C.H. Accts Chem. Res. **1975**, 8, 125. b) Walling, C.H. Proc. Natl. Acad. Sci. USA **1975**, 72, 140. c) Walling, C.H.; Goosen, A. J. Amer. Chem. Soc. **1973**, 95, 2987. d) Koslov, Y.N.; Nadezhchin, A.D.; Pourmal, A.P. Int. J. Chem. Kinetics **1974**, 6, 383, e) Dixon, W.T.; Norman, R.O.C. Nature (London), **1962**, 196, 891. f) Haber, F.; Weiss, J.J. Proc. Roy. Soc. London, Ser. A. **1934**, 147, 332.

62. a) Kurimura, Y.; Ochiai, R.; Matsuura, N. Bull. Chem. Soc. Japan **1968**, 41, 2234. b) Bhattacharyya, S.N.; Kunda, K.P. Int. J. Radiat. Phys. Chem. **1974**, 4, 31. c) Ilan, Y.A.; Czapski, G. Biochim. Biophys. Acta, **1977**, 498, 386. d) Fridovich, I. Ann. Rev. Biochem., **1975**, 44, 147. e) Borgaard, O.K.; Farrer, D.; Anderson, V.S. Acta Chem. Scand. **1971**, 25, 3541. f) Kachanova, Zh.P.; Kudryautseva, E.L.; Purmal, A.P. Russ. J. Phys. Chem. **1974**, 48, 849. g) Bull, C.; McClure, G.; Fee, J. J. Amer. Chem. Soc. **1983**, 105, 5290.
63. Repine, J.E. Proc. Natl. Acad. Sci. USA **1981**, 78, 1001.
64. For reviews see: a) Zimmer, Ch. Prog. Nucl. Acids Res. Mol. Biol. **1975**, 15, 285. b) Gale, E.F. et al. in "The Molecular Basis of Antibiotic Action", Wiley-Interscience, New York, 1981, p. 345.
65. Hahn, F.E. in "Antibiotics III. Mechanism of Action of Anti-microbial and Antitumor Agents", Corcoran, J.W. ed., Spring Verlag, Heidelberg, 1975, p. 79.
66. a) Luck, G.; Zimmer, Ch.; Reinert, K.E.; Arcamore, F. Nucleic Acids Res. **1977**, 4, 2655. b) Wartell, R.M.; Larson, J.E.; Wells, R.D. J. Biol. Chem. **1974**, 249, 6719. c) Malcolm, A.D.B.; Snounou, G. Symposia of Quantitative Biology, XLVII Cold Spring Harbor, **1982**, 323. d) Krey, A.K.; Hahn, F.E. Febs. Letts **1970**, 10, 175. e) Kolchinski, A.M.; Mirzabekhov, A.D. Molec. Biol. USSR **1975**, 9, 14. f) Reinert, K.E. J. Molec. Biol. **1972**, 72, 593. g) Nosikov, V.; Jain, B. Nucl. Acids Res. **1977**, 4, 2263. h) Pullman, B.; Pullman, A. Stud. Biophys. **1981**, 86, 95.
67. Luck, G.; Triebel, H.; Waring, M.; Zimmer, Ch. Nucl. Acids Res.

1974, 1, 503.

68. Mazza, G.; Galizzi, A.; Minghetti, A.; Siccardi, A. in "Anti-microbial Agents and Chemotherapy", G.L. Hobby, ed., Vol. 3, 1973, p. 384.
69. Krylov, A.S.; Grokhovsky, S.L.; Zasedatelev, A.S.; Zhuze, A.L.; Gursky, G.V.; Gottikh, B.P. Nucl. Acids Res. **1979**, 1, 289.
70. a) Patel, D.J.; Canuel, L.L. Proc. Natl. Acad. Sci. USA **1977**, 74, 5207. b) Zimmer, Ch.; Marck, C.; Schneider, C.; Guschlbauer, W. Nucl. Acids Res. **1979**, 6, 2831. c) Reinert, K.E.; Stutler, E.; Schweiss, H. Nucl. Acids Res. **1979**, 7, 1375. d) Wilkins, R.J. Nucl. Acids Res. **1982**, 10, 7273. e) Marky, L.; Blumenfeld, K.; Breslauer, K. Nucl. Acids Res. **1983**, 11, 2857.
71. a) Sutherland, J.C.; Duval, J.F.; Griffin, K.P. Biochemistry **1978**, 17, 5088. b) Zimmer, Ch.; Marck, C.; Schneider, C.; Thiele, D.; Luck, G.; Guschlbauer, W. Biochim. Biophys. Acta **1980**, 607, 232.
72. a) Patel, D. Eur. J. Biochem. **1979**, 99, 369. b) Patel, D.; Canuel, L. Proc. Natl. Acad. Sci. USA **1977**, 74, 5207. c) Pardi, A.; Morden, K.; Patel, D.; Tinoco, Biochemistry **1983**, 22, 1107. d) Patel, D. Proc. Natl. Acad. Sci. USA **1982**, 79, 6424.
73. Berman, H.M.; Neidle, S.; Zimmer, Ch.; Thrum, H. Biochim. Biophys. Acta **1979**, 561, 124.
74. Kolchinsky, A.M. et al. Molekularnaya Biologiya **1975**, 2, 19.
75. Zasedatlev, A.S.; Gursky, G.V.; Zimmer, Ch.; Thrum, H.

- Mol. Biol. Rep. **1974**, 1, 337.
76. a) Sveshnikov, P.G. et al. Molekularnaya Biologiya **1978**, 12, 557. b) Krey, A.K.; Hahn, F.E. Febs Lett. **1970**, 10, 175.
77. Krey, A.K.; Allison, R.G.; Hahn, F.E. Febs Lett. **1973**, 29, 58.
78. Bialer, M.; Yagen, B.; Mechoulam, R. Tetrahedron **1978**, 34, 2389.
79. Koenig, W.; Geigen, R. Chem. Ber. **1970**, 103, 788.
80. Paul, R.; Anderson, G.W. J. Org. Chem. **1962**, 27, 2094.
81. a) Hay, R.W.; Nolan, K.B. J. Chem. Soc., Dalton Trans. **1975**, 1348. b) Anderson, G.W.; Zimmerman, J.E.; Callahan, F.M. J. Amer. Chem. Soc. **1964**, 86, 1839.
82. a) Strong, J.E.; Crooke, S.T. in "Bleomycin: Chemical, Biochemical and Biological Aspects", Hecht, S.M., ed., Springer-Verlag, New York, 1979, p. 244. b) Johnson, P.H.; Grossman, L.I. Biochemistry, **1977**, 16, 4217.
83. Friefelder, D. Biopolymers **1969**, 7, 681.
84. McGhee, J.D.; von Hippel, P.H. J. Mol. Biol. **1974**, 86, 469.
85. Hertzberg, R.H., Ph.D. Thesis, California Institute of Technology, Pasadena, California 1983.
86. Kachanov, Z.P.; Purmal, A.P.; Skurlatov, Y.I. Russ. J. Phys. Chem. **1973**, 47, 951.
87. Gurskaya, G.V.; Grokhovskii, J.L.; Zhuze, A.L.; Gottikh, B.P. Biochim. Biophys. Acta **1979**, 563, 336.
88. Stent, G.S.; Calender, R. "Molecular Genetics", Freeman and Co., San Francisco, 1978, p. 163.
89. Segel, I., "Enzyme Kinetics", Wiley, New York, 1975.

90. Maniatis, T.; Fritsch, E.F.; Sambrook, J. "Molecular Cloning", Cold Spring Harbor, New York, 1982.
91. The sequence of pBR-322 plasmid DNA has been determined: Sutcliffe, J.G. Symposia on Quantitative Biology Cold Spring Harbor, **1979**, 43, 77.
92. Maxam, A.M.; Gilbert, W. Methods Enzymol. **1980**, 65, 499.
93. Sanger, F.; Coulson, A.R. J. Mol. Biol. **1980**, 94, 441.
94. a) Murai, S.; Sonada, N.; Tsutsumi, S.; Bull. Chem. Soc. Japan **1963**, 36, 527. b) Digman, R.V.; Anderson, D.F. J. Org. Chem. **1963**, 28, 239. c) Schultz-Frohlinde, D. Red. Res. Okuda, S., ed., Manusen, 1979, 407.
95. a) Zimmer, Ch. Prog. Nucl. Acids Res. Mol. Biol. **1975**, 15, 285. b) Zimmer, Ch.; Kakiuchi, N.; Guschlbauer, W. Nucl. Acids Res. **1982**, 10, 1721. c) Wartell, R.M.; Larson, J.E.; Wells, R.D. J. Biol. Chem. **1974**, 249, 6719.
96. Dickerson, R.E.; Drew, H.R.; Conner, B.N.; Wing, R.M.; Fratini, A.V.; Kopka, M.L. Science **1982**, 216, 475.
97. a) Miller, J.H.; Resnikoff, W.S., eds., "The Operon", Cold Spring Harbor, New York, 1978. b) Dickson, R.C.; Abelson, J.; Barnes, W.; Reznikoff, W.S. Science **1975**, 10, 186. c) Wang, J.C.; Jacobsen, J.H.; Saucier, J.M. Nucl. Acids Res. **1977**, 4, 1225. d) Epstein, W.; Rothman-Denes, L.B.; Hesse, J. Proc. Natl. Acad. Sci. USA **1975**, 72, 2300.
98. Martin, R.; Holmes, N. Nature **1983**, 302, 452.
99. Itnatowich, D.J. et al. Science **1983**, 220, 613.
100. Hogan, M.; Dattagupta, N.; Crothers, D.M. Nature **1979**, 278, 521.

101. a) Zunio F.; Di Marco, A. Biochem. Pharmacol. **1972**, 21, 867.
b) Zimmer, Ch.; Luck, G.; Thrum, H.; Pitra, C. Eur. J. Biochem. **1972**, 26, 81. c) Arcamone, F.; Nicoletta, V.; Penco, S. Gazz. Chim Ital. **1969**, 99, 632.
102. Bell, C.F. "Metal Chelation, Principles and Applications", Oxford University Press, Oxford, 1977.
103. a) Khorlin, A.A.; Krylov, A.S.; Grokhovsky, S.L.; Zhuze, A.L.; Zasedatelev, A.S.; Gursky, G.V.; Gottikh, B.P. Febs Lett. **1980**, 118, 311. b) Gursky, G.V.; Zasedatelev, A.S.; Zhuhze, A.L.; Khorlin, A.A.; Grokhovsky, S.L.; Streltsov, S.A.; Surovaya, A.N.; Nikitin, S.M.; Krylov, A.S.; Retchinsky, V.O.; Mikhaililov, M.V.; Beabealashvili, R.S.; Gottikh, B.P. Symposia on Quantitative Biology Cold Spring Harbor **1982**, 367.
104. Tanaka, T.; Weisblum, B. J. Bacteriol. **1974**, 121, 354.
105. Muller, W.; Hattesoht, I.; Schuetz, H.; Meyer, G. Nucl. Acids. Res. **1981**, 9, 95.
106. Birks, J.B. "Photophysics of Aromatic Molecules", John Wiley, New York, 1970, Chpt. 10.
107. "Handbook of Chemistry and Physics", Weast, R.C., ed., CRC Press, USA, 1973.
108. Equilibration of the 3' end labeled 381 bp fragment (3×10^{-3} M bp) with 10^{-4} M **P5E**·Fe(II) followed by addition of unlabeled 381 bp (3×10^{-3} M bp) fragment/DTT afforded the same amount of double strand cleavage as did equilibration of unlabeled DNA with **P5E** followed by addition of labeled DNA/DTT. This crossover experiment however, is inconclusive in the absence of a **P5E**·Fe(II) binding constant.